Novel ECG and Intracardiac Electrograms Signal Processing Schemes for Predicting the Outcome of Atrial Fibrillation Catheter Ablation

PAR

Andréa BUTTU

EPFL

ÉCOLE POLYTECHNIQUE
FÉDÉRALE DE LAUSANNE

« On ne force pas une curiosité,
on l'éveille. »

Daniel Pennac

Abstract

Atrial fibrillation (AF) is the most common encountered cardiac rhythm disorder (*arrhythmia*) in clinical practice. It is responsible for about one third of arrhythmia-related hospitalizations. This arrhythmia, which increases in prevalence with age, leads to severe complications and subsequently decreases the quality of life for the affected patients. Lifetime risks for developing AF are ~ 25% in subjects older than 40 years old. Currently, this arrhythmia is considered as a major public health concern.

AF is a progressive disease, starting by short and rare episodes which further develop into longer and more frequent occurrences. When the arrhythmia becomes sustained for more than one year, it is labelled as *long-standing persistent*. AF advancement gives rise to an electrical of the atria (the upper chambers of the heart) resulting from abnormal high frequency atrial activations.

The main goals of therapeutic management for patients with AF are to prevent severe complications associated with this arrhythmia, and ultimately to restore a normal rhythm. Currently, the cornerstone of non-pharmacological therapy is the radiofrequency catheter ablation of AF, which consists in delivering at strategic locations within the atria high-frequency electrical impulses. However, catheter ablation for patients with long-standing persistent AF involves extensive ablation of the atria and the success rate reported in various publications is associated with conflicting results.

Over the last twenty years, an important effort has been made by the scientific community to develop signal processing algorithms to quantify the complexity of temporal or spectral characteristics of AF dynamics in terms of *organization*. As such, multiple approaches have been proposed to quantify AF organization either based on time-domain or frequency-domain analysis. All these methods shared one common goal : the development of *organization indices* which are interpretable from an electrophyisiological viewpoint. In the context of catheter ablation of patients with long-standing persistent AF, the success rate appears limited as the "classical" organization indices are not performant in assessing the amount of ablation required to achieve AF termination. Thus, there is a strong interest in predicting the procedural outcome from the surface electrocardiogram (ECG) recorded at baseline, i.e., prior to ablation.

The main objective of this thesis was to derive novel organization indices from surface ECG and intracardiac signals acquired at baseline which could discriminate patients in whom AF was terminated from patients in whom AF persisted during catheter ablation within the left atrium. As the standard surface ECG is not appropriate for measuring the atrial activity, we aimed at adapting the placement of at least one ECG lead such that additional electrical information from the atria was provided. In our ECG signals study, we hypothesized that a quantification of the harmonic structure of AF signals brings more insight into AF complexity. Time-invariant and time-varying approaches were used to derive the ECG organization indices, and their performance for predicting the acute outcome of catheter ablation were compared. In the first scheme, the harmonic components of AF waves were extracted using linear time-invariant filters. In the second one, the components were extracted using an adaptive harmonic frequency tracking algorithm. In both schemes, two indices were developed each of which aiming at quantifying the

regularity of the oscillations of the AF waves and the morphological regularity of the AF waves. We have shown that the ability of the organization measures derived from the adaptive scheme were more robust for predicting the outcome of catheter ablation. We also investigated the impact of epoch durations on these organization indices for predicting the procedural outcome of catheter ablation. The predictive performance of the organization indices derived from the adaptive algorithm were better than that of the measures derived from the time-invariant approach on more epoch durations and ECG leads.

Before ablation, multiple catheters were inserted within both atria and recordings were acquired sequentially at several atrial segments. A frequency analysis was performed on these acquisitions in order to characterize the frequency of the activation wavefronts within both atria. We have shown that for patients in whom AF was terminated, the frequency of activations were significantly lower within both atria than for patients in whom AF was not terminated. We also studied the correlation between the frequency activity assessed endorcardially with that from the surface ECG. We have shown that the contribution of the left and right atria during AF can be independently determined using specific regions of the thorax. From the intracardiac signals we also derived novel organization indices from a temporal study on the variability of the AF activation wavefronts. Our results suggest that for patients in whom AF was terminated, the temporal stability of the activation wavefronts was higher than for patients in whom AF persisted.

Collectively, the results of this thesis showed that patients with long-standing persistent AF for whom catheter ablation successfully restored a normal rhythm, the electrical remodelling was less important than that in patients for whom the arrhythmia persisted. The ECG organization indices derived from the adaptive harmonic frequency tracking algorithm can be used to predict the outcome of catheter ablation in patients with long-standing persistent AF. The use of such measures in clinical application would provide an upstream tool for the cardiologists to help establishing the appropriate therapeutic strategy.

Keywords : atrial fibrillation, catheter ablation, prediction, organization index, ECG, intracardiac electrograms, instantaneous frequency, adaptive frequency tracking, adaptive filter, dominant frequency, phase difference, atrial fibrillation cycle length, variability of atrial activation wavefronts.

Résumé

La fibrillation auriculaire (FA) est le trouble du rythme cardiaque (*arythmie*) le plus diagnostiqué en soins cliniques et est la cause d'environ un tiers des hospitalisations liées aux arythmies. Cette arythmie, dont la prévalence augmente avec l'âge, engendre des complications sévères et diminue considérablement la qualité de vie des patients. Au-delà de 40 ans, les risques de développer une FA sont d'environ 25%. Cette arythmie est considérée actuellement comme un problème majeur de santé publique.

La FA est une maladie progressive, commençant par des épisodes brefs et rares devenant progressivement longs et fréquents. Lorsque l'arythmie devient soutenue pendant plus d'une année, elle est classifiée comme *FA chronique*. L'avancement de la FA provoque une réorganisation électrique des oreillettes (les chambres supérieures du cœur) résultant en l'activations anormale des oreillettes à une fréquence élevée.

Les objectifs principaux de la gestion thérapeutique des patients atteints de FA sont d'empêcher les graves complications associées à cette arythmie et de restaurer un rythme cardiaque normal. Actuellement, la pierre angulaire des thérapies non-médicamenteuses est l'ablation par radiofréquence de la FA, consistant à délivrer par le moyen de cathéters introduits à l'intérieur des oreillettes des impulsions électriques à haute fréquence. Cependant, chez les patients souffrant de FA chronique, l'ablation par cathéter implique la création de lésions importantes dans l'oreillette. Par ailleurs, les taux de succès publiés dans la littérature sont contradictoires.

Durant les vingt dernières années, un effort conséquent a été entrepris par la communauté scientifique pour développer des algorithmes de traitement des signaux afin de quantifier la complexité des caractéristiques temporelles ou spectrales de la dynamique de la FA. Ainsi, dans le domaine fréquentiel, plusieurs approches basées sur des méthodes invariantes ou variantes dans le temps ont été proposées pour quantifier l'organisation de la FA. Toutes ces méthodes avaient un but commun : le développement d'indices d'organisation qui peuvent être interprétés d'un point de vue électrophysiologique. Dans le contexte de l'ablation par cathéter chez les patients souffrant de FA chronique, le taux de succès apparaît limité étant donné que les indices d'organisation "classiques" ne sont pas assez performants pour évaluer la quantité d'ablation requise pour terminer la FA. En conséquence, il y a un fort intérêt à pouvoir prédire l'issue procédurale à partir de signaux provenant de l'électrocardiogramme de surface (ECG) enregistrés avant l'ablation.

L'objectif principal de cette thèse a été de définir des nouveaux indices d'organisation à partir de signaux d'ECG ou intracardiaques enregistrés avant l'ablation, dans le but de discriminer les patients chez qui la FA a été terminée des patients chez qui la FA a persisté pendant l'ablation par cathéter dans l'oreillette gauche. Étant donné que l'ECG de surface n'est pas approprié pour mesurer l'activité auriculaire, nous avions pour but d'adapter le placement standard des électrodes de surface afin de disposer d'une meilleure résolution spatiale de l'activité électrique atriale. Dans notre étude des signaux ECG, nous avons fait l'hypothèse que la structure harmonique des signaux de FA améliore la quantification de la dynamique de FA. Des méthodes invariantes et variantes dans le temps ont été utilisées pour définir des indices d'organisation, et leurs performances pour la prédiction de l'issue procédurale de l'ablation ont été comparées.

Dans la première approche, les composantes harmoniques des signaux de FA ont été extraites avec des filtres linéaires et invariants dans le temps. Dans la deuxième approche, les composantes ont été extraites par le biais d'un algorithme adaptatif de poursuite en fréquence. Dans les deux approches, deux mesures d'organisation furent développées chacune d'elle quantifiant respectivement la régularité des oscillations des signaux de FA et leur la régularité morphologique. Nous avons montré que les indices d'organisation définis à partir de l'algorithme adaptatif sont plus robustes pour prédire le succès de l'ablation. Nous avons aussi étudié l'impact de la durée d'enregistrement sur les performances statistiques de ces mesures d'organisation. Les performances de prédictions ont été meilleures, sur plus de durées et d'électrode ECG, pour les indices d'organisation issus de l'algorithme adaptatif que pour les indices issus de la méthode invariante dans le temps.

Avant l'ablation, plusieurs cathéters sont introduits dans les deux oreillettes afin d'enregistrer séquentiellement des signaux à divers endroits anatomiques. Une analyse fréquentielle a été effectuée sur ces signaux afin de caractériser la fréquence d'activation des fronts d'ondes de la FA. Nous avons montré que chez les patients pour qui la FA termina pendant l'ablation, cette fréquence était significativement plus basse dans les deux oreillettes que chez les patients pour qui l'ablation fut un échec. Nous avons aussi étudié la corrélation entre le contenu fréquentiel intracardiaque et celui mesuré depuis l'ECG de surface. Nous avons montré que la contribution des oreillettes gauche et droite peut être déterminée à partir de régions spécifiques du thorax. Pour finir, à partir des signaux intracardiaques, nous avons développé de nouveaux indices d'organisation dans le but de mesurer la variabilité temporelle des fronts d'activation de la FA. Nos résultats ont montré que, pour les patients chez qui la FA terminait, les fronts d'activations étaient plus stables au cours du temps que pour les patients chez qui l'ablation fut un échec.

Pris collectivement, les résultats de cette thèse montrent que chez les patients atteints de FA chronique, pour qui l'ablation par cathéter a rétabli avec succès un rythme cardiaque normal, la réorganisation électrique des oreillettes est moins avancée que chez les patients pour qui l'ablation fut un échec. Les indices d'organisation définis à partir de l'algorithme adaptatif peuvent être utilisés afin de prédire l'issu procédurale de l'ablation par cathéter de la FA chronique. Dans un contexte clinique, l'utilisation de ces indices peut permettre à l'électrophysiologue d'établir en amont une thérapie appropriée dans le but de restaurer un rythme cardiaque normal.

Mots-clés : fibrillation auriculaire, ablation par cathéter, prédiction, indice d'organisation, ECG, électrogramme intracardiaque, fréquence instantanée, poursuite adaptative de fréquence, filtre adaptatif, fréquence dominante, différence de phase, variabilité des fronts d'activations.

Remerciements

Ce travail de thèse n'aurait pas été possible sans les contributions, directes ou indirectes, de nombreuses personnes que j'aimerais sincèrement remercier :

- Merci au président du jury, Prof. Jean-Philippe Thiran, ainsi qu'aux rapporteurs, Prof. Catherine Dehollain, Prof. Leif Sörnmo et Dr. Laurent Roten pour les discussions et commentaires lors de l'examen oral de cette thèse.

- Je tiens à remercier l'équipe du CHUV en salle d'électrophysiologie : Hélène, Françoise, Andrei, Patrizio, et tout particulièrement Claude, sans qui je n'aurais eu aucune donnée ! MERCI !

- Merci à Susanna et Vanessa de Biosense pour leur soutien et surtout leur patience et disponibilité pour m'expliquer les méandres techniques du Carto.

- Je tiens à remercier tous les membres des différents laboratoires de traitement du signal (ASPG, LTS et MMSPG) pour l'ambiance conviviale et amicale qui règne dans nos couloirs. Un merci tout particulier à Rosie pour m'avoir rappelé à chaque fois que je devais tenir à jour le "cahlandhryhey".

- Je tiens à remercier tout particulièrement les "Jean-Marc Boys and Girls" pour tous les bons moments que nous avons partagés. Je n'oublierai jamais tous ces moments remplis de fous-rires. J'ai eu beaucoup de chance d'avoir des collègues et amis aussi formidables que vous : Florian, Cédric, Yannou, Alain et Maîtresse Aline. Un merci particulier à mes collègues de bureau : Laurent et Jérôme, que de fous-rires nous avons partagés ! Leila (alias oeil de lynx) et Adrian, merci pour votre soutien pendant l'écriture de ce manuscrit ! Vous m'avez tellement aidé. MERCI ! Merci aussi aux membres honoraires de l'ASPEGIC : Elda, Martin, Benoît, Ashkan et tous les autres pour tous les bons moments passés à Sat et en dehors de l'EPFL. "T'chieu c'téquipe ! ! ! !"

- Je tiens également à exprimer toute ma gratitude à ma famille et mes proches pour leur soutien inconditionel : merci à mes parents qui ont toujours cru en moi. Merci aussi à mes beaux-parents pour leur soutien. Un énorme merci à Seb pour m'avoir soutenu pendant l'écriture de cette thèse. Rédiger une thèse n'est pas facile, mais m'avoir supporté pendant cette période stressante le fut encore moins. MERCI !

- Merci à mon co-directeur de thèse, Etienne, pour sa pédagogie et son soutien. Merci de m'avoir donné l'opportunité d'assister aux procédures, j'ai énormèment appris grâce à toi. Merci pour tous les bons moments que nous avons partagé pendant les conférences. J'ai eu beaucoup de chance d'avoir un coach médical aussi brillant que toi !

- Le meilleur, et sûrement le plus important, pour la fin : un énorme merci à Jean-Marc, mon directeur de thèse. Ta passion et ton enthousiasme pour l'enseignement, ton sens de l'humour et de la répartie, ton érudition sans limite ont rendu ces années de thèse inoubliables. J'ai de la chance d'avoir eu un boss comme toi. Au fil de ces années rendues magiques en grande partie grâce à toi, tu es devenu bien plus qu'un directeur de thèse. Je ne pourrai

jamais assez te remercier pour tout ce que tu m'as apporté. MERCI POUR TOUT !

Contents

List of Acronyms

AA	Atrial activity
ABS	Average beat subtraction
AF	Atrial fibrillation
AFCL	Atrial fibrillation cycle length
$AFCL_{RI}$	Resampled instantaneous atrial fibrillation cycle length
ANOVA	Analysis of variance
AOI	Adaptive organization index
aPD	Adaptive phase difference
ASPG	Applied signal processing group
AT	Atrial tachycardia
AUC	Area under the curve
AV	Atrioventricular
BMI	Body mass index
bpm	Beats per minute
BSPM	Body surface potential maps
CFAE	Complex fractionated atrial electrograms
CHUV	Centre Hospitalier Universitaire Vaudois
CS	Coronary sinus
DCC	Direct-current cardioversion
DF	Dominant frequency
DFT	Discrete Fourier transform
DTFT	Discrete-time Fourier transform
ECG	Electrocardiogram
EGM	Electrogram
ERP	Effective refractory period
f-waves	Fibrillatory waves
HFT	Harmonic frequency tracker

LA	Left atrium
LAA	Left atrial appendage
LAT	Local activation time
LIPV	Left inferior pulmonary vein
LOOCV	Leave-one-out cross validation
LSPV	Left superior pulmonary vein
LT	Left terminated
NLT	Not left terminated
OI	Organization index
PD	Phase difference
PSD	Power spectral density
PV	Pulmonary vein
PVI	Pulmonary vein isolation
RA	Right atrium
RAA	Right atrial appendage
RF	Radiofrequency
RIPV	Right inferior pulmonary vein
ROC	Receiver operating characteristic
RSA	Respiratory sinus arrhythmia
RSPV	Right superior pulmonary vein
SA	Sinoatrial
SB	Single beat
SFT	Single frequency tracker
sPD	Slope of the phase difference
SR	Sinus rhythm
step-CA	Stepwise catheter ablation
TIPD	Time-invariant phase difference
VA	Ventricular activity
YI	Youden index

List of Tables

List of Figures

Introduction

<div style="text-align: right; font-size: 3em;">**1**</div>

1.1 Motivation and problem statement

Clinical importance of atrial fibrillation

Atrial fibrillation (AF) is the most commonly encountered cardiac disorder (*arrhythmia*) in clinical practice and is responsible for about one third of arrhythmia-related hospitalizations. In contrast to a regular rhythm, the so-called *sinus rhythm* (SR), an AF episode is characterized by rapid and irregular activation of the upper chambers of the heart (*the atria*). AF is complicated by a severe impairment of the atrial and ventricular (lower chambers) contractile functions resulting in a decrease of the cardiac output. The loss of the contractile functions promotes the formation of blood clots and, thus, considerably increases the risks for stroke. The conditions associated with AF may lead to a severe decrease in quality of life for affected patients. Worldwide epidemiological data on AF suggest that this disease can be considered as an emergent global epidemic [1]. Lifetime risks for developing AF are $\sim 25\%$ in subjects older than 40 years, independently of gender [2]. As life expectancy increases, AF prevalence is estimated to double in the next fifty years [1]. Consequently, AF is considered as a major public health concern [3].

The natural time-course of the evolution of AF starts by short and rare episodes (usually the arrhythmia self-terminates within 48 hours, and in this case AF is classified as *paroxysmal*), to longer and more frequent occurrences (the arrhythmia becomes *persistent*). The numerous conditions associated with AF contribute to a progressive process in the development of the disease by favoring either the occurrence responsible to its initiation (the *focal triggers*) and/or the formation of a *substrate* responsible for its perpetuation. These mechanisms are not mutually exclusive and are likely to be present simultaneously at various times of the disease, in particular when the arrhythmia becomes persistent [4]. When the arrhythmia becomes sustained for a duration greater than one year, it is labelled as *long-standing persistent AF* (also termed chronic AF).

AF advancement gives rise to an electrical and structural remodellings of the atria that may, in turn, favor the maintenance of the arrhythmia. More precisely, the electrical remodelling results from abnormal high frequency atrial activations. The structural remodelling engenders a significant enlargement of the atria. The electrical and structural remodelling affect the atrial function and structure at different stages of the disease. In the development of sustained AF, the atrial remodelling is important and may quench therapeutic success.

<div style="text-align: center;">1</div>

Management of atrial fibrillation

The main goals of therapeutic management for patients with AF are to reduce the symptoms, to prevent severe complications associated with AF, and ultimately to restore a normal SR. These objectives may be pursued in parallel. Nowadays, pharmacological and non-pharmacological treatments constitute the most prevailing options. Most commonly, pharmacological therapies involve the prescription of drugs, such as beta-blockers. Pharmacological approaches, however, suffer from poor efficacy, in particular in patients with long-standing persistent AF. When a pharmacological approach fails to reduce the heart rate or to terminate AF, a non-pharmacological strategy should be considered. Currently, radiofrequency catheter ablation of AF is the cornerstone of non-pharmacological therapy. This approach consists in delivering high-frequency electrical impulses endocardially (within the atria) in order to eliminate the trigger(s) and/or alter the arrhythmogenic substrate and ultimately restore a normal SR.

Various ablation strategies have been deployed in order to terminate AF in different patient populations. For patients with paroxysmal AF, it has been reported that ablation procedures involving eliminations of the focal triggers achieved 70% of AF termination, whereas in patients with non-paroxysmal AF the success dropped to 30% [5]. Once AF becomes sustained, ablation of the triggers alone is not sufficient for terminating the arrhythmia, suggesting that the triggers play a less critical role in maintaining AF and that some level of structural or electrical remodelling enables the atria to perpetuate the AF independently of the triggers. Consequently, in patients with a sustained form of AF, some additional ablation strategy targeting the substrate responsible for the maintenance of AF should be considered, notably for patients with long-standing persistent AF. These approaches consist of performing linear ablations and/or ablation of complex fractionated electrograms (CFAEs). These electrograms are characterized by low-voltage with multiple potentials signals and are visually identified by the operator during the ablation procedure, which can be challenging and highly subjective. CFAEs are currently believed to be involved in AF maintenance as fractionated and continuous activity may be indicative of the presence of fibrillatory wave collisions. CFAEs ablation, however, results in extensive atrial lesions that may preclude any recovery of atrial contractile function despite SR restoration. For patients with long-standing persistent AF, some groups have reported the benefit of using a *stepwise* approach consisting in performing a sequential ablation strategy involving the ablation of the focal triggers, linear and CFAEs ablations [6–8].

The success rate of stepwise catheter ablation of long-standing persistent AF reported in various publications is associated with conflicting results, and usually requires several attempts in order to restore a long-term SR [6–8]. Originally, this sequential approach has been proposed by the Bordeaux group which reported in one study the termination of persistent AF in 87% of patients [6], whereas in another study the single-procedure success rate was 55% [7]. Outside of this group, Rostock et al. achieved a lower single-procedure success rate of 38% [8]. There is therefore a clear need for additional studies from different research centers to validate this ablation strategy for patients with long-standing persistent AF.

The concept of atrial fibrillation organization

For a long time, the atrial fibrillatory activation patterns have been described as totally chaotic and random. In 1978, the first study aiming at establishing visual differences of AF intracardiac electrograms resulted in the classification of AF recordings into different categories based on the discreteness of the electrograms and the baseline perturbations [9]. An important issue with such an approach is that the classification is highly subjective on operators judgement. However, this graduation of the fibrillatory waveforms pointed out an important aspect of AF recordings: they can be characterized in terms of temporal regularity and repeatability. This avant-garde perception of AF activity has motivated the scientific community to develop signal processing

algorithms to quantify the complexity of temporal or spectral characteristics of AF dynamics in terms of *organization*.

As such, multiple approaches have been proposed to quantify AF organization either based on time-domain analysis, frequency-domain analysis or non-linear dynamical systems theory. All these methods shared one common goal: the development of *organization indices* which are interpretable from an electrophysiological viewpoint. For instance, the most commonly used index in clinical practice is computed from intracardiac electrograms as the average time difference between consecutive atrial activation wavefronts and is named the *AF cycle length* (AFCL). Clinical studies have established a fine correspondence between the intracardiac AFCL and depolarization properties of atrial tissues [10–12]. Furthermore, indices computed from frequency-domain approaches constitute a logical alternative to time-domain methods, in particular if the goal is to characterize the repeatability of AF activation patterns. As such, the most widely used method is to locate the peak of highest amplitude in the power spectral density (PSD) of an atrial signal. This frequency, the so-named *dominant frequency* (DF), can be computed either from an atrial signal recorded from the surface electrocardiogram (ECG) or endocardially. This measure has been used as an organization index in clinical studies in order to quantify the atrial electrical remodelling [13–15], and to predict the response to several therapies [16–20]. Another spectrum-based index estimated from the study of the harmonic structure of AF signals is the organization index (OI) which is computed as the ratio between the power under the harmonic peaks to the total power of intracardiac signals [21]. Although no physiological meaning of the OI was provided by the authors, they have used this index in order to optimize the success of electrical AF cardioversion [21] [1].

Because of the variety of signal processing indices proposed in the literature, the term *AF organization* has become ambiguous and hence no consensus on a precise definition has been established. As a consequence, comparing results from different studies is a difficult task. One might argue therefore that measures of AF organization may instead be developed based on their clinical application and interpretation from an electrophysiological viewpoint.

Challenges in predicting catheter ablation outcome of atrial fibrillation

The prediction of the procedural outcome of catheter ablation is an important information for the physician, in particular for patients with long-standing persistent AF for which the success rate in terminating AF is lower compared to non-sustained AF. Furthermore, for AF sustained for more than one year, the duration of the stepwise ablation procedure is considerably longer and extensive ablation of the atria is necessary for terminating the arrhythmia. The availability of a prediction tool using ECG signals would possibly lead to the establishment of upstream therapies for patients with long-standing persistent AF. As such, patients comfort would be greatly enhanced and the ablation procedural time could be reduced.

Predicting AF catheter ablation outcome from ECG signals has the main advantage that it can be performed before the procedure, without the need of inserting any catheter within the atria. The idea is to identify in patients with long-standing persistent AF a broad pathophysiological behaviour of the AF dynamics using novel organization indices. Importantly, these indices estimated on ECG signals should be interpretable from an electrophysiological viewpoint, and therefore should correspond to a certain degree with intracardiac measurements. However, from a signal processing viewpoint, several constraints should be taken into account. First, the signal processing methods should not be computationally expensive and ideally should run in real-time. As such, the prognosis of the catheter ablation outcome could be established from recordings acquired on embedded devices. Second, the minimal recording duration necessary to get stable and statistically robust organization indices should be established.

---

1. An electrical cardioversion consists in performing an electric shock which will eventually reset the atrial activity towards a normal rhythm.

1.2   Objectives

The goal of the present thesis is to investigate the performance of innovative organization indices derived from the surface ECG in predicting the outcome of first-time catheter ablation in patients with long-standing persistent AF. As such, a logical first step was to define the ablation and the baseline (prior to ablation) data acquisition protocols. From a clinical aspect, care was taken in establishing a detailed record of the patient population.

The standard surface ECG was specifically designed to follow the depolarization and repolarization of the ventricles, which considerably compromise the estimation of the spatial information of the atrial activity. Thus, we aimed at adapting the placement of at least one ECG lead such that additional electrical information from the atria was provided. Moreover, a correspondence between the activity recorded from the surface ECG and that from intracardiac segments must be established, providing us a spatial interpretation of the measures of organization derived from ECG signals.

Signals acquired within the atria are a direct measurement of the local activity and a surrogate of the level of atrial remodelling. Therefore, before ablation, multiple catheters were inserted within both atria and recordings were acquired sequentially at several atrial segments. We aimed at performing an intracardiac DF analysis in order to characterize the frequency of the activation waveforms within both atria. Moreover, the intracardiac AFCL reflects the average regularity of the local AF dynamic and is not suitable for assessing the temporal variations in the fibrillatory activation wavefronts. We intend to define intracardiac organization indices which quantify the temporal variations of the atrial activation wavefront around the mean AFCL.

In this thesis, for the derivation of organization indices from the surface ECG, we hypothesized that the quantification of the harmonic structure of AF signals might bring more insight into the AF complexity rather than characterizing the AF dynamic with one component such as the DF. We aimed at deriving organization indices from time-invariant and time-varying methods and compare their performance for predicting the acute outcome of catheter ablation.

In the context of predicting the outcome AF catheter ablation, defining organization indices from baseline ECG signals should be accomplished with the aim of answering the following questions. Are the organization indices reflecting specific characteristics of the AF dynamics? Are the organization indices useful for discriminating patients in whom AF catheter ablation terminates AF from patients in whom AF persisted? What is the impact of epoch durations on the performance of the organization indices for predicting the acute procedural outcome of AF catheter ablation?

To summarize, the main objective of this dissertation are:
- to provide a clinical study of patients with long-standing persistent AF in the context of AF catheter ablation,
- to improve the recording of the atrial activity using a modified surface ECG lead placement,
- to establish a correspondence between the AF activity recorded endocardially with that from the surface ECG,
- to quantify the variability of atrial activation intervals,
- to define novel organization indices from ECG signals to predict the outcome of catheter ablation,
- to assess the impact of the epoch durations on the ECG organization indices in discriminating patients with AF termination from those without termination,
- to assess the predictive performance values of these measures of organization.

The ultimate goal of this thesis is to define organization indices from the surface ECG that could be used as an upstream tool for predicting the outcome of catheter ablation in patients with long-standing persistent AF.

This work has been carried out in the framework of a collaboration between the Applied Signal Processing Group [2] (ASPG) and the cardiology department at the Centre Hospitalier Universitaire Vaudois [3] (CHUV).

1.3 Organization

The dissertation is divided into four parts. The first two parts are organized as follows:

I **Introduction to cardiac electrophysiology, electrography, atrial fibrillation and catheter ablation.** In Chapter 2, after a review of the anatomy of the cardiovascular system and a description of the initiation and propagation of electrical impulses across the heart, the different conventional electrocardiographic measures (surface ECG and intracardiac) are also presented. Then, Chapter 3 is devoted to the main clinical aspects of AF, and to the presentation of the alleged pathophysiological mechanisms by which cardiac conditions favor AF. Chapter 4 briefly introduces the technologies and tools necessary for performing AF catheter ablation. The current ablation strategies performed for eliminating AF triggers and for modifying the substrate maintaining AF are also presented.

II **Patients characteristics and data acquisition.** The second part (Chapter 5) is dedicated to the presentation of the patient population clinical characteristics used in the present dissertation. Also, the various technologies available during the ablation procedure for the ECG and intracardiac signals acquisitions are described. Additionally, a description of the baseline endocardial signal acquisition and ablation protocol defined during this thesis is provided. Finally, the databases, which were constructed off-line, are briefly expounded.

Parts III and IV are devoted to the development of novel organization indices from ECG and intracardiac signals respectively. Figure 1.1 illustrates the organization of these parts. In this schematic view, the node with shapes and colors □ denote a part of the dissertation, ○ a thesis chapter, and ○ a section of a chapter.

III **ECG signal processing.** This part is divided into two chapters. Chapter 6 presents organization indices derived from time-invariant spectral approaches and harmonic analysis of ECG signals. The performance of these indices to correctly and robustly identify patients in whom catheter ablation was successful in terminating AF is investigated through an exhaustive statistical analysis. Then, Chapter 7, presents the adaptive harmonic frequency tracking algorithm from which novel organization indices were estimated. For comparison purposes, the prediction performance of the adaptive derived organization indices was assessed with the same statistical analysis as in Chapter 6.

IV **Intracardiac signal processing.** As illustrated in Figure 1.1, this part is divided into two chapters. Chapter 8 is devoted to the spectral analysis of intracardiac signals using a classical time-invariant spectral estimation of the DF as well as a time-varying scheme for assessing the temporal evolution of the frequency content of atrial signals. In this chapter, two types of study are presented. The first one, aims at evaluating the intracardiac contribution of several atrial segments to ECG chest leads. While the second study is aimed at studying the distribution of the DFs assessed in several atrial segments prior to ablation. Then, Chapter 9 presents a novel method for characterizing the temporal variability of intracardiac atrial activation wavefronts around the mean AFCL before ablation.

---

2. `http://aspg.epfl.ch/`
3. `http://www.cardiologie.chuv.ch/`

Finally, Chapter 10 summarizes the results achieved during this thesis and provides a global conclusion. Possible future directions of research are also covered.

Three appendices are included in this dissertation. Appendix A provides various medical definitions and a mathematical background on the concept of instantaneous frequency, the Hilbert transform, the binary logistic regression, and the receiver operating characteristic curves analysis. Appendix B presents the technical details on the catheters as well as the recording system used during the ablation procedure. Appendix C presents the ventricular cancellation method used on the ECG signals.
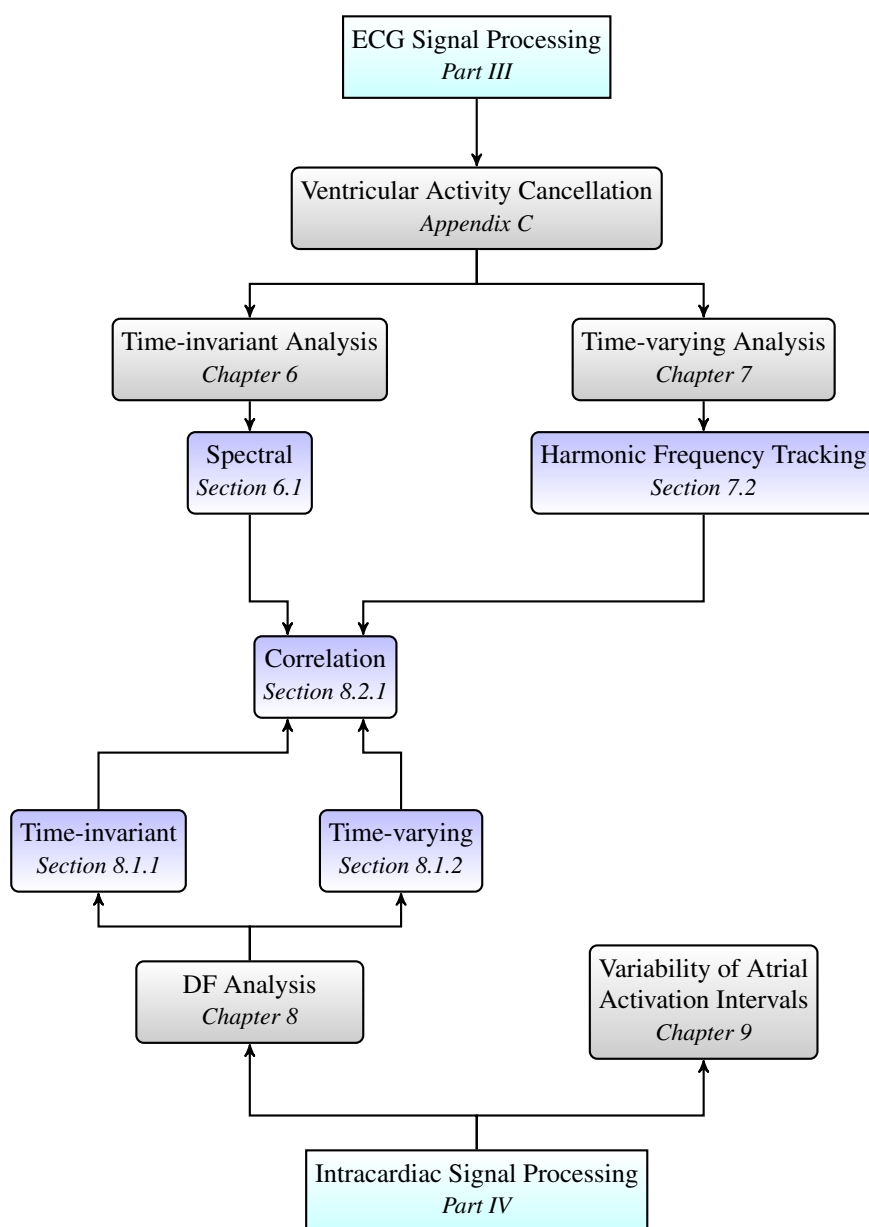
Figure 1.1: Organization of Parts III and IV of the dissertation. The shapes and colors of the nodes are defined as such. □: thesis part. ○: thesis chapter. ○: section of a chapter.

1.4   Original contributions

The main contribution [4] of this work are:

- **Electrophysiological study**

  - Clinical study of long-standing persistent AF catheter ablation.
  - Use of a modified 12-lead ECG placement.

- **Signal processing and measures of organization estimated on recordings prior to ablation**

  - *Surface ECG*
    * Characterization of the AF instantaneous frequency and phase relationship between the AF fundamental component and its first harmonic using an adaptive harmonic frequency tracking algorithm.
    * Assessment of the impact of the epoch durations on the performance of the organization indices for predicting the procedural outcome of catheter ablation.
    * Exhaustive statistical analysis on the predictive performance of ECG organization indices.
    * Comparison between organization indices derived from time-invariant and time-varying signal processing schemes.

  - *Intracardiac*
    * Bi-atrial frequency mapping.
    * Evaluation of intracardiac contribution to ECG fibrillation waves.
    * Correspondence between the intracardiac activity and the ECG outputs of the adaptive frequency tracking algorithm.
    * Characterization of the temporal variability of atrial activation wavefronts.

---

4. See also the list of publications at the end of the manuscript (page 175).

Part I

Introduction to Cardiac Electrophysiology, Electrocardiography, Atrial Fibrillation and Catheter Ablation

Cardiac Electrophysiology and Electrography

2

This chapter reviews the anatomy of the cardiovascular system and describes the initiation and propagation of electrical impulses across the heart (Section 2.1). In the second part of this chapter, the different conventional electrocardiographic measures are explained (Section 2.2).

2.1 Cardiac electrophysiology

2.1.1 The anatomy of the heart and of the cardiovascular system

The heart is a muscular organ of the size of a fist located in the middle of the chest above the diaphragm, between the lungs and behind the sternum. The heart weights between 200 to 425 grams and its walls are composed of cardiac muscle, called myocardium. It is surrounded by a double-layered membrane called the pericardium.

The heart receives venous blood at a low pressure, then increases it to a higher pressure by contracting its cardiac chambers, and finally ejects the blood into the arterial blood vessels [22]. Its anatomy (Figure 2.1) consists of two pumps working in parallel. Each pump is made of two chambers: the atrium (where the blood enters) and the ventricle (where the blood exits the heart). Each side is responsible for pumping synchronously different circulatory networks. The non-oxygenated blood (i.e., coming from the systemic circulation, blue arrows in Figure 2.1) enters the right atrium through the superior and inferior vena cava. The blood flows from the right atrium into the right ventricle through the tricuspid valve. The blood is then expulsed into the pulmonary artery through the pulmonary valve. The pulmonary artery then branches into two pulmonary arteries (left and right), which deliver the blood to the corresponding lung. The oxygenated blood (red arrows in Figure 2.1) returns from the lungs and enters the left atrium via four pulmonary veins. The blood flows from the left atrium into the left ventricle through the mitral valve and is ejected from the left ventricle across the aortic valve into the aorta.

2.1.2 The cardiac cycle

In order to understand how the cardiac function is regulated, one must know the sequence of mechanical events during a complete cardiac cycle and how these mechanical events relate to the electrical activity of the heart.

The successive mechanical events characterizing the contractile function of the heart during the cardiac cycle can be divided into two general events: **diastole** (filling) and **systole** (ejection).
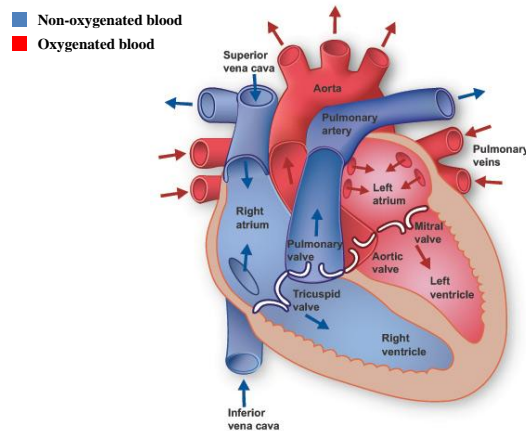
Figure 2.1: Anatomy of the heart and associated vessels. The blue arrows denote the non-oxygenated blood. The red arrows denote the oxygenated blood. *Image adapted from:* `http://www.texasheartinstitute.org`.

The diastole refers to the resting time in the cardiac cycle, i.e., the period of time when the ventricles are undergoing relaxation and filling with atrial blood (Figure 2.2).

Ventricular filling is primarily passive, although atrial contraction has a variable effect on the final extent of ventricular filling (end-diastolic volume). The systole refers to the ventricular contraction and ejection and is initiated by the electrical depolarization of the ventricles. Ventricular ejection begins when ventricular pressure exceeds the pressure within the outflow tract (aorta or pulmonary artery) and continues until ventricular relaxation causes the ventricular pressure to fall below the aortic and pulmonary artery pressures closing the aortic and/or pulmonic valves. The volume of blood remaining within the ventricle at the end of the ejection is the end-systolic volume. The cardiac cycle is further divided into seven phases: atrial systole, isovolumetric contraction, rapid ejection, reduced ejection, isovolumetric relaxation, rapid filling, and reduced filling [22].
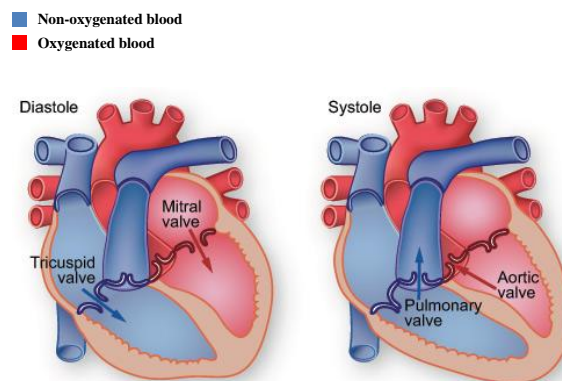
Figure 2.2: The cardiac cycle which is primarily divided into two phases: diastole (panel A, filling of the ventricles) and systole (panel B, ejection from the ventricles). *Image adapted from:* `http://www.texasheartinstitute.org`.

2.1.3   Cardiac electrical activity

Cardiac muscle cells

The cardiac tissue can be illustrated as a dense array of cells arranged into bundles. These cells are called the cardiac myocytes. Their primary function is to contract. The contractions are initiated by electrical changes. This section explains: (1) the electrical activity of individual myocytes, and (2) how a coordinated contraction of the heart is initiated.

Cell membrane potentials

Cardiac potentials can be measured by means of microelectrodes placed into the cell. These microelectrodes allow to measure the electric potential in millivolts (mV) inside the cell relative to its outside. The *transmembrane potential V_m* is defined by the difference in voltage between the interior and exterior of a cell. The resting membrane potential is primarily determined by the concentrations of positively and negatively charged ions across the cell membrane. At rest, cardiac cells are electrically polarized (i.e., their insides are negatively charged with respect to their outsides). In the resting state, the membrane potential of a myocardiac cell is around -80 to -90 mV (Figure 2.3).

The cell membrane is a thin film of lipid and protein molecules held together by non-covalent interactions [23]. The lipid molecules are arranged in a continuous double layer of about 5 nm thick. Protein molecules embedded in this lipid bilayer form ionic channels allowing specific ions to cross the membrane. Of the many different ions present inside and outside of the cells, the most important in determining the membrane potentials are sodium (Na^+), potassium (K^+), chloride (Cl^-), and calcium (Ca^{++}). Ions channels have both opened (activated) and closed (inactivated) states that are regulated either by membrane voltage or by receptor-coupled signal transduction mechanism [22]. The electrical polarity is maintained by transmembrane pumps that ensure the appropriate distribution of ions to keep the insides of the cardiac cells relatively electronegative compared to the extracellular space. Cardiac cells can reverse their internal negativity in a process called *depolarization*. This happens when a normal depolarization current spreads from one cardiac cell to another during electrical activation of the heart. After depolarization is complete, the cardiac cells are able to restore their resting polarity through a process called *repolarization*. The electrical cycle from a single cell of depolarization and repolarization is called an action potential. By convention, the action potential has five phases numbered from 0 to 4.

The two general types of cardiac action potentials include nonpacemaker and pacemaker action potentials. Nonpacemaker action potentials are triggered by depolarization currents from neighboring cells, whereas pacemaker cells are capable of spontaneous action potential generation.

Nonpacemaker action potentials

Nonpacemaker action potentials are typically found in cells such as atrial and ventricular myocytes and Purkinje cells. Figure 2.3 illustrates the phases of a nonpacemaker action potential.

  – **Phase 0.** Phase 0 is the rapid depolarization phase caused by a transient increase of Na^+ ions into the cell (I_{NA}) resulting in a shifting of the membrane potential away from the potassium equilibrium potential and closer to the sodium equilibrium potential.
  – **Phase 1.** Phase 1 represents the initial fast repolarization caused by the inactivation of the fast Na^+ channel and the opening of a specific type of K^+ channel (transient outward, I_{to1}).
  – **Phase 2.** Phase 2 is the "plateau" phase due to a delay in the repolarization. This delay is sustained by a balance between inward movement of Ca^{++} ions (I_{ca}, through L-type cal-
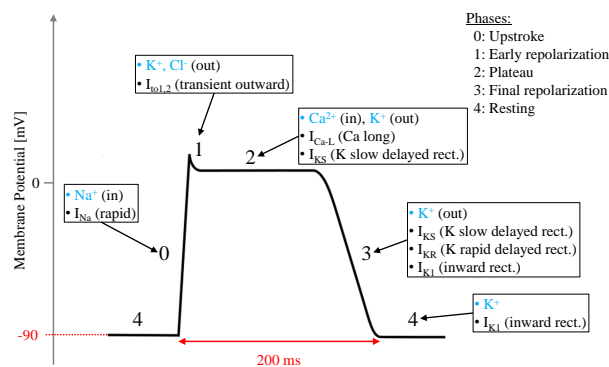
Figure 2.3: The five phases of the nonpacemaker action potential. For each phase, the types of ion channels (blue) and the currents (black) are indicated in the corresponding text boxes. The sharp rise in voltage (phase 0) is primarily produced by a transient increase in sodium (Na^+) conductance. The two decays (phases 1 and 3) correspond to the sodium channel inactivation and the repolarizing efflux of potassium (K^+) ions. The plateau (phase 2) is principally generated by inward calcium channels (Ca^{++}). *Figure adapted from Wikipedia (cc by-sa).*

cium channels) and outward movement of K^+ ions (I_{KS}, through the slow delayed rectifier potassium channels).

   – **Phase 3.** Phase 3 is the rapid repolarization process. During this phase, the L-type calcium channels close while the slow delayed rectifier potassium channels (I_{Ks}) are still open. This ensures a net outward current, corresponding to a negative change in the membrane potential, thus allowing more types of potassium channels to open (I_{Kr} and I_{K1}). This net outward current causes the cell to repolarize.

     The delayed rectifier K^+ channels close when the membrane potential is restored to about -80 to $-85\,mV$, while the inward rectifier K^+ channels (I_{K1}) remain conductive throughout phase 4, contributing to set the resting membrane potential [24].

   – **Phase 4.** Phase 4 is the resting membrane potential described previously. When the non-pacemaker cells are rapidly depolarized from the resting potential of $-90\,mV$ to a threshold voltage of about $-40\,mV$ (owing to an external stimulus, typically an action potential conducted by an adjacent cell), phase 0 is initiated.

During phases 0, 1, 2, and part of phase 3, the cell is refractory (i.e., unexcitable) to the initiation of a new action potential, which defines the *effective refractory period* (ERP). The ERP limits the frequency of action potentials (and therefore contractions) that the heart can generate and thus, acts as a protective mechanism. This enables the heart to have adequate time to fill and eject blood. The ERP is followed by the *relative refractory period* during which high intensity stimuli are required to elicit action potentials. Because not all the sodium channels have fully recovered at this time, the action potentials generated during this phase have a decreased phase 0 slope and lower amplitude.

Atrial cells have action potentials similar in many aspects to the ventricular action potentials. The most distinguishable feature of the atrial action potential is that it has a more triangular appearance than the ventricular one [25]. This feature seems to be due to a prominent phase 1. In atrial cells, phases 1, 2, and 3 tend to run together, producing a triangular shape, with a plateau not always apparent.

Pacemaker action potentials

Pacemaker cells have no true resting potential, but instead generate regular, spontaneous action potentials. These types of cells possess the property of automaticity, that is, they have the ability to spontaneously depolarize. The depolarization current of the action potential is carried primarily by relatively slow, inward Ca^{++} currents (instead of fast Na^+ currents).

Cells within the sinoatrial (SA) node, located in the right atrium at the junction of the superior vena cava (crista terminalis), constitute the primary pacemaker site within the heart. Other pacemaker cells exist within the atrioventricular (AV) node (located at the boundary between the atria and ventricles) and the ventricular conduction system, but their firing rates are driven by the higher rate of the SA node. This is due to a mechanism called overdrive suppression in which the intrinsic pacemaker activity of the secondary pacemakers is suppressed. Through this mechanism, the secondary pacemaker becomes hyperpolarized when driven at a rate above its intrinsic rate. In this case, a secondary site can take over to the pacemaker of the heart. When this phenomenon occurs, the new pacemaker site is called an *ectopic foci*.

SA nodal action potential is divided into three phases (illustrated in Figure 2.4):
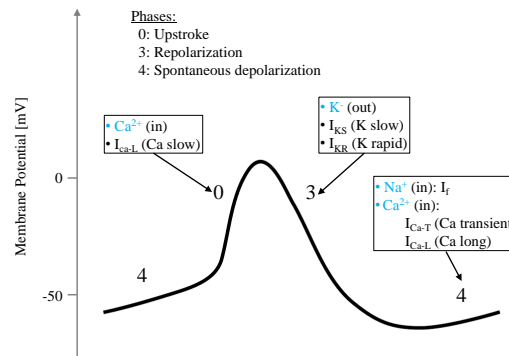
Figure 2.4: The three phases of the SA nodal action potential. For each phase, the types of ion channels (blue) and the currents (black) are indicated in the corresponding text boxes. Phase 0 (depolarization) is due to an increase in calcium (Ca^{++}) conductance. Phase 3 (repolarization) results from an increase in potassium (K^+) conductance. Phase 4 undergoes a spontaneous depolarization.

– **Phase 0.** Phase 0 corresponds to the upstroke of the action potential. When the membrane is depolarized to a threshold value of about $-40\ mV$, specific slow calcium channels open, causing a slow inward movement of Ca^{++} ions. For pacemaker cells, the slope of phase 0, which corresponds to the rate of depolarization, is much slower than that of nonpacemaker cells.

– **Phase 3.** Phase 3 corresponds to the repolarization. The depolarization in phase 0 causes the potassium channels to open, repolarizing the cell toward the equilibrium potential for K^+ ions. At the same time, the slow inward Ca^{++} channels that opened during phase 0 become inactivated, which also contributes to the repolarization process. When the membrane potential reaches $-65\ mV$, phase 3 ends.

– **Phase 4.** Phase 4 undergoes a spontaneous depolarization from $-65\ mV$ to a threshold voltage of about $-40\ mV$ owing in part to special pacemaker currents (also called "funny" currents, I_f). As the depolarization reaches the threshold voltage, the slow calcium chan-

nels begin to open, causing an increase in calcium conductance and phase 0 is initiated.

The intrinsic rate of the SA node is the highest at rest (60 to 100 beats per minute - *bpm*), followed by the AV node (40 to 50 *bpm*), then the ventricular muscle (20 to 40 *bpm*). The heart rate, however, can vary between low resting values of about 60 *bpm* to over 200 *bpm* during exercise. These rate variations are controlled by autonomic nerves acting directly on the rate of the SA node. Pacemaker activity is regulated by sympathetic and parasympathetic (*vagal*) nerves as well as circulating hormones. At rest, SA nodal activity is principally influenced by vagal activity which significantly reduces the intrinsic SA nodal firing rate to 60 to 80 *bpm*. Autonomic nerves increase SA nodal firing rate by both decreasing vagal tone and increasing sympathetic activity.

The firing rate of pacemaker cells can be altered (i.e., the rate will increase or decrease) by autonomic influences in the following manners (Figure 2.5):

1. Modification of the slope in phase 4.

2. Altering the threshold for triggering phase 0.

3. Altering the degree of hyperpolarization at the end of phase 3.

SA nodal activity		
	Sympathetic	Vagal
Slope of phase 4	*Increases*	*Decreases*
Threshold	*Decreases*	*Increases*
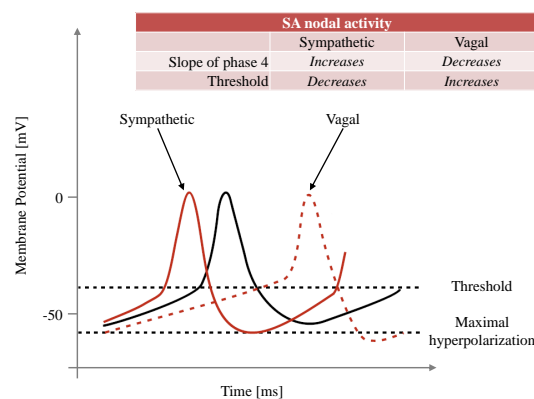
Figure 2.5: Effects of sympathetic and vagal stimulation on the SA nodal activity. Sympathetic stimulation increases the firing rate (the slope of phase 4 increases and the threshold for the action potential decreases). Vagal stimulation decreases the firing rate (the slope of phase 4 decreases and the threshold for the action potential increases). During vagal stimulation, the cell is hyperpolarized. *Figure adapted from [22].*

The electrical conduction system of the heart

Cardiac cells are connected together by low-resistance *gap junctions*. When one cell depolarizes, depolarizing currents can pass through the junctions and depolarize adjacent cells, resulting in a cell-to-cell propagation of the action potential. The action potentials generated by the SA node spread throughout the atria primarily through cell-to-cell conduction. Action potentials in the atrial muscle have a conduction velocity of about 0.5 *m/sec*, which is similar to that of the ventricular muscle.

Non-conducting tissue separates the atria from the ventricles. Normally, action potentials have only one pathway available to enter the ventricles, a specialized region of cells called the *AV node*. The AV node is located at the junction between the interatrial septum and the ventricular one, between the origin of the coronary sinus and the septal leaflet of the tricuspid valve
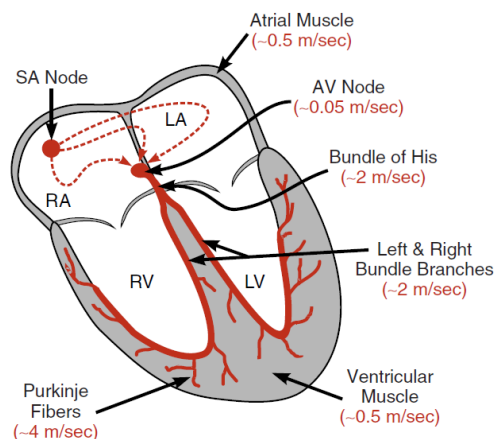
Figure 2.6: The electrical conduction system within the heart. Conduction velocities of different regions are noted in parenthesis. *Image from [22].*

(Figure 2.6. The AV node serves two important features. The first is to relay the wave of depolarization from the atria to the ventricles. A skeleton of connective tissue associated with the valves separates the atria from the ventricles, and the AV node is normally the only conductive link between the atria and the ventricles. The second function of the AV node is to delay the spread of excitation from the atria to the ventricles. The impulse conduction velocity is slowed down to about 0.05 m/sec (one-tenth the velocity found in atrial or ventricular myocytes). This conduction delay is important. First, it allows sufficient time for complete atrial depolarization, contraction, and emptying of atrial blood into the ventricles prior to ventricular depolarization and contraction. Second, the low conduction velocity limits the frequency of impulses travelling through the AV node and activating the ventricle. This is important during atrial arrhythmias (such as atrial fibrillation or flutter, see Chapters 3 and 5 respectively), in which the atria rate is excessively high. If these abnormal and rapid contractions propagate to the ventricles, it will lead to severe tachycardia and reduced cardiac output caused by inadequate time for ventricular filling.

Action potentials leaving the AV node enter the base of the ventricle at the *bundle of His* and then follow the left and right bundle branches along the interventricular septum (Figure 2.6). These specialized bundle branch fibers conduct the action potential at a high velocity (about 2 m/sec). These branches then divide into an extensive network of *Purkinje fibers* that conduct the impulse at high velocity through the ventricles (about 4 m/sec). These fibers are interconnected among the contractile cells of the ventricles and serve to quickly spread the wave of excitation throughout the ventricles. The rapidly conducting Purkinje fibers cause the ventricular cardiomyocytes to contract almost simultaneously.

2.2 Electrocardiography

2.2.1 Electrocardiogram: the standard 12-lead ECG

An electrocardiogram (ECG) is the most commonly used tool in clinical practice for recording the electrical activity of the heart. It is especially useful in diagnosing abnormal rhythms, variations in electrical conduction, and myocardial ischemia and infarction. The first human ECG was measured in 1887 by Augustus Walter. The essential contribution to ECG-recording technology still in use nowadays has been developed by Willem Einthoven in 1908 by using a string galvanometer which greatly increased the sensitivity [26].

The ECG records the electrical activity of the heart by attaching to the skin an array of electrodes at specific locations on the body surface. The convention requires that electrodes are placed on each arm and leg, and additional electrodes at defined locations on the chest. The difference between two electrodes voltage is defined as a *lead*. Typically, the ECG includes unipolar and bipolar leads. A unipolar lead has a single positive electrode and the voltage variation is measured in relation to a reference electrode commonly called the central terminal. A bipolar lead is composed of two electrodes (positive and negative) and reflects the voltage difference between these two electrodes. Typically, the ECG magnitude ranges from a few *mV* to 1 *V*.

In practice different standardized placement of recording electrodes exist. The most widely used in clinical practice is, however, the standard 12-lead ECG.

The standard 12-lead ECG is composed of three different leads: the bipolar limb leads, the augmented unipolar limb leads, and the unipolar precordial chest leads.

ECG limb leads

Bipolar limb leads   Figure 2.7 shows the three bipolar limb leads, denoted *I*, *II*, and *III*. Lead *I* has the positive electrode on the left arm and the negative electrode on the right arm. In this way, the potential difference across the chest between the two arms is measured. Lead *II* has the positive electrode on the left leg and the negative electrode on the right arm. Lead *III* has the positive electrode on the left leg and the negative electrode on the left arm. By noting V_{LA}, V_{RA} and V_{LL} as the voltage recorded on the left arm, the right arm and the left leg respectively, one can derive the following combinations:

$$I = V_{LA} - V_{RA}$$
$$II = V_{LL} - V_{RA}$$
$$III = V_{LL} - V_{LA}$$

The three limb leads roughly form an equilateral triangle with the heart at its center, known as the Einthoven's triangle. It is interesting to note that only two of these three leads are independent. Indeed, according to Kirchhoff's law, these lead voltages have the following relationship:

$$II = I + III$$

Augmented unipolar limb leads   The augmented unipolar limb leads are derived from the three limb leads. Each of these augmented leads has a single positive limb electrode which is referred against a combination of the two other limb electrodes. These augmented limb leads are
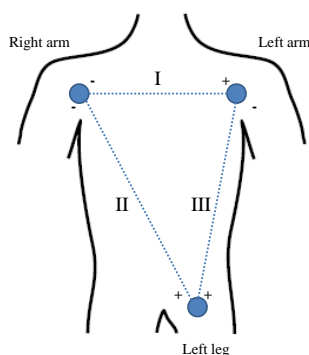
Figure 2.7: Standardized placement of the bipolar limb leads *I*, *II*, and *III* and the location of the positive and negative recording electrodes.

defined as the voltage difference between one limb electrode and the average of the remaining two limb electrodes:

$$aVR = V_{RA} - (V_{LA} + V_{LL})/2$$
$$aVL = V_{LA} - (V_{RA} + V_{LL})/2$$
$$aVF = V_{LL} - (V_{LA} + V_{RA})/2$$

Therefore, *aVL* has the positive electrode located on the left arm, *aVR* on the right arm and *aVF* on the left leg (the "F" stands for "foot").

These six limb leads are the base of the conventional axial reference system as shown in Figure 2.8. The positive electrode for lead *I* is defined as being at zero degrees relative to the heart, forming the horizontal axis. Similarly, relative to the heart, the positive electrode for lead *II* is located at $+60°$ and the positive electrode for lead *III* is at $+120°$. By definition, the lead *aVL* is at $-30°$ relative to the horizontal axis (e.g. lead *I*); *aVR* is at $-150°$, and *aVF* is at $+90°$.

These six limb leads record the electrical activity of the heart along a single plane, namely the frontal plane relative to the heart. The axial reference system is used to determine the direction of an electrical vector. For example, if a wave of depolarization is spreading from right to left along the horizontal axis, lead *I* shows the maximum positive amplitude. Likewise, if the depolarization direction is heading towards $+90°$, then *aVF* shows the maximum positive deflection.

ECG precordial chest leads

The six precordial chest leads are unipolar recordings obtained by electrodes placed on the surface of the chest over the heart to record electrical activity in a horizontal plane perpendicular to the frontal place (Figure 2.9, panel A). The six leads are labelled $V_1, \ldots, V_6$. V_1 is located to the right of the sternum over the fourth intercostal space. V_2 is located to the left of the sternum over the fourth intercostal space. V_3 is located midway between V_2 and V_4, while V_4 is located on the midclavicular line, over the fifth intercostal space. V_5 is located at the same level as V_4 but on the anterior axillary line. Finally, V_6 is located laterally on the midaxillary line at the same level as V_4 and V_5.
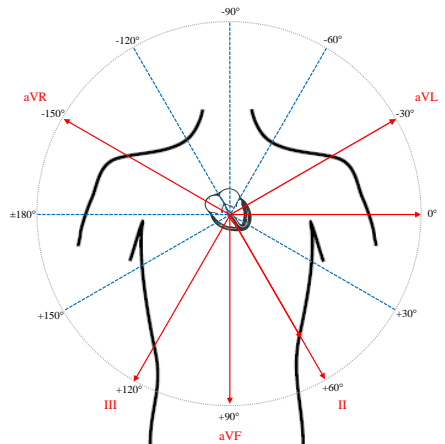
Figure 2.8: The axial reference system giving the location and direction for all six limb leads.
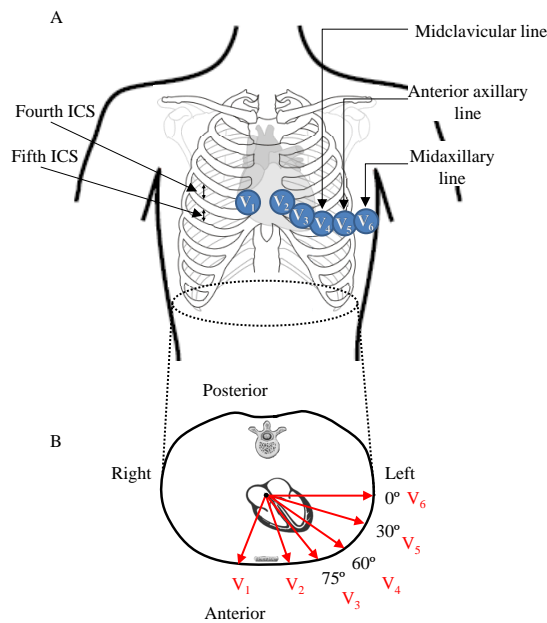
Figure 2.9: ECG chest leads positions and vectors. Panel A: electrodes position for the precordial chest leads within the horizontal place. Panel B: directions of the precordial leads on the horizontal plane. ICS: intercostal space.

With this electrode placement, leads V_1 and V_2 reflect the activity of the right ventricular free wall. Leads V_3 and V_4 reflect the activity of the left ventricular anterior wall, while lead V_5 and V_6 reflect the lateral wall of the left ventricle. Panel B on Figure 2.9 illustrates the lead vectors for the six unipolar precordial chest leads along the horizontal plane. As it can be observed, only the left anterior part of the heart (mostly representing the ventricles) is reflected with this electrodes positioning.

The normal electrocardiogram

We will now describe some important ECG characteristics along with the wave-naming convention and the relations between the different ECG complexes and the heart activation.

As cardiac cells depolarize and repolarize (Section 2.1.3), electrical currents spread throughout the body because the tissues surrounding the heart are able to conduct electrical currents generated by the heart. The repeating waves of the ECG represent the sequence of depolarization and repolarization of the atria and ventricles (Figure 2.10). The ECG does not measure absolute voltages, but voltage changes from a baseline (isoelectric) voltage. The duration of a wave is defined by the two time instants at which the wave either deviates significantly from the baseline or crosses it. A normal 12-lead ECG (in sinus rhythm) is shown in Figure 2.11.
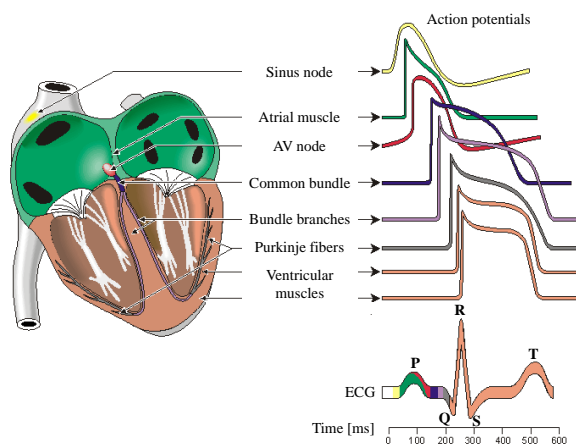
Figure 2.10: ECG wave definition of the cardiac cycle. *Image adapted from [27].*

By convention, the first wave of the ECG is the **P wave** which represents the wave of depolarization that spreads from the SA node across the atria. Once the impulse leaves the SA node, atrial activation spreads in several directions following a specific pattern determined by the complex anatomical and functional properties of the atrial musculature. The propagation is rapid and moves anteriorly toward the lower portion of the right atrium. It also spreads across the anterior and posterior surfaces of the atria toward the left atrium. At the same time, activation spreads through the interatrial septum, entering high on the right side and moving toward the interventricular septum. Although the right atrium is first activated, activation occurs simultaneously in both atria. The duration of the P wave is usually between 80 to 100 *msec*. Normal atrial activation projects positive as an upright P waves in leads *I*, *II*, *aVL*, and *aVF* and negative one in lead *aVR* (Figure 2.11). In the precordial leads, P wave patterns correspond to the direction of atrial activation wavefronts in the horizontal plane. The early activation in the P wave is over the right atrium and is oriented anteriorly and later, as activation moves toward the left atrium, it shifts posteriorly. Thus, the P wave in the right precordial leads (mostly V_1, and occasionally

V_2) is biphasic, with an initial positive deflection followed by a negative one. In the lateral leads, the P wave is upright and reflects right-to-left spread of the activation wavefronts. The amplitude in the limb leads is normally less than 0.25 mV and the terminal negative deflection in the right precordial leads is normally less than 0.1 mV in depth.

Atrial depolarization is followed by an atrial repolarization wave that is rarely visible on the surface ECG because of its very low amplitude (usually less than 100 μV) which also occurs during ventricular depolarization. The brief isoelectric period after the P wave represents the time in which the atrial cells are depolarized and the impulse is travelling within the AV node, where the conduction velocity is greatly reduced.

The **QRS complex** represents the ventricular repolarization and its duration is normally between 0.06 to 0.11 seconds. The period of time from the onset of the P wave to the beginning of the QRS complex, the **P-R interval**, normally ranges from 0.12 to 0.20 seconds. This interval starts with the onset of atrial depolarization and ends with the onset of ventricular depolarization. It is during this period that occur the activation of the AV node, the Bundle of His and the bundle branches.

The isoelectric period (**ST segment**) following the QRS is the period at which the entire ventricles are depolarized and roughly corresponds to the plateau phase of the ventricular action potential (Figure 2.10). The **T wave** represents ventricular repolarization (phase 3 of the action potential) and lasts longer than depolarization. During the **Q-T interval**, both ventricular depolarization and repolarization occur and roughly estimates the duration of the ventricular action potential. On some ECGs, a small wave follows the T wave, named the **U wave**, may be visible and is thought to represent the late repolarization of ventricular segments [27].
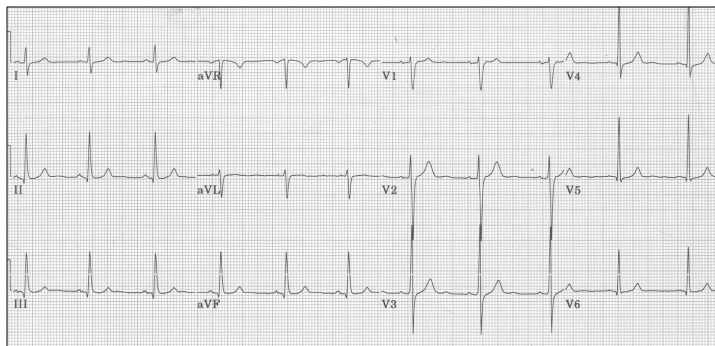
Figure 2.11: Normal electrocardiogram. The vertical lines of the grid represent time, with line spaced at 40 *msec* interval. Horizontal lines represent voltage amplitude, with lines spaced at 0.1 *mV* intervals. *Figure from* `http://ecg.utah.edu/lesson/3`

2.2.2   Intracardiac electrograms

The recording of cardiac potentials from electrodes directly in contact with the heart is called an *intracardiac electrogram (EGM)*. The electrode is an electrical conductor which is used to make contact with the heart and convert ionic currents (ions passing trough transmembrane channels) into electrical currents that can be detected by electronic devices. Intracardiac EGMs record therefore the local electrical activity of the heart, that is, the cardiac tissue surrounding the electrode in contact. All electrical potentials measured by any device are actually measuring difference in potentials between two electrodes. By convention, all clinical EGMs are differential recordings from one source connected to the anodal (positive) input of the recording amplifier and a second source connected to the cathodal (negative) input. *Unipolar EGMs* represent the potential difference between the electrode in contact with the heart (also called the exploring electrode) and a reference electrode distant from the heart (referred as an indifferent electrode and in theory placed at and infinite distance). In practice, the Wilson central terminal is used to approximate the indifferent electrode [26]. *Bipolar EGMs* represent the potential difference between two electrodes and are calculated as the algebraic difference between the two unipolar EGMs at the two sites (using the same reference).

The following characteristics of unipolar and bipolar EGMs are separately mentioned and summarized in Table 2.1 at page 26:
– Spatial resolution: ability to locate the discrete area of excited tissue generating the recorded potentials [28].
– Temporal resolution: ability to identify the local activation time which coincides best with the arrival of the depolarization wavefront.
– Directionality: ability to provide information regarding the direction and the origin of wavefronts.

Unipolar EGM

Spatial resolution   Unipolar EGMs record the activity occurring between the exploring electrode and the reference electrode and, therefore, contain substantial far-field signal generated by the depolarization of remote tissue. Typically, the far-field activity is of much higher amplitude than the local signal occurring at the exploring electrode, and therefore, distant activity can be difficult to separate from local activity.

Unipolar EGMs have also poor signal-to-noise ratio. Filtering may improve the signal quality by eliminating noise, but it may also alter the signal.

Unipolar EGMs reflect the potential generated by the tissue in direct contact with the exploring electrode as well as far field activity.

Temporal resolution   In unipolar recording, the local activation time is positioned at the point of maximum downslope (i.e., maximum negative dV/dt), which corresponds to the maximum sodium channel conductance [5]. It has been shown that using this fiducial point, the error in determining the local activation time is less than 1 millisecond [29].

Directionality   The morphology of unipolar recordings indicates the direction of wavefront propagation (and therefore its origin). Figure 2.12 illustrates the case when a wavefront originates outside of the tissue in contact with the electrode (top plot), reaches the electrode (middle plot), and then moves away from the electrode (bottom plot). When the depolarization wavefront is moving towards the recording electrode, a positive deflection is produced (Figure 2.12, top plot). When the depolarization wavefront is moving away from the recording electrode, a negative deflection is produced (Figure 2.12, bottom plot).
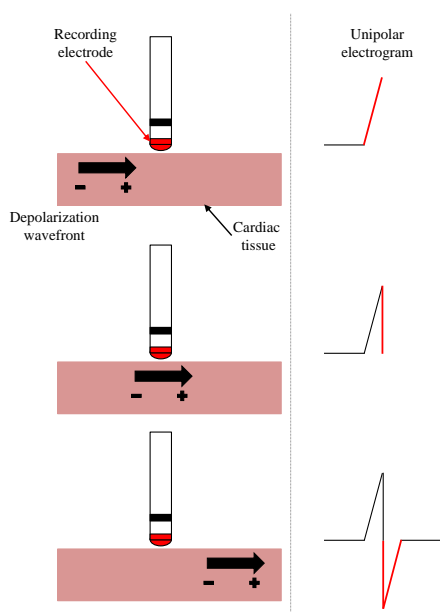
Figure 2.12: Hypothetical morphology of a unipolar recording. A unipolar EGM is recorded from the distal electrode (red). When the depolarization wavefront originates from outside of the tissue in contact with the recording electrode (top plot), a positive deflection is produced. When the depolarization wavefront moves away, a negative deflection is produced. *Figure adapted from [28].*

Bipolar EGM

Spatial resolution   Bipolar EGMs, by virtue of subtraction of closely spaced electrodes, eliminate noise and far-field activity, hence improving the signal-to-noise ratio. As a byproduct, high frequency components are more accurately seen. Indeed, when the distance from a signal or noise source to the electrodes is larger than the distance between the two electrodes, the noise is recorded quasi-identically by the two electrodes, and efficiently eliminated by subtraction. Moreover, as the distance from the recording site increases, amplitude and frequency of the recorded signal decrease depending on the inter-electrode distance.

Bipolar EGMs reflect the local electrical activity produced by the area of tissue in contact with and between the two electrodes. As the distance between the two electrodes of bipolar recording decreases, the spatial resolution increases.

Temporal resolution   For bipolar EGMs, the detection of local activation times is more problematic due to the generation of the bipolar recordings. Multiple methods were proposed [28]. Most commonly, the absolute maximum electrogram amplitude is chosen, which correlates with the local activation time that corresponds to the maximal negative downslope (dV/dt) of the unipolar recording as shown in Figure 2.13. However, in the case of complex fractionated EGMs, this fiducial point cannot be reliably used for determining the local activation time.

Directionality   The orientation of the bipolar recording axis with respect to the direction of propagation of the activation wavefront has a direct influence on the morphology and amplitude of bipolar EGMs [29]. When the depolarization wavefront is propagating in the direction exactly perpendicular to the bipolar recording axis, no difference in potential between the recording
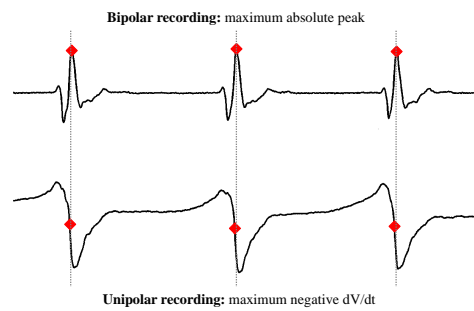
Figure 2.13: Local activation time in unipolar and bipolar EGMs. In unipolar EGMs, the local activation time is located at the maximum negative downslope (*dV/dt*). In bipolar EGMs, the local activation time is most commonly estimated by the maximum absolute peak. In this particular example, only one unipolar derivation is shown.

electrodes is produced, and hence no resulting signal is recorded. As opposed to unipolar EGMs, the direction of wavefront propagation cannot be reliably inferred from the morphology of the bipolar signal, although a change in morphology can be a useful finding [29].

		Unipolar		Bipolar
Spatial resolution	+	Good spatial resolution	+	Reflect the local electrical activity
	–	Contain far-field activity	+	Far-field activity is removed
	–	Poor signal-to-noise ratio	+	High frequency components more accurately seen
			–	Loss of spatial resolution depending on electrode distance
Temporal resolution	+	Precise measure for estimating the local activation time	+	Good for visual or manual assessment of local activation time
	–	Visually difficult to assess the local activation time	–	Less precise for estimating the local activation time
Directionality	+/–	Morphology indicates the direction of wavefront propagation	+/–	Morphology dependent on wavefront direction

Table 2.1: Summary of unipolar and bipolar EGMs properties.

Atrial Fibrillation

<div style="text-align: right; font-size: 4em;">3</div>

Atrial fibrillation (AF) is the most commonly encountered cardiac arrhythmia in clinical practice. Hospitalizations related to AF problems account for one third of all admissions for cardiac arrhythmia. AF alters the mechanical function of the left atrium leading to blood stasis and thrombus formation causing an increasing number of complications and deaths. The available data from epidemiological studies suggest that, independently of other known predictors of mortality, AF is the cause for doubling death rates [30]. It is estimated that 20% of all strokes are caused by AF and that AF-related events are more severe than strokes of other origin [4]. AF is complicated by hemodynamic impairment (loss of atrial contractile function, irregular and fast ventricular rate). These conditions may lead to a decrease in quality of life for affected patients. In the context of the *Global Burden of Disease 2010 Study*, using data from 184 publications it was concluded that worldwide in 2010, 33.5 millions of individuals suffered from AF, with 5 millions new cases occurring each year and that over the last two decades both the prevalence and incidence of AF have increased meaningfully [1]. As life expectancy increases, AF prevalence is estimated to double in the next fifty years.

In this chapter, we will first cover the clinical definition of AF (Section 3.1) and important clinical aspects related to AF will be introduced (Section 3.2). In Section 3.3, the different stages of the disease will be covered. Section 3.4 presents the most common symptoms of AF. Then, Section 3.5 presents the pathophysiological mechanisms by which cardiac conditions favor AF. Finally, the management of AF will be briefly presented in Section 3.6.

3.1 Definition

AF is a supraventricular arrhythmia characterized by rapid and irregular atrial activation leading to a consequent deterioration of atrial mechanical functions. On the ECG, AF is distinguishable by the replacement of the P wave with rapid oscillations called atrial fibrillatory waves (f-waves). A 12-lead ECG with AF is shown in Figure 3.1. Generally, atrial fibrillatory activity is best seen in lead V_1. The rate of the f-waves is generally between 300 and 600 *bpm*. The f-waves vary in amplitude, morphology and period, which may be reflective of various simultaneous atrial activations present at different locations and time within the atria.
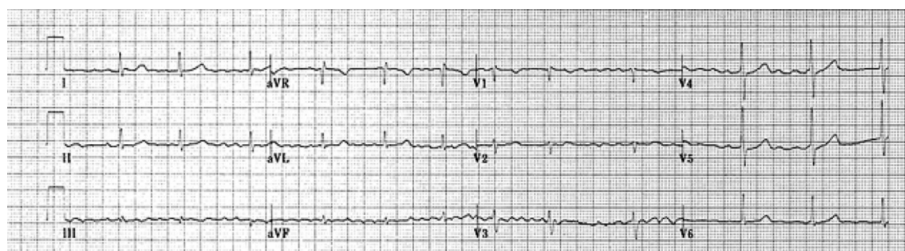
Figure 3.1: 12-lead ECG tracing of AF. Note the replacement of P waves by f-waves and the irregular response of the ventricles. *Figure from [31].*

3.2 Clinical considerations

3.2.1 Epidemiology

Worldwide epidemiological data on AF suggest that this disease can be considered as an emergent global epidemic [1]. It is important to mention that AF may be undiagnosed, and that many patients with AF will never present to hospital [32]. The prevalence of AF increases with age (from < 0.5% at $40 - 50$ years, to $5 - 15\%$ at 80 years) and AF incidence rates are higher in males compared to females [4]. Lifetime risks for developing AF are $\sim 25\%$ in subjects older than 40 years, independently of gender [2].

AF is associated with different cardiovascular events the prevention of which is the main goal of therapeutic strategies. Outcomes related to AF are summarized in Table 3.1.

Outcome parameters	Relative changes in AF patients
Death	Death rate doubled.
Stroke	Stroke risk increased; AF is associated with more severe strokes.
Hospitalizations	Hospitalizations related to AF account for $\sim$ 30% of all admission for cardiac arrhythmias.
Quality of life	Wide variation, from no effect to major reduction.
Left ventricular function	May be impaired.

Table 3.1: Clinical outcomes associated with AF. *Table from [4].*

3.2.2 Conditions associated with atrial fibrillation

AF is related to numerous conditions. Most of them contribute to a progressive process in the development of the disease by favoring either the occurrence of AF "triggers" (i.e. responsible for the initiation) and/or the formation of "substrate" for AF (i.e. responsible for its perpetuation). Several conditions are listed below:

– **Age:** increases the risk of developing AF.

- **Hypertension:** found in most of AF patients. It is an independent predictor of AF and contributes to its progression.
- **Thyroid dysfunction:** in particular hyperthyroidism is associated with AF and may be the only cause for its development.
- **Obesity:** found in more than a quarter of AF patients [4].
- **Sleep apnea:** may be a pathophysiological factor for AF (especially in association with hypertension or diabetes).

Other conditions are also coronary artery disease, valvular heart disease, obstructive lung disease, symptomatic heart failure, cardiomyopathies, diabetes and chronic renal diseases [4].

3.3 Types of atrial fibrillation

Various classifications of AF have been used, making the comparison between studies or therapy effectiveness difficult. In clinical practice, a classification is useful for the management of AF patients. Typically, it is important to characterize the arrhythmia at a given moment based on the clinical presentation and duration of the arrhythmia. In this manuscript, the recent classification published by *the Task Force for the Management of Atrial Fibrillation of the European Society of Cardiology* [4] has been chosen. The types of AF are as follows (also illustrated in Figure 3.2):

1. **First diagnosed AF:** a patient presents an AF for the first time, independently of the severity of AF-related symptoms.

2. **Paroxysmal AF:** the arrhythmia self-terminates, usually within 48 hours.

3. **Persistent AF:** the arrhythmia becomes sustained for a duration longer than 7 days or requires termination by cardioversion (see the AF management Section 3.6).

4. **Long-standing persistent AF:** the arrhythmia becomes sustained for a duration greater than one year.

5. **Permanent AF:** when the presence of the arrhythmia is accepted by the physician and the patient. In this category, the cardioversion has failed (see the AF management Section 3.6). If a rhythm control strategy is chosen, the arrhythmia is reclassified in long-standing persistent.

3.4 Symptoms

Patients can experience periods of both symptomatic and asymptomatic AF. Most commonly, AF can be recognized by a sensation of palpitations. In patients in whom the arrhythmia has become permanent, palpitations may decrease with time. Other symptoms of AF are chest pain, dyspnea (e.g. a respiratory distress), or dizziness.

3.5 Pathophysiological mechanisms of atrial fibrillation

It is important to separate the underlying AF mechanisms into two main components: arrhythmia triggers and arrhythmia perpetrators. The onset and maintenance of the arrhythmia require both triggers for its initiation and substrates for its maintenance. These mechanisms are, however, not mutually exclusive and are likely to be present simultaneously at various times [4].
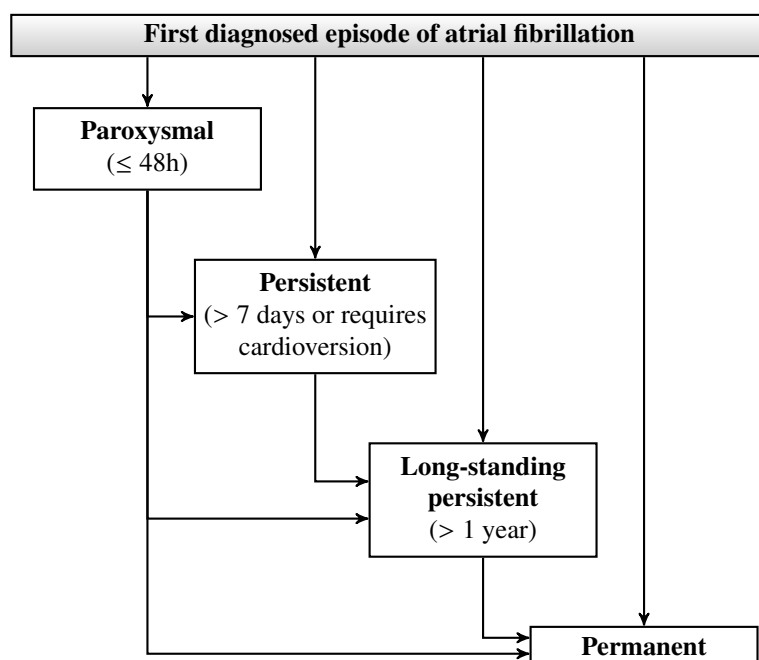
Figure 3.2: Types of atrial fibrillation. *Figure adapted from [4].*

3.5.1   Initiation

Focal mechanisms

Many studies have suggested that in most cases AF begins with a rapid focal activity in the pulmonary veins (PVs), and less commonly in the superior vena cava, the coronary sinus (CS), or the left atrial posterior wall [5, 31]. Figure 3.3 shows a posterior view of the atria, and the corresponding locations of the common triggers. The identification of these triggers is of major clinical importance because any treatment that may eliminate them may be successful in terminating AF. Haisseguerre et al. have shown in 1998 that the ablation of focal triggers around the PVs could terminate paroxysmal AF [33]. It is now well established and accepted by the medical community that the PVs are a crucial source of triggers in the initiation of AF. The underlying mechanism responsible of focal firing remains unclear yet.

3.5.2   Maintenance

Once initiated, an AF episode may be brief and may end spontaneously. Maintenance of AF is ensured by various factors. On one hand, focal triggers which initiated AF may persist, acting as drivers for the maintenance of AF. On the other hand, AF can persist even in the absence of triggers. In this case, AF maintenance results from additional factors including various amount of electrical and structural remodeling characterized by shortening of atrial refractoriness and atrial dilation. These factors are presumably responsible for favoring the development of a common pathway for AF throughout the atria [5]. This mechanism is known as the "multiple wavelet hypothesis".

Posterior view
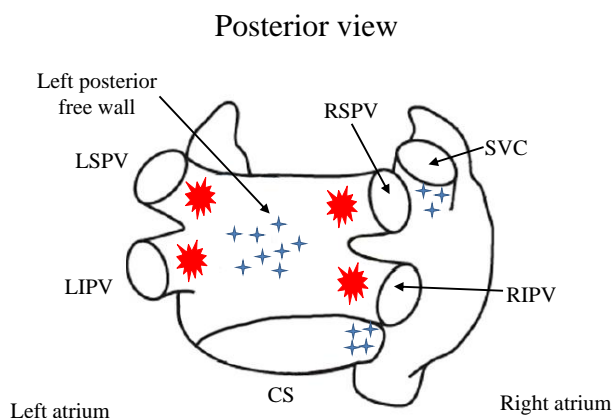
Figure 3.3: Common locations of focal triggers responsible for initiating AF. The four pulmonary veins (PVs, in red) are the most common source of foci. The four PVs are: left superior PV (LSPV), left inferior PV (LIPV), right superior PV (RSPV), right inferior PV (RIPV). Other sites of AF sources (blue) are the coronary sinus (CS), the superior vena cava (SVC), and the left posterior free wall. *Figure adapted from [34].*

Multiple wavelet hypothesis

For many years, the multiple wavelet hypothesis for AF maintenance was widely accepted as the dominant AF mechanism. The hypothesis was advanced by Moe et al., who proposed a model in which AF is sustained by multiple randomly wandering wavelets colliding with each other [35]. These wavelets occur simultaneously throughout the left and right atria and continuously undergo either self-extinction or self-perpetuation (e.g. wavebreaks) into "daughter" wavelets. Figure 3.4 shows a schematic drawing of the large and small reentrant wavelets.

Posterior view
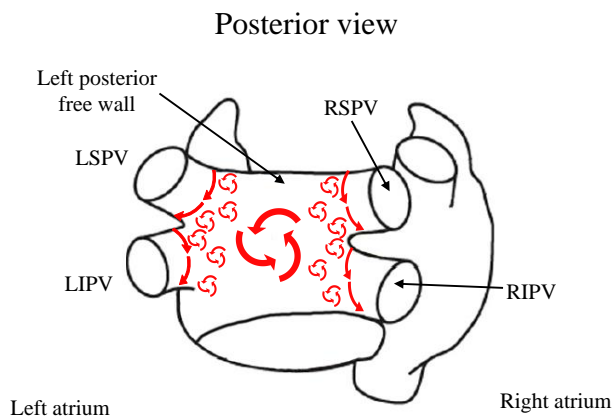
Figure 3.4: Schematic drawing of the large and small reentrant multiple wavelets favouring AF initiation and maintenance. *Figure adapted from [34].*

Typically, these circuits have a variable and short cycle length. AF requires the presence of at least four to six independent wavelets to perpetuate [5]. In this model, the number of wavelets depends at any time on the excitable mass, atrial conduction velocity and refractory period in

different parts of the atria. The presence of anatomical obstacles (such as the PVs) also favours the creation of daughter wavelets. The number of wavelets increases with a larger atrial mass, shorter refractory period and delayed conduction. It is more likely that AF is sustained when the number of wandering wavelets increases. The multiple wavelet hypothesis has been subsequently confirmed by experimental work [36, 37].

Mother circuit

Some authors have shown in isolated sheep hearts that, in the presence of an appropriate heterogeneous AF substrate, a focal trigger usually localized in one PV can result in a single meandering functional reentrant AF driver (*rotor*) [38]. This model is illustrated in Figure 3.5 which shows the presence of a single source of stable reentrant activity, i.e., the mother circuit, with high frequency wavefronts emanating from a focal trigger located within the left superior PV (LSPV). When conditions of heterogeneity are adequate, the wavefronts break and initiate two counter-clocking vortices. Alternatively, only one of the vortices remains (drawn in red plain line), and is responsible for maintaining AF.

Posterior view

Figure 3.5: Schematic drawing of the mother circuit mechanism. High frequency wavefronts emanate from a focal trigger located within the LSPV. When conditions of heterogeneity are adequate, the wavefronts break and initiate two counter-clockwise vortices. Alternatively, only one of the vortices remains (drawn in red plain line) and is responsible for maintaining AF. *Figure adapted from [34, 38].*

The waves emerging from the rotor may undergo spatial fragmentation upon anatomical obstacles (such as PVs or scars), leading to the formation of multiple wavelets spreading out in multiple directions at varying conduction velocity (fibrillatory conduction). The dominant rotors responsible for driving AF generally originate and anchor within the left atrium (LA), while the right atrium (RA) is being activated passively [39].

3.5.3   Atrial remodeling and atrial fibrillation

The atria may display some electrical and structural remodeling over time that may, in turn, favor the maintenance of AF. More specifically, modifications primarily affecting excitability and action potentials characteristics are termed *electrical remodeling*, while the changes in atrial volume and tissue structure are referred to as *structural remodeling*. The hemodynamic impairment

such as loss of atrial contractile function is referred as *contractile remodeling*. Experimental studies have shown that electrical and structural remodeling play a major role in the initiation and maintenance of AF. These modifications in atrial structure and conduction have provided a possible explanation for the progressive and self-perpetuating nature of AF ("AF begets AF" [12]). Figure 3.6 illustrates the different types of remodeling and their interactions [13]. Each of these remodelings affects the atrial function and structure at different stages of the disease. The electrical remodeling develops within the first days of AF and results from high frequency atrial activations, decreasing rapidly the atrial ERP. It has been observed in clinical practice that the time course for persistent AF development is slower than that of the electrical remodeling. Indeed, the structural remodeling takes weeks to months after AF onset. This observation suggests that in the development of sustained AF (such as long-standing or permanent AF), the structural remodeling is important.
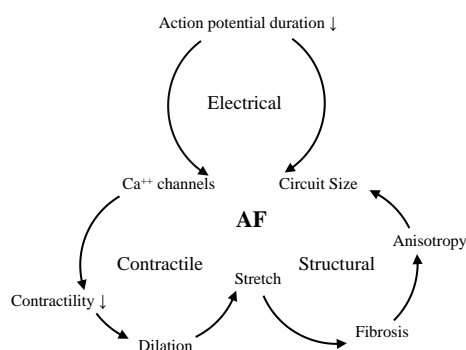
Figure 3.6: Three proposed positive feedback-loops associated with remodelings: electrical, contractile and structural. The primary cause for electrical and contractile remodeling is considered to be the down regulation of Ca^{++} channels function. The structural remodeling of the atria is due to its dilation. Atrial regions with advanced fibrosis can be the harbinger for local sources of AF. The resulting electro-anatomical substrate of AF consists of dilated atria and increased tissue heterogeneity. *Figure adapted from [13].*

3.6 Management

The clinical management of patients with AF is aimed at:
– **Preventing thromboembolism.** For each patient, the evaluation of stroke risk determines the need for anticoagulation. Numerous studies have shown that in the presence of risk factors, patients with paroxysmal AF appear to have an equivalent stroke risk to those with persistent or permanent AF [4].

– **Rate control.** AF is characterized by a rapid heart rate that may decrease the cardiac output. During AF, rate control is important to prevent haemodynamic distress in AF patients. The main goal of a rate control therapy is to target a ventricular rate between 60 to 80 *bpm* at rest and 90 to 115 *bpm* during exercise. The criteria for rate control vary with patient age. However, an adequate ventricular rate control therapy should target a decrease in

symptoms and improve haemodynamics.

– **Rhythm control.** Rhythm control is aimed at restoring and maintaining the sinus rhythm. The restoration of the heart normal rhythm is called a *cardioversion* .

These three objectives are not mutually exclusive; they can be pursued in parallel. For each patient, the clinician shall establish an overall strategy considering several factors such as the patient's age, the type and duration of AF, the severity of symptoms, the associated cardiovascular disease or medical conditions, short or long-term treatment goals, and therapeutic options (e.g. pharmacological or non pharmacological approach).

3.6.1   Pharmacological therapies

Rate control

During AF, the conduction characteristics and refractoriness of the AV node as well as the sympathetic and parasympatetic tones are the main determinants of the ventricular rate. Moreover, the functional refractory period of the AV node is inversely correlated with the ventricular rate [31]. Drugs prolonging the AV node refractory period are generally effective for rate control. The most commonly prescribed drugs are beta-blockers, non-dihydropyridine calcium channel antagonists, digoxin, digitalis, and amiodarone. When a pharmacological approach fails to reduce the heart rate, a non pharmacological strategy should be considered (such as an AV node ablation after pacemaker implantation [4]).

Rhythm control

Pharmacological cardioversion of AF may be initiated by the administration of antiarrhythmic drugs such as flecainide, propafenone, sotalol, amiodarone or ibutilide [4]. When the pharmacological cardioversion fails to terminate AF, a non pharmacological approach may be considered (such as a direct-current cardioversion, Section 3.6.2, or a catheter ablation ablation, Section 3.6.2 and Chapter 4)

Rhythm versus rate control

For patients in whom AF related symptoms are considered tolerable (typically the elderly), a rate control strategy may be appropriate. Two major prospective studies (Atrial Fibrillation Follow-up Investigation of Rhythm Management - AFFIRM - and Rate Control vs Electrical cardioversion - RACE) that compared rate control and rhythm control therapies, have shown that, regardless of the selected strategy, embolic events occur with equal frequency after interruption of anticoagulation [40, 41].

The clinical management of symptomatic AF may differ from one patient to another. For symptomatic patients with AF lasting several weeks, the initial therapy should be rate control and anticoagulation. When rate control does not provide sufficient symptom relief, restoration of sinus rhythm may become a long-term goal, that may be achieved with non pharmacological approaches.

3.6.2   Non pharmacological therapies

Direct-current cardioversion of atrial fibrillation

Direct-current cardioversion (DCC) is a non pharmacological method for restoring sinus rhythm in AF patients and is generally preferred to a pharmacological approach because of

greater efficacy. As cardioversion is associated with an increased risk of thromboembolism, anticoagulation must be initiated several weeks before.

DCC consists in delivering an electrical shock in synchronization with the ventricular activation. Indeed, it is important to ensure that the electrical shock does not occur during the vulnerable phase of the cardiac cycle (i.e., the T-wave) [42]. Most commonly, the current is delivered through special external chest electrodes (or paddles) which are located on either side of the heart or in an antero-posterior configuration. In both configurations, the electrical current delivered between the patches spreads through the heart. Traditionally, the energy output is successively increased in increments of 100 J to a maximum of 400 J [31].

Because the shock is uncomfortable, DCC is performed under general anaesthesia. Recurrences after cardioversion can be divided into three phases: a) immediate (seconds to minutes after DCC); b) early (five days after DCC); c) late. Importantly, factors that predispose to AF recurrence are age, AF duration, number of previous DCCs, and a dilated left atrium.

Surgical ablation

In the 1980s, several studies have identified important factors involved in the termination of AF surgically. The main hypothesis for the surgical approach is that reentry underlies the development and maintenance of AF and, that atrial incisions at critical locations would produce barriers to the conduction of AF [43]. Following this assumption, the surgical procedure developed was called *maze* [44]. Since its introduction, the procedure has gone through different iterations. Results appeared quite effective (over fifteen years of follow-up success rates from $75 - 95\%$ have been reported) but decreased in the most recent studies using long-term ECG recordings [4]. The maze procedure is complex mainly because of the need for cardiopulmonary bypass and requires extensive lesions precluding the atrial function.

Catheter ablation

Radiofrequency catheter ablations techniques were developed for terminating AF in the 90$'s$ following the maze procedure by performing linear lesions from the atrial endocardium, i.e., inside the atria [45]. Currently, AF catheter ablation is the cornerstone of non pharmacological AF therapy. Radiofrequency catheter ablation of AF is covered in more details in Chapter 4.

Catheter Ablation of Atrial Fibrillation

4

Since the late $90's$, treatment of AF by catheter ablation has evolved from an experimental procedure to one that is nowadays widely performed in a large number of medical centres worldwide. It has become the cornerstone of non pharmacological AF therapy.

As shown in the previous chapter, the development of AF requires both a trigger for its initiation and a substrate for its perpetuation (Section 3.5 page 29). Catheter ablation is aimed at eliminating the trigger(s) and/or altering the arrhythmogenic substrate. Importantly, various ablation strategies have been deployed in order to terminate AF in different patient populations. However, the optimal ablative strategy remains to be established.

In this chapter, we will first cover the technologies and tools necessary for performing AF catheter ablation (Section 4.1). Then, in Section 4.2, the ablation strategy for eliminating AF triggers is explained whereas the last two Sections (4.3 and 4.4) focus on different approaches for modifying the substrate maintaining AF.

4.1 Technologies and tools

4.1.1 Left atrial access

Catheter ablation is considered as a minimally invasive procedure as no major incision is necessary. Catheters are inserted within the heart using blood vessels, typically the left and/or right femoral veins as illustrated in Figure 4.1. The catheters are then advanced into the right atrium via the inferior vena cava. Drivers of AF are thought to be mainly localized within the left atrium (Section 3.5), which is separated from the right atrium by an *interatrial septum*. In order to access the left atrium, a transseptal puncture must be performed. Figure 4.1 illustrates the situation when a mapping and ablation catheters have been introduced within the left atrium.

4.1.2 Energy sources

The most dominant energy source used for catheter ablation is by far the radiofrequency energy (RF) which is electrically conducted. A unipolar alternating current (typically 500 kHz) is delivered from the ablation catheter tip to a dispersive indifferent electrode (or patch) applied on the patient's skin. RF current heats up the cardiac tissue to produce variable amount of myocardial oedema an necrosis. The assumption of successful AF ablation is the creation of lesions that
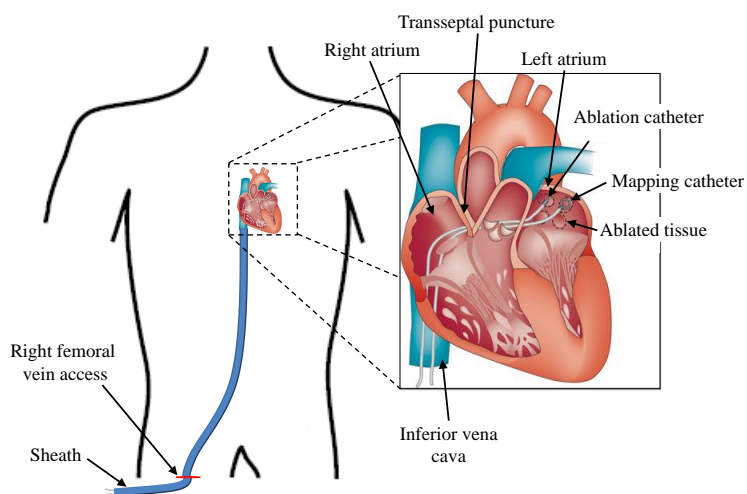
Figure 4.1: Catheters are inserted within the heart using the right femoral vein and enter the right atrium through the inferior vena cava. A transseptal puncture is performed in order to introduce the catheter within the left atrium. *Figure adapted from [46].*

block the propagation of AF wavefronts.

When the contact between the electrode and the tissue is constant, only a fraction of the power is effectively applied to the cardiac tissue. The rest is dissipated in the blood pool because the electrode has better conductance with blood than tissue. Also, the blood is a better conductor and has significantly lower impedance than the tissue. Therefore, much more power will be delivered to the blood. When the surface is excessively heated, coagulum or steam popping can form which may tear apart the tissue. In order to increase the efficiency of RF delivery to the tissue, a cooling system of the ablation catheter has been developed. There are two types of irrigated catheters:

1. Internal closed-loop: a saline fluid continuously circulates within the electrode, internally cooling the electrode.

2. External open-loop: the electrode cooling is performed by flushing a saline fluid through multiple irrigation holes located around the distal electrode. This method provides both internal and external cooling.

With an irrigated ablation catheter, higher amounts of RF energy for a longer duration can be delivered creating larger and deeper myocardial lesions. Open irrigation appears to be more effective than closed-loop irrigation.

4.1.3   Electroanatomical mapping system

Mapping and ablation require accurate navigation within the atria. The CARTO® 3 System [1] is aimed both at reconstructing a 3D shell of any cardiac structures, including the atria, and at visualizing on a real-time basis all catheters simultaneously. Also, it allows to tag specific sites of interest for future diagnostic manoeuvres and ablations.

---

1. http://www.biosensewebster.com/carto3.php

4.2 Pulmonary veins isolation

In Section 3.5.1, we have seen that paroxysmal AF is commonly initiated by a rapid focal activity coming from the PVs. Haissaguerre et al. was the first to introduce an ablation procedure in which the PVs were electrically isolated [33]. This technique was segmental and involved the sequential identification and ablation of the earliest sites of activation of each PV. To achieve this goal, a circumferential mapping catheter (similar to the one shown in Figure 4.1) was positioned within the PV ostium. Another ablation strategy was subsequently developed by Pappone et al., in which each PV was totally encircled with RF lesions [47, 48].

4.2.1 Endpoints of pulmonary veins isolation

The main endpoint of the PV isolation (PVI) procedure is the complete electrical isolation/disconnection of all four PVs.

4.2.2 Outcome of pulmonary veins isolation

Successful PVI does not ensure permanent disconnection. In patients with paroxysmal AF, it has been reported that in the first 3 months post-PVI, 70% of the patients were AF free [5]. In patients with non-paroxysmal AF, however, the success dropped to 30% [5]. Once AF becomes sustained, it is more likely that PVI alone is not sufficient for terminating the arrhythmia, and that some additional ablation strategy should be considered. The lower success of PVI ablation in non-paroxysmal AF suggests that once AF has become sustained, the PVs play a less critical role in maintaining AF and that some level of structural remodelling enables the atria to perpetuate the AF independently of the triggers, i.e., the PVs.

4.3 Linear atrial ablation

In patients with non-paroxysmal AF, when PVI alone is performed, the recurrence rate is higher than in patients with paroxysmal AF, suggesting that a residual substrate is responsible for maintaining AF. Alternative ablation strategies have been attempted in non-paroxysmal AF. One of these strategies is to perform linear lesions in the atria similar to those produced during the maze procedure (Section 3.6.2).
The main linear ablations involve the LA roof line, LA mitral isthmus line, and/or RA cavotricuspid line and are illustrated in Figure 4.2.

Left atrial roof line

The LA roof line (shown in green in Figure 4.2) connects the postero-superior lesions (red dashed lines) of the left and right upper PVs. Although the exact mechanism by which the LA roof is involved in AF maintenance remains unclear, clinical evidences have established a clear implication of this LA region in the AF substrate [5].

Left atrial mitral isthmus line

The LA mitral isthmus line (shown in blue in Figure 4.2) is made of a complete line of conduction block that transects the lateral part of the LA starting from the infero-lateral antrum of the LIPV to the mitral isthmus. The LA mitral isthmus ablation line (in adjunction to other AF ablation strategies) eliminates perimitral reentry and is associated with an increased organization in AF after its completion [6].

A   Anterior view   B   Posterior view
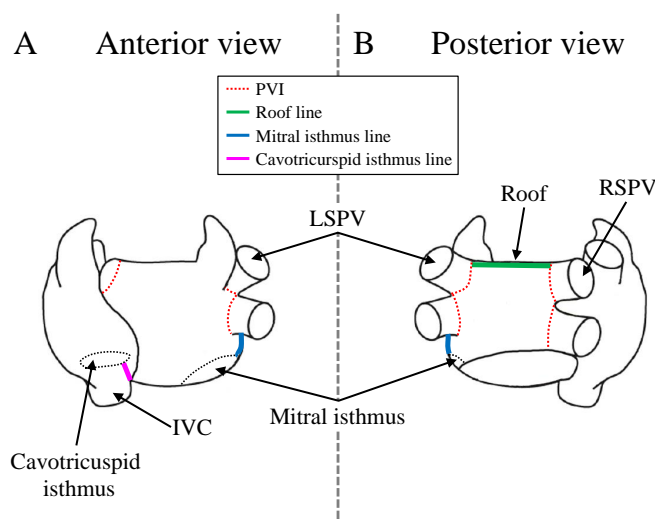
Figure 4.2: Linear atrial ablation may involve the LA roof line (green), LA mitral isthmus line (blue), and/or the RA cavotricuspid line (pink). Panel A shows an anterior view of the atria and panel B a posterior view. IVC: inferior vena cava.

Right atrial cavotricuspid isthmus line

The RA cavotricuspid isthmus line (shown in pink in Figure 4.2) connects the inferior vena cava and the tricuspid annulus.

4.3.1   Endpoints of linear atrial ablation

The electrophysiological endpoint of linear ablation is the effectiveness of bidirectional conduction block across each line. To prove the effectiveness of linear ablation, differential pacing is performed on either sides of the lines [5].

4.3.2   Outcome of linear atrial ablation

Many studies have shown the benefit of linear atrial ablation [6, 49, 50]. Prospective clinical studies have shown that in patients with non-paroxysmal AF, linear ablation of the mitral isthmus or linear ablation of the LA roof were associated with an improved clinical outcome compared to PVI alone [49]. In patients with long-standing persistent AF, Haissaguerre et al. have shown that linear lesions following PVI produced a significant prolongation of AF cycle length, which is indicative of the role played by these structures in maintaining AF and its substrate [6, 50].

Importantly, other studies have shown that incomplete block across linear ablation lines were the most predictive factor for AF recurrence [51, 52]. It is therefore crucial to assess the effectiveness of bidirectional conduction block across each ablation line.

4.4 Complex fractionated atrial electrograms ablation

Nademanee et al. proposed to target sites with high continuous frequency activities described as complex fractionated atrial electrograms (CFAEs) defined as [53]:

1. Atrial EGMs that are fractionated and composed of ≥ two deflections, and/or have a perturbation of the baseline with continuous deflections of prolonged activation complex over a 10 *sec* recording epoch.

2. Atrial EGMs with a very short cycle length (≤ 120 *ms*) averaged over a 10 *sec* recording epoch.

Typically, CFAEs are of low-voltage with multiple potential signals between 0.06 and 0.25 *mV* [34]. During the ablation procedure, their visual identification by the operator can be challenging and is highly subjective.

CFAEs are believed to be involved in AF maintenance as fractionated and continuous activity may be indicative of the presence of wave collision, and/or pivot points where the wavelets turn around [5]. CFAEs areas may locally represent a reentry circuit, or a collision of different wavelets. Also, a short cycle length may be indicative of the presence of AF drivers or rotors [38].

In their seminal study, Nademanee et al. suggested that any atrial site displaying CFAEs activity can be targeted for ablation and that once CFAEs are eliminated AF can no longer be maintained [53]. While PVI aims at removing the AF triggers, CFAEs ablation aims at removing the AF substrate.

4.4.1 Endpoints of complex fractionated atrial electrograms ablation

The primary endpoints of CFAEs ablation are either complete elimination of areas with CFAEs, and/or AF termination.

4.4.2 Outcome of complex fractionated atrial electrograms ablation

In long-standing persistent AF, CFAEs ablation throughout the atria can restore sinus rhythm [53]. Recently, the ablation of CFAEs with given characteristics was of benefit in terms of organization over PVI [54], including RA CFAEs when the RA AF cycle length became shorter than that of the LA [49]. CFAEs ablation, however, results in extensive atrial lesions that may preclude any recovery of atrial contractile function despite sinus rhythm restoration.

Part II

Patients Characteristics and Data Acquisition

Patients Characteristics and Data Acquisition

5

The first step in this thesis was to elaborate a detailed medical study design. This chapter aims at presenting the various settings used during each ablation procedure. First, the characteristics of the patient population (Section 5.1) are presented. In the second part, one can find all information regarding the various tools used for the acquisition of ECG and intracardiac signals (i.e., also known as the electrophysiological study, Section 5.2). This section also covers the acquisition and ablation protocols which were meticulously followed during each procedure. Finally, the different databases, which were constructed off-line, are described in Section 5.3.

5.1 Patient population

Overall, 33 consecutive patients of a mean age of 61 ± 7 years made the study population. They suffered on average from AF for 6 ± 4 years that was sustained for 19 ± 11 months before ablation, and resistant to pharmacological and electrical cardioversion. Among the population, the left atrium was extremely dilated as the average volume was 173.81 ± 43.59 *ml* for a normal value of approximately 70 *ml*. Table 5.1 at page 51 reports the other clinical characteristics of the study population. Medical definitions of the clinical characteristics are provided in Section A.1 of Appendix A. Numerical data are expressed as mean ± standard deviation.

5.2 Electrophysiological study

All patients had effective oral anticoagulation for > 1 month before the intervention. All antiarrhythmic drugs, with the exception of amiodarone and beta-blockers, were discontinued for ≥ five half-lives before the procedure. The procedure was performed under general anesthesia.

5.2.1 Surface ECG

In order to improve the recording of the antero-posterior activity of the atria [55], chest lead V_6 was placed in the back of each patient, and denoted V_{6b} as illustrated in Figure 5.1. More specifically, the dorsal site for each patient was placed facing the left atrial silhouette using X-Ray.

In the testing phase, an extra unipolar chest lead derivation was used. The signal shown in panel A of Figure 5.2 was of too poor quality for further analysis of its frequency content due
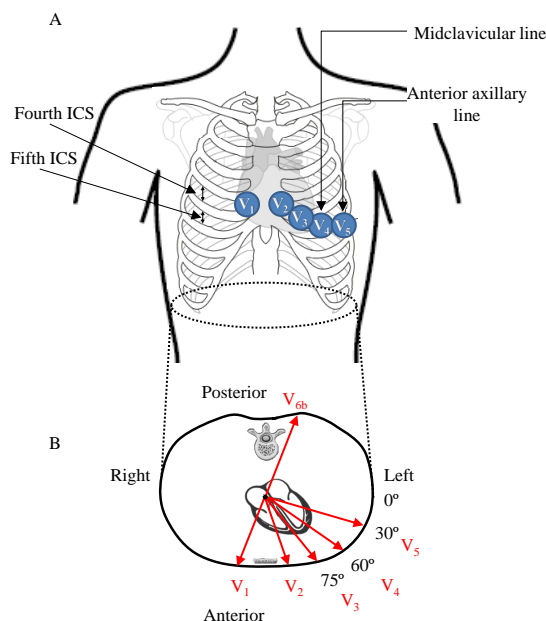
Figure 5.1: Modified ECG chest leads positions and vectors. The electrode V_6 was placed in the back of each patient and denoted V_{6b} in order to improve the recording of antero-posterior activity. Panel A: electrodes position for the precordial chest leads within the horizontal plane. Panel B: directions of the precordial leads on the horizontal plane. ICS: intercostal space.

to high frequency noise. Several cables and notch filters were unsuccessfully used. Therefore, chest lead V_6 was moved to the patient's back as the regular ECG cables and electrophysiology system offered a better shielding. Panel B of Figure 5.2 shows a snapshot of the resulting ECG signal whose quality was much improved with respect to the first attempt.

5.2.2 Intracardiac electrograms

The following catheters were introduced via the right and/or left femoral veins:

1. A 3.5 *mm* cooled-tip catheter for mapping and ablation (Navistar, Biosense Webster). In this manuscript, this catheter is denoted as the *MAP* catheter.

2. A steerable decapolar catheter within the CS (electrodes spacing $2-8-1$ *mm*, tip electrode of size 1 *mm*, Biosense Webster). In this manuscript, this catheter is denoted as the *CS-cath* catheter.

3. A circumferential duodecapolar Lasso catheter within the LA (electrodes spacing $2-6-2$ *mm*, Biosense Webster).

4. A quadripolar catheter into the RA appendage (RAA) (electrodes spacing $5-5-5$ *mm*, tip electrode of size 4 *mm*, St Jude). In this manuscript, this catheter is denoted as the *HRA* catheter.

More technical details of the catheters are provided in section B.1 of the appendix B.
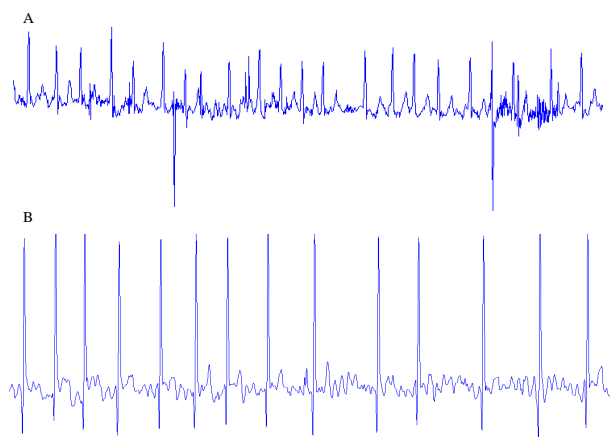
Figure 5.2: Signal quality for different back electrode placements. Panel A: first attempt with the back electrode using an extra unipolar derivation. Panel B: second attempt with V_6 placed in the back.

5.2.3 Study protocol

The general overview of the study protocol is illustrated in Figure 5.3. The first step consisted in reconstructing a precise $3D$ model of the LA using the CARTO® 3 system. During the second step, baseline data were systematically acquired (Section 5.2.3). Finally, the ablation was performed following a specific protocol (Section 5.2.3).
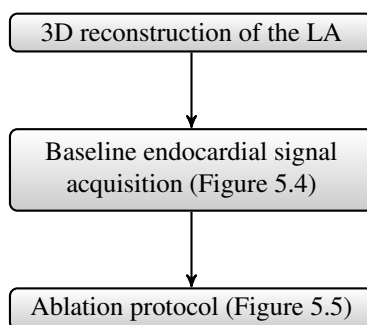
Figure 5.3: General overview of the study protocol.

Baseline endocardial signal acquisition

Once the $3D$ volume had been reconstructed with the CARTO® 3 system, the Lasso was placed consecutively in a stable position at thirteen different locations within the LA for a minimum duration of 20 seconds. The locations are the following which are illustrated in Figure 5.4:
– The ostium of the four PVs.
– The base of the LAA.
– The anterior and posterior parts of the roof.
– The middle and inferior parts of the posterior wall.
– The mitral isthmus.
– The superior, middle and inferior parts of the septum.
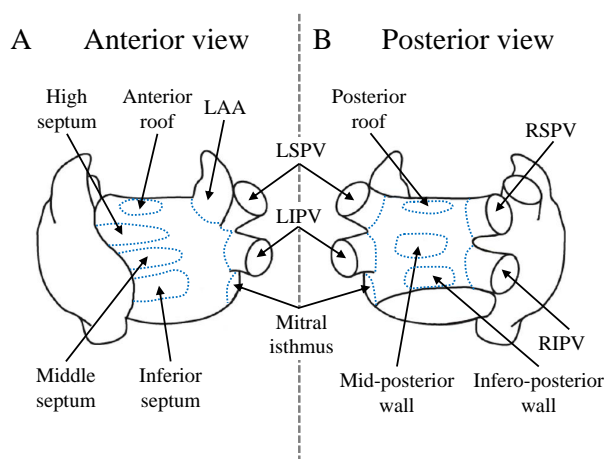
Figure 5.4: Baseline mapping of the left atrium. The Lasso is placed consecutively in a stable position at different locations within the LA for a minimum duration of 20 seconds. Panel A shows an anterior view of the atria and panel B a posterior view.

Ablation protocol

As described in Section 3.5.3, in long-standing persistent AF significant electrical and structural remodeling of the atria was observed providing a diffuse substrate for AF perpetuation [12]. The ablation strategy must therefore target the different substrate responsible for initiating and maintaining AF. Some groups have reported the benefit of using a stepwise approach in long-standing persistent AF [6, 8, 49, 50]. Haïssaguerre et. al. have shown the incremental benefit of linear ablation of long-standing persistent AF over PVI [50]. In another study, they reported termination of persistent AF in 87% of patients by stepwise catheter ablation consisting of PVI, CFAEs and linear ablation of the roof and mitral isthmus [6].

During this study, the stepwise radiofrequency catheter ablation (step-CA), illustrated in Figure 5.5, was performed within the LA as follows:

1. **PVI:** all PVs were electrically disconnected in this specific order: LSPV, LIPV, RSPV and RIPV. Following each isolation, the Lasso was placed within the LAA in a stable position to provide a recording for a minimum duration of 20 seconds.

2. **CFAEs:** CFAEs were visually identified as such by the ablating physician. CFAEs were ablated sequentially in a specific order in the following regions of the LA:
   – The posterior wall. The ablation started in the inferior part along the CS, then it progressively moved upwards by first defragmenting the middle part and finishing at the superior region near the posterior area of the roof.
   – The anterior wall (defined as the separation between the septum and the base of the LAA).
   – The septum.
   – The lateral wall (defined as the left lateral region of the LA).
   – The base of the LAA.

3. **Linear:** two ablation lines were performed within the LA, first on the roof, and then at the mitral isthmus (see Figure 4.2 at page 40).

The ablation protocol was approved by the Human Research Ethics Committee of the Lausanne University Hospital and all patients provided informed consent.
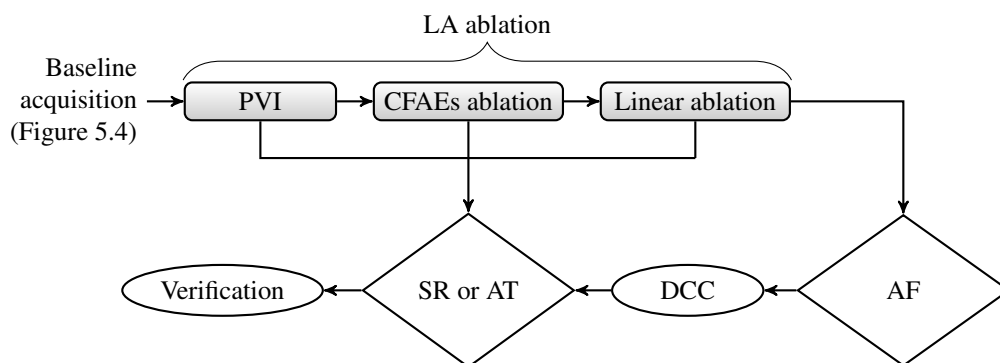
Figure 5.5: Stepwise radiofrequency catheter ablation (step-CA) protocol starting with PVI, followed by CFAEs ablation and LA linear ablation (roof and mitral isthmus). If AF was non terminated within the LA, a cardioversion (DCC) was performed. At the end of step-CA, the effectiveness of PVI and bidirectional conduction block across the lines was verified and completed when needed.

Procedural endpoint

The study endpoint was reached when AF was terminated into SR or atrial tachycardia (AT). AT is defined as a regular atrial rhythm at a constant rate more than 100 bpm [5]. The term AT encompasses several types of tachycardia that originate within the atria. Mechanisms include abnormal automaticity, triggered activity (focal AT), or micro/macroreentry. Focal AT is initiated and maintained by a focus from which its activation spreads out centrifugally. In contrast, macroreentrant AT occurs around an anatomical obstacle. This type of AT includes the atrial flutter. Atrial flutter refers to a pattern of very organized and rapid atrial activation with a rate of 240 bpm or more and is frequently observed after catheter ablation of AF. When AF was terminated in atrial flutter, the tachycardia was mapped by identifying the earliest site of activation and was ablated.

Non terminated AF cases were cardioverted electrically. At the end of step-CA, following AF termination or electrical cardioversion, the effectiveness of PVI and bidirectional conduction block across the lines was checked and completed when needed. To prove the effectiveness of ablation, differential pacing was performed on either side of the lines.

Based on the clinical outcome of the procedure, the study population was divided into two groups:

1. **Left terminated (LT,** N = 22**)**: patients in whom AF was terminated into SR or AT during ablation within the LA.

2. **Not left terminated (NLT,** N = 11**)**: patients in whom ablation within the LA failed to terminate AF and required a cardioversion.

Among these two groups, the level of significance of the distribution of the clinical characteristics presented in Table 5.1 was assessed using the ANOVA framework for numerical data and the Kruskal-Wallis test for categorical data. Importantly, the average duration of sustained AF was found to be significantly lower (16 ± 8 months) for the LT patients than for the NLT patients (25 ± 14 months, $p < 0.05$).

Table 5.2 reports several characteristics during step-CA such as the cumulative time of ablation within the LA, and the sites of AF termination within the LA. The average duration of each ablation step is given in minutes. Numerical data are expressed as mean ± standard deviation. The level of significance of the average duration between each group was assessed using the

ANOVA framework. For the LT patients, 45 ± 16 minutes of ablation were delivered to terminate the AF, while for the NLT patients the ablation time was slightly longer (53 ± 12 minutes), although non significantly. During each ablation step, the average ablation duration of both groups was similar.

5.3 Databases

Surface ECG and endocardial EGMs were continuously monitored and recorded at $2kHz$ sampling rate (AXIOM Sensis XP, Siemens, see Section B.2 of Appendix B) for off-line analysis. Two databases were constructed off-line. Importantly, in both databases, recordings during ablation were discarded.

The first database contained continuous and synchronous recordings of both ECG and EGM signals (except when an ablation was performed). This database was named DB_{full}.

The second database is a subset of DB_{full}; it has been manually segmented according to the timing of the different acquisition steps at baseline (i.e., before ablation) and during ablation (see Section 5.2.3).

Characteristics	All	LT	NLT	
	($N = 33$)	($LT = 22, 67\%$)	($NLT = 11, 33\%$)	
Age, (years)	61 ± 7	61 ± 8	60 ± 4	
Sex, (male/female)	31/2	19/2	11/0	
AF duration, (years)	6 ± 4	7 ± 5	4 ± 2	
Duration of sustained AF, (months)	19 ± 11	16 ± 8	25 ± 14	*
BMI, (kg/m^2)	30 ± 6	30 ± 6	29 ± 7	
High blood pressure, n (%)	24 (73)	16 (73)	8 (73)	
Valvular disease, n (%)	5 (15)	4 (18)	1 (9)	
Diabetes, n (%)	6 (18)	4 (18)	2 (18)	
Tobacco, n (%)	5 (15)	3 (14)	2 (18)	
Hypercholesterolemia, n (%)	15 (45)	11 (50)	4 (36)	
Coronary artery disease, n (%)	0 (0)	0 (0)	0 (0)	
Sleep apnea syndrome, n (%)	19 (58)	13 (59)	6 (55)	
Chronic kidney disease, n (%)	1 (3)	1 (5)	0 (0)	
CHA$_2$DS$_2$ VASc score	1.5 ± 1.1	1.7 ± 1.1	1.1 ± 1	
Dilated cardiomyopathy, n (%)	12 (36)	9 (41)	3 (27)	
Hypertrophic cardiomyopathy, n (%)	2 (6)	2 (9)	0 (0)	
Left ventricular fraction ejection, %	48.9 ± 10.9	47.1 ± 11.2	52 ± 9.6	
Left atrial volume, (ml)	173.81 ± 43.59	173.14 ± 44.14	175.1 ± 44.63	
Beta-blockers, n (%)	25 (76)	18 (82)	7 (64)	
Calcium channel blockers, n (%)	6 (18)	5 (23)	1 (9)	
Amiodarone, n (%)	7 (21)	6 (27)	1 (9)	
Other antiarrhythmics, n (%)	5 (15)	2 (9)	3 (27)	
Enzyme conversion inhibitor, n (%)	8 (24)	5 (23)	3 (27)	
Angiotensin receptor inhibitor, n (%)	5 (15)	4 (18)	1 (9)	
Number of antiarrhythmics drugs, (n)	2.2 ± 0.9	2.4 ± 0.85	1.7 ± 0.7	*
Statins, n (%)	5 (15)	2 (9)	3 (27)	

Table 5.1: Study population clinical characteristics. The left atrial volume was measured with the Carto® software (Biosense Webster®) after exclusion of the pulmonary veins. The level of significance of the distribution of numerical data was inferred through the ANOVA framework, while for categorical variables the Kruskal-Wallis test was used. Levels of significance are indicated as such: $*: p < 0.05$, $**: p < 0.01$, $\dagger: p < 0.005$ and $\ddagger: p < 0.001$.

Characteristics	All (N = 33)	LT (LT = 22)	NLT (NLT = 11)
LA cumulative ablation time, (*min*)	48 ± 15	45 ± 16	53 ± 12
LSPV ablation, (*min*)	6 ± 3	6 ± 3	4 ± 2
LIPV ablation, (*min*)	4 ± 3	5 ± 3	3 ± 1
RSPV ablation, (*min*)	6 ± 3	7 ± 3	5 ± 2
RIPV ablation, (*min*)	5 ± 2	5 ± 2	5 ± 2
CFAEs ablation, (*min*)	25 ± 10	23 ± 10	29 ± 10
Linear ablation, (*min*)	8 ± 4	9 ± 4	7 ± 4
LA sites of AF-termination:			
Mitral isthmus		7	
Roof		4	
Septum		3	
Coronary sinus		3	
Left atrial appendage		2	
Left superior pulmonary vein		1	
Right inferior pulmonary vein		1	
Lateral		1	

Table 5.2: Characteristics during step-CA. Average ablation durations are provided for each ablation step as well as the cumulative ablation duration within the LA. Importantly, all ablation durations between the two groups were non-significantly different. For the LT patients, sites of AF-term are reported.

Part III

ECG Signal Processing

Time-invariant Analysis

<div style="text-align: right; font-size: 3em; font-weight: bold;">6</div>

The ECG of AF is characterized by the replacement of the P waves with f-waves made of rapid but variable oscillations. Spectral time-invariant approaches have been widely used for analysing the rate of the f-waves. The ECG comprises both ventricular and atrial components. Hence, the PSD computed from a raw ECG signal is typically characterized by a peak within the low frequency band reflecting the ventricular activity that may prevent the accurate determination of the atrial activation PSD because of some overlap in their frequency content. The first step is to separate the ventricular activity from the atrial one. This task is non-trivial as extracting the atrial signal cannot be achieved using linear filters. Appendix C covers in more details the schemes proposed in the literature for subtracting the ventricular activity from the ECG during AF. In this thesis, we chose to use the approach developed by Lemay et al. [56], which is presented in details in Appendix C, page 149. Their approach has the main advantage to be independent of the duration of the ECG recordings as opposed to other techniques.

Following the extraction of the atrial signal devoid of ventricular activity, the PSD is computed. The spectral peak of highest amplitude is taken as an estimate of AF frequency and is named the dominant frequency (DF). Previous studies have shown that the DF computed from the ECG reflects the average frequency of atrial activation during AF [16, 17, 57, 58]. This measure has been used as an organization index in clinical studies in order to quantify the atrial electrical remodeling [13–15], and to predict the response to several therapies [16–20].

Once the DF has been identified, its harmonics can be localized. In a perfectly periodic signal, the power is concentrated at the DF and its harmonics. Conversely, for an irregular signal, the PSD is characterized by a broader spectrum with multiple spectral peaks. In this case, the power concentrated at the DF and its higher harmonics represents a fraction of the entire PSD. Harmonic analysis can therefore be used to quantify the organization of any AF signal. Everett et al. proposed such an index computed as the ratio between the power under the harmonic peaks to the total power of bipolar intracardiac signals [21]. Another method for characterizing the fibrillatory content of the ECG signals from their AF harmonic component was presented by Stridh et al. [59] in which time-invariant bandpass filters were used to extracted the AF harmonic components. Once the AF harmonic components were extracted, the phase difference between them was computed. The phase difference between harmonic components is a direct indicator of their relative timing and subsequently of their synchronization. Hence, an index quantifying the phase difference between the DF and its higher harmonics reflects the regularity of the morphology of the f-waves.

This chapter is aimed at 1) presenting ECG organization indices derived from time-invariant approaches and harmonic analysis, and 2) analysing the performance of these indices to discriminate patients in whom catheter ablation terminated long-standing persistent AF from patients in

whom SR could not be restored.

This chapter is organized as follows. In Section 6.1 the methods for computing the time-invariant based organization indices are presented. Then, in Section 6.2, the results of these indices on the study population for predicting the procedural outcome are given. Finally, Section 6.3 covers the discussion of the results and concludes this chapter.

6.1 Methods

6.1.1 Measures of AF organization

Dominant frequency

The frequency spectra from all ECG chest leads were computed using Welch's method (Hamming window of segment length of $\lfloor N/4 \rfloor$, where N is the length of the input signal, and 50% overlap between segments). The DF was estimated as the frequency of the highest peak between 3 and 20 Hz in the PSD estimate of each lead. The mean ECG DF was then calculated for each patient over different epoch durations from chest leads V_1 to V_{6b}. Typically, a lower DF is indicative of an organized atrial signal.

Organization index

The second measure computed from the surface ECG is similar to the organization index (OI) introduced by Everett, et al. [21]. Originally, the OI was defined as the ratio between the power under the harmonic peaks (over a 1 Hz band centered around the fundamental and up to the 4th harmonic) to the total power of bipolar intracardiac signals.

In the present thesis, we developed a similar ratio that only used the fundamental and the first harmonic as the power of higher harmonics was negligible and did not contribute significantly to the overall power. The power spectrum was estimated using Welch's method (segment length of 1 second, with 50% overlap).

Phase difference

The phase difference (PD) between two waveforms measures their relative timing, and is therefore an indicator of their synchronization [59]. An approach for characterizing the complexity of fibrillatory waves using phase information was proposed in [59]. More specifically, the power spectrum was estimated using Welch's method (segment length of 512 samples, 50% overlap). The estimate f_0 of the fundamental frequency was determined by locating the highest peak in the interval from 3 to 12 Hz. The mth harmonic frequency f_m was found by searching an interval centered around $(m+1)f_0$. Then, the fundamental and harmonic signal components were extracted by $(m+1)$ linear, time-invariant band-pass Kaiser filters, centered around the identified peaks [59].

In [59], the phases of the fundamental and harmonic components were recovered using a maximum likelihood estimation. A typical method for extracting the phase information is the discrete Hilbert transform and the associated analytic representation [60]. A definition of the Hilbert transform is provided in Appendix A.2. It has been shown that proper estimation of phase parameters can only be performed on narrow-band signals [61, 62]. Importantly, the vast majority of ECG recordings display narrow-banded frequency spectra [63]. In this thesis, we chose to extract the phase information using the Hilbert transform.

The approach for computing the PD in this chapter is closely related to the one proposed in [59]. The PD was computed between the fundamental component (i.e., the DF) and its first

harmonic component extracted with the linear, time-invariant bandpass filters as in [59]. The phase of the first harmonic component was divided by 2 to ensure that both quantities were comparable. Once the PD was computed, its slope (sPD) was locally estimated by fitting a polynomial of degree 1 to centered sliding windows of odd length ($L = 101$). The sPD therefore reflects the variations of the PD. If the shape of the oscillations does not vary over time, the PD is constant, and therefore the sPD is null. Conversely, a change in the oscillations morphology translates into a change in the slope. By computing the variance of the sPD, the regularity of the oscillations between the fundamental and its first harmonic can be quantified. The resulting index is called the time-invariant phase difference (TIPD). The closer to zero the TIPD, the higher the coupling between the fundamental and its first harmonic. Small TIPD values are therefore indicative of organized AF oscillations.

6.1.2 Material

Most ECG-based clinical studies are performed on durations of 10 seconds. In this chapter, we aimed at evaluating the performance of classical ECG-based methods on longer durations. As such, durations of 10 to 60 seconds were compared by steps of 10 seconds.

The analysis was performed on DB_{full}, as this database contains continuous recordings [1]. For each patient, the signals at baseline (before any ablation) were considered. More specifically, on average, 21 ± 10 minutes of continuous recordings were available per patient at baseline. For each patient, the recordings were split into non-overlapping epochs of fixed durations (10 to 60 seconds by steps of 10 seconds). Then, the organization indices were computed on each epoch and averaged over all available epochs. As such, for each patient and each epoch duration, this led to one average value for the corresponding organization index.

Importantly, all ECG methods presented in this chapter were applied after QRST cancellation. Once the ECG was devoid of ventricular activity, the atrial signals were down sampled to 50 Hz [57, 64]. Previous studies have shown that the atrial rate rarely goes above 10 Hz. Therefore, reducing the sampling rate to 50 Hz does not only guarantee the conservation of the atrial frequency components, but also speeds up subsequently the analysis process.

Finally, only the ECG chest leads were included in this study (i.e., from V_1 to V_{6b}, where V_{6b} denotes the dorsal electrode, see Section 2.2.1).

6.1.3 Statistical analysis

The statistical analysis aims at comparing the various indices between the LT and NLT groups before the first ablation step. The distribution of the mean values at baseline of the three indices was inferred through the analysis-of-variance (ANOVA) framework. First, the statistical significance between the LT and NLT groups was assessed on the different epochs (from 10 to 60 sec, by steps of 10 seconds).

In the second step, the longest available duration (i.e, 60 seconds) was selected to perform an advanced statistical analysis. When the ANOVA p-value was significant for a given index/lead, a binary logistic regression model was applied to the corresponding index values. The definition of the binary logistic regression is provided in Section A.3 of Appendix A. The performance of the binary logistic regression model was evaluated using the odds ratio and its 95% confidence interval. Another method to evaluate the binary logistic regression model is to make use of the receiver operating characteristic (ROC) curve analysis, in which the power of the predicted values by the model to discriminate between a LT and a NLT patient is investigated. Section A.4 of Appendix A briefly presents the technique involved in ROC analysis. In this study, the area under the curve (AUC) is reported as well as the Youden index (YI) with its corresponding sensitivity, specificity and cut-off threshold value. Since the available data set is not large, and in

---

1. See Section 5.2.3 of Chapter 5 for the description of the study protocol

order to assess the generalization ability of the analysis to an independent data set, a leave-one-out cross validation was performed (LOOCV). LOOCV is a simple cross validation technique in which the validation set is created by taking all the available samples except one (in our case the samples are the patients). ROC characteristics, AUC values and cut-off thresholds were averaged over all possible validation sets.

6.2 Results

6.2.1 Illustrative examples

Figure 6.1 shows an example of DF and OI measures on an LT (6.1a) and on an NLT patient (6.1b) respectively, computed on a 60 *sec* epoch acquired from lead V_1. The PSD was estimated after QRST cancellation. The DF (red square) for the LT patient is located at 5.08 *Hz* and the first harmonic (H_1, green diamond) at 10.16 *Hz*. In both figures, the bandwidth limits of ± 1 *Hz* for OI computation are represented by vertical dashed lines.

For the LT patient, most of the power lies within the bandwidth limits resulting in an OI of 0.77, which is indicative of a high spectral organization and hence a rather organized AF signal.

For the NLT patient, the DF is located at 4.93 *Hz* and H_1 at 9.86 *Hz*. Note the widely distributed frequency components with multiple peaks of high magnitude, some outside the bandwidth limits. This wide distribution results in a low OI value of 0.35 indicative of a low spectral organization and hence a disorganized AF signal.

(a) LT patient, $DF = 5.08$ *Hz*, $H_1 = 10.16$ *Hz*, $OI = 0.77$

(b) NLT patient, $DF = 4.93$ *Hz*, $H_1 = 9.86$ *Hz*, $OI = 0.35$
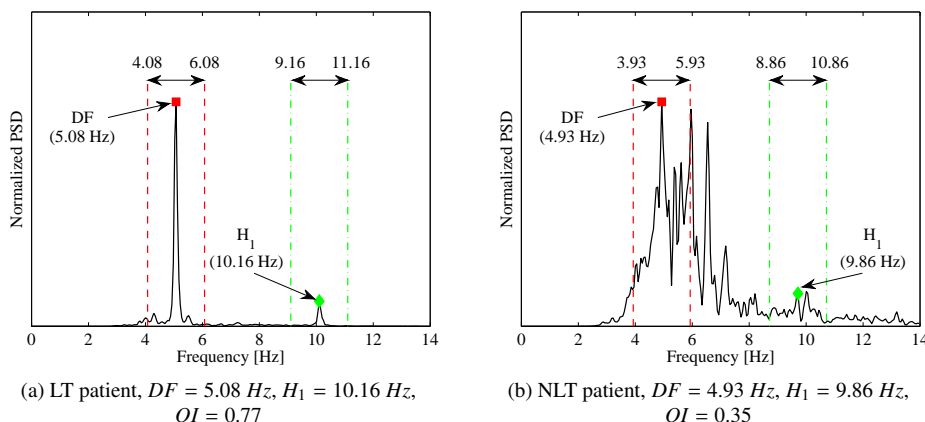
Figure 6.1: Examples of DF and OI measures on an LT patient (a) and on an NLT patient (b) both computed on a 60 *sec* epoch acquired from chest lead V_1. PSDs were estimated after QRST cancellation. On both figures the DF (red square) and the first harmonic (H_1, green diamond) are shown. In both examples the PSD, estimates were normalized.

Figure 6.2 shows the time-invariant sPD (top plots) estimated from the outputs of the time-invariant filters. For both patients, the input signals were the same AF signals as in the previous figure.

For the LT patient (Figure 6.2a), $TIPD$ equals $2 \cdot 10^{-3}$ $(rad/s)^2$. Interestingly, one can notice three short periods (highlighted in gray, time intervals $[13.7; 17.3]$, $[30.3; 32.4]$, and $[37.6; 42.6]$ *sec*) during which the sPD remains close to zero. In other words, these intervals correspond to a *phase lock* between the fundamental component and its first harmonic. The bottom plot shows an excerpt of the initial ECG signal on a time interval covering the last two phase locks. The original

V_1 is shown in blue (top), while the same signal devoid of ventricular activity is plotted in black (bottom). Note the regular morphology of the atrial ECG during the phase locks, while at the time following the last phase lock, the shape of the atrial ECG transitions into an irregular pattern. Nevertheless, between the two phase locks, the morphology of the AF waveforms does not change much as compared to the shapes during the two phase locks.

For the NLT patient (Figure 6.2b), a higher TIPD was found ($TIPD = 7.4 \cdot 10^{-3} \ (rad/s)^2$). Note the erratic sPD during the whole recording duration, with larger deviations than for the LT patient and the lack of phase lock as well. The AF waveform morphology after QRST cancellation appears highly irregular without any apparent organization.

(a) LT patient, $TIPD = 2 \cdot 10^{-3} \ (rad/s)^2$.   (b) NLT patient, $TIPD = 7.4 \cdot 10^{-3} \ (rad/s)^2$.
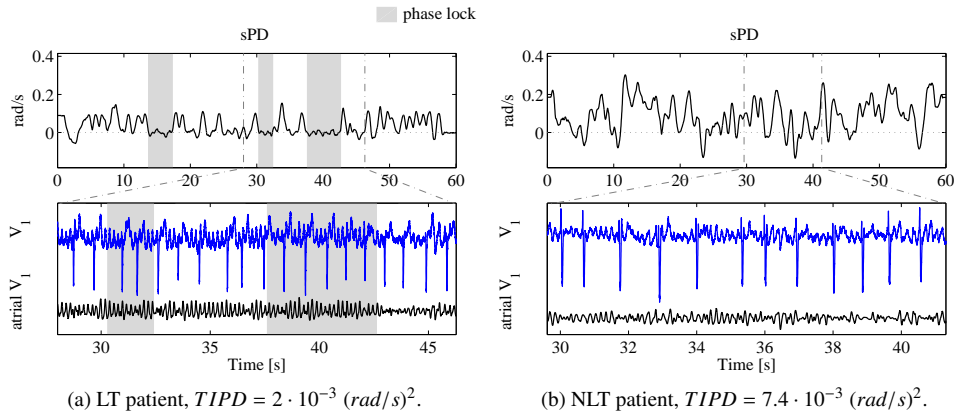
Figure 6.2: Examples of the TIPD index on an LT (a) and an NLT (b) patient. On both figures the top plot shows the time-invariant sPD, while the bottom plot displays an excerpt of the corresponding input ECG signals. The blue signal corresponds to the original ECG whereas the black signal corresponds to the ECG after QRST cancellation. The highlights in gray illustrate time intervals during which a phase lock occurs between the DF and its first harmonic.

6.2.2 Epoch durations

Figure 6.3 shows the baseline p-values obtained when comparing LT and NLT patients for the all three indices computed from each ECG chest lead (x-axis) and on the different epoch durations (y-axis). White squares denote non-significant differences between groups ($p = ns$). When the ANOVA test was found significant, the square was filled with gray, from light (less significant, $p < 0.05$) to dark (most significant, $p < 0.001$).

DF analysis   Figure 6.3a reports the p-values for the DF analysis. Among the six leads and all available epochs, only V_1 and V_{6b} display significant p-values. On lead V_1, the significance level was constant on all epoch durations ($p < 0.005$). On the dorsal lead V_{6b}, the statistical significance between the two groups was higher for epoch durations < 50 sec ($p < 0.001$), while for 60 sec epochs the p-value slightly decreased ($p < 0.005$). Chest lead V_4 showed a significant difference on the 10 sec epochs ($p < 0.05$). On the remaining leads (V_2, V_3, and V_5), no significant difference between the two groups was observed ($p = ns$).

(a)

(b)

(c)
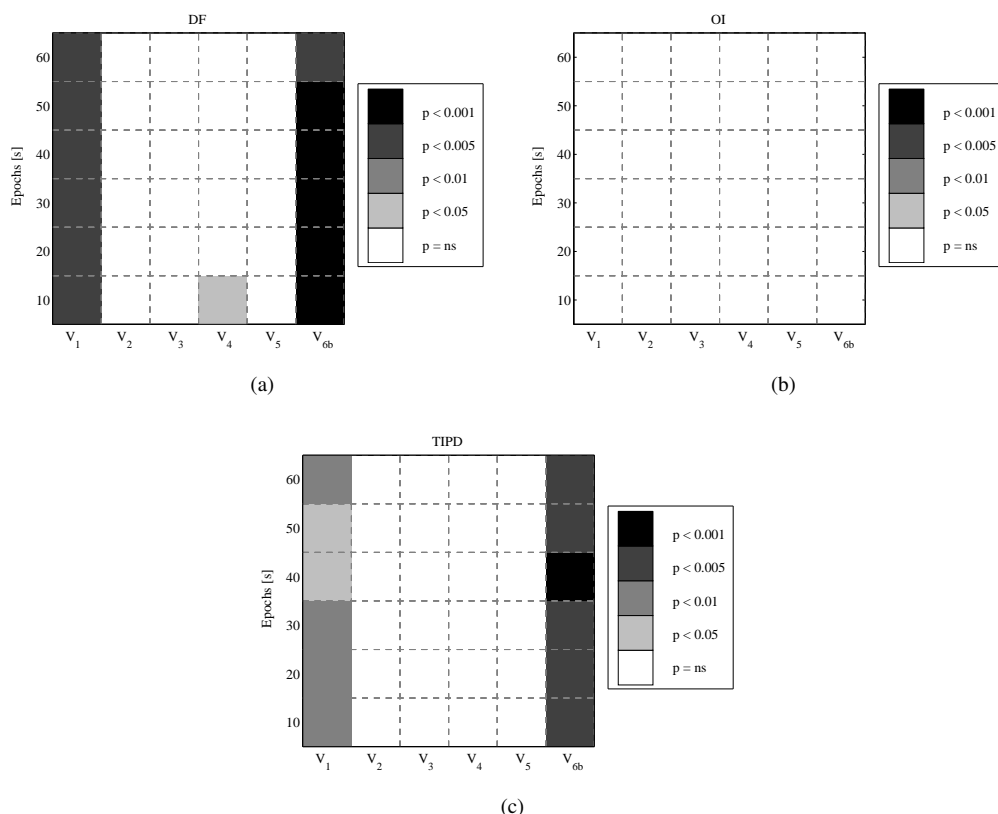
Figure 6.3: Statistical significance levels for all epoch durations (*y*-axis) and chest leads (*x*-axis) for DF (a), OI (b) and TIPD (c). White squares denote non-significant differences between groups ($p = n.s.$). When the difference was significant, the corresponding square was filled with gray, from light (less significant, $p < 0.05$) gradually to dark (most significant, $p < 0.001$).

OI analysis   Figure 6.3b shows the p-values for the OI analysis. Among all chest leads and all epoch durations, no significant differences were found between the two groups ($p = ns$).

TIPD analysis   Figure 6.3c shows the significance levels for the TIPD. Among all precordial leads and all epoch durations, significant differences between groups were only found on V_1 and V_{6b}. For the remaining leads, the p-values were non-significant ($p = ns$). On chest lead V_1 and on durations of 40 and 50 *sec*, the levels of discrimination between LT and NLT groups were lower as compared to the remaining periods ($p < 0.05$ vs. $p < 0.01$). Finally, on the dorsal lead V_{6b}, the level of significance for all epoch durations was estimated to $p < 0.005$ (except on 40 *sec* duration for which $p < 0.001$).

6.2.3   Group comparisons on the procedural outcome

Figure 6.4 reports the distribution of DF (a), OI (b) and TIPD (c) on all chest leads for the LT (blue) and the NLT (red) groups. Mean and median values are displayed as circle and square respectively. The vertical lines indicate one standard deviation. ANOVA was used to determine significant differences between the two groups. The following annotations were used for the dif-

Lead	DF [Hz]		OI		TIPD [$\cdot 10^{-3}(rad/s)^2$]	
	LT	NLT	LT	NLT	LT	NLT
V_1	5.52 ±0.72 (5.36)	6.33 ±0.46 † (6.28)	0.37 ±0.07 (0.36)	0.34 ±0.11 (0.34)	6.31 ±1.56 (6.23)	7.8 ±0.92 ∗∗ (7.72)
V_2	5.45 ±0.73 (5.42)	5.49 ±0.92 (5.45)	0.32 ±0.10 (0.29)	0.33 ±0.08 (0.30)	7.19 ±0.88 (7.11)	7.62 ±0.75 (7.49)
V_3	5.22 ±0.72 (5.13)	5.35 ±0.66 (5.31)	0.31 ±0.09 (0.28)	0.35 ±0.09 (0.32)	7.40 ±0.80 (7.42)	7.60 ±0.64 (7.46)
V_4	5.21 ±0.55 (5.23)	5.48 ±0.61 (5.46)	0.32 ±0.06 (0.32)	0.37 ±0.10 (0.40)	7.30 ±0.91 (7.38)	7.76 ±0.8 (7.65)
V_5	5.32 ±0.64 (5.27)	5.61 ±0.71 (5.51)	0.38 ±0.10 (0.36)	0.43 ±0.11 (0.43)	7.38 ±0.95 (7.51)	7.92 ±0.91 (7.90)
V_{6b}	5.38 ±0.61 (5.34)	6.08 ±0.36 † (6.13)	0.32 ±0.05 (0.32)	0.33 ±0.09 (0.3)	6.82 ±1.07 (6.63)	8.13 ±0.90 † (8.24)

Table 6.1: Mean ± standard deviation and median (in brackets) of the time-invariant based indices before ablation computed on 60 *sec* epochs. From left to right: DF, OI and TIPD. The following annotations were used for the different level of significance: $\ast$: $p < 0.05$, $\ast\ast$: $p < 0.01$, † : $p < 0.005$ and ‡ : $p < 0.001$.

ferent levels of significance: $\ast$: $p < 0.05$, $\ast\ast$: $p < 0.01$, † : $p < 0.005$ and ‡ : $p < 0.001$. The respective values are reported in Table 6.1.

DF analysis   LT patients displayed significantly lower DF values in V_1 and V_{6b} compared to NLT patients (5.52±0.72 vs 6.33±0.46 Hz, $p < 0.005$ for V_1 and 5.38±0.61 Hz vs. 6.08±0.36 Hz, $p < 0.005$ for V_{6b} respectively). Interestingly, for the LT patients, DF analysis had similar values between leads V_1 and V_{6b} (5.52 ± 0.72 Hz and 5.38 ± 0.61 Hz respectively), whereas a gradient was observed in NLT patients with significantly higher DF values in V_1 compared to V_{6b} (6.33 ± 0.46 Hz vs. 6.08 ± 0.36 Hz).

The binary logistic parameters estimated for leads V_1 and V_{6b} are reported in Table 6.2. On
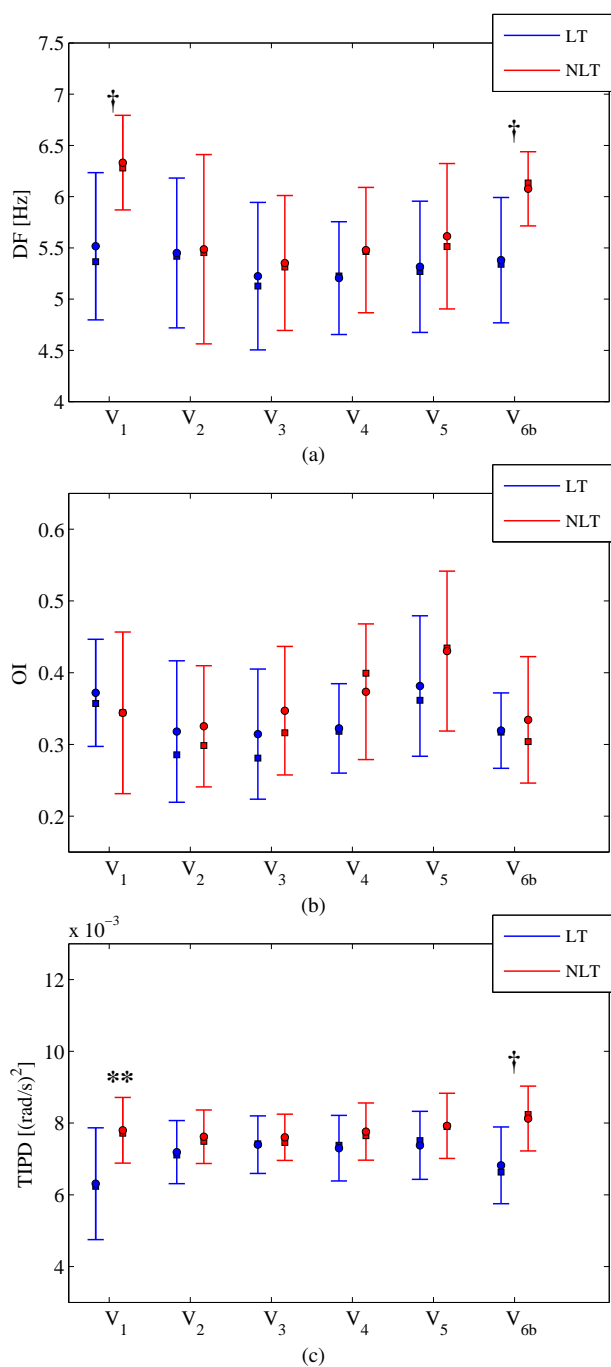
Figure 6.4: Distributions of the baseline DF (a), OI (b) and TIPD (c) for the LT (blue) and NLT (red) groups computed on 60 *sec* epochs. The mean (circle) as well as the median (square) of each group are shown. The vertical lines delimit the mean ± the standard deviation. The following annotations were used for the different level of significance: $*$: $p < 0.05$, $**$: $p < 0.01$, † : $p < 0.005$ and ‡ : $p < 0.001$.

both leads, the odds ratio was slightly smaller than one (0.97996 for V_1 and 0.96995 for V_{6b}) and their corresponding 95% confidence intervals were relatively small, indicative of a reliable precision on the odds ratio ([0.96502 − 0.99513] for V_1 and [0.94798 − 0.99243] for V_{6b}). Finally, on both leads, the respective p-values were < 0.01.

Figure 6.5 shows the ROC curves estimated for leads V_1 (a) and V_{6b} (b), while Tables 6.3a and 6.3b report the values of the estimated AUCs and YIs (a) as well as the results of the LOOCV (b). On both leads, the AUC was estimated at 0.84 and this value was corroborated by the average AUC from the LOOCV (0.84 ± 0.02). On lead V_1, however, the YI was slightly inferior than that on lead V_{6b}, suggesting that the correct classification rate was higher on the dorsal lead compared to V_1 (0.6 with 59% sensitivity and 100% specificity for V_1 vs. 0.66 with 75% sensitivity and 91% specificity for V_{6b}). Interestingly, the cut-off value for discriminating LT patients from NLT patients was smaller for lead V_1 (5.4 Hz) as compared to the cut-off on the dorsal lead V_{6b} (5.82 Hz) suggesting that the organization quantified on lead V_1 has to be somewhat higher than that on lead V_{6b} for a patient to be labelled as LT. Finally, it is also worth mentioning that the standard deviation of the average cut-off estimated from the LOOCV was higher on V_1 as compared to lead V_{6b} (0.16 Hz vs. 0.005 Hz).

OI analysis   For the OI (Figure 6.4b and middle column of Table 6.1), no significant differences were observed between groups on any lead ($p = ns$). Importantly, on leads V_3, V_4 and V_5, the OI for the NLT patients was on average slightly larger than that for the LT patients, however non significantly. The largest difference can be observed for lead V_5, on which the average OI for the NLT group was estimated at 0.43 ± 0.11 whereas for the LT group, the average OI lay within the interval 0.38 ± 0.1. These results are indicative of a higher organization in the NLT group, though non-significant. For both groups and on most leads, the mean and median diverged considerably.

TIPD analysis   LT patients displayed significantly lower TIPD values in leads V_1 and V_{6b} compared to NLT patients suggestive of a higher coupling between the DF and its first harmonic Figure 6.4c and right column of Table 6.1). More precisely, on lead V_1, the average TIPD for the LT patients was significantly lower than for the NLT ones ((6.31 ± 1.56) $\cdot 10^{-3}$ $(rad/s)^2$ vs (7.8 ± 0.92) $\cdot 10^{-3}$ $(rad/s)^2$ respectively, $p < 0.001$). Likewise, on the dorsal lead V_{6b}, the average TIPD for the LT group was significantly lower than for the NLT group ((6.82 ± 1.07) $\cdot 10^{-3}$ $(rad/s)^2$ vs. (8.13 ± 0.9) $\cdot 10^{-3}$ $(rad/s)^2$ respectively, $p < 0.005$). On the remaining leads, no significant difference between the groups was observed ($p = ns$).

The binary logistic regression parameters estimated for leads V_1 and V_{6b} are reported in Table 6.2. On both leads, the odds ratio was lower than one. On lead V_1 the odds ratio was higher than that on lead V_{6b} (0.91513 and 0.871 respectively). Furthermore, the 95% confidence interval was narrower on lead V_1 compared to that on lead V_{6b}, indicating that the odds ratio was more precisely estimated on lead V_1 than on lead V_{6b} ([0.8504 − 0.98479] for V_1 and [0.78341 − 0.96838] for V_{6b}).

Figure 6.6 displays the ROC curves estimated for leads V_1 (a) and V_{6b} (b) while Table 6.2 reports the values of the estimated AUCs and YIs (a) as well as the results of the LOOCV (b). The AUC as well as the YI estimated on lead V_1 were lower compared to lead V_{6b}. More specifically, the AUC on lead V_1 measured 0.8, while on the dorsal lead it was 0.84. The value of the YI on lead V_1 was estimated at 0.55 with 64% sensitivity and 91% specificity, while on lead V_{6b}, the YI was estimated at 0.63 with 90% sensitivity and 73% specificity. Interestingly, the estimated cut-off threshold for discriminating LT from NLT patients was lower on V_1 ($6.73 \cdot 10^{-3}$ $(rad/s)^2$) compared to V_{6b} ($8.07 \cdot 10^{-3}$ $(rad/s)^2$), suggesting that a higher level of organization was required on V_1 to increase the probability of terminating AF (the same behavior was observed previously

for the DF). All these values were corroborated by the respective average values estimated from the LOOCV. These results suggest a better classification performance on lead V_{6b} than on lead V_1.

Lead	Index	Odds ratio	95% confidence interval	p-value
V_1	DF	0.97996	[0.96502 − 0.99513]	0.0098163
	TIPD	0.91513	[0.8504 − 0.98479]	0.01781
V_{6b}	DF	0.96995	[0.94798 − 0.99243]	0.0090481
	TIPD	0.871	[0.78341 − 0.96838]	0.010641

Table 6.2: Binary logistic regression parameters of the time-invariant based indices/leads before ablation computed on 60 *sec* epochs. The binary logistic model was estimated when the ANOVA declared a significant difference for a pair of lead/index. The table reports the corresponding odds-ratio, its 95% confidence interval and associated p-value.
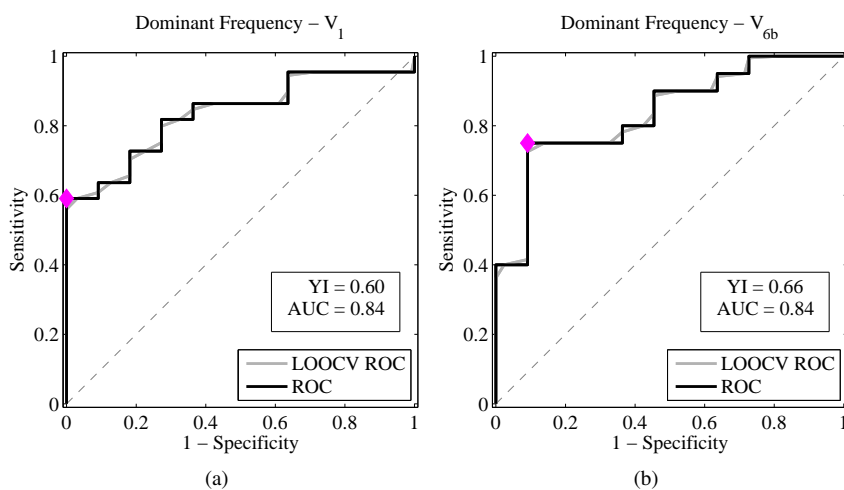
Figure 6.5: ROC curves (black) for the DF on lead V_1 (a) and V_{6b} (b) assessed on recordings of 60 *sec* duration. The corresponding AUCs and YI (pink diamond) estimated from the ROC curve are also reported. The average LOOCV ROC curves is plotted in gray.

Lead	Index	AUC	Youden index			
			Cut-off	Value	Sensitivity	Specificity
V_1	DF	0.84	5.40 [Hz]	0.60	0.59	1
	TIPD	0.80	$6.73 \cdot 10^{-3}$ [$(rad/s)^2$]	0.55	0.64	0.91
V_{6b}	DF	0.84	5.82 [Hz]	0.66	0.75	0.91
	TIPD	0.84	$8.07 \cdot 10^{-3}$ [$(rad/s)^2$]	0.63	0.90	0.73

(a)

Lead	Index	LOOCV		
		AUC	Cut-off	Youden index
V_1	DF	0.84 ± 0.02	5.46 ± 0.16 [Hz]	0.60 ± 0.02
	TIPD	0.80 ± 0.02	$(6.74 \pm 2.97 \cdot 10^{-2}) \cdot 10^{-3}$ [$(rad/s)^2$]	0.55 ± 0.03
V_{6b}	DF	0.84 ± 0.02	5.82 ± 0.005 [Hz]	0.66 ± 0.03
	TIPD	0.83 ± 0.02	$(8.07 \pm 4.05 \cdot 10^{-3}) \cdot 10^{-3}$ [$(rad/s)^2$]	0.63 ± 0.03

(b)

Table 6.3: ROC (a) and LOOCV (b) estimations for the DF and TIPD assessed on epochs of 60 *sec* duration. Results are reported for the leads which were declared significant through the ANOVA framework, i.e., leads V_1 and V_{6b}. Table (a) reports the AUCs, Youden indices with their respective sensitivities/specificities as well as the cut-off thresholds for discriminating LT patients from NLT patients. Table (b) reports the average AUCs, Youden indices and cut-off values assessed with LOOCV.
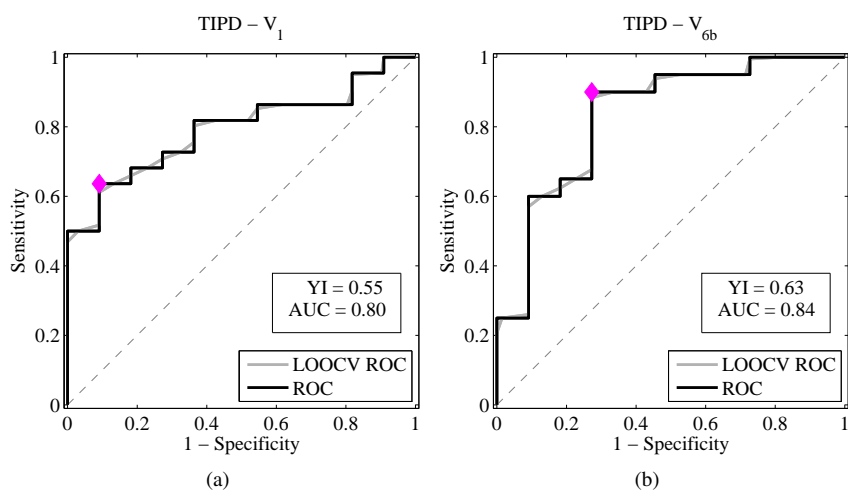
Figure 6.6: ROC curves (black) for the TIPD on lead V_1 (a) and V_{6b} (b) assessed on recordings of 60 *sec* duration. The corresponding AUCs and YI (pink diamond) estimated from the ROC curve are also reported. The average LOOCV ROC curves is plotted in gray.

6.3   Discussion

In this chapter, organization indices derived from time-invariant approaches for characterizing the frequency content (the DF) as well as the harmonic structure (the OI and TIPD) of ECG AF signals were presented. Importantly, all measurements aiming at quantifying the amount of organization during AF were computed on AF signals devoid of ventricular activity.

The first index presented in this chapter is the DF defined as the peak of highest amplitude in the PSD from AF signals. This index is widely used in the literature for assessing the amount of organization in AF signals. It has been established that the frequency content of f-waves computed from ECG signals can be used as a surrogate of the average AF cycle length, and subsequently of the atrial refractoriness [16, 17, 57, 58]. The atrial fibrillatory rate has been used in clinical studies to quantify the atrial electrical remodeling [13–15], and to predict the success following several therapies such as with antiarrhythmic drugs or electrical cardioversion [16–18]. For instance, an increase in the fibrillatory frequency measured in lead V_1 was associated with more advanced remodeling [14, 15]. Moreover, several studies have demonstrated that a lower fibrillatory rate was associated to AF termination by cardioversion whereas a higher AF frequency predicted an early arrhythmia recurrence [16–18].

The second spectrum-based index analyzed in detail in the present thesis is the OI defined as the ratio between the power under the DF and the first harmonic to the total power of the signal. This index was originally presented by Everett et al. in order to optimize the success of AF electrical cardioversion [21]. Although no physiological meaning was given by Everett et al., in another study performed by Dibs et al., a significant correlation between the intracardiac OI and the DF was observed in patients with persistent AF [65]. Others also showed that AF successfully terminated by pharmacological cardioversion was associated with a higher intracardiac OI [66].

The third organization index presented in this chapter is directly inspired from an approach proposed by Stridh et al. based on the extraction of AF harmonic components [59]. Using linear, time-invariant bandpass filters, the atrial activity is divided into fundamental (i.e., the DF) and harmonic components from which a phase relationship is extracted. As the PD between harmonic components measures their relative timing, it is therefore an indicator of their coupling. Quantifying the PD between harmonic components to characterize the atrial complexity is also an indirect measure of the f-waves morphological regularity. In this chapter, we proposed a novel approach for quantifying the variations of the PD over time. The resulting index, the TIPD, was computed as the variance of the slope of the PD between the fundamental and harmonic components.

6.3.1   Relevance of the epoch durations

To the best of our knowledge, no prior studies have investigated the impact of epoch durations on organization indices derived from the ECG at baseline for predicting the procedural outcome of catheter ablation. Typically, segments ranging between 7 to 10 seconds are used [14, 20]. ECG segments of short durations have been shown to reproducibly represent the average AF dynamics [18], while some used epochs of one minute duration [19].

In our study, we found that the mean DF and TIPD computed on leads V_1 and V_{6b} were the most robust for separating LT from NLT patients on all epoch durations. A significant level was observed for the DF on lead V_4, but only for an epoch duration of 10 seconds. The levels of significance for the DF were higher as compared to the TIPD. Among all leads and epoch durations, the OI was not predictive of the procedural outcome. Thus, the spectral organization of harmonic components can not be assessed using a time-invariant approach regardless of the epoch duration.

6.3.2   Prediction of the procedural outcome before ablation

DF computed on atrial ECG has been used to predict the outcome of first-time catheter abla-
tion in patients with persistent [19] and chronic AF [20]. It has been shown that the baseline DF
on lead V_1 was significantly lower in patients with AF termination than in patients without AF
termination [20, 67]. The OI, in association with the DF, was used in several studies in order to
predict the success of AF catheter ablation [68–71]. Takahashi et al. showed that the intracardiac
OI was more predictive of AF termination than the mean DF [68]. In another study, during ab-
lation of persistent AF, the mean intracardiac OI was unchanged whereas a significant decrease
in the DF was observed [69]. More recently, ablation of intracardiac segments displaying high
OIs was associated with an increase of the OI assessed remotely within the LAA [70]. Lately,
Jones et al. have used the ECG OI and DF measured at baseline to identify patients in whom
brief ablation of focal impulses and stable rotors achieved acute AF termination [71]. In their
results, the OI had a better ROC with AUC of 0.67 as compared to the DF, which yielded an
AUC of 0.38. In their study, however, the DF and OI were assessed in three pseudo-orthogonal
ECG planes [2].

In our study, we found that the average DF and TIPD were significantly lower on leads V_1 and
V_{6b} for LT patients compared to NLT patients. For both indices, the statistical analysis showed
that the classification performance was better on the dorsal lead V_{6b} than on lead V_1. However,
the significance level was higher for DF than for TIPD. For both indices, the discriminative cut-
off values were lower on lead V_1 than on the dorsal lead V_{6b}, suggesting that a higher level of
organization on lead V_1 was necessary to increase the probability of terminating AF. For the OI,
no statistical significance could be observed between the groups. It even showed an opposite
trend as the organization appeared slightly higher, though non significantly, in NLT patients than
in LT patients.

6.3.3   Limitations of time-invariant approaches

Using time-invariant approaches, the number of ECG leads displaying a significant difference
between the LT and NLT groups was limited. For the DF and TIPD, only two leads (V_1 and the
dorsal V_{6b}) were predictive of procedural outcome. The OI computed on all ECG precordial
leads was unable to separate the two groups. Several arguments can be put forward in order to
explain these poor performances.

First, classical PSD analysis typically reflects the average frequency content of a signal. Mul-
tiple peaks can be seen in the frequency spectrum as the results of the temporal variations in AF
frequency. Also, linear time-invariant filters shall be restricted to well organized signals, which is
seldom in biological signals. Even in the case of well organized signals such as in the illustrative
example of the LT patient (page 59), the long period of regular morphology was not correctly
identified. Indeed, only some short excerpts of phase locks were observed.

Second, in order to explain the inability of the OI to discriminate LT and NLT patients, one
may refer to the recent study of Lee et al. [72]. In their work, the authors used simulated atrial
electrograms of varying amplitudes on which the OI was computed. Importantly, the repetition
of the atrial wavefronts was similar in each simulated electrograms, only their amplitudes were
variable. They observed that the amplitude variations of the signal greatly influenced the value
of the OI, even if the DF was correctly detected. It was established that the amplitude measure-
ments of ECG f-waves were repeatable over time within patient, but that inter-patient variability
was considerable [73]. One might therefore argue that this substantial inter-patient variability re-

---

2. The pseudo-orthogonal ECG space is a three dimensional space defined as such: the X axis corresponds to the
signal from lead I, the Y axis corresponds to the signal from aVF, and the Z axis corresponds to the signal from V_1. The
spectral analysis was performed on the signal characterizing the phase angle [71].

duces the potential of the OI to discriminate one group of patients from another when computed on ECG signals.

In conclusion, time-invariant schemes are not optimal in characterizing the temporal variations of long-standing persistent AF, which is typically described as a disorganized arrhythmia with considerable short-term rate variations. The performance of the time-invariant based organization indices in predicting the acute procedural outcome was relatively poor. The time-invariant quantification of the spectral content of the fundamental and first harmonic components (the OI) did not show any discrimination between the two groups of patients, while those based on the DF and TIPD did with a limited success. In the next chapter, we propose a novel time-varying (adaptive) approach in order to circumvent these issues.

Time-varying Analysis

7

In the previous chapter, we showed the inaccuracy of time-invariant methods to track rapid temporal variability of AF waveforms. Classical approaches for retrieving the frequency information from a signal are based on the estimation of its PSD. Typically, these methods are limited to stationary signals. The temporal information is lost as the frequency information assessed from the power spectrum estimates the average oscillations embedded within a signal during the study duration. When the frequency content is stable over time, no matter how long the epoch is, the signal properties remain unchanged. However, in practical applications, this assumption is rarely valid as most of the signal properties (amplitude, frequency and phase) vary over time. This issue can be circumvented by using time-varying approaches, such as time-frequency techniques. With these schemes, the energy at a given instant and frequency can be adequately estimated.

Time-frequency techniques were developed for characterizing short- and long-term AF frequency temporal variations from ECG f-waves [74]. Separate algorithms were proposed for short- and long-term analyses. The short-term scheme was specifically designed to investigate spontaneous AF frequency temporal variations in recordings of about ten seconds to several minutes. Conversely, the long-term method was elaborated for tracking temporal variations in AF frequency on recordings ranging from several minutes to hours. Their results revealed considerable temporal variations of the AF frequency.

Although time-frequency representations are aimed at analyzing the temporal evolution of the frequency content of a signal, these techniques suffer from three major drawbacks. The first one comes from the fact that time-frequency representations are estimated block-by-block. A classical approach, namely the short-term Fourier transform, consists in using a sliding window along the signal such that at each sample value a new portion of the signal is used to estimate its frequency content. The primary purpose of this sliding window is based on the assumption that the spectral characteristics of the signal are reasonably stationary over the duration of this window. The more rapidly the frequencies of the signal vary over time, the shorter the window shall be. However, as the window shortens, the frequency resolution decreases. Consequently, the choice of the window length carries an inherent trade-off between frequency resolution and time resolution. Secondly, it may be difficult to extract the instantaneous frequency from a time-frequency distribution estimation, especially in the presence of random noise. In this case, the estimation of the instantaneous frequency can be very arduous and unreliable. Additionally, in practical situations, the component corresponding to the estimated frequency is often needed, and in order to retrieve this component with time-frequency techniques, further non-trivial processing is required. Lastly, the important computational costs of time-frequency approaches are often limiting the development of applications running in real-time and on embedded devices.

These issues can be avoided by using adaptive frequency tracking algorithms. Basically, these

algorithms are composed of two elementary parts: a time-varying filter (band-pass or notch) for extracting the oscillations present in the input signal and an adaptive mechanism for controlling the central frequency of this filter and subsequently for estimating the instantaneous frequency of the extracted oscillations.

The previous chapter was focused on characterizing the harmonic structure of ECG f-waves oscillations. Specific organization indices were presented for quantifying in an ECG AF signal the harmonic content in the power spectrum (the OI) and to assess the PD between the fundamental component and its first harmonic (the TIPD). The current chapter is therefore aimed at 1) presenting a novel adaptive harmonic frequency tracking algorithm, 2) from the output of this algorithm, deriving innovative organization indices that extend the time-invariant ones, and 3) analyzing the performance of these indices in predicting the procedural outcome of catheter ablation in patients with long-standing persistent AF.

This chapter is organized as follows. Section 7.1 illustrates in details the motivations of developing an adaptive frequency tracking algorithm for characterizing the temporal evolution of the harmonic components of ECG f-waves. Then, Section 7.2 presents the adaptive frequency tracking algorithm and the derived organization indices. Section 7.3 covers the results of these organization indices in predicting the outcome of catheter ablation in patients with long-standing persistent AF. Finally, Section 7.4 covers the discussion on the results and concludes this chapter.

7.1   Motivations

In Chapter 6, the harmonic structure of an ECG atrial signal was characterized using linear, time-invariant band-pass filters centered around the peaks defining the AF DF and its harmonics. Of note, for a perfectly regular oscillation, the harmonic frequencies are exact multiples of the fundamental one, while for irregular oscillations, the expected harmonics deviate from the actual ones on a long duration signal (typically, longer than 10 seconds). If the filter is too narrow, the oscillations may escape from the filter passband, whereas a filter that is too large may render the phase estimates unreliable. Hence a compromise must be made when setting the filter bandwidth, whose reliability may be affected by the large temporal variations of AF waveforms. Figure 7.1 illustrates the limitations of using time-invariant band-pass filters as described in [59]. In this example, a 60 *sec* signal from the dorsal electrode V_{6b} of an LT patient was used. Following QRST cancellation, the power spectrum (Figure 7.1a) was estimated as in [59] (Section 6.1.1 page 56). The estimate of the fundamental frequency (red square) was found to be $f_0 = 5.6\ Hz$, and the first two harmonics (green diamonds) were located at $f_1 = 11.2\ Hz$ and $f_2 = 16.9\ Hz$. The filter response centered around f_0 is shown in red, and the filter responses centered around the harmonics are shown in green. On top of each filter the respective pass-band and stop-band limits are displayed. Figure 7.1b shows the time-frequency representation of the same 60 *sec* signal after QRST cancellation. The time-frequency was computed using the short-time Fourier transform (Hamming window of 255 samples, and a segment length of 512 samples for the discrete Fourier transform). The filter responses are plotted using the same colors as in Figure 7.1a. At each sample, the instantaneous spectrum was extracted and the new corresponding fundamental and harmonic components were estimated using the same method as in [59], i.e., the one used in Figure 7.1a. The lower yellow dots indicate the instants when at least one of the frequencies (f_0 or $f_m, m = 1, 2$) was outside of its corresponding filter. In total, this occurred 62.7% of the time, meaning that during this 60 *sec* epoch only 37.73% of the time the fundamental and harmonic components were correctly extracted by their corresponding filters. Therefore, using time-invariant band-pass filters on a long duration segment appears less accurate for extracting the AF components. However, note that these yellow segments are stable on a short duration (< than 10 *sec*), which corresponds to the analysis duration set in [59]. Figure 7.1c shows a

snapshot of the instantaneous spectrum at time $t_1 = 32.2$ *sec* when all the instantaneous frequencies were outside of their corresponding filter bandwidths. Note that the fundamental frequency as well as its harmonic are too low to be extracted by their corresponding filter. We chose to circumvent this limitation by using adaptive band-pass filters. Section 7.2 presents the adaptive scheme used in our study.

7.2 Methods

7.2.1 Adaptive frequency tracking

The harmonic frequency tracking algorithm presented in this chapter is an extension of a scheme exploited previously [75, 76], which has been originally proposed by our group [77]. First, the basic tracking scheme is briefly introduced before the extension for harmonic components is described. These adaptive algorithms are presented within the complex-valued signal framework which leads to a simplification of several computational aspects. Clearly, the ECG signals are real-valued, but the presented methods are still applicable to their analytic representation obtained with the discrete Hilbert transform [78] (see Section A.2 of Appendix A for the definition of the discrete Hilbert transform and for an introduction on the concept of instantaneous frequency). Reverting to real-value data is always possible as the real part of the analytic representation is the original signal itself.

Single frequency tracking

The single frequency tracker (SFT) is composed of two elementary parts (Figure 7.2): a time-varying band-pass filter for extracting the components and an adaptive mechanism controlling the filter.

The input signal is considered to be a noisy cisoid,

$$x[n] = c[n] + v[n] = A_0 e^{j\omega_0 n} + v[n], \qquad (7.1)$$

where A_0 and ω_0 are the complex amplitude and frequency of the cisoid, and $v[n]$ is an additive white complex centered noise. The output signal, $y[n]$, is obtained by filtering the input signal with a time-varying band-pass filter whose transfer function is given by:

$$H(z; \omega[n]) = \frac{1 - \beta}{1 - \beta e^{j\omega[n]} z^{-1}}. \qquad (7.2)$$

The parameter β ($0 \ll \beta < 1$) controls the bandwidth and $\omega[n]$ is the current estimate of the instantaneous frequency that determines the central frequency of the filter. More specifically, these parameters are respectively the modulus and argument of the pole of the transfer function. The frequency response of the filter is shown in Figure 7.3 for three values of β when the central frequency is set to $\omega[n] = 0.4\pi$. Importantly, this filter has unit gain and zero phase at $\omega[n]$ ensuring that the extracted component is not distorted.

The adaptive mechanism is based on the complex discrete oscillator equation,

$$c[n] = e^{j\omega_0} c[n - 1], \qquad (7.3)$$

which is satisfied for any cisoid at frequency ω_0. From this equation, it is possible to estimate the frequency of a noiseless cisoid with only two samples. However, in a noisy environment and if the frequency can change over time, this is not applicable. Therefore, the estimation of the instantaneous frequency is performed by minimizing the mean square error of the discrete oscillator equation (7.3) for the filtered signal, $y[n]$,

$$J[n] = \mathrm{E}\left\{ \left| y[n] - e^{j\omega[n+1]} y[n - 1] \right|^2 \right\}. \qquad (7.4)$$

(a)

(b)

(c)
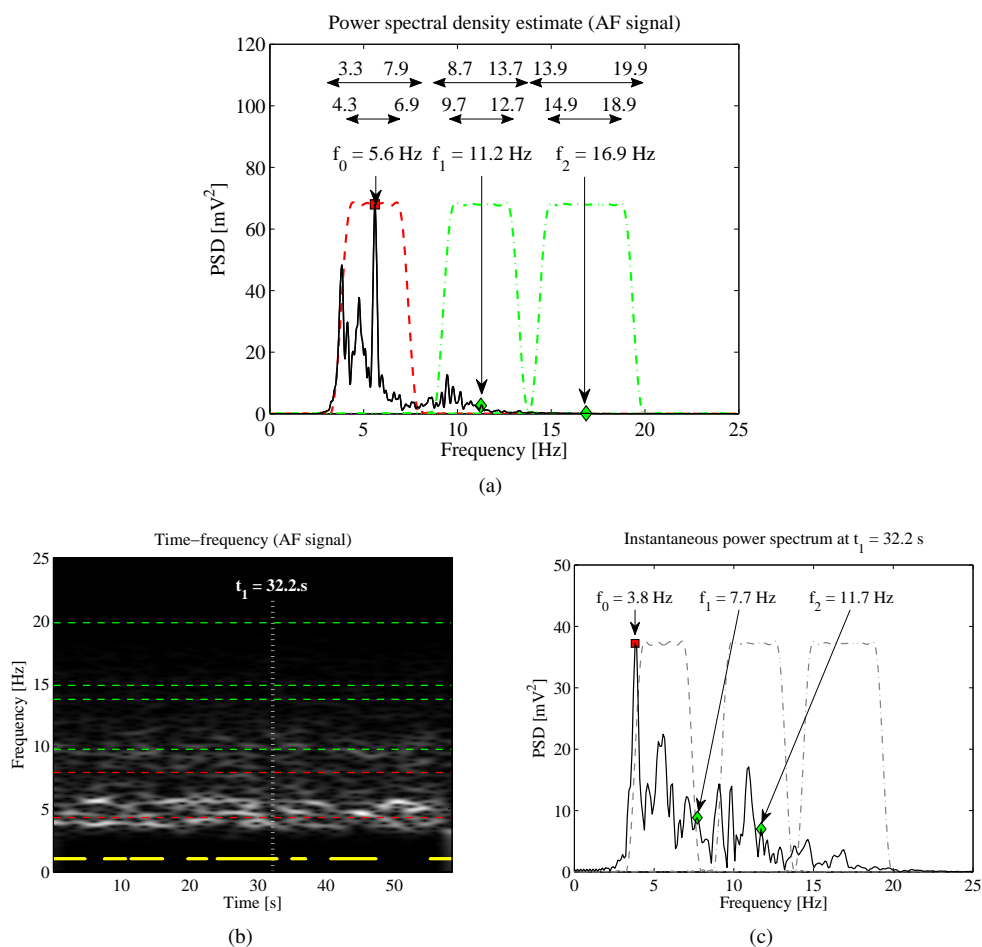
Figure 7.1: Illustration of the limitation of using linear, time-invariant band-pass filters for the extraction of AF components on a long duration epoch. Following QRST cancellation, a 60 *sec* signal from the dorsal electrode V_{6b} of an LT patient was used. Figure (a) shows the power spectrum estimate on the entire signal. The locations of the fundamental (f_0) and the first two harmonics ($f_m, m = 1, 2$) were computed as in [59]. In this example, $f_0 = 5.6$ *Hz* (red square), $f_1 = 11.2$ *Hz* and $f_2 = 16.9$ *Hz* (green diamonds). The fundamental and harmonic components are isolated by three linear, time-invariant band-pass Kaiser filters centered around the identified peaks [59]. The pass-band and stop-band are given above each filter. The filter response for isolating the fundamental component is plotted in red, while the filter responses for the harmonics are plotted in green. Figure (b) shows a time-frequency representation of the 60 *sec* signal after QRST cancellation. At each sample, the instantaneous spectrum was extracted and the corresponding fundamental and harmonic frequencies were estimated. When the new values were not fitting their initial corresponding filters, it was indicated by a yellow dot at the bottom of the time-frequency representation. In total, these excursions occurred 62.27% of the time. Figure (c) shows a snapshot of the instantaneous spectrum at time $t_1 = 32.2$ *sec* where the fundamental (red square, $f_0 = 3.8$ *Hz*) and harmonic frequencies (green diamonds, $f_1 = 7.7$ *Hz* and $f_2 = 11.7$ *Hz*) were outside of their initial corresponding filters response. In this particular case, all three frequencies are outside the initial pass-bands/stop-bands.
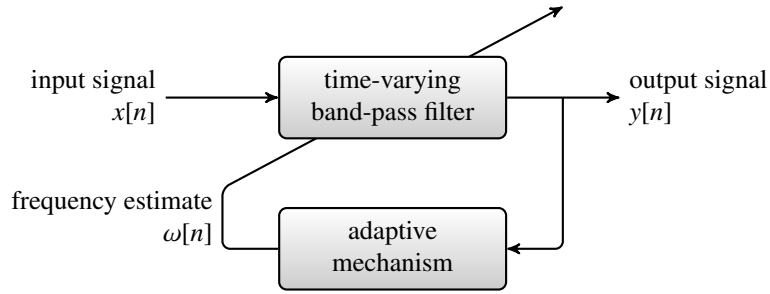
Figure 7.2: Structure of the SFT. *Figure from [77].*
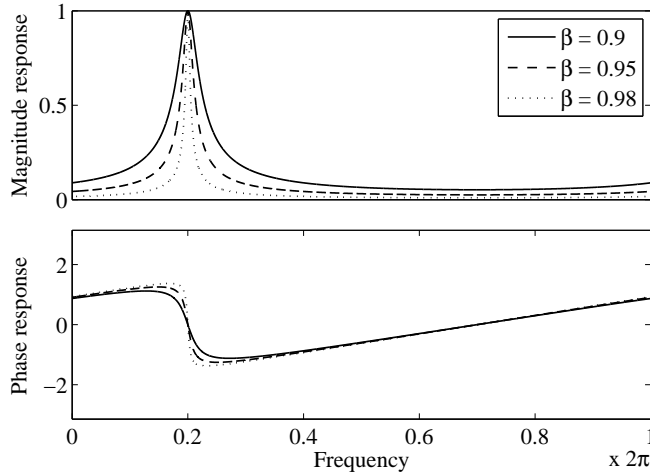
Figure 7.3: Response of the band-pass filter (7.2) for three values of β with the central frequency set to $\omega[n] = 0.4\pi$. *Figure from [77].*

The optimal solution of this cost function is obtained by setting its derivative with respect to $\omega[n + 1]$ to zero. The derivative with respect to $\omega[n + 1]$ is obtained as follows:

$$
\begin{aligned}
\frac{\partial J}{\partial \omega[n + 1]} &= \mathrm{E}\left\{ je^{-j\omega[n+1]}y[n]\bar{y}[n-1] - je^{j\omega[n+1]}\bar{y}[n]y[n-1] \right\} \\
&= je^{-j\omega[n+1]}\,\mathrm{E}\{y[n]\bar{y}[n-1]\} - je^{j\omega[n+1]}\,\mathrm{E}\{\bar{y}[n]y[n-1]\} \\
&= 2\,\mathrm{Re}\left\{ je^{-j\omega[n+1]}\,\mathrm{E}\{y[n]\bar{y}[n-1]\} \right\} \\
&= -2\,\mathrm{Im}\left\{ e^{-j\omega[n+1]}\,\mathrm{E}\{y[n]\bar{y}[n-1]\} \right\}.
\end{aligned}
\tag{7.5}
$$

where the upper bar in $\bar{y}$ denotes the complex conjugate. The optimal value for $\omega[n + 1]$ is therefore:

$$
\omega[n + 1] = \arg\{\, \mathrm{E}\{y[n]\bar{y}[n-1]\}\, \},
\tag{7.6}
$$

This solution cannot be obtained exactly in practice. Therefore, the expectation is replaced by an exponentially weighted average [79], and the adaptive mechanism is now given by

$$
Q[n] = \delta Q[n - 1] + (1 - \delta)y[n]\bar{y}[n - 1],
\tag{7.7}
$$

$$
\omega[n + 1] = \arg\{Q[n]\},
\tag{7.8}
$$

where $Q[n]$ is an internal variable and δ $(0 \ll \delta < 1)$ is a forgetting factor. The convergence rate of the SFT is directly determined by the parameter δ.

Harmonic frequency tracking

The SFT can be extended in order to estimate the instantaneous fundamental frequency and extract the harmonic components. The basic idea behind this extension is to use one time-varying band-pass filter (equation (7.2)) for the fundamental and one for each harmonic component. Therefore, each harmonic component is extracted with the same type of time-varying bandpass filter as in the SFT. An adaptive mechanism is used to estimate the fundamental frequency from all the filtered components with a weighting procedure. Finally, in order to obtain a global estimate, a linear combination is applied. The structure of the harmonic frequency tracker (HFT) is illustrated in Figure 7.4.
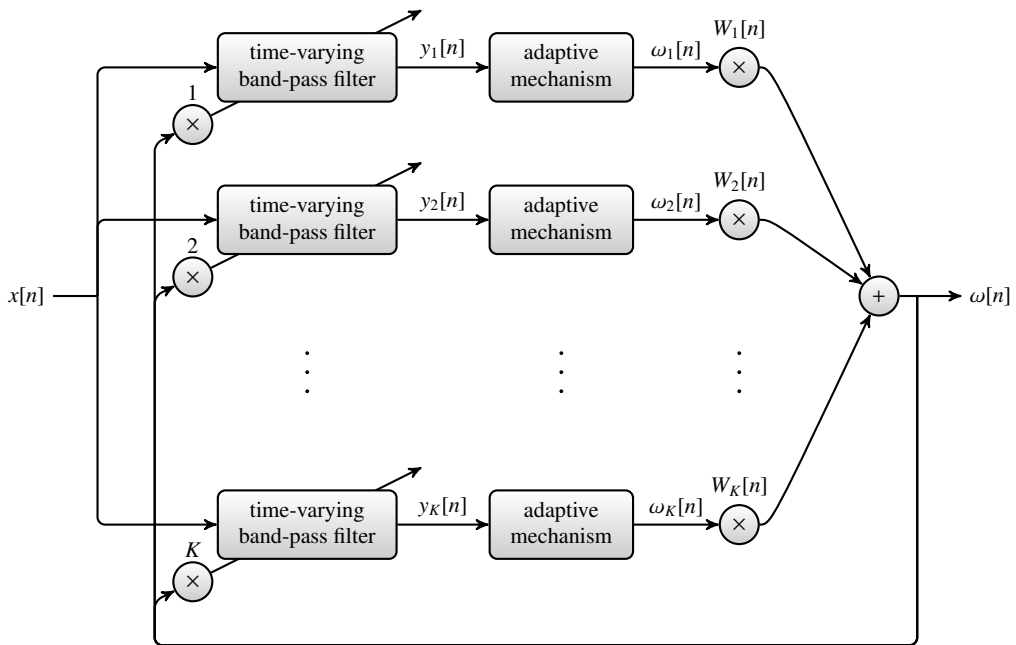
Figure 7.4: Structure of the harmonic frequency tracking algorithm. The figure shows one time-varying bandpass filter for the fundamental and one for each harmonic component; $x[n]$ is the input signal, $y_k[n]$ are the filtered output signals, and $\omega[n]$ is the estimated instantaneous frequency. The instantaneous frequency of each extracted component is estimated independently. After this, a linear combination is used to obtain a global estimate. *Figure from [77].*

In this case, the input signal is defined as:

$$x[n] = \sum_{k=1}^{K} c_k[n] + v[n] = \sum_{k=1}^{K} A_k e^{jk\omega_0} + v[n], \qquad (7.9)$$

where K is the number of harmonic components, $\{A_k\}$ their complex amplitudes, ω_0 is the fundamental frequency, and $v[n]$ is the additive complex noise. Each harmonic component, $y_k[n]$, is extracted with a band-pass filter whose central frequency is an integer multiple of the current estimate of the fundamental frequency, $k \cdot \omega[n]$, $k = 1, 2, \ldots, K$. The filtered outputs are therefore given by:

$$y_k[n] = \beta e^{jk\omega[n]} y_k[n-1] + (1-\beta)x[n], \qquad k = 1, \ldots, K. \qquad (7.10)$$

The adaptive mechanism of the HFT is more complex than the one of the SFT because in this case the instantaneous frequency is estimated from all the filtered harmonic compoments, $y_k[n]$, $k = 1, 2, \ldots, K$. First, an instantaneous estimate of the fundamental frequency is obtained for each extracted component with the same approach as in the SFT (i.e., using the oscillator-based recursion):

$$Q_k[n] = \delta Q_k[n-1] + (1-\delta) y_k[n] \bar{y}_k[n-1], \qquad k = 1, \ldots, K, \tag{7.11}$$

$$\omega_k[n+1] = \frac{\arg\{Q_k[n]\}}{k}, \qquad k = 1, \ldots, K. \tag{7.12}$$

In order to obtain a global estimate of the instantaneous fundamental frequency all the estimates are weighted. The weighting procedure favors the components for which the discrete oscillator in equation (7.3) is best satisfied [80]. The output variance is used to yield a scale-independent scheme. For this purpose, the cost function and variance of the instantaneous estimates are computed with exponentially weighted averages:

$$\hat{J}_k[n] = \delta \hat{J}_k[n-1] + (1-\delta) \left| y_k[n] - e^{jk\omega[n]} y_k[n-1] \right|^2,$$

$$\hat{S}_k[n] = \delta \hat{S}_k[n-1] + (1-\delta) \left| y_k[n] \right|^2,$$

for $k = 1, 2, \ldots, K$, where δ is the same forgetting factor as the one used in equation (7.7). Using these two equations, the weights are defined as follows,

$$W_k[n] = \frac{S_k[n]/J_k[n]}{\sum_{i=1}^{K} S_i[n]/J_i[n]}, \qquad k = 1, \ldots, K. \tag{7.13}$$

Finally, the global estimate of the instantaneous fundamental frequency is given by:

$$\omega[n+1] = \sum_{k=1}^{K} W_k[n] \omega_k[n]. \tag{7.14}$$

It is also important to mention that although the HFT algorithm was presented for all harmonic components $k = 1, 2, \ldots, K$, the tracking can also be performed on a restricted set of components. For instance, the fundamental frequency can be estimated with the 1st and 3rd harmonic component only when the signal under study has no 2nd harmonic component.

Performance analysis

The theoretical analysis of the performance of the SFT and HFT is widely detailed in the work of Van Zaen et al. [77] in which the following aspects are studied in depth: the behavior of the cost function (equation (7.4)), the frequency estimation bias and the variance of the adaptive estimates. A brief summary is provided below.

SFT In the extreme situation when the oscillation is of low amplitude compared to the noise level, the SFT is able to correctly extract the oscillation. This is mainly due to the fact that the algorithm is scale-independent. Indeed, its cost function (equation 7.4) is specifically designed to maximize the oscillatory behavior at the output, instead of, for instance, maximizing the output power. Another important aspect of the SFT is its time-varying band-pass filter (equation 7.2) which has unit gain and zero phase at the central frequency, avoiding therefore any distortion at the filtered component.

The effect of each parameter on the performance of the algorithm was substantially analyzed both through theoretical calculations and Monte Carlo simulations. In most situations, the bias is negligible, as long as the filter is correctly adjusted and its bandwidth is sufficiently narrow.

When the input signal is the analytic representation of a real signal, the discrete Hilbert transform introduces long-term correlations in the noise process which in turn induce a bias, however limited.

An important limitation has to be acknowledged. Since the SFT is an adaptive scheme, it induces an adaptation delay that depends upon the update coefficients δ and the filter bandwidth defined by β.

HFT   As for the SFT, Monte Carlo simulations were used to measure the estimation bias and variance of the HFT. The HFT is biased since the band-pass filters do not cancel the other harmonic components. However, setting the filters bandwidth sufficiently narrow ensures a negligible bias. Compared to the SFT, the HFT produces a more accurate estimate of the instantaneous fundamental frequency as additional information is contained in all harmonic components.

In this thesis, the HFT was always set to track the fundamental (i.e., the DF) and the first harmonic components, as higher harmonics in ECG atrial signals have typically a very low amplitude. In addition, the bandwidth and update parameters of this adaptive tracking scheme were set respectively to $\beta = 0.95$ and $\delta = 0.95$. Using these parameter values, the convergence time of the algorithm is less than than 50 samples for a sampling frequency of 50 Hz [77].

7.2.2   Measures of AF organization

Once the fundamental and the first harmonic components were extracted with the HFT, they were used to derive two novel measures of AF organization.

Adaptive organization index

Similarly to the OI defined in Section 6.1.1 of Chapter 6, an adaptive OI (AOI) was defined as the ratio between the power of the components (the fundamental and its first harmonic) extracted with the HFT and the total power of the input signal. The local estimates of these powers were computed by low-pass filtering the squared input and outputs with a Hamming window of length $L = 101$, to ensure a good tradeoff between temporal resolution and estimation accuracy [81]. This yielded an organization measure localized in time. Whenever a global value was needed, the local AOI was averaged over the whole signal duration.

This complexity measure quantifies the cyclicity of the oscillations of the fundamental and its first harmonic and, by definition, is bounded between zero and one. The closer to one, the more organized the atrial signal is, as most of the frequency content is concentrated in the components extracted by the HFT (fundamental and its first harmonic). Conversely, an AOI close to zero indicates that the frequency components are widely distributed across the whole spectrum of the atrial signal.

Adaptive phase difference

The two outputs of the HFT represent the harmonic components of the AF waveforms. These two signals were used to define a second organization index derived from the phase difference between harmonic components. Similarly to the TIPD presented in Section 6.1.1 of Chapter 6, an index characterizing the PD between the first harmonic and the fundamental component extracted by the HFT was estimated following the same computational steps as for the TIPD. This index was named the *adaptive PD* (aPD). For convenience, the procedure for estimating the aPD is repeated here. The PD was estimated between the first harmonic and the fundamental component extracted by the HFT, and its slope, the adaptive sPD, was locally estimated by a linear fit on centered sliding windows ($L = 101$). The aPD was defined as the variance of the adaptive sPD. The aPD characterizes the regularity of the oscillations between the components extracted by the

HFT. Small values of aPD are indicative of organized AF oscillations since they correspond to stronger couplings between the fundamental and its first harmonic.

7.2.3 Material

Synthetic signal

For illustration purposes, the complete analysis procedure (i.e., the extraction of the harmonic components with the HFT followed by the computation of organization measures) was performed on a synthetic signal inspired from [59] of duration 10 *sec* composed of two frequency-modulated harmonic components:

$$x[n] = A_1 \sin\left(2\pi f_0 n + \frac{f_d}{f_m}\cos(2\pi f_m n)\right) + A_2 \sin\left(2\pi 2 f_0 n + \frac{2f_d}{f_m}\cos(2\pi f_m n) - \frac{4\pi}{500}n\right) + v[n],$$
(7.15)

where $A_1 = 1$ and $A_2 = 0.5$ are the amplitudes, $f_0 = 8.9$ is the fundamental frequency, $f_d = 1.78$ is the frequency deviation, $f_m = 0.178$ is the frequency of the modulation, and $v[n]$ is an additive white Gaussian noise with a signal-to-noise ratio (SNR) of 10 dB. The 2nd harmonic component also included a linear phase drift.

Surface ECG

For comparison purposes, the analysis was performed on the same ECG signals as those used in the time-invariant analysis (Section 6.1.2, page 57). For convenience, they are briefly summarized here.

The analysis was performed on the DB_{full} database. Durations of 10 to 60 seconds by steps of 10 seconds were selected.

Importantly, QRST cancellation was performed as a first step (Appendix C, page 149). Once the ECG was devoid of the ventricular activity, the atrial signals were down sampled to 50 Hz [57, 64].

Finally, only the ECG precordial chest leads were included in this study (i.e., from V_1 to V_{6b}, where V_{6b} denotes the dorsal electrode, see Section 2.2.1 page 18).

7.2.4 Statistical analysis

For purposes of comparison, the statistical analysis performed in this study was the same as the one performed using the time-invariant analysis (Section 6.1.3, page 57). For convenience, this statistical analysis is briefly repeated here.

First, the distribution of the mean values at baseline of the two indices was inferred on the different epochs through the ANOVA framework (from 10 to 60 *sec*, by steps of 10 seconds). Second, the results on the longest available epoch (60 *sec*) were selected to perform an advanced statistical analysis. When the ANOVA p-value was significant for a given pair of index/lead, a binary logistic regression was applied to the corresponding index/lead values. The performance of the binary logistic regression model was evaluated using the odds ratio and its 95% confidence interval. ROC curve analysis was also performed and the AUC and YI are reported. A LOOCV was performed on the ROC curve parameters previously mentioned.

7.3   Results

7.3.1   Illustrative examples

Synthetic signal

Figure 7.5 shows the different steps of organization measurements computation on the synthetic signal defined in equation (7.15). The HFT is able to precisely estimate the instantaneous fundamental frequency and to extract the harmonic components which are later used for measuring the slope of the phase difference and its variance, the *aPD* of value $2.3 \cdot 10^{-5}$ and the AOI of value 0.7. Both aPD and AOI indicate a well-organized signal.
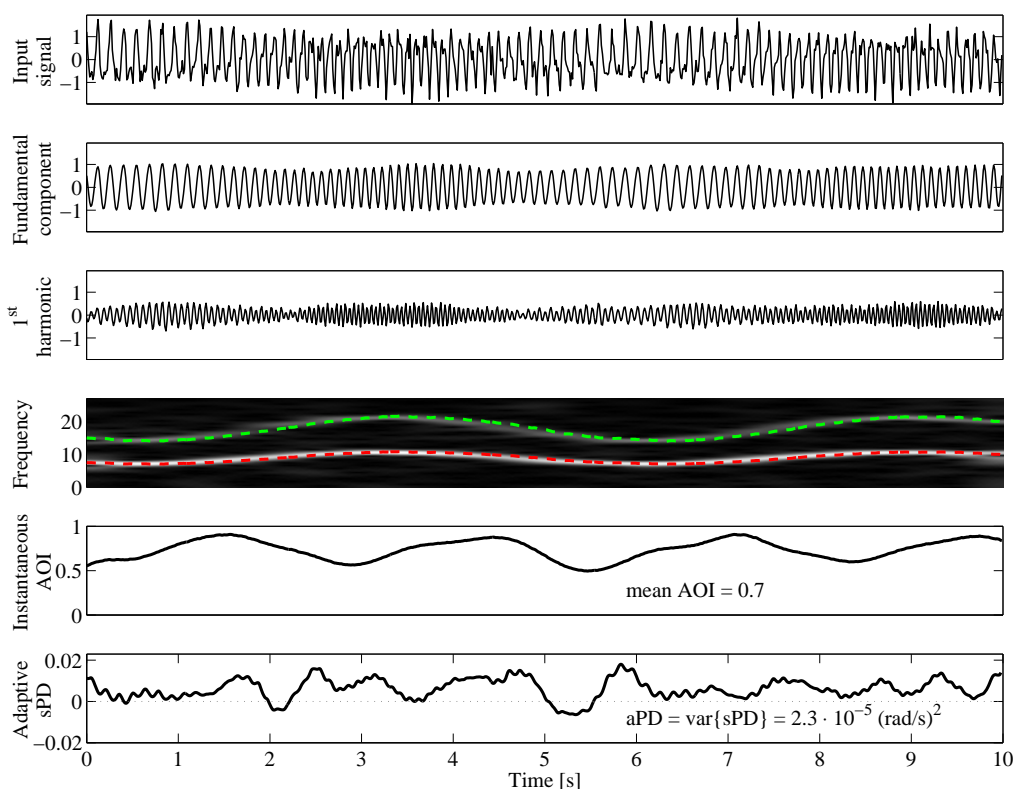
Figure 7.5: Harmonic frequency tracking example on a synthetic signal. From top to bottom, the input signal, the fundamental component, the first harmonic component, the instantaneous estimates extracted with the HFT of the fundamental and its first harmonic on top of a short-time Fourier transform of the input signal, the corresponding instantaneous AOI, and adaptive sPD. The synthetic input signal is composed of two frequency-modulated harmonic components. Both measurements of organization indicate a relatively well organized signal.

AF signals

For comparison purposes, the AF signals used here are the same as those used in the illustrative examples from the previous Chapter in Section 6.2.1, i.e., the recordings from one LT and NLT patient of 60 *sec* duration from lead V_1. After QRST cancellation, both adaptive measures of AF organization (AOI and aPD) were estimated from the outputs of the HFT.

Figure 7.6 shows a time-frequency representation (top plot) estimated from the 60 *sec* ECG from lead V_1 after QRST cancellation for the LT (Figure 7.6a) and NLT (Figure 7.6b) patients. For both figures, the time-frequency was computed using the short-term Fourier transform (255-sample Hamming window, 512-sample segment length for the discrete Fourier transform). The bandwidths of ±1 *Hz* for the OI computation (Chapter 6, Section 6.1.1) are represented by the horizontal dashed lines (red for the DF, and green for the first harmonic H_1). The instantaneous frequencies estimated with the HFT are shown in red for the DF and in green for H_1. The bottom plot displays the instantaneous AOI during the 60 *sec* epoch.

For the LT patient (Figure 7.6a), the instantaneous frequency estimates (top plot) remains stable between $t = 4.5$ and $t = 43$ *sec*. During this period, the values of the AOI (bottom plot) are larger than 0.5 (highlighted in gray), which is indicative of a high spectral concentration within the extracted components (apart for some short excerpts). Some limited excursions outside the bandwidth limits are observed at 46 *sec* matching a drop in the AOI.

The NLT patient (Figure 7.6b) displays erratic instantaneous frequencies (top plot) over time and repetitive excursions across the bandwidth limits (during the intervals [12; 17] and [36; 52.5] *sec*. Consequently, the AOI (bottom plot) remains below 0.5 during the entire recording.

(a) LT patient, $AOI = 0.7$ (b) NLT patient, $AOI = 0.35$
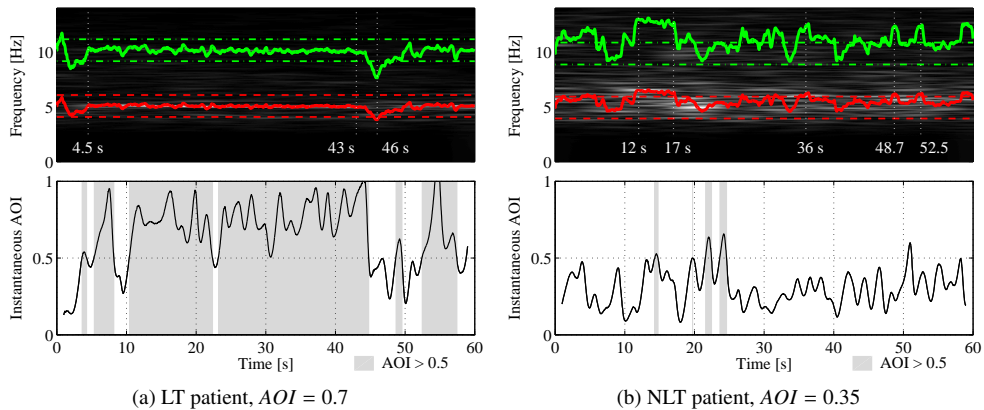
Figure 7.6: Examples of AOI index computed in an LT (a) and an NLT (b) patients. On both figures the top plot shows the time-frequency representation of V_1 after QRST cancellation. The horizontal lines denote the bandwidth for the OI computation (red for the DF, and green for the first harmonic H_1). The instantaneous frequencies estimated with the HFT are shown in red for the DF and in green for H_1. The AOI over the entire epoch is shown in the bottom plot. Periods when AOI ≥ 0.5 are emphasized in gray.

Figure 7.7 shows the adaptive sPD [1] (top plot) estimated from the outputs of the HFT. For the LT patient (Figure 7.7a), there are four periods during which a phase-lock occurred (highlighted in light gray), especially sustained between $t = 14$ and $t = 42$ *sec*. For comparison purposes, the time-invariant sPD is also plotted (dashed dot line) as well as the corresponding periods of phase-locks (dark gray). Interestingly, these periods constitute a subset of the long period of

_____
1. For the recall, the sPD corresponds to the slope of the phase difference

phase-lock observed on the adaptive sPD. The bottom plot shows an excerpt of lead V_1 (blue) and the atrial V_1 devoid of QRST (black) between seconds 30 and 50, corresponding to this long phase-lock episode. Note the regular morphology during the phase-lock observed on the adaptive sPD on the left hand side of the recording transitioning into an irregular atrial ECG pattern at the time of high adaptive sPD variations on the right hand side. The time-invariant sPD is not able to catch the time spent in phase-lock during the regular AF waveforms. Moreover, the aPD index is $10^{-3} \ (rad/s)^2$, whereas the TIPD is twice as high $2 \cdot 10^{-3} \ (rad/s)^2$ (see Chapter 6, Section 6.2.1 page 58 for the computation of the TIPD on the same atrial waveform).

For the NLT patient (Figure 7.7b) the adaptive sPD (top plot) appears erratic during the entire duration resulting in a relatively high value of $9.7 \cdot 10^{-3} \ (rad/s)^2$. Importantly, this value is much higher than that for the LT patient. The atrial ECG morphology is irregular without any apparent organization (bottom plot).

(a) LT patient, $aPD = 10^{-3} \ (rad/s)^2$.   (b) NLT patient, $aPD = 9.4 \cdot 10^{-3} \ (rad/s)^2$.
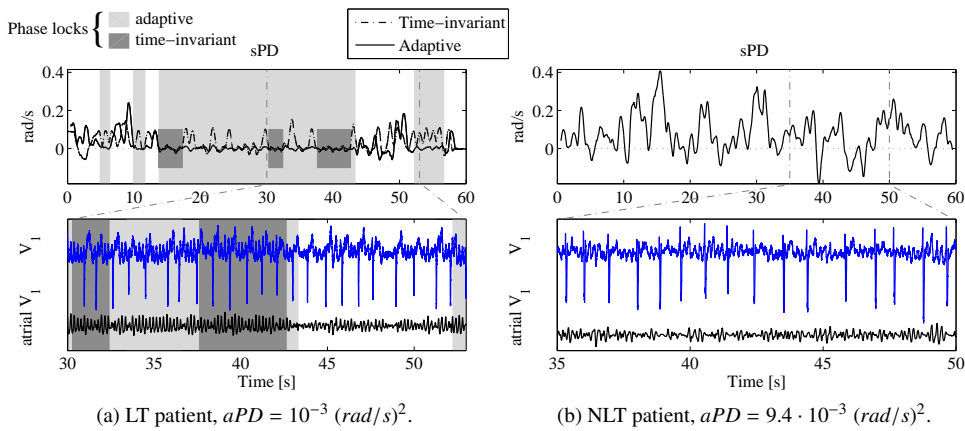
Figure 7.7: Examples of aPD index computed in an LT (a) and an NLT (b) patients. On both figures the top plot shows the adaptive sPD, and the bottom plot the corresponding input ECG signals. The blue signal corresponds to the raw ECG and the black one to the ECG after QRST cancellation. The highlights in light gray illustrate the time intervals during which a phase-lock between the fundamental and the first harmonic component extracted with the HFT occurs. For comparison purposes, the time-invariant sPD is also shown (dashed dot line) as well as its corresponding episodes of phase-locks in dark gray (see Chapter 6, Section 6.2.1 page 58 for the computation of the TIPD on the same atrial waveforms).

7.3.2   Epoch durations

Figure 7.8 shows the baseline p-values obtained when comparing LT and NLT patients for the AOI and aPD computed from all ECG chest leads (x-axis) and on the different epoch durations (y-axis). White squares denote non-significant differences between groups ($p = ns$). When the difference was found significant, the square was filled with gray shades proportional to the level of significance (from light, $p < 0.05$ to dark gray for $p < 0.001$).

AOI analysis   Figure 7.8a reports the statistical significance levels for the AOI. From chest leads V_1 to V_4, significant differences were found between LT and NLT groups on all epoch durations. Interestingly, on lead V_1, shorter durations (less than 30 *sec*, $p < 0.001$) were more discriminative than longer periods ($p < 0.005$). On leads V_2 and V_3, the statistical significance

levels were similar ($p < 0.005$, except for the 10 *sec* epoch duration on which $p < 0.01$). No significant difference was found between the groups on chest lead V_5 regardless of the epoch duration ($p = ns$). Finally, the p-values estimated on the dorsal lead V_{6b} were only significant for recording of short durations (10 and 20 *sec*, $p < 0.05$).

aPD analysis   Figure 7.8b shows the p-values estimated for the aPD. Lead V_1 displayed significant p-values on epochs from 20 to 60 *sec* ($p < 0.05$). For chest leads V_2, V_3, and V_5 and on all epoch durations, no significant difference were observed between the groups ($p = ns$). Lead V_4 showed significant p-values on epochs from 40 to 60 *sec* ($p < 0.05$). Finally, on all epoch durations, only chest lead V_{6b} showed a significant difference between groups with a stronger discrimination on 20 and 60 *sec* epochs for which $p < 0.005$.
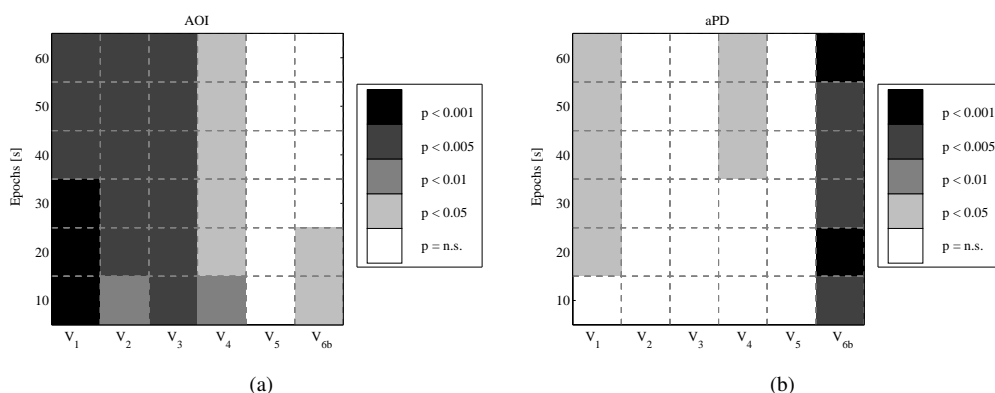
Figure 7.8: Statistical significance levels for all epochs durations (*y*-axis) and chest leads (*x*-axis) for AOI (a), and aPD (b). White squares denote non-significant differences between groups ($p = ns$). When the difference was significant, the corresponding square was filled with gray, from light (less significant, $p < 0.05$) to dark (most significant, $p < 0.001$).

7.3.3   Group comparisons on the procedural outcome

Figure 7.9 reports the distribution of AOI (a) and aPD (b) on all chest leads for the LT (blue) and NLT (red) groups. Mean and median values are displayed as circle and square respectively. The vertical lines indicate ± one standard deviation. ANOVA was used to determine significant differences between groups. The following annotations were used for the different level of significance: $*$: $p < 0.05$, $**$: $p < 0.01$, † : $p < 0.005$ and ‡ : $p < 0.001$.

AOI analysis   The AOI (Figure 7.9a and left column of Table 7.1) computed on leads V_1, V_2, V_3 and V_4 revealed a significantly higher organization for the LT group than for the NLT one. On the remaining leads the mean AOI was also higher for the LT group, but non-significantly. More specifically, the significance level between groups was higher on leads V_1, V_2 and V_3 ($p < 0.005$), than on V_4 ($p < 0.05$). Interestingly, among all significant leads in the LT group, V_1 displayed the highest organization with an average AOI of 0.45 ± 0.08, while on leads V_2, V_3 and V_4 the average was lower (0.36 ± 0.05, 0.34 ± 0.04 and 0.32 ± 0.05 respectively).

The binary logistic parameters estimated for all the significant leads are reported in Table 7.2. Importantly, the odds ratio on all four leads was greater than one, which is indicative that the AOI
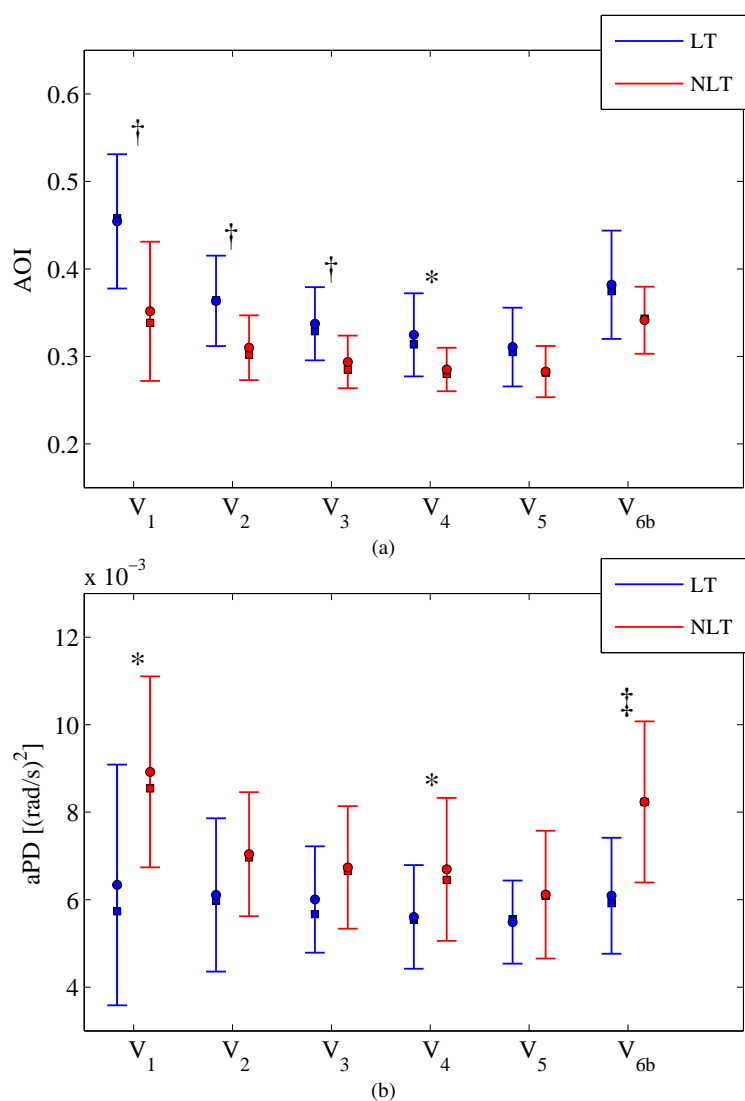
Figure 7.9: Distributions of the baseline AOI (a) and aPD (b) for the LT (blue) and NLT (red) groups computed on 60 *sec* epochs. The mean (circle) as well as the median (square) of each group are shown. The vertical lines delimit one standard deviation. The following annotations were used for the different level of significance: $* : p < 0.05$, $** : p < 0.01$, $† : p < 0.005$ and $‡ : p < 0.001$.

on these specific leads was a strong predictor of AF termination. More specifically, the narrowest associated 95% confidence interval and lowest p-value were found on lead V_1, which is indicative of a more reliable precision of the odds ratio for this lead ($[1.0538 - 1.4011]$ with $p < 0.01$ for V_1, compared to $[1.0589 - 1.646]$ with $p < 0.05$ for V_2, $[1.0772 - 1.9291]$ with $p < 0.05$ for V_3, and $[1.036 - 1.8852]$ with $p < 0.05$ for V_4). The odds ratio was, however, lower on V_1 compared to the remaining leads (1.2151 for V_1, 1.3202 for V_2, 1.4415 for V_3, and 1.3975 for V_4). But keeping in mind that the associated 95% confidence interval and p-values were lower on V_1, we can state with confidence that the AOI computed on V_1 was the most effective in predicting AF termination among the four significant leads.

Lead	AOI		aPD $[\cdot 10^{-3}(rad/s)^2]$	
	LT	NLT	LT	NLT
$\mathbf{V_1}$	0.45 ±0.08 (0.46)	0.35 ±0.08 † (0.34)	6.34 ±2.75 (5.74)	8.92 ±2.18 * (8.54)
$\mathbf{V_2}$	0.36 ±0.05 (0.36)	0.31 ±0.04 † (0.3)	6.11 ±1.75 (5.97)	7.04 1.42 (6.97)
$\mathbf{V_3}$	0.34 ±0.04 (0.33)	0.29 ±0.03 † (0.29)	6 ±1.22 (5.67)	6.74 ±1.4 (6.65)
$\mathbf{V_4}$	0.32 ±0.05 (0.31)	0.28 ±0.02 * (0.28)	5.61 ±1.18 (5.55)	6.69 ±1.63 * (6.45)
$\mathbf{V_5}$	0.31 ±0.04 (0.31)	0.28 ±0.03 (0.28)	5.49 ±0.95 (5.55)	6.12 ±1.46 (6.09)
$\mathbf{V_{6b}}$	0.38 ±0.06 (0.37)	0.34 ±0.04 (0.34)	6.09 ±1.32 (5.91)	8.23 ±1.84 ‡ (8.23)

Table 7.1: Mean ± standard deviations and median (in brackets) of the AOI (left column) and aPD (right column) before ablation computed on epochs of duration 60 *sec*. The following annotations were used for the different level of significance: $*$: $p < 0.05$, $**$: $p < 0.01$, † : $p < 0.005$ and ‡ : $p < 0.001$.

Figure 7.10 shows the ROC curves estimated for leads V_1 (Figure (a)), V_2 (Figure (b)), V_3 (Figure (c)) and V_4 (Figure (d)) while Tables 7.3a and 7.3b report the values of the estimated AUCs and YIs as well as the results of the LOOCV respectively. Among the four leads, the highest AUC was obtained on V_1 (0.86 for V_1 compared to 0.81 for the remaining leads). Similarly, the maximum YI was estimated on lead V_1 (0.69 with 78% sensitivity and 91% specificity on V_1, as compared to 0.5 with 50% sensitivity and 100% specificity for V_2, 0.6 with 78% sensitivity and 82% specificity for V_3, and 0.64 with 82% sensitivity and 82% specificity for V_4). Interestingly, the cut-off value for separating LT from NLT patients was higher on lead V_1 (0.43) as compared to the cut-off values on the remaining leads (0.32). All the obtained estimates were corroborated by the LOOCV in terms of average values and low standard deviations. These results suggest a better classification performance for lead V_1 than for leads V_2, V_3, and V_4.

aPD analysis The aPD values (Figure 7.9 and right column of Table 7.1) computed on leads V_1, V_4, and V_{6b} were significantly lower for the LT patients than that for the NLT patients, which is suggestive of a higher coupling between the fundamental and the first harmonic extracted with the HFT for the first group. The overlap between the groups is, however, less important on the dorsal lead V_{6b} leading to a higher significance level on this lead than on the other two ($p < 0.001$ for V_{6b} vs. $p < 0.05$ for V_1 and V_4). Interestingly, on lead V_1 the average aPD for the LT group was significantly lower than for the NLT group. For both groups the standard deviations were rather large (($6.34 \pm 2.75) \cdot 10^{-3}$ $(rad/s)^2$ for the LT group and $(8.92 \pm 2.18) \cdot 10^{-3}$ $(rad/s)^2$ for the NLT group, $p < 0.05$). On the dorsal lead V_{6b} the average aPD for the NLT patients was significantly higher than that for the LT patients suggestive of a larger degree of disorganization (($8.23 \pm 1.84) \cdot 10^{-3}$ $(rad/s)^2$ compared to $(6.09 \pm 1.32) \cdot 10^{-3}$ $(rad/s)^2$ for the LT group, $p < 0.001$). One can also observe that, for the NLT patients, the average aPD on leads V_1 and V_{6b} were similar. On the remaining leads V_2, V_3, and V_5, no significant difference was observed between the groups ($p = ns$).

The binary logistic parameters estimated for leads V_1, V_4, and V_{6b} are reported in Table 7.2. On the three leads, the odds ratio are slightly smaller than one, with a maximum value on lead V_1 (0.96234 for V_1 compared to 0.94307 for V_4 and 0.90853 for V_{6b}). Reciprocally, the associated 95% confidence interval is narrower on chest lead V_1 ([$0.93002 - 0.99578$] as compared to [$0.88988 - 0.99944$] for V_4 and [$0.84548 - 0.97627$] for V_{6b}). The related p-values indicated the most significant level on the dorsal lead V_{6b} on which $p < 0.01$, while on V_1 and V_4 $p < 0.05$.

Figure 7.11 shows the ROC curves estimated for leads V_1 (Figure (a)), V_4 (Figure (b)) and V_{6b} (Figure (c)) while Tables 7.3a and 7.3b report the values of the estimated AUCs and YIs as well as the results of the LOOCV respectively. ROC curves parameters were similar for leads V_1 and V_{6b} but differed for lead V_4. AUCs estimated on leads V_1 and V_{6b} were similar (for the dorsal lead V_{6b} the AUC was estimated to 84, while on V_1 to 0.82). Conversely, the YI was slightly larger on lead V_1 as compared to lead V_{6b} (0.69 with 77% sensitivity and 91% specificity for V_1 vs. 0.63 with 90% sensitivity and 73% specificity for V_{6b}). The cut-off value for separating LT patients from NLT patients was similar on these two leads ($\approx 7.5 \cdot 10^{-3}$ $(rad/s)^2$). Finally, lead V_4 showed lower classification performance, with a AUC of 0.69 and an YI of 0.37 with 82% sensitivity and 55% specificity. Compared to V_1 and V_{6b}, the cut-off value was lower on V_4, i.e., $6.45 \cdot 10^{-3}$ $(rad/s)^2$. Finally, the values of the parameters estimated from ROC curves were corroborated by the respective average estimates from the LOOCV, except for the cut-off threshold on V_4, for which the LOOCV indicated an average cut-off larger than the one estimated from the ROC curve analysis.

Lead	Index	Odds ratio	95% confidence interval	p-value
V_1	AOI	1.2151	$[1.0538 - 1.4011]$	0.0073402
	aPD	0.96234	$[0.93002 - 0.99578]$	0.027617
V_2	AOI	1.3202	$[1.0589 - 1.646]$	0.013558
V_3	AOI	1.4415	$[1.0772 - 1.9291]$	0.013884
V_4	AOI	1.3975	$[1.036 - 1.8852]$	0.028414
	aPD	0.94307	$[0.88988 - 0.99944]$	0.047826
V_{6b}	aPD	0.90853	$[0.84548 - 0.97627]$	0.0089364

Table 7.2: Binary logistic regression parameters of the AOI and aPD indices/leads before ablation computed on 60 *sec* epochs. The binary logistic model was estimated when ANOVA declared a significant difference for a pair of index/lead. The table reports the corresponding odds ratio, its 95% confidence interval and associated p-value.
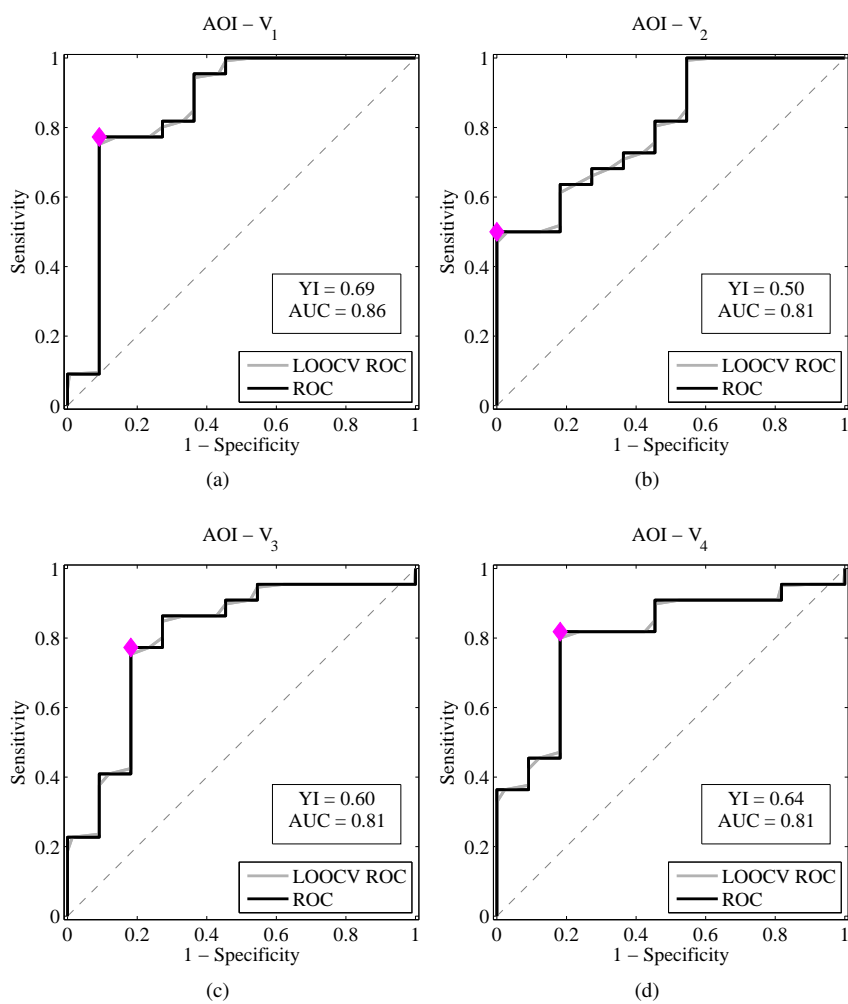
Figure 7.10: ROC curves (black) for the AOI on lead V_1 (a), V_2 (b), V_3 (c), and V_4 (d) assessed on recordings of 60 *sec* duration. The corresponding estimated AUCs and YI (pink) estimated from the ROC curves are also reported. The average LOOCV ROC curve is plotted in gray.
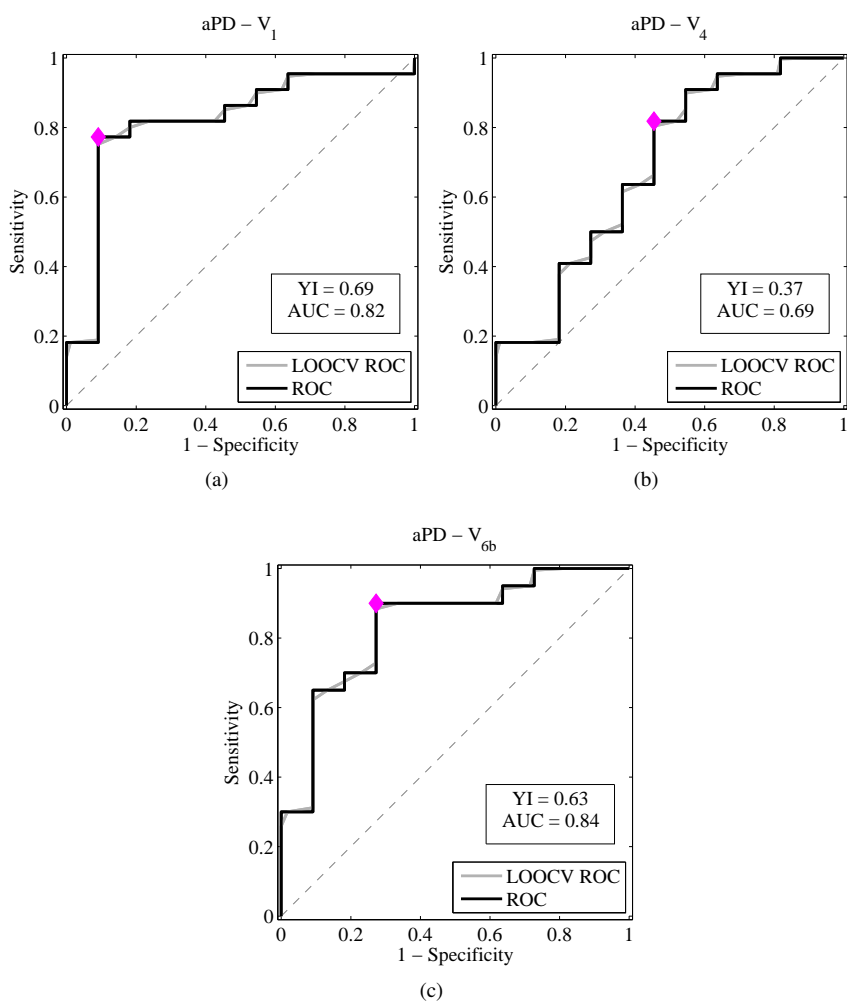
Figure 7.11: ROC curves (black) for the aPD on lead V_1 (a), V_4 (b), and V_{6b} (c) assessed on recordings of 60 *sec* duration. The corresponding estimated AUCs and YI (pink) estimated from the ROC curves are also reported. The average LOOCV ROC curve is plotted in gray.

Lead	Index	AUC	Youden index			
			Cut-off	Value	Sensitivity	Specificity
V_1	**AOI**	0.86	0.43	0.69	0.77	0.91
	aPD	0.82	$7.55 \cdot 10^{-3}\ [(rad/s)^2]$	0.69	0.77	0.91
V_2	**AOI**	0.81	0.32	0.5	0.5	1
V_3	**AOI**	0.81	0.33	0.6	0.78	0.82
V_4	**AOI**	0.81	0.32	0.64	0.82	0.82
	aPD	0.69	$6.45 \cdot 10^{-3}\ [(rad/s)^2]$	0.37	0.82	0.55
V_{6b}	**aPD**	0.84	$7.52 \cdot 10^{-3}\ [(rad/s)^2]$	0.63	0.9	0.73

(a)

Lead	Index	LOOCV		
		AUC	Cut-off	Youden index
V_1	**AOI**	0.86 ± 0.02	0.43 ± 0.01	0.68 ± 0.02
	aPD	0.82 ± 0.02	$(7.56 \pm 2.56 \cdot 10^{-2}) \cdot 10^{-3}\ [(rad/s)^2]$	0.68 ± 0.02
V_2	**AOI**	0.81 ± 0.01	0.32 ± 0.01	0.5 ± 0.02
V_3	**AOI**	0.81 ± 0.02	0.33 ± 0.01	0.6 ± 0.03
V_4	**AOI**	0.8 ± 0.02	0.32 ± 0.01	0.64 ± 0.03
	aPD	0.69 ± 0.02	$(6.99 \pm 0.39) \cdot 10^{-3}\ [(rad/s)^2]$	0.37 ± 0.03
V_{6b}	**aPD**	0.84 ± 0.01	$(7.53 \pm 2.14 \cdot 10^{-2}) \cdot 10^{-3}\ [(rad/s)^2]$	0.63 ± 0.03

(b)

Table 7.3: ROC (a) and LOOCV (b) estimations for the AOI and aPD assessed on epochs of 60 *sec* duration. Results are reported for the leads which were declared significant through the ANOVA framework: leads V_1, V_2, V_3 and V_4 for the AOI and leads V_1, V_4 and V_{6b} for the aPD. Table (a) reports the estimation from the ROC curve of the AUCs, YIs with respective sensitivities/specificities as well as the cut-off thresholds for discriminating LT patients from NLT patients. Table (b) reports the average AUCs, YIs and cut-off values assessed with LOOCV.

7.4   Discussion

In this chapter, an adaptive algorithm for extracting the harmonic components of ECG f-waves was presented. The adaptive algorithm takes as input the ECG signal devoid of ventricular activity and outputs two signals corresponding to the fundamental and first harmonic components of the AF signal. From these outputs, two novel organization indices were estimated. The first one, the AOI, quantifies the cyclicity of the oscillations of the harmonic components over time. The second one, the aPD, quantifies the regularity of the PD between the harmonic components, and is an indicator of the f-waves morphological regularity.

7.4.1   Relevance of the epochs durations

In this study, we found that the AOI yielded a better separation between LT and NLT groups on shorter epoch durations. Significant differences on segments of duration ≤ 20 *sec* were observed on all chest leads except for V_5. Among the significant leads, V_1 showed the highest level of significance. For longer epochs, significant differences were observed on chest leads V_1 to V_4. Interestingly, the aPD yielded more discriminative p-values between the two groups on longer epoch durations. On segments of duration ≥ 40 *sec*, the average aPD was statistically different between LT and NLT patients on leads V_1, V_4, and V_{6b}. Among these leads, the highest level of significance was observed on the dorsal lead V_{6b}.

Thus, the AOI was statistically more robust on shorter epochs, in particular on lead V_1. Conversely, the aPD was statistically stronger on longer epochs, notably on the dorsal lead V_{6b}. In terms of the relevance of the epochs duration, these two indices appear complementary.

7.4.2   Prediction of the procedural outcome before ablation

Other studies based on time domain analysis have shown that the procedural outcome of AF catheter ablation can be predicted from the analysis of f-wave amplitude [82, 83]. Nault et al. manually performed their analysis on individual leads; f-waves amplitudes were correlated to clinical and echocardiographic variables and to ablation outcome [82]. The best correlation accuracy was obtained using ECG electrodes V_1 and *II*. High f-wave amplitude was shown to be predictive of procedural termination. However, manual analysis carries an important limitation due to operator's subjectivity. Meo et al. used an automatic method taking into account the inter-variability between ECG leads [83]. They found that a large spatial diversity is present in surface ECG signals and that exploiting this feature increases the predictive power of the amplitude parameter.

In our study, the AOI showed a significant higher organization on leads V_1 to V_4 in patients with AF termination compared to patients whose AF did not terminate. More specifically, the best statistical performance of the AOI was achieved on chest lead V_1. The discriminative cut-off value was the highest on this lead compared to the remaining ECG electrodes. The aPD was significantly lower on leads V_1, V_4, and V_{6b} for the LT group compared to NLT patients. These results also suggest that LT patients had a higher organization on these specific ECG leads as compared to NLT patients. The highest statistical performance was achieved on leads V_1 and V_{6b}, with a better discriminative power on the dorsal lead. Importantly, the aPD cut-off values on leads V_1 and V_{6b} were lower than on lead V_4.

7.4.3   Comparison with time-invariant approaches

In the previous chapter, organization indices derived from time-invariant approaches for characterizing the harmonic structure of the ECG f-waves were presented. The discussion below is aimed at comparing the performance in predicting the procedural outcome of these time-invariant measures with that of the adaptive indices presented the current chapter. A summary of the predictive power of the organization indices on the ECG precordial chest leads is provided in Table 7.4 in which the comparison has been separated in short epochs (≤ 30 *sec*) and long epochs (≥ 30 *sec*) durations. For each table cell, the indices are ordered from more predictive (top) to less predictive (bottom).

AOI vs. OI   The OI was not predictive of the outcome of catheter ablation, regardless of the ECG leads and epochs duration. The results were in contradiction with those obtained with the other organization indices since the average OI indicated a tendency of higher organization in NLT patients than in the LT one. On the opposite, the AOI showed on several ECG leads a significant higher organization in LT patients than in the NLT ones. Clearly, the AOI outperformed the OI for predicting the procedural outcome of catheter ablation in long-standing persistent AF.

aPD vs. TIPD   The computational steps for deriving an organization index based on the PD between the harmonic components were the same for the aPD and TIPD indices. These measures were defined as the variance of the slope of the PD between the fundamental component and its first harmonic. The prominent difference between these two indices resided in the schemes for extracting the harmonic components from the ECG f-waves. On one hand, the TIPD was assessed on the harmonic components extracted with linear, time-invariant filters. On the other hand, the aPD was computed on the harmonic components extracted with the adaptive HFT algorithm. The illustrative examples showed that the adaptive slope of the PD detected longer periods of phase-locks than the PD slope estimated between the harmonic components extracted with the time-invariant approach. The periods of phase-locks assessed with the latter scheme were actually a subset of the phase-locks periods computed on the components extracted by the adaptive HFT. Moreover, on shorter epochs durations (≤ 30 *sec*) the average TIPD and aPD were statistically different between the two groups on leads V_1 and V_{6b} (except for the aPD on V_1 for a duration of 10 *sec* on which $p = ns$). On lead V_1, for these epoch durations the level of statistical significance was slightly higher for the TIPD than for the aPD. On the dorsal lead V_{6b}, however, the p-values were similar for the TIPD and aPD (except for a duration of 20 *sec* for which the p-value was lower for the aPD than for the TIPD). On longer epoch durations (≥ 40 *sec*), the average aPD was statistically different between the two groups on leads V_1, V_4 and V_{6b} whereas the average TIPD was discriminative on leads V_1 and V_{6b}. For these durations, the levels of significance were slightly better on lead V_1 for the TIPD, while on the dorsal lead V_{6b} the aPD was more discriminative. On 60 *sec* epochs, the performance of the binary logistic regression as well as the ROC parameters on leads V_1 and V_{6b} were better for the aPD than for the TIPD, in particular on the dorsal lead V_{6b}.
Taking all these results together, the PD assessed between the harmonic components extracted with the adaptive algorithm is more appropriate than the time-invariant one for predicting the ablation outcome in patients with long-standing persistent AF, in particular on long epochs duration and using a dorsal ECG lead.

	ECG leads					
	V_1	V_2	V_3	V_4	V_5	V_{6b}
Short epochs durations ($\leq$ 30 sec)	AOI TIPD aPD	AOI	AOI	AOI		aPD TIPD AOI
Long epochs durations ($\geq$ 30 sec)	AOI TIPD aPD	AOI	AOI	AOI aPD		aPD TIPD

Table 7.4: The predictive power of catheter ablation outcome of the equivalent indices derived from the time-invariant approach (OI and TIPD) and the adaptive scheme (AOI and aPD) are compared on all ECG precordial chest leads. The comparison has been separated in short epochs ($\leq$ 30 *sec*) and long epochs ($\geq$ 30 *sec*) durations. For each table cell, the indices are ordered from more predictive (top) to less predictive (bottom).

7.4.4 Conclusion

As ECG f-waves rapidly vary over time, the ability of classical organization indices to track these variations and detect potential differences between patients appears limited. The organization indices derived from the adaptive algorithm presented in the current chapter are more suitable for characterizing the temporal evolution of the harmonic components of ECG f-waves. The AOI and aPD are complementary indices in terms of temporal and spatial performance. Indeed, the AOI is statistically more robust on shorter epochs and on lead V_1, while the aPD is statistically more powerful on longer epochs and on the dorsal lead V_{6b}.

After cancellation of the ventricular activity, the ECG f-waves reflect the global activity of the atria. It has been observed separately for the DF, TIPD, AOI and aPD that the respective cut-off values estimated for discriminating LT patients from NLT ones were not the same on all ECG leads. Each ECG lead is positioned at a specific location on the patient's thorax (or in the back in the case of V_{6b}). Hence, each ECG electrode is facing different parts of the left and right atria. These observations suggest that the different amount of organization assessed by the various organization indices computed from ECG leads are indicative of a heterogeneous organization within both atria. Therefore, it would be of relevant information to correlate the global activity assessed from the ECG with the activity measured inside the atria. This analysis is performed in the next part of this manuscript.

Part IV

Intracardiac Signal Processing

Dominant Frequency Analysis

8

During AF, the intracardiac signals display complex and variable patterns. Time-invariant spectral techniques have been widely used to characterize the periodic components embedded into these complex signals. Similarly to ECG analysis, power spectral analysis is the most extensively used approach to estimate the frequency of AF. The frequency corresponding to the peak of highest amplitude is defined as the DF. The DF computed from intracardiac signals has been used as an estimate of the local atrial activation rate. In Chapters 6 and 7, we showed that the frequency content of AF ECG signals is characterized by important temporal variations, and that classical time-invariant approaches are not suitable for tracking these variations. Hence, in this chapter, a new time-varying approach for estimating the intracardiac instantaneous frequency is proposed.

Several studies have shown that AF waves in ECG chest lead V_1 adequately reflect the RAA activity during AF [16, 20, 55, 57, 58, 65, 84–86]. During this thesis, we had the unique opportunity to extend these results by analyzing the contribution of the LAA and CS in addition to the RAA, to the frequency content of the AF waves of ECG chest leads before ablation of long-standing persistent AF. These contributions were investigated using time-invariant and time-varying techniques.

Many electrophysiological studies have used the DF of intracardiac recordings as a tool for understanding the pathophysiology and dynamics of AF in humans [13, 14, 87, 88]. One such approach has been to map the activation rates in the frequency domain throughout the atria. Most of these studies have used the DF in order to assess the change of AF dynamics during catheter ablation and it was observed that a decrease in intracardiac DF was associated with AF termination [67, 89, 90]. Lazar et al. observed that a left-to-right atrial frequency gradient was present in patients with paroxysmal AF, but not in patients with persistent AF [91]. To the best of our knowledge, very few studies investigated the baseline distribution of the DF as a tool for predicting procedural outcome [90, 92]. Thus, we aimed at studying the distribution of the baseline DFs assessed in several atrial segments prior to ablation for patients with long-standing persistent AF.

This chapter is organized as follows. In Section 8.1, the classical time-invariant approach for DF estimation is presented as well as a novel time-varying scheme for estimating the instantaneous DF. Then, in Section 8.2, the correlation between ECG and intracardiac DFs is investigated. Finally, in Section 8.3, the distribution of baseline DFs is presented.

8.1   Estimation of the intracardiac dominant frequency

8.1.1   Time-invariant approach

The following time-invariant spectral analysis was performed in order to estimate the intracardiac dominant frequency from the bipolar EGMs [93]. In the first step, the EGMs were rectified (i.e., the absolute value of the signal was computed). Signal rectification is a crucial step because all biphasic waveforms are transformed to monophasic waveforms, making the peaks and deflections after rectification closer to sinusoids [94]. Then, a band-pass Butterworth filter with bandwidth $[1-20]$ Hz was applied to the rectified signal in order to ensure that the estimated frequencies lie within an admissible physiological range. Frequency spectra were estimated using fast Fourier transform. Finally, the intracardiac DF was defined as the highest peak within the power spectrum between $[3-15]$ Hz.

8.1.2   Time-varying approach

The signal processing steps for computing the instantaneous frequency of intracardiac EGMs are described here. In the first step, the local activation time (LAT) was defined as the time of the maximum positive peak of each detected activation wave using sliding windows of 150 ms. False detections were removed using temporal and amplitude thresholding. The upper plot in Figure 8.1 illustrates a 20 sec epoch acquired from the HRA_d dipole placed within the RAA in an LT patient with its detected LATs (red dot). The bottom plot shows an excerpt of two seconds.
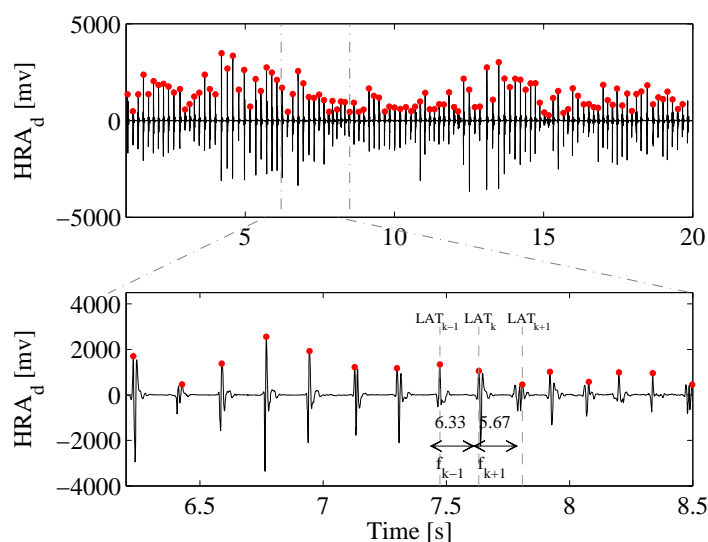
Figure 8.1: Intracardiac LATs and instantaneous frequencies. The top plot illustrates a 20 sec epoch acquired from the HRA_d dipole placed within the RAA in an LT patient with its detected LATs (red dots). The bottom plot shows an excerpt of two seconds. The numbers displayed between consecutive LATs indicate the corresponding instantaneous frequencies in Hz.

Let LAT_{k-1}, LAT_k, and LAT_{k+1} be three consecutive LATs in a given signal with a total of $k = 2, \cdots, N - 1$ LATs, as illustrated in the bottom plot of Figure 8.1. We denoted $f_{k-1} = 1/(LAT_k - LAT_{k-1})$ as the instantaneous frequency between LAT_k and LAT_{k-1}. Likewise, $f_{k+1} = 1/(LAT_{k+1} - LAT_k)$ was set as the instantaneous frequency between LAT_{k+1} and LAT_k. As displayed in the bottom plot of Figure 8.1, $f_{k-1} = 6.33\ Hz$ and $f_{k+1} = 5.67\ Hz$.

The following set of data points was defined (Figure 8.2, bottom plot):

$$\begin{cases} x_k = \text{LAT}_k, \\ y_k = (f_{k+1} + f_{k-1})/2 \end{cases} \tag{8.1}$$

where $k = 2, \cdots, N - 1$. The instantaneous frequency (f_{inst}) was defined as the cubic interpolation of these data points at a sampling frequency of 50 Hz. The top plot of Figure 8.2 shows the f_{inst} computed for the intracardiac signal shown in Figure 8.1.
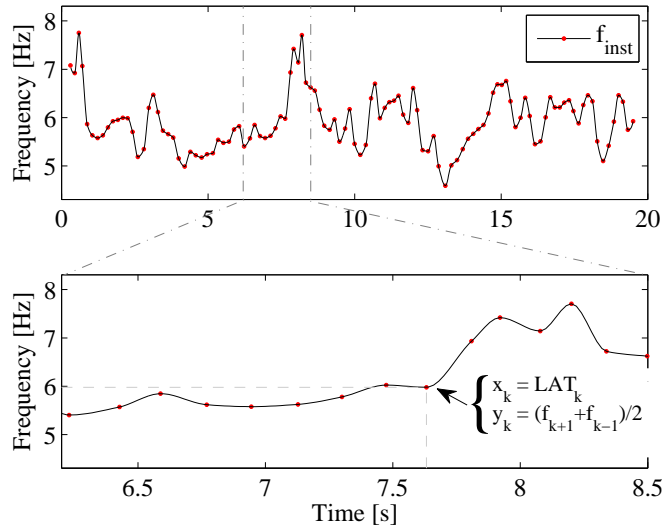
Figure 8.2: Example of an intracardiac instantaneous frequency signal, f_{inst} estimated from the signal displayed in Figure 8.1.

8.2 Intracardiac contribution to ECG fibrillation waves

8.2.1 Methods

Time-invariant approach

Synchronous baseline recordings from the RAA, LAA and CS were used (see Section 5.2.3 at page 47 of Chapter 5 for further details of the study protocol). For convenience, the data recording setup is briefly repeated here [1]:

1. the Lasso catheter was placed within the LAA for a duration of 20 *sec*.

2. the HRA catheter was placed within the RAA during the entire procedure. In this study, the distal bipolar EGM was considered.

3. the CS-cath was placed within the CS during the entire ablation procedure, with the proximal electrode CS_{9-10} placed at the ostium. All five bipolar EGMs were further analyzed.

The DF of each atrial location was computed using the time-invariant approach presented in Section 8.1.1. The epoch duration of the study was set to 10 *sec*. Synchronous recordings were considered for this analysis, and when more than two epochs of 10 *sec* were available for a particular patient, the intracardiac DF was temporarily averaged. For the Lasso, when the DF was computed on more than one dipole, the DF was spatially averaged.

The ECG DF was also estimated from the synchronous epochs corresponding to the intracardiac acquisitions. The method for computing the ECG DF has been presented in Section 6.1.1. In short, the frequency spectra from all chest leads were computed from the ECG signals after QRST subtraction and the DF was estimated as the frequency of the highest peak between 3 and 20 Hz in the PSD estimate for each lead. The ECG DF was then averaged for each patient on all available epochs.

The relation between surface ECG and intracardiac baseline DFs was investigated using Pearson's correlation coefficients, which were computed between each combination of ECG chest leads and intracardiac bipolar EGMs, between each combination of ECG chest leads (i.e., V_1 with the remaining ECG leads, V_2 with the remaining ECG leads, etc...), and finally between each combination of bipolar EGMs (i.e., averaged LAA with RAA as well as all CS bipolar EGMs, and RAA with all CS bipolar EGMs).

Time-varying approach

The intracardiac instantaneous frequency f_{inst} was compared to the ECG instantaneous frequency of the dominant component extracted by the adaptive HFT algorithm. Indeed, the adaptive scheme proposed in Section 7.2 takes as input an ECG signal devoid of ventricular activity, and outputs estimates of the dominant component and its first harmonic. In this study, the estimated instantaneous frequency of the dominant component was taken as the central frequency of the filter tracking at each time instant the dominant component. Importantly, the delay induced by the adaptive algorithm was compensated [77].

The method presented in Section 8.1.2 for computing the intracardiac f_{inst} is dependent on the accuracy of LATs detection, and subsequently on the quality of the intracardiac signal. If the EGM is fractionated, LATs may be inaccurate, which is typically the case for the CS-cath during long-standing persistent AF, preventing the use of CS-cath dipoles for estimating their respective f_{inst}. In contrast, the baseline signals recorded from the RAA and LAA rarely display fractionation and are hence suitable for estimating f_{inst}. As a consequence, in this study, synchronous baseline recordings of 10 *sec* from the HRA_d and Lasso dipoles were included to estimate f_{inst} of

---

1. The technical characteristics of the catheters are presented in Section B.1 of Appendix B.

the RAA and LAA respectively. Unfortunately, the number of synchronous recordings satisfying the quality criterion for LATs detection was not sufficient to perform a robust analysis on the entire population. As such, case studies were selected in order to investigate the correspondence between the surface and intracardiac instantaneous frequencies.

8.2.2 Results

Time-invariant approach

Correlation values are reported in Table 8.1. Figure 8.3 shows the correlation between the DF estimated from ECG chest leads V_1 to V_{6b} with that estimated from the LAA, RAA and CS EGMs. The RAA DF (blue solid line) was best correlated with chest lead V_1 ($r = 0.9, p < 0.001$), and this correlation progressively dropped until V_5 ($r = 0.37, p < 0.05$) with a moderate rise for V_4 and V_{6b} ($r = 0.56$ and $r = 0.73, p < 0.001$). Interestingly, the LAA DF (green solid line) showed the opposite pattern with the highest correlation in V_{6b} ($r = 0.90, p < 0.001$) and the lowest one in V_2 ($r = 0.09, p = ns$). The correlation between the LAA DF and the one estimated on V_1 was moderate ($r = 0.59, p < 0.005$). Among the dipoles of the CS (dashed lines), the correlation pattern with the ECG leads was divergent. Two groups of dipoles could be identified. The first one was composed of the dipole CS_{9-10} (red dashed dot line) which was best correlated with the precordial leads V_1 ($r = 0.58, p < 0.001$) and V_{6b} ($r = 0.68, p < 0.001$). The remaining dipoles of the CS constituted the second group. These dipoles had similar correlation coefficients on all ECG precordial leads, with the highest correlation on chest leads V_1 and V_{6b} ($r \cong 0.5, p < 0.05$ and $r \cong 0.6, p < 0.001$ respectively).
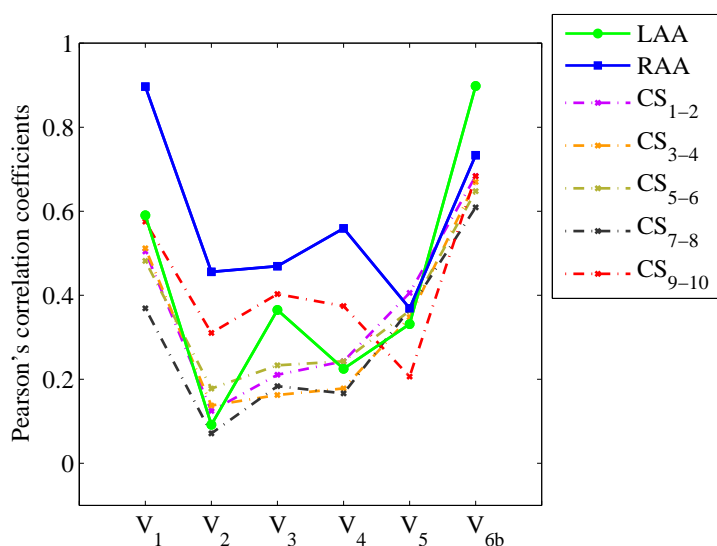
Figure 8.3: Pearson's correlation coefficients between all ECG precordial leads (x axis) and intracardiac sites LAA (green solid line with circle markers), RAA (blue squared marked solid line) and CS (dashed lines).

The correlation values between each combination of ECG chest leads indicated a strong correlation between the subgroup of leads V_1, V_2, and V_3. Chest lead V_4 was strongly correlated with leads V_1 and V_3 ($r = 0.73$, and $r = 0.66$ respectively $p < 0.001$), while its correlation with lead V_2 was moderate ($r = 0.49, p < 0.005$). Interestingly, the dorsal lead V_{6b} was highly

correlated with chest lead V_1 ($r = 0.71, p < 0.001$) and reasonably correlated with lead V_5 ($r = 0.55, p < 0.05$).

Figure 8.4 shows the correlation between the DF estimated from the LAA (green line) and RAA (blue line) with that from each CS dipole (x-axis). The correlation coefficient pattern for both appendages appeared similar. The correlation coefficients on dipoles CS_{1-2} and CS_{3-4} were slightly higher for the LAA as compared to the RAA (for the LAA, $r = 0.7, p < 0.001$ and $r = 0.75, p < 0.001$, while for the RAA $r = 0.62, p < 0.001$ and $r = 0.7, p < 0.001$ respectively).

As the CS dipoles were highly correlated with both appendages, we then tested whether the LAA and RAA DFs displayed some correlation as well. The correlation coefficient between both appendages was indeed high ($r = 0.74, p < 0.001$).
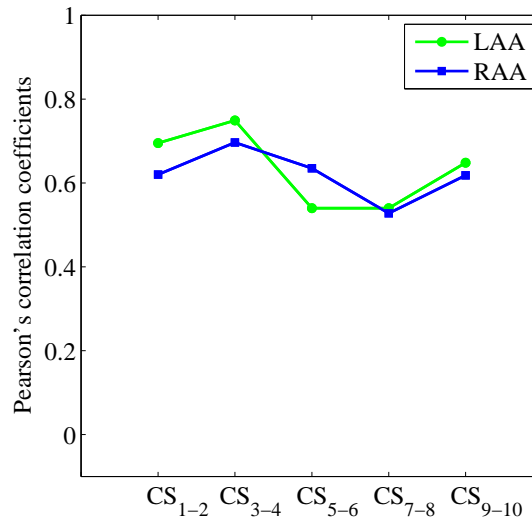
Figure 8.4: Pearson's correlation coefficients between all CS dipoles (x axis) and the LAA (green line with circle markers) and RAA (blue squared marked line).

Time-varying approach

In order to illustrate the correspondence between the instantaneous frequencies estimated from the surface ECG and that from both appendages, 10 *sec* recordings of two LT patients were selected. Figures 8.5 and 8.6 illustrate the estimated instantaneous frequencies for the two case studies. The correspondence between the instantaneous frequencies estimated from ECG lead V_1 and that from the distal dipole of the HRA catheter placed within the RAA is illustrated in Figure 8.5a for the first case study and Figure 8.6a for the second one. Also, the correspondence between the instantaneous frequencies estimated from the dorsal lead V_{6b} and that from the dipoles of the Lasso catheter placed within the LAA are displayed in Figure 8.5b for the first case study and Figure 8.6b for the second one.

On all figures, the display is the following: the top plot shows the 10 *sec* recording of the considered ECG chest lead in blue and the corresponding signal after QRST subtraction in black. The middle plot displays the 10 *sec* recording of the intracardiac dipoles with their corresponding LATs (circle markers). The bottom plot illustrates the instantaneous frequencies estimated from the ECG chest lead ($f_{inst_{ECG}}$, black solid line with square markers), and all intracardiac dipoles,

	V_1	V_2	V_3	V_4	V_5	V_{6b}	RAA	LAA
V_1	-	0.67 ‡	0.63 ‡	0.73 ‡	0.34	0.71 ‡	0.90 ‡	0.59 †
V_2	0.67 ‡	-	0.79 ‡	0.49 †	-0.12	0.14	0.46 **	0.09
V_3	0.63 ‡	0.79 ‡	-	0.66 ‡	-0.09	0.15	0.47 **	0.36 *
V_4	0.73 ‡	0.49 †	0.66 ‡	-	0.37 *	0.43 *	0.56 ‡	0.23
V_5	0.34	-0.12	-0.09	0.37 *	-	0.55 †	0.37 *	0.33
V_{6b}	0.71 ‡	0.14	0.15	0.43 *	0.55 †	-	0.73 ‡	0.90 ‡
CS_{1-2}	0.50 **	0.12	0.21	0.24	0.41 *	0.68 ‡	0.62 ‡	0.70 ‡
CS_{3-4}	0.51 †	0.14	0.16	0.18	0.35	0.67 ‡	0.70 ‡	0.75 ‡
CS_{5-6}	0.48 **	0.18	0.23	0.24	0.36 *	0.65 ‡	0.64 ‡	0.54 †
CS_{7-8}	0.37 *	0.07	0.18	0.17	0.37 *	0.61 ‡	0.53 †	0.54 †
CS_{9-10}	0.58 †	0.31	0.40 *	0.37 *	0.21	0.68 ‡	0.62 ‡	0.65 ‡
RAA	0.90 ‡	0.46 **	0.47 **	0.56 ‡	0.37 *	0.73 ‡	-	0.74 ‡
LAA	0.59 †	0.09	0.36 *	0.23	0.33	0.90 ‡	0.74 ‡	-

Table 8.1: Person's correlation coefficients between the DF estimed at the CS, RAA, and LAA and ECG precordial leads. The significance level of correlation is indicated ($* : p < 0.05$, $** : p < 0.01$, $† : p < 0.005$ and $‡ : p < 0.001$).

$f_{inst_{EGM}}$. The time intervals highlighted in gray correspond to epochs where the absolute difference between $f_{inst_{ECG}}$ and $f_{inst_{EGM}}$ was $\leq$ than $0.2\ Hz$, which is indicative of a good correspondence between the ECG and intracardiac instantaneous frequencies.

For the first case study (Figure 8.5), an adequate match during the 10 sec window can be observed between the instantaneous frequencies estimated from the ECG and those from both appendages. More specifically, the correspondence between the instantaneous frequencies estimated from the Lasso dipoles and the dorsal lead V_{6b} was more consistent than those from the HRA_d dipole and ECG chest lead V_1. Importantly, on both figures, the variations over time of $f_{inst_{ECG}}$ and $f_{inst_{EGM}}$ were highly similar. Interestingly, on Figure 8.5a, at $t = 6.4\ sec$, $f_{inst_{HRA_d}}$ increased up to 5.9 Hz while $f_{inst_{V_1}}$ increased to 5.6 Hz. Then, at $t = 7\ sec$, $f_{inst_{HRA_d}}$ suddenly dropped while $f_{inst_{V_1}}$ remained stable. However, at $t = 7.3\ sec$ $f_{inst_{V_1}}$ also dropped and matched with $f_{inst_{HRA_d}}$. In Figure 8.5b, the $f_{inst_{EGM}}$ computed from the four dipoles of the Lasso within the LAA increased to 5.6 Hz, while $f_{inst_{V_{6b}}}$ decreased to 5.3 Hz at $t = 7.3\ sec$.

For the second case study (Figure 8.6), periods of adequate match between the instantaneous frequencies estimated from the ECG and those from both appendages were shorter than those for the first case study. During the first three seconds, $f_{inst_{HRA_d}}$ (Figure 8.6a) varied between 4.8 Hz and 5.9 Hz with multiple maxima and minima, while the instantaneous frequency estimated from the ECG lead V_1 decreased almost monotonically from 5.7 Hz to 5.4 Hz. Then, the instantaneous frequencies variations from lead V_1 and that from HRA_d matched until $t = 5\ sec$, with a significant decrease in both values. Interestingly, this frequency drop was not perceived within the LAA (Figure 8.6b) suggesting that the RAA was not remotely driving the LAA.
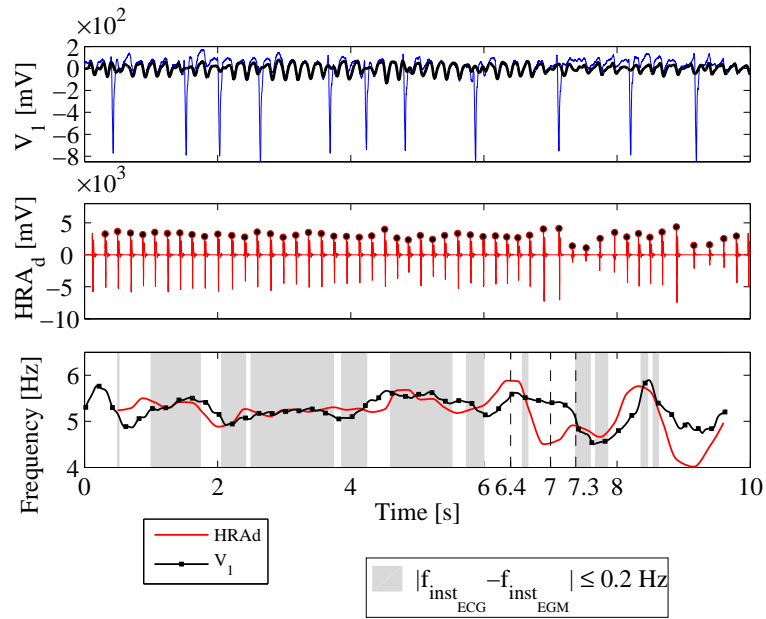
(a)
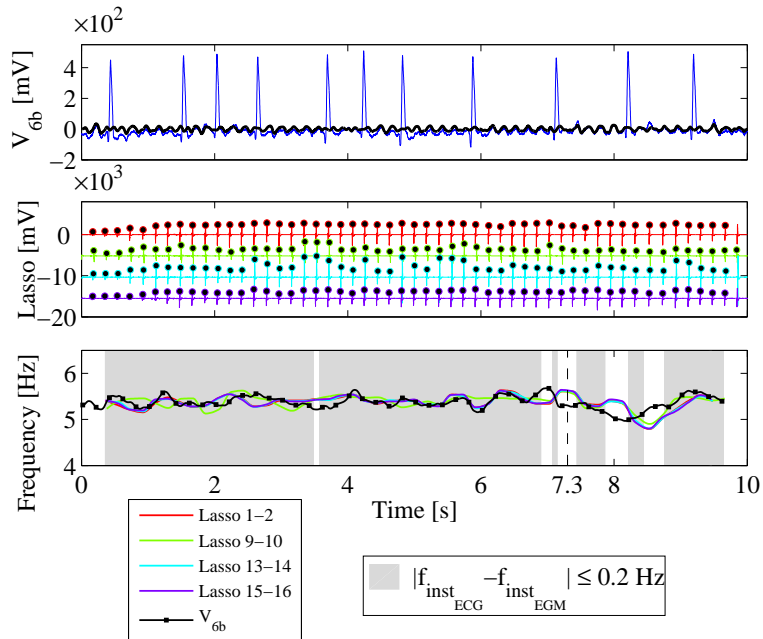
(b)

Figure 8.5: Illustrative examples of the instantaneous frequencies estimated from the ECG and intracardiac EGMs, first case study. Figure (a) illustrates the instantaneous frequency estimated from ECG lead V_1 and that from the HRA_d placed within the RAA. Figure (b) displays the instantaneous frequency estimated from the dorsal lead V_{6b} and that from four dipoles of the Lasso placed within the LAA. Top plots: 10 *sec* recording from the ECG lead (blue) after QRST subtraction (black). Middle plots: synchronous recordings from the intracardiac dipoles. Bottom plots: $f_{inst_{ECG}}$ (black squared marked line) and $f_{inst_{EGM}}$ (colored lines). The periods in gray denote when $|f_{inst_{ECG}} - f_{inst_{EGM}}| \leq 0.2$ *Hz*.
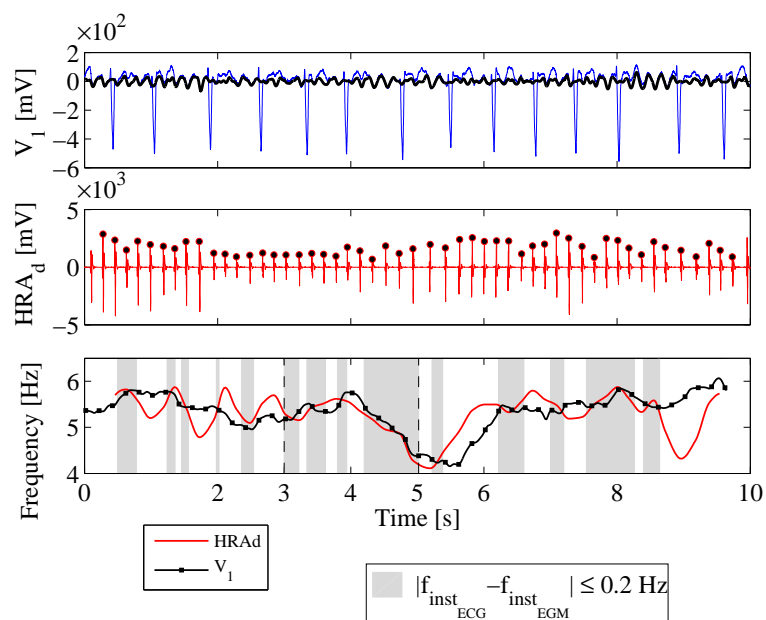
(a)
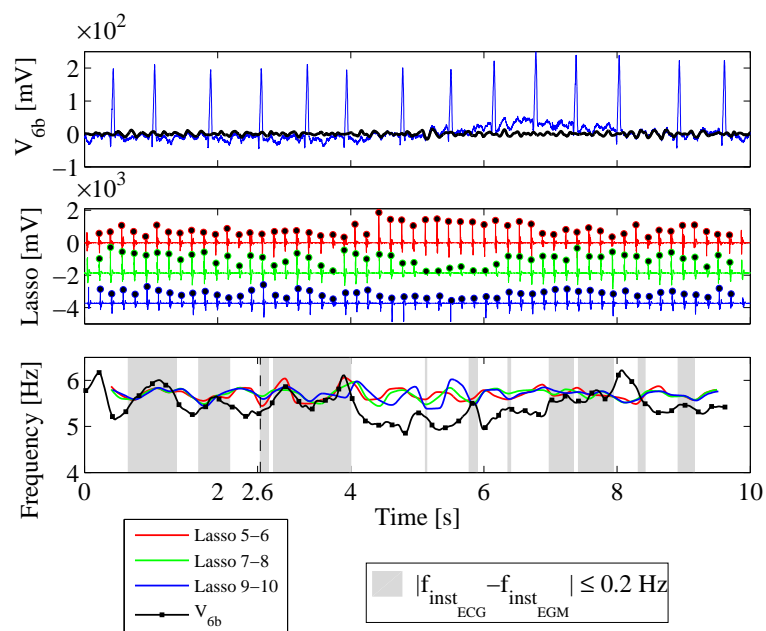
(b)

Figure 8.6: Illustrative examples of the instantaneous frequencies estimated from the ECG and intracardiac EGMs, second case study. Figure (a) illustrates the instantaneous frequency estimated from ECG lead V_1 and that from the HRA_d placed within the RAA. Figure (b) displays the instantaneous frequency estimated from the dorsal lead V_{6b} and that from three dipoles of the Lasso placed within the LAA. Top plots: 10 *sec* recording from the ECG lead (blue) after QRST subtraction (black). Middle plots: synchronous recordings from the intracardiac dipoles. Bottom plots: $f_{inst_{ECG}}$ (black squared marked line) and $f_{inst_{EGM}}$ (colored lines). The periods in gray denote when $|f_{inst_{ECG}} - f_{inst_{EGM}}| \leq 0.2 \ Hz$.

8.2.3   Discussion

Time-invariant approach

Over the last two decades, many studies have established the correspondence between the atrial activity measured from the surface ECG with that of various intracardiac segments. These studies are summarized in Table 8.2.

Correspondence between surface ECG and intracardiac activity.   All reported studies have shown that RA activity during AF is a major contributor to the f-waves recorded from chest lead V_1 [16, 20, 55, 57, 58, 65, 84–86]. Dibs et al. have shown that the strongest correspondence between RA activity and ECG chest leads was found on V_2 and that the LA activity was mostly correlated with that of chest leads V_4 and V_6 [65]. Petrutiu et al. extended these findings by showing that posterior leads were best correlated with LA activity [55]. Recently, Guillem et al. reported a detailed study of the correlation between intracardiac atrial and body surface DFs map in patients with persistent AF [86]. They found a high correlation between the region covered by lead V_1 and RA DF, and the posterior paravertebral region and the LA DF. In our study, a strong correlation was found between RAA activity and the DF measured on lead V_1, and between LAA activity and the DF of dorsal lead V_{6b}, which is in line with the results of these recent studies.

Regarding the correspondence between the activity measured from the CS and that from the surface ECG, the results reported in the literature are contradictory. On one hand, some studies have shown a strong correlation between the activity of the proximal, mid-portion and distal segments of the CS and that from chest lead V_1 [14, 16, 58, 65, 95]. On the other hand, Holm et al. found a poor correlation between the frequency content measured at the proximal part of the CS and that of ECG chest lead V_1 [57]. These results should be, however, interpreted with care as the CS follows the curvature of the LA and of the left ventricle that might have "polluted" the atrial signal. In our study, a moderate correlation was found between the DF estimated from the proximal and distal dipoles of the CS-cath and that of ECG chest lead V_1. In fact, the correlation level of the proximal CS-cath dipole with V_1 was similar to that of the LAA with V_1. Importantly, the correlation of all CS-dipoles was slightly stronger for the dorsal lead V_{6b} as compared to the remaining ECG chest leads.

Other correspondences.   To the best of our knowledge, no study has investigated the cross-correlation of intracardiac segments or the cross-correlation between the ECG chest leads. In our study, we found that the DFs estimated from the proximal and distal dipoles of the CS-cath were strongly correlated with the DFs from the RAA and LAA. The correlation was, however, stronger on the distal dipoles of the CS-cath with the LAA than with the RAA.

The significant correlations obtained on the CS-cath with lead V_{6b} and with several intracardiac segments might be slightly surprising. Indeed, the ECG lead V_{6b} is not directly facing the CS-cath. We hypothesized that these findings are a result of an indirect correlation from both appendages.

Regarding the correlation between each combination of ECG lead, a significant correlation was found between the first four precordial leads V_1 to V_4, as these leads are placed close to each other on the patient's chest. Surprisingly, the correlation between chest lead V_1 and the dorsal lead V_{6b} was strong. In summary, we have the following; a) the correlation between both appendages was high, b) the activity from V_1 corresponded to the activity from the RAA, and c) the frequency content from the dorsal lead V_{6b} was strongly correlated with that of the LAA. Thus, we hypothesized that the correlation observed between ECG leads V_1 and V_{6b} is a consequence of their respective correlations with both appendages and the significant correlation between the LAA and the RAA.

		Appendages	
Leads	Correspondence	RAA	LAA
V1	Strong	Holm et al. [57] Bollmann et al. [16] Hsu et al. [84] Petrutiu et al. [55] Matsuo et al. [20] Platonov et al. [85] Raitt et al. [58]	Matsuo et al. [20] Platonov et al. [85]
	Poor		Hsu et al. [84] Petrutiu et al. [55]
V2	Strong	Dibs et al. [65]	
V4	Strong		Dibs et al. [65]
V6	Strong		Dibs et al. [65]
Posterior	Strong		Petrutiu et al. [55] Guillem et al. [86]

(a)

		CS		
Leads	Correspondence	Proximal	Middle	Distal
V1	Strong	Dibs et al. [65] Raitt et al. [58] Walters et al. [14]	Bollmann et al. [16] Husser et al. [95]	Walters et al. [14]
	Poor	Holm et al. [57]		

(b)

Table 8.2: Studies on the correspondence of atrial activity measured from the surface ECG and that from the atrial appendages (a) and from the CS (b).

Time-varying approach

In Chapter 7, a novel method for characterizing the dominant component of atrial ECG signals was presented. The output of the adaptive scheme estimates the ECG atrial f-waves dominant component and its first harmonic. In the present chapter, a method for computing the instantaneous frequency of intracardiac signals was presented.

Typically, the frequency content of intracardiac signals is assessed by computing the DF using a time-invariant scheme. This approach, however, is not appropriate for characterizing the variations of the intracardiac DF over time. We reported two study cases, in which the instantaneous frequencies were estimated from catheters placed within the RAA and the LAA. The ECG instantaneous frequency was highly similar to the intracardiac instantaneous frequencies. More specifically, the instantaneous frequency estimated from ECG leads V_1 and V_{6b} had similar values with that of the RAA and LAA respectively. Importantly, there was a high correspondence in the temporal variations of the ECG and intracardiac instantaneous frequencies. Some discrepancies were observed punctually between the ECG and intracardiac instantaneous frequencies suggesting the existence of a remote driver located in another atrial segment and not perceived by the ECG electrode.

8.3   Baseline dominant frequency mapping

8.3.1   Methods

Sequential mapping of the LA was performed following the baseline acquisition protocol described in Section 5.2.3 at page 47. For convenience, the sequential acquisition is briefly repeated here.

Within the LA, the Lasso was placed consecutively in a stable position for a minimum duration of 20 seconds at thirteen different locations:
- The ostium of the four PVs.
- The base of the LAA.
- The anterior and posterior parts of the roof.
- The middle and inferior parts of the posterior wall.
- The mitral isthmus.
- The superior, middle and inferior parts of the septum.

In addition to these locations, the recordings acquired at baseline with the distal pole of the HRA catheter placed within the RAA as well as the recordings from all dipoles from the CS-cath were considered.

The DF of each bi-atrial location was computed as presented in Section 8.1. For the Lasso, the DF was spatially averaged when computed on multiple dipoles. The epoch duration of this study was set to 10 *sec*. The intracardiac DF was then temporarily averaged for each patient. Finally, the mean and standard deviation DF values were estimated for the LT and NLT groups.

Two statistical analyses were performed. The first one assessed the statistical significance between the average DF of the two groups using the ANOVA framework. Levels of statistical significance were set to 0.05, 0.01, 0.005 and 0.001. The second statistical analysis was aimed at studying the presence at baseline of an inter-atrial gradient within each group. More specifically, the inter-atrial gradient between appendages was estimated as the DF difference between LAA and RAA. Within each group, the significance level of the inter-atrial gradient was assessed through a one-tailed t-test for values of DF gradients ranging from 0.2 to 1 *Hz*. The level of statistical significance was set to 0.05.

8.3.2   Results

Baseline bi-atrial DF mapping

Table 8.3 reports the mean ± standard deviation of the DF computed on each bi-atrial segment. If the ANOVA test declared a significant difference, the corresponding level is indicated: $* : p < 0.05$, $** : p < 0.01$, $\dagger : p < 0.005$ and $\ddagger : p < 0.001$.

Figure 8.7 shows the distribution of DF values for the LT (blue) and NLT (red) groups for all dipoles estimated within the CS. The average DF was significantly lower for the LT group than for the NLT one on all CS dipoles (except CS_{1-2}). The most significant difference was found on the CS_{9-10} dipole.

Figure 8.8 shows the distribution of DF values for the LT (blue) and NLT (red) groups for all mapped structures within both atria (RAA, LAA, and the four PVs). The average DF was significantly lower for the LT group than for the NLT one in all mapped structures. Interestingly, the level of statistical significance was more pronounced for the superior PVs than for to the inferior ones. Concerning the atrial appendages, the most significant difference between the groups could be observed within the RAA ($p < 0.001$, while for the LAA $p < 0.05$). For the LT patients, one can observe that the average DF within the LAA (5.78 ± 0.66 *Hz*) was slightly higher than the mean DF within the RAA (5.61 ± 0.66 *Hz*) suggestive of a possible LA driver.

It was the opposite for the NLT group, as the average DF within the RAA (6.60 ± 0.55 *Hz*) was higher than that of the LAA (6.49 ± 0.68 *Hz*), suggestive in this case of a possible RA driver.

Figure 8.9 shows the distribution of the DF values for the LT (blue) and NLT (red) groups for all LA segments. The DF values of the LT patients were significantly lower than that of the NLT patients for each LA segment, except for the inferior part of the septum.
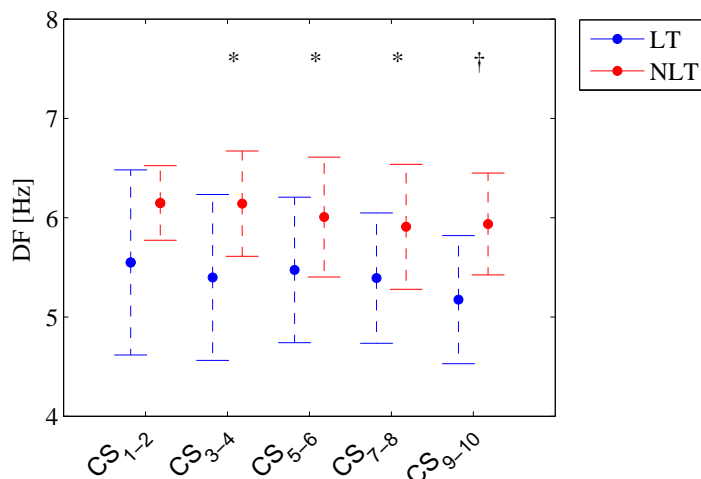
Figure 8.7: Distribution of the baseline DF within the CS for the LT (blue) and NLT (red) groups ($*: p < 0.05$, $**: p < 0.01$, $\dagger: p < 0.005$ and $\ddagger: p < 0.001$).
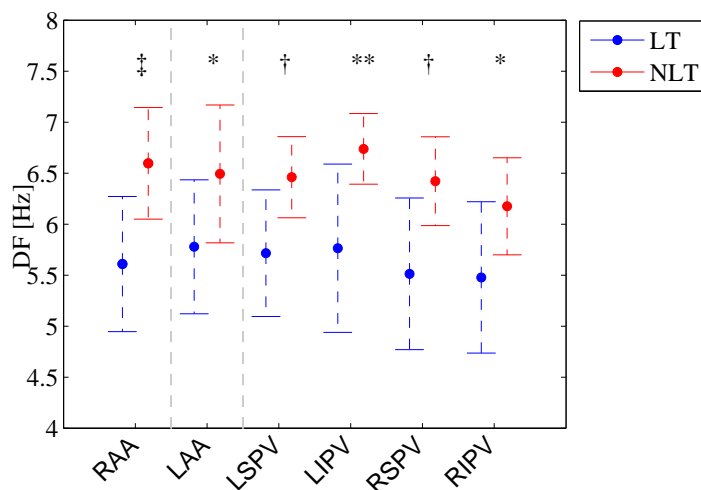
Figure 8.8: Distribution of the baseline DF within the RAA, LAA and the four PVs for the LT (blue) and NLT (red) groups ($*: p < 0.05$, $**: p < 0.01$, $\dagger: p < 0.005$ and $\ddagger: p < 0.001$).
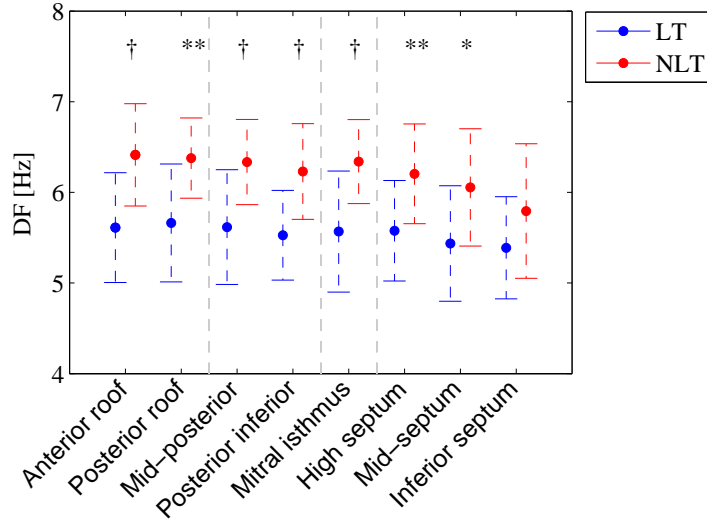
Figure 8.9: Baseline left atrium DF mapping.

	Dominant frequency [Hz]			Dominant frequency [Hz]	
	LT	NLT		LT	NLT
CS_{1-2}	5.55 ± 0.93	6.15 ± 0.38	Anterior roof	5.61 ± 0.61	$6.41 \pm 0.56^{\dagger}$
CS_{3-4}	5.40 ± 0.84	$6.14 \pm 0.53^{*}$	Posterior roof	5.66 ± 0.65	$6.38 \pm 0.44^{**}$
CS_{5-6}	5.47 ± 0.73	$6.01 \pm 0.60^{*}$	Mid-posterior	5.62 ± 0.63	$6.33 \pm 0.47^{\dagger}$
CS_{7-8}	5.39 ± 0.66	$5.91 \pm 0.63^{*}$	Posterior inferior	5.53 ± 0.50	$6.23 \pm 0.53^{\dagger}$
CS_{9-10}	5.17 ± 0.64	$5.94 \pm 0.51^{\dagger}$	Mitral isthmus	5.57 ± 0.67	$6.34 \pm 0.46^{\dagger}$
RAA	5.61 ± 0.66	$6.60 \pm 0.55^{\ddagger}$	High septum	5.58 ± 0.55	$6.20 \pm 0.55^{**}$
LAA	5.78 ± 0.66	$6.49 \pm 0.68^{*}$	Mid-septum	5.44 ± 0.64	$6.05 \pm 0.65^{*}$
LSPV	5.72 ± 0.62	$6.46 \pm 0.40^{\dagger}$	Inferior septum	5.39 ± 0.56	5.79 ± 0.74
LIPV	5.76 ± 0.82	$6.74 \pm 0.35^{**}$			
RSPV	5.51 ± 0.74	$6.42 \pm 0.44^{\dagger}$			
RIPV	5.48 ± 0.74	$6.18 \pm 0.48^{*}$			

Table 8.3: Distribution of the baseline DF at various LA segments for the LT and NLT groups ($*: p < 0.05$, $**: p < 0.01$, $\dagger: p < 0.005$ and $\ddagger: p < 0.001$).

Baseline inter-atrial frequency gradient

Figure 8.10 shows the statistical significance levels (p-values) of the inter-atrial DF gradient for the LT (blue solid line) and the NLT (red solid line) groups as a function of the variations in Hertz of the inter-atrial gradient denoted as ∇DF. The bottom green area represents a significant statistical level < 0.05. For the LT (blue solid line) and NLT (red solid line) groups, no significant LA-to-RA frequency gradient was observed. As the results of the bi-atrial DF mapping showed that for the NLT group the average DF within the RAA was slightly larger than that within the LAA, the same statistical analysis was performed, but the inter-atrial gradient was defined as the DF difference between the RAA and the LAA as shown by the red dashed line. For the NLT patients, no significant RA-to-LA gradient was observed.
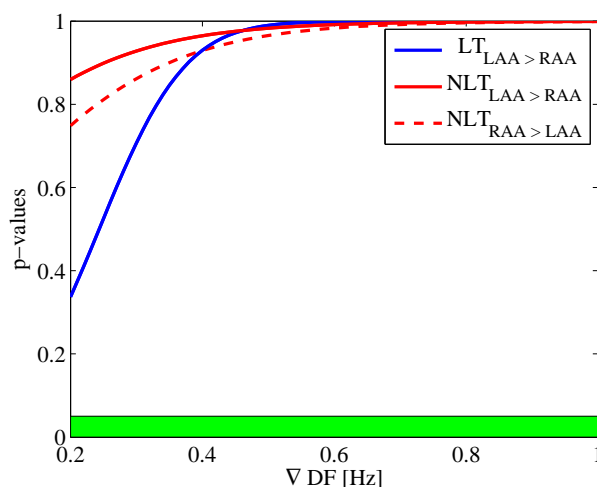
Figure 8.10: Statistical significances of the LAA to RAA DF gradient for the LT (blue solid line) and NLT (red solid) groups as a function of the variations in Hertz of the inter-atrial gradient (∇DF). The bottom green area represents statistical significance level < 0.05. The red dashed line shows the statistical significance levels for the NLT group when the inter-atrial gradient was defined as the difference between the RAA and LAA DFs.

8.3.3 Discussion

Baseline bi-atrial DF mapping

The intracardiac DF has been used as an estimate of the local underlying atrial activation rate during AF. Many electrophysiological studies have used the DF of intracardiac recordings as a tool for understanding the pathophysiology and dynamics of AF in humans [13, 14, 87, 88]. One such approach has been used to map the activation rates in the frequency domain throughout the atria. Sahadevan et al. reported a detailed study of intra-operative mapping in patients with long-standing persistent AF [87]. These patients manifested a rapid, regular rhythm, most exclusively located at the posterior wall of the LA, whereas the rest of the atria was characterized by irregular electrograms, suggesting that local drivers (rotors) may be responsible for maintaining chronic AF. Using an animal model, it was shown that the DFs of the rotors were of high frequency values [88]. Moreover, in patients with persistent AF, a higher DF in the LA has been associated to a greater degree of electroanatomical remodeling and slowing of atrial conduction [13, 14].

More recently, the DF was used as a tool for assessing the change of AF dynamics during catheter ablation [67, 89, 90, 96]. In [96], Sanders et al. showed that in patients with permanent AF, sites of high frequency activity were localized in several segments of the atria, including RA sites, and that ablation at these specific sites resulted in a significant slowing of the fibrillatory process. Others reported that in patients with permanent AF, freedom from recurrent AF was associated with a significant reduction in the DF measured from the CS [67, 89, 90].

To the best of our knowledge, studies investigating the baseline intracardiac DF as a predictor of procedural AF termination are scarce, in particular for patients with non-paroxysmal AF. In [90], the baseline DF measured from the CS in patients with persistent AF was similar, regardless of the procedural outcome during catheter ablation. Another study showed that in patients with non-paroxysmal AF, a lower average DF acquired from the RA was associated with acute AF termination by catheter ablation [92].

In our study, we measured the baseline DF in several segments of the atria including the right and left atrial appendages, the CS, the four pulmonary veins, the mitral isthmus, the LA roof, the posterior wall and septum. In all mapped atrial locations, we found that a significant lower baseline DF was associated to termination of long-standing persistent AF during stepwise catheter ablation. Patients in whom ablation failed to terminate AF had, on average, a significantly higher DF as compared to patients in whom AF was terminated. These results suggest that the electroanatomical remodeling in NLT patients was more important than that of LT patients.

Baseline inter-atrial frequency gradient

Lazar et al. showed that patients with paroxysmal AF displayed a significant LA-to-RA frequency gradient of 1.1 ± 0.7 Hz, which was absent in patients with long-lasting persistent AF [91]. The DF recorded within the RA was significantly higher for the chronic AF group compared to the paroxysmal group. In another study, patients with persistent AF showed no significant LA-to-RA DF gradient [55]. Conflicting results, however, were reported by Dibs et al who observed a mean LA-to-RA DF gradient of 0.4 ± 0.2 Hz in patients with persistent AF [65].

In our study, no significant LA-to-RA frequency gradient was observed for the LT and NLT groups. Moreover, for the NLT group, the average RA DF was slightly higher than that of the LA, however, no significant RA-to-LA gradient for these patients was found. One possible reason for our divergent results with those of Dibs et al. may come from differences in patients characteristics. Our study population had on average an AF sustained for 19 ± 11 months, while Dibs et al. included nine patients with sustained durations of AF varying between one month and more than one year [65].

8.4 Conclusion

In the first part of this chapter, we have shown that the contributions of the RA and LA during AF can be independently determined using specific regions of the thorax, and that the main contributors to the surface ECG f-waves come from the appendages rather than that from the smooth parts of the atria such as the CS. We have also demonstrated that the temporal variations of the ECG instantaneous frequency estimated from the outputs of the adaptive scheme corresponds to a high degree with that of intracardiac instantaneous frequencies.

In the second part of this chapter, we observed that the electroanatomical remodeling in NLT patients is higher than that in LT patients. Also, no inter-atrial DF gradient was observed in both group. Taken together, these observations suggest that the frequency of the atrial activation rate in long-standing persistent AF is predictive of the procedural outcome during stepwise catheter ablation and that it is also an indicator of the degree of electroanatomical remodeling.

In conclusion, the analysis of intracardiac AF signals frequency spectra provides valuable insights into its dynamics, and it appears as a promising clinical tool for predicting the procedural outcome during catheter ablation of patients with long-standing persistent AF.

Variability of Atrial Activation Intervals

9

Prior studies on animals and humans have shown that during AF, the average interval between local depolarizations, the so-called intracardiac AFCL, approximates the local atrial refractoriness [10–12]. A very good correlation was established between local atrial refractory periods and the AFCL measured at the same atrial location [10–12]. Hence, the AFCL estimated from various endocardial sites has been widely used as a useful clinical tool for monitoring the effect of substrate modification during AF catheter ablation [6, 49, 50, 97–100]. In all reported studies, a gradual increase of the intracardiac AFCL during ablation was associated with AF termination. Conflicting results were, however, reported regarding the ability of intracardiac AFCL to assess AF organization before step-CA [6, 49, 100–103]. For instance, baseline AFCL was found significantly longer in patients in whom long-standing persistent AF terminated during step-CA [49, 101], while in persistent AF continuing despite PVI, the baseline AFCL did not differ between patients whose long-standing persistent AF did and did not terminate [100]. Other studies reported that, in patients with persistent AF, the baseline intracadiac AFCL was not predictive of the procedural outcome [99, 102]. Thus, in this chapter, we aim at characterizing the intracardiac AFCL prior to ablation in patients with long-standing persistent AF.

According to the multiple wavelet hypothesis (Section 3.5.2 page 30), the presence of regular reentrant circuits is associated to a higher degree of organization [35–37]. A longer mean AFCL is suggestive of a high organization. During AF, intracardiac electrograms are characterized by short and variable atrial intervals and, thus, display irregular activations. The AFCL is computed as the average interval between local depolarizations and is therefore not suitable for reflecting the variability of these intervals. In this chapter, we hypothesize that the temporal variability of atrial activation wavefronts around the mean AFCL before ablation may help characterizing the AF dynamics and furthermore, may help identifying patients whose long-standing persistent AF will terminate within the LA during stepwise catheter ablation. This approach evaluates the oscillations of time intervals between consecutive AF wavefronts similarly to that of heart rate variability analysis [104].

This chapter is organized as follows. Section 9.1 presents the signal processing steps for characterizing the variability of atrial activation waveforms and Section 9.2 presents the material used for this study. The results are provided in Section 9.3. Finally, Secion 9.4 covers the discussion for the current study.

9.1 Characterization of the variability of atrial activation intervals

The signal processing steps for characterizing the variability of atrial activation waveforms are described here. First, the LAT was defined as described in the previous chapter in Section 8.1.2. Namely, the LAT was set as the time of the maximum positive peak of each activation wave detected using sliding windows of 150 *ms*. False detections were removed using temporal and amplitude thresholding. The upper plot in Figure 9.1 illustrates a 20 *sec* epoch acquired from the HRA$_d$ dipole placed within the RAA in an LT patient with its detected LATs (red dot). The bottom plot shows an excerpt of two seconds.
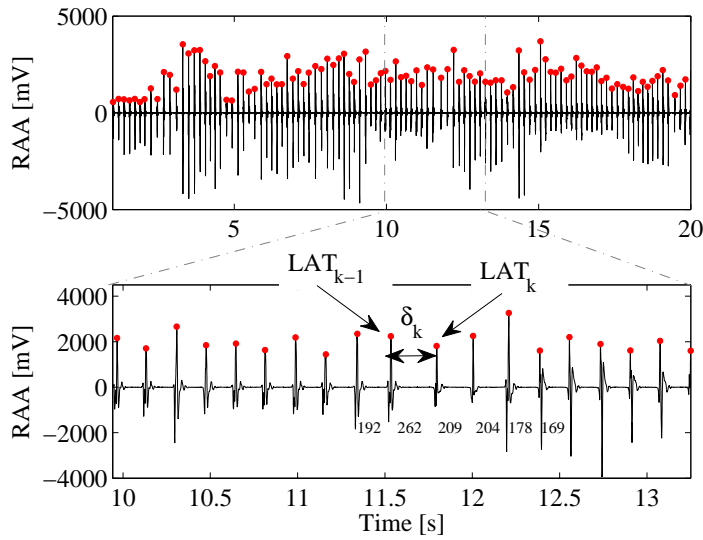
Figure 9.1: Intracardiac local activations times and instantaneous AFCL. The top plot illustrates a 20 *sec* epoch acquired from the HRA$_d$ dipole placed within the RAA in an LT patient with its detected LATs (red). The bottom plot shows an excerpt of two seconds. The numbers displayed between consecutive LATs indicate the corresponding duration of interval in milliseconds.

Let N be the total number of LATs in a given signal. We set δ_k (Figure 9.1, bottom plot) as the time difference between two consecutive LATs:

$$\delta_k = \text{LAT}_k - \text{LAT}_{k-1} \tag{9.1}$$

where $k = 2, \cdots, N$. The value of δ_k corresponds to the instantaneous AFCL of the consecutive atrial activation waveforms $k - 1$ and k. In the example displayed in Figure 9.1, the values of δ_k are not constant during this 20 *sec* epoch; faster intervals alternate with slower ones. In the bottom plot, the numbers indicate the value in milliseconds of five consecutive δ_k. It can be observed that at $t \approx 11.5$ *sec* the instantaneous AFCL slows down to 262 *ms* and that three wavefronts after, at $t = 12.5$ *sec*, $\delta_k = 169$ *ms*.

The intracardiac AFCL is classically computed as the mean difference in LATs. In this example, the estimated AFCL value was 179 *ms*. This value is much lower than the instantaneous difference observed in Figure 9.1 at $t \approx 11.5$ *sec* which can be therefore interpreted as a local
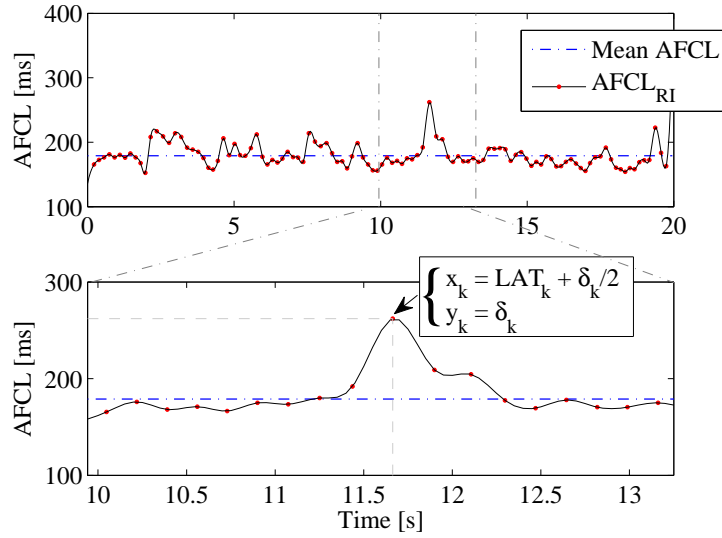
Figure 9.2: Resampled instantaneous AFCL computed from the signal displayed in Figure 9.1. The blue horizontal dashed-dotted line corresponds to the average AFCL.

slowing down of the instantaneous AFCL with respect to the average AFCL.

In order to characterize the variability of the instantaneous AFCLs around the average AFCL, we defined the set of data points (Figure 9.2, bottom plot) as:

$$\begin{cases} x_k = \mathrm{LAT}_k + \delta_k/2, \\ y_k = \delta_k \end{cases} \tag{9.2}$$

The resampled instantaneous AFCL (AFCL$_{RI}$) was defined as the cubic interpolation of these data points at a regular sampling frequency of 20 Hz. From equation (9.2), the mean of AFCL$_{RI}$ corresponds to the AFCL. The top plot of Figure 9.2 shows the AFCL$_{RI}$ computed for the intracardiac signal shown in Figure 9.1, while the bottom plot of Figure 9.2 displays an excerpt of two seconds in the same interval as in the bottom plot of Figure 9.1. The blue horizontal dashed-dotted line corresponds to the average AFCL. It can be observed that the local slowing down of the instantaneous AFCL identified at time ≈ 11.5 sec is emphasized by an abrupt rise of the AFCL$_{RI}$ which lies above the mean AFCL.

In order to characterize the variability of the atrial activation intervals, the AFCL$_{RI}$ PSD was estimated using Welch's method (Hamming window of length of 512 samples, 50% overlap). Let L be the number of power spectrum density estimates, $\mathbf{f}$ and $\mathbf{p}$ be the vectors of frequency and power spectral density estimates. Two indices were computed:

1. The mean frequency μ_f:

$$\mu_f = \frac{\sum_{i=1}^{L} p_i f_i}{\sum_{i=1}^{L} p_i} \quad [Hz] \tag{9.3}$$

   From equation (9.3), μ_f quantifies the mean frequency at which the AFCL oscillates. Low values of μ_f are indicative of a slower temporal variability of LATs, and consequently of a higher organization.
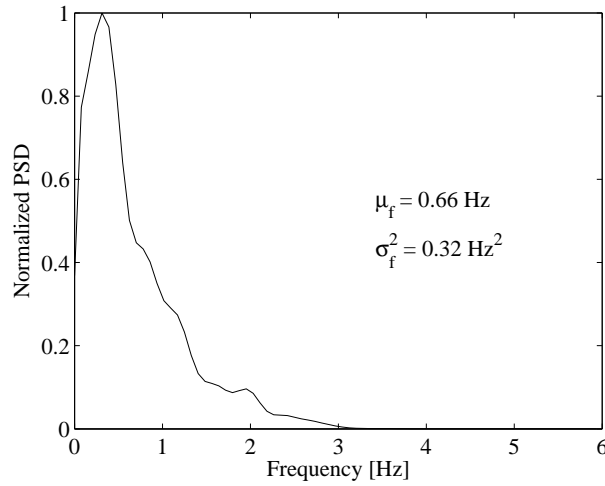
Figure 9.3: PSD of the resampled instantaneous AFCL computed in Figure 9.2. The values of μ_f and σ_f^2 are indicated.

2. The variance σ_f^2

$$\sigma_f^2 = \frac{\sum_{i=1}^{L} p_i(f_i - \mu_f)^2}{\sum_{i=1}^{L} p_i} \quad [Hz^2] \tag{9.4}$$

From equation (9.4), σ_f^2 characterizes the spread of μ_f. Low values of σ_f^2 are indicative of a stable μ_f, i.e., a more regular variability; conversely, large σ_f^2 values reflect a more erratic variability.

Figure 9.3 shows the PSD of the AFCL$_{RI}$ computed in Figure 9.2. In this example, $\mu_f = 0.66\ Hz$ and $\sigma_f^2 = 0.32\ Hz^2$.

9.2   Material

The average AFCL, μ_f and σ_f^2 were computed on 20 *sec* epochs duration from recordings acquired at baseline from the HRA$_d$ placed within the RAA and from the Lasso placed within the LAA [1]. For the Lasso, when the computation was performed on multiple dipoles, the corresponding indices were spatially averaged on all available dipoles. Then, for each measure, the temporal mean was computed resulting in one value for each measure, subject and intracardiac location.

The statistical significance between the two groups and within each group was assessed through the ANOVA framework. Levels of statistical significance were set to 0.05, 0.01, 0.005 and 0.001.

---

1. It is important to mention that in this study, the signals acquired from the CS-cath were not used because for only a few number of patients were signals of sufficient quality available for correctly detecting the LATs. Most of the patients of our study population displayed a considerable amount of signal fractionation at the CS. Our scheme for detecting the LATs is not appropriate in case of high fractionation.

9.3   Results

9.3.1   Illustrative examples

Figure 9.4 displays representative examples of AFCL$_{RI}$s from an LT (blue solid line with circle markers) and an NLT (red solid line with plus sign markers) patients [2]. The mean AFCL for the LT patient was of 179 ms, while for the NLT patient, the mean AFCL was smaller, 152 ms. Note the presence of high frequency oscillations in the AFCL$_{RI}$ for the NLT patient. In contrast, the AFCL$_{RI}$ for the LT patient appeared more regular, with less rapid oscillations.

Figure 9.5 shows the normalized AFCL$_{RI}$ PSD for the LT (blue solid line) and for the NLT patient (red dashed line). The PSD estimates for the LT patient were mostly concentrated below 2 Hz with low values for μ_f and σ_f^2 (0.66 Hz and 0.32 Hz^2 respectively) as opposed to the NLT patient displaying a widespread PSD distribution with higher μ_f and larger σ_f^2 (1.26 Hz and 0.87 Hz^2 respectively).

As a parenthesis, for both patients, a predominant peak in the lower frequencies can be observed ($\approx$ 0.3 Hz for the LT patient and $\approx$ 0.08 Hz for the NLT patient). One might argue that the presence of this peak is due to modulation induced by the respiration. However, all patients underwent the ablation under general anaesthesia and consequently the respiration was regulated by mechanical ventilation at a frequency of $\approx$ 0.2 Hz. Due to the lack of experiments describing this modulation in anaesthetised patients, one cannot draw a clear interpretation as to the origin of the oscillations around 0.3 Hz. The lower oscillations for the NLT patient could be a manifestation of the fluctuations of the arterial pressure regulation [105]. However, this phenomenon has not extensively been studied in anaesthetised patients. Therefore, no clear interpretation can be drawn from these illustrative examples regarding the exact nature of these observations. It must be noted that this aspect is clearly beyond the scope of the present work.
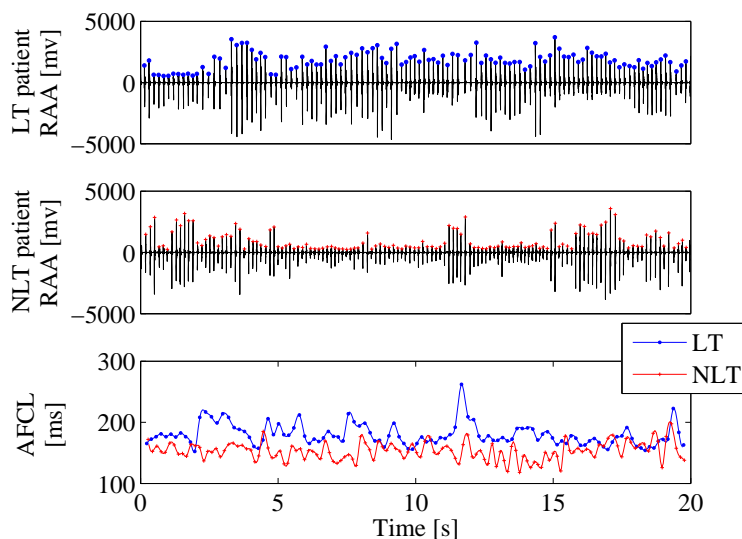
Figure 9.4: Representative examples of AFCL$_{RI}$ signals for an LT (blue solid line with circle markers) and an NLT (red solid line with plus sign markers) patients. The mean AFCL for the LT patient is of 179 ms, while for the NLT patient, the mean AFCL is smaller, 152 ms.

---

2. The LT patient is the same as the one used in Section 9.1
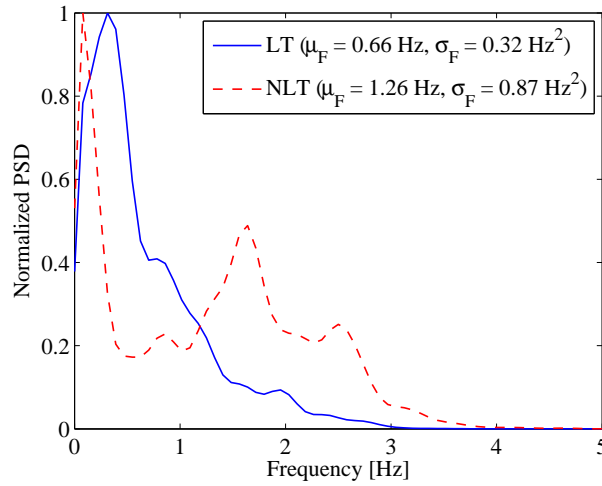
Figure 9.5: Representative examples of the $AFCL_{RI}$ power spectrum density of an LT (blue solid line) and an NLT patient (red dashed line). Note the broader spectrum for the NLT patient indicative of a lower AF organization as compared to the LT patient.

9.3.2   Clinical results

Figure 9.6 and Table 9.1 report the mean ± standard deviation and median values of μ_f (Figure 9.6a), σ_f^2 (Figure 9.6b) and average AFCL (Figure 9.6c) for the LT (blue) and NLT (red) groups computed at baseline within the RAA and LAA.

On both appendages, all indices were on average significantly different between the LT and NLT groups. Before ablation, LT patients displayed significantly longer bi-atrial AFCL for both LA and RA appendages. Likewise, LT patients displayed significantly smaller μ_f and σ_f^2 values on both appendages as compared to NLT patients. Interestingly, for all organization indices, the most significant differences between the LT and NLT groups were observed within the RAA ($p < 0.001$).

For the LT group, the mean AFCL computed from the RAA (180 ± 22 ms) was similar to that from the LAA (178 ± 25 ms), suggestive of a similar organization within both appendages. Likewise, the average σ_f^2 was similar within both appendages (0.56 ± 0.16 Hz^2 for the RAA and 0.58 ± 0.17 Hz^2 for the LAA). However, a tendency for a higher LAA μ_f (0.98 ± 0.2 Hz) as compared to the RAA one (0.89 ± 0.14 Hz, $p = ns$) was observed, suggesting that wavefront variability was lower within the RAA. Thus, for the LT group, the average indices characterizing the variability of atrial activation wavefronts indicated a higher organization within the RA as compared to the LA.

For the NLT group, the mean AFCL computed from the RAA (151 ± 11 ms) was also similar to that from the LAA (153 ± 13 ms). The average μ_f was similar within both appendages (1.2 ± 0.17 Hz for the RAA and 1.22 ± 0.22 Hz for the LAA). However a tendency of larger RAA σ_f^2 (0.89 ± 0.17 Hz^2) as compared to the LAA (0.78 ± 0.23 Hz^2, $p = ns$) was observed, suggesting that the variance of the oscillations around the mean AFCL was on average higher in the RAA than in the LAA.

(a)

(b)

(c)
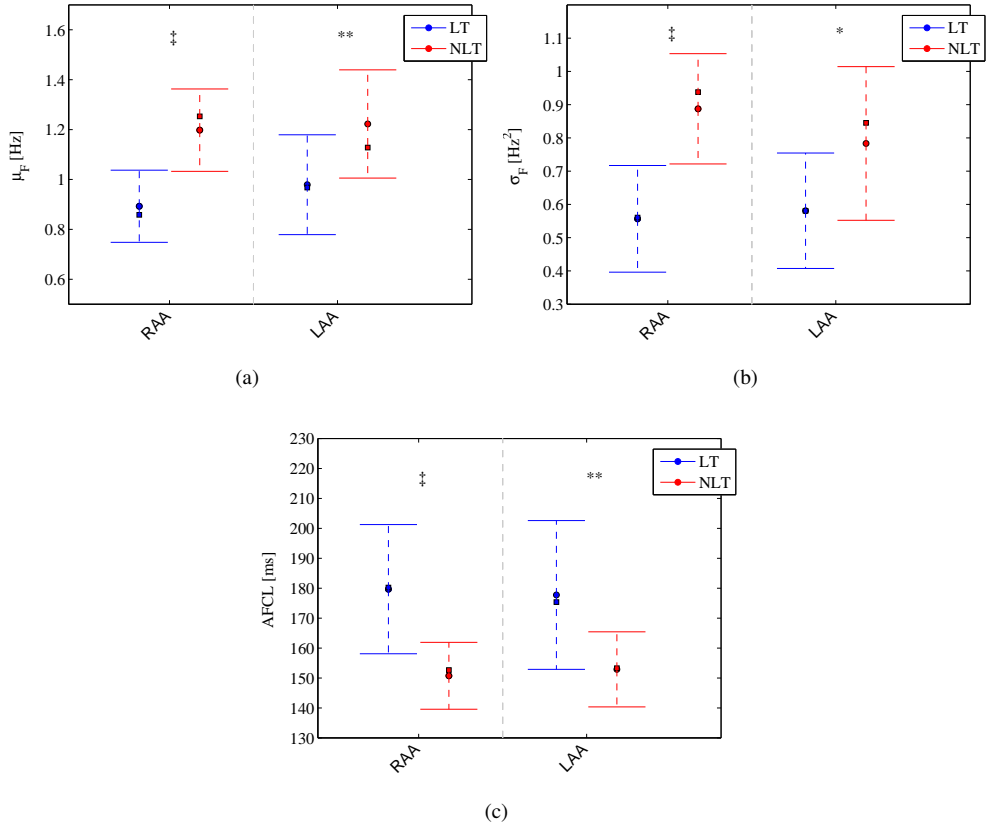
Figure 9.6: Mean (circles) ± standard devation and median (squares) of the baseline μ_f (a), σ_f^2 (b) and average AFCL (c) for the LT (blue) and NLT (red) groups computed on 20 *sec* epochs. If the ANOVA test declared a significant difference, the corresponding level is indicated ($*$: $p < 0.05$, $**$: $p < 0.01$, $\dagger$: $p < 0.005$ and $\ddagger$: $p < 0.001$).

	RAA		LAA	
	LT	NLT	LT	NLT
μ_f [Hz]	0.89 ± 0.14	1.20 ± 0.17 $\ddagger$	0.98 ± 0.2	1.22 ± 0.22 $**$
	(0.86)	(1.25)	(0.97)	(1.13)
σ_f^2 [Hz^2]	0.56 ± 0.16	0.89 ± 0.17 $\ddagger$	0.58 ± 0.17	0.78 ± 0.23 $*$
	(0.56)	(0.94)	(0.58)	(0.85)
AFCL [ms]	180 ± 22	151 ± 11 $\ddagger$	178 ± 25	153 ± 13 $**$
	(180)	(153)	(175)	(153)

Table 9.1: Mean ± standard deviations and median (in brackets) of μ_f, σ_f^2 and average AFCL before ablation computed on 20 *sec* epochs at the RAA and LAA. If the corresponding ANOVA declared a significant difference, the corresponding level is indicated ($*$: $p < 0.05$, $**$: $p < 0.01$, $\dagger$: $p < 0.005$ and $\ddagger$: $p < 0.001$).

9.4   Discussion

The AFCL estimated from various endocardial locations has been widely used as a useful clinical tool to monitor the effect of substrate change during AF catheter ablation [6, 49, 50, 97–100]. Typically, the AFCL was monitored in one or both appendages [6, 49, 98, 99]. Some studies also assessed the AFCL from the CS [6, 50, 97, 99, 100]. In all reported studies, a gradual prolongation of the AFCL has been observed prior to AF termination. Divergent results were, however, reported regarding the ability of intracardiac AFCL estimated from baseline recordings (i.e., before any ablation) to predict the procedural outcome of AF catheter ablation [6, 49, 100–103]. Some studies have shown that the baseline AFCL estimated from both appendages was significantly longer in patients in whom AF was terminated within the LA by catheter ablation [6, 49, 98, 101, 103]. In contrast, other studies observed that the baseline intracardiac AFCLs estimated from the CS and from both appendages were not predictive of the procedural outcome [99, 102]. In another study, after the exclusion of AF of shorter duration, the AFCL measured within the CS failed to predict AF termination in patients whose AF continued despite PVI [100]. All reported studies, however, included patients with paroxysmal, persistent or long-standing persistent AF of variable durations with assessment of AFCL at different atrial locations. No definite explanation can be given for these discrepancies but one may hypothesize that the AFCL from the CS reflects the composite activation of neighboring structures including the CS itself, the left ventricle and the LA [106]. In our study, however, we found that the baseline AFCL was significantly longer in both appendages in patients in whom AF terminated by stepwise catheter ablation within the LA compared to patients in whom AF continued despite extensive ablation.

In this chapter, we proposed to extend the analysis of the intracardiac AFCL by measuring its variability using novel indices. These indices characterized the mean frequency (μ_f) and variance (σ_f^2) of the oscillations around the mean AFCL. We observed that LT patients displayed a significantly lower variability of atrial activation wavefronts as compared to NLT patients in both appendages, with a more significant difference within the RA. These results are suggestive of a high temporal stability of the activation wavefronts within the appendages, and in particular within the RA.

A recent study has proposed an index of AFCL stability based on the histogram of the inverse of intervals between consecutive atrial activation wavefronts [107]. The authors observed that when AF terminated into SR, it displayed higher AFCL stability than that of unterminated AF during step-CA. Our results extend these findings by showing that the frequency of variation and range of variability of atrial activation wavefronts offer potential discriminative values that deserve further clinical validation.

Conclusion

10

Over the last twenty years, an important effort has been made by the scientific community to develop measures of AF organization with the goal to provide a better understanding of the AF pathophysiological mechanisms. Organization indices, such as the AFCL or the DF, have been successfully used in clinical studies for quantifying the electrical remodelling [13–15], and for predicting the response to pharmacologial or non-pharmacological AF cardioversion [16–20]. Despite these achievements in quantifying AF complexity, important aspects of AF therapeutic management remain unclear, in particular in the context of AF catheter ablation of long-standing persistent AF. Indeed, the performance of these "classical" organization indices computed on ECG signals for predicting the acute outcome of catheter ablation appears limited. There is an obvious need of a close collaboration between cardiologists and scientists. As an engineer in biomedical science, it is our role to develop organization indices that can predict AF catheter ablation from the surface ECG and consequently to provide an upstream tool for the cardiologists to help establishing the appropriate therapeutic strategy. Importantly, these measures of organization must remain interpretable from an electrophysiological viewpoint. This multidisciplinary collaboration has been the core spirit of the ASPG, whose collaboration with the CHUV has been ongoing for more than two decades. Moreover, the work presented in this thesis could not have been developed without former PhD theses accomplished through this partnership [77, 108]. First, the thesis completed by Mathieu Lemay was used to retrieve the ventricular activity from ECG signals [108]. Then, the second thesis, which was used for the time-varying analysis of ECG signals, was carried out by Jérôme Van Zaen, who developed efficient schemes for adaptive frequency tracking [77]. The present dissertation can be considered as a continuation of these past developments.

During this thesis, the first step consisted in defining the ablation and data acquisition protocols. From a clinical viewpoint, care was taken in establishing a detailed record of the patient population characteristics. Among other clinical characteristics, the duration of sustained AF was significantly lower in LT patients than in NLT ones. It was shown recently that a longer AF duration favors a higher degree of AF complexity [109]. Given that the average sustained duration was longer for NLT patients, the novel organization indices developed in this work from intracardiac as well as from surface ECG signals were in agreement with this clinical observation.

The baseline DF was estimated at several atrial segments. In all mapped atrial locations, a significant lower baseline DF was found in LT patients. Patients in whom catheter ablation failed to terminate AF had, on average, a significantly higher bi-atrial DF than patients in whom AF terminated. These observations are in agreement with the hypothesis of a higher complexity in

NLT patients. Moreover, in patients with persistent AF, a higher intracardiac DF has been associated to a greater degree of electroanatomical remodelling [13, 14]. Hence, higher bi-atrial DFs for the NLT patients suggest that the electrical remodelling in these patients was more advanced than that of LT patients. Furthermore, in patients with long-standing persistent AF, the presence of a LA-to-RA gradient has been poorly characterized [55, 65]. In our study, no significant LA-to-RA frequency gradient was observed for the LT and NLT groups. Our results suggest that for this particular type of sustained AF, the LA-to-RA DF gradient cannot be associated with the procedural outcome. The remodelling induced by atrial fibrillation also engenders a structural remodelling in which the atria are enlarged, in particular the left one. The average left atrial volume in our study population was large, however, it was non-significantly different between LT and NLT patients. Taken all together, these observations suggest that, in patients with long-standing persistent AF, a higher degree of electrical remodelling, rather than a large left atrial volume, is associated to failure of terminating AF by stepwise catheter ablation.

The intracardiac AFCL estimated within both appendages prior to ablation was significantly longer for LT patients than for NLT ones. The organization indices derived from the analysis of the temporal variations of the atrial activation wavefronts extended these results. It was observed that LT patients displayed in both appendages a significantly lower variablity of atrial activation wavefronts than NLT patients. These results suggest that for patients in whom AF was terminated, the temporal stability of the activation wavefronts within the appendages was higher than for patients in whom AF persisted. We can thus hypothesize that the drivers responsible for maintaining AF displayed different characteristics in terms of average frequency and temporal stability in our study population. For LT patients, these drivers had a lower frequency of activation as well as a higher temporal stability, and consequently a lower complexity than for NLT patients.

The main objective of this thesis was to derive organization indices from surface ECG signals. These signals, after cancellation of the ventricular activity, reflect the global activity of the atria. However, a correspondence between the activity recorded from the surface ECG and that from intracardiac segments is clearly of valuable information for interpreting any results derived from the analysis of ECG signals. As such, we have shown that the contributions of the right and left atria during AF can be independently determined using specific regions of the thorax, and that the main contributors to the surface ECG f-waves come from the appendages. More precisely, a strong correlation was found between the RA activity and the DF measured on lead V_1, and between the LA activity and the DF on the dorsal lead V_{6b}.

The ECG organization indices presented in the current dissertation were derived using time-invariant and time-varying approaches. In both schemes, we hypothesized that a quantification of the harmonic structure of AF signals brings more insight into the AF complexity compared to assessing the DF. In the first scheme, the harmonic components of AF f-waves were extracted using linear time-invariant filters. Such an approach is largely affected by the rapid temporal variability of AF waveforms. As such, the adaptive harmonic frequency tracking algorithm is more suitable for extracting the harmonic components of AF f-waves. Indeed, we have shown through illustrative examples that the temporal variations of the instantaneous frequency of the DF component were matching that of the intracardiac instantaneous frequency. In both schemes, two indices were developed each of which aiming at quantifying the regularity of the f-waves oscillations (OI and AOI) and the morphological regularity of the f-waves (TIPD and aPD). We have shown that the ability of the organization measures derived from the adaptive scheme were more robust for discriminating LT from NLT patients than those derived from the time-invariant approach. The AOI and aPD were significantly different between the two groups on more epoch durations and ECG leads than the OI and TIPD. The AOI and aPD are complementary indices in terms of temporal and spatial performance. Indeed, for discriminating LT from NLT patients, the AOI was statistically more robust on shorter epochs and on lead V_1, while the aPD was

statistically more robust on longer epochs and on the dorsal lead V_{6b}. More precisely, the aPD measured on the posterior lead V_{6b} was significantly lower in LT patients compared to NLT patients. As the left atrial activity was best reflected on the dorsal lead V_{6b}, our results are suggestive of a higher LA organization in patients whose AF can be terminated within the left atrium. Also, our findings of a higher coupling between the DF and its first harmonic in the LT population might be indirectly indicative of the presence within the LA of highly organized AF sources, such as rotors. We have also shown that LT patients were successfully separated from NLT ones by the AOI measured on lead V_1. As the right atrial activity was best reflected on chest lead V_1, this finding suggests that for LT patients, the organization within the RA was higher than for NLT patients. The discriminative cut-off value for classifying LT from NLT patients estimated for the AOI was highest on V_1 than on the remaining ECG leads. This result suggests that, within the RA the spectral organization over time of the cyclicity of the AF harmonic components is higher than that within the LA and is associated to AF termination. The cut-off value for the aPD was highest on leads V_1 and V_{6b}, suggesting that a higher coupling between the DF and its first harmonic within both atria is associated to AF termination. One can hypothesize that in patients in whom AF can be terminated by catheter ablation, a highly organized LA source will drive the RA in a more organized manner.

10.1 Summary of achievements

The major achievements of this thesis are summarized below.

Cinical study

The patient population in the current thesis is extremely homogeneous. Indeed, all patients suffered from long-standing persistent AF. Most of the clinical studies aiming at characterizing sustained AF include persistent and long-standing persistent AF in their study population. As AF is a progressive disease, the pathophysiological mechanisms might be different for these two types of AF. However, this rigorous inclusion criteria had a severe impact on the total number of the patients.

In this study, we report a success rate of long-standing persistent AF termination within the LA of 67%. Among the clinical characteristics of the study population, only the duration of sustained AF was significantly different between the two groups. However, AF can be asymptomatic, and therefore this duration can be wrongly assessed or even unknown in clinical practice.

The importance of ECG leads placement

In this thesis, it was decided to use a modified placement of the standard 12-lead ECG. As such, chest lead V_6 was placed in the back of the patient with the desire to improve the spatial recording of the posterior part of the atria. The main contributors to the surface ECG f-waves came from the activity in the atrial appendages. More precisely, a strong correlation was found between the RA activity and the DF measured on lead V_1, and between the LA activity and the DF on the dorsal lead V_{6b}. Measuring the LA activity non-invasively is essential, since the triggers as well as the drivers responsible for maintaining AF are predominantly present in this atrium.

Predicting AF catheter ablation outcome from the surface ECG

The organization indices derived from the adaptive harmonic frequency tracking algorithm were suitable to characterize the different AF dynamics in our study population in order to predict the outcome of AF catheter ablation. They were appropriate for quantifying non-invasively

the higher complexity in patients in whom catheter ablation failed to terminate AF than in patients in whom AF was terminated. The organization indices derived from the adaptive harmonic frequency tracking algorithm are complementary measures in terms of temporal and spatial predictive performance. The harmonic frequency tracking algorithm used is not computationally expensive, and as such, the estimation of the AOI or aPD could be implemented for a real-time application, or on embedded devices.

Baseline atrial frequency mapping

The higher bi-atrial DFs for patients in whom catheter ablation failed to terminate AF indicated that the electrical remodelling in these patients was more important than that of LT patients. No LA-to-RA frequency gradient was observed in our study population. The results obtained from the baseline DF analysis suggest that a higher degree of electrical remodelling is associated to failure of terminating long-standing persistent AF by catheter ablation.

Characterization of the variability of atrial activation intervals

The AFCL measured from intracardiac signals reflects the average regularity of the local AF dynamic. The characterization of the temporal variations of atrial activation wavefronts around the mean AFCL provides an extension for assessing the local AF dynamic. The results from this study suggested that for LT patients, the drivers responsible for maintaining AF had a lower frequency of activation as well as a higher temporal stability than for NLT patients.

10.2   Perspectives

The novel ECG organization indices presented in this thesis can be used in different types of acquisition systems or biophysical signals.

The data acquired during this thesis are unique in the sense that, for each patient, the recording was continuous during the ablation procedure and the events were meticulously timestamped and annotated. As a matter of fact, this implies that for each patient, between two to four hours of continuous recordings are available. Consequently, the databases constructed for off-line analysis have a great potential for future work, in particular for studying the evolution of AF organization during catheter ablation.

The phase difference measure for detecting sleep apnea

In this thesis, an index measuring the phase coupling between two waveforms was presented. In the present work, the two waveforms were the components characterizing the DF and its first harmonic, which were extracted from an ECG AF signal. This index quantifying the phase synchronization between these two waveforms was computed as the variance of the slope of their phase difference. But this phase coupling index can be computed on other types of biophysical signals. For instance, in a recent work published by our group, the phase coupling was assessed between the respiration signal and the respiratory sinus arrhythmia (RSA) [1] in order to detect sleep apnea episodes [110] [2]. The gold standard in detecting sleep apnea is to make use of polysomnography performed at a sleep laboratory, where the subject sleeps while wearing multiple and uncomfortable sensors [111]. Over 20 physiological signals such as nasal airflow, ECG and the electroencephalogram are acquired and later manually analyzed by a specialist in order

---

1. RSA is a natural modulation of the heart rate induced by the respiration. This phenomenon is visible on the ECG as a subtle modifications in the R-R interval in relation with respiration.
2. A medical definition of the sleep apnea syndrome is provided in Section A.1 of Appendix A

to detect episodes of sleep apnea. These cumbersome acquisitions can be performed only in a clinical facility, precluding therefore a widespread tool for diagnosing sleep apnea. In contrast, in our work [110], the ECG and respiration waveforms were acquired during a night sleep using an instrumented t-shirt worn by the subjects [112]. During normal breathing, the respiration and the RSA are mostly in phase opposition, as an inspiration corresponds with a shortening of the R-R interval [113]. However, during an episode of sleep apnea, it is assumed that this relationship is often disturbed as the respiration is altered. For this reason, the phase coupling index was assessed between the respiration and the RSA. The results have shown that this coupling was significantly lower during episodes of sleep apnea as compared to normal breathing [110].

These promising and encouraging results may have a potential and practical applications in detecting sleep apnea episodes. As opposed to polysomnography, the acquisition process is highly facilitated by the convenience of the instrumented t-shirt. Sleep apnea may be a patho-physiological factor for developing hypertension, AF and other types of heart diseases, and most often it is largely underdiagnosed. With this technology associated to the phase-coupling index, one can envisage the development of an "at-home" monitoring product, avoiding therefore the need of a bulky and uncomfortable diagnosis process.

Organization indices evolution during catheter ablation

The evolution of classical organization indices during catheter ablation has been the subject of several studies. The most widely used measure of organization assessed during catheter ablation is the AFCL estimated from various endocardial locations [6, 49, 50, 97–99]. In all reported studies, a gradual prolongation of the AFCL was observed prior to AF termination. However, in patients with long-standing persistent AF in whom AF continued despite PVI, AFCL did not change during stepwise catheter ablation, while other indices based on large intracardiac dipoles did [100]. There is thus a need to develop novel organization indices computed on intracardiac recordings, which would provide a better spatio-temporal quantification of substrate modification during catheter ablation. These measures would reflect the dynamical variations within the atria. The novel ECG organization indices developed in the present thesis can also be used to assess the global evolution of AF organization during catheter ablation. Ideally, these indices should predict the additional amount of ablation to perform in order to terminate AF during the procedure.

During this thesis, two novel methods for quantifying the evolution of AF organization during catheter ablation were developed [114, 115]. They were not presented in the current dissertation, as it was entirely dedicated to the outcome prediction of catheter ablation. However a short summary is provided below.

The first method was aimed at analyzing the structural and temporal evolution of the morphology of bipolar intracardiac signals [114]. In this study, atrial activation times were estimated by computing the local activation wave barycenters [116]. The morphological similarity between two activation waves was defined as their cosine distance [117]. Recurring patterns in the morphological regularity were assessed with recurrence plot analysis, from which three measures of organization were derived. The first one reflected the average recurrence of morphological similarity. The second one measured the percentage of consecutive activation waves that were morphologically similar. The third one was computed as the Shannon entropy of the distribution of the number of consecutive morphologically similar activations. The significance of these parameters was assessed using surrogate data and a one-sided rank-order test. Recordings acquired within the RAA were used in this study. These parameters were compared to the local AFCL. The relative evolution of the mean recurring parameters and AFCL were compared during PVI vs baseline conditions. In our preliminary results, the AFCL did not change, while the recurring parameters revealed positive and negative variations after PVI, suggestive of a greater sensitivity to the modification of the left atrial substrate by catheter ablation. Hence, these measures appear as promising parameters to titrate the amount of additional ablation required to restore long-term

SR.

The second method aimed at analyzing the synchronization between nearby bipolar intracardiac electrograms [115]. In this study, the LAT was defined as the maximum positive peak from each activation wave. Series of LATs were transformed into trains of impulses on which the cross-correlation was computed. For multiple wavefronts, the cross-correlation presents several peaks. Therefore, the peak concentration of the cross-correlation reflects the local complexity of AF dynamics. From this cross-correlation, a novel organization index was computed on the smoothed cross-correlation (Hamming window) on which the area around the largest peak was divided by the sum of the components of the cross-correlation. Low values of this index are indicative of a weak dominance of the largest peak, and consequently of a weak LAT synchronization. In contrast, high values are indicative of a single sharp dominant peak and therefore of a high coupling between LATs. Bipolar recordings acquired within the RAA were used for estimating this synchronization index as well as the AFCL. The relative evolution of their mean values was compared between PVI vs baseline conditions, CFAEs ablation vs PVI and the last two steps preceding AF termination. The preliminary results have shown that the synchronization measure was more sensitive than the AFCL for estimating changes of AF dynamics induced by catheter ablation. These results, however, must be corroborated with simulated data provided by a biophysical model of AF [118] in order to establish their electrophysiological significance.

Considering all these observations, the AFCL is not suitable for assessing the substrate modification induced by catheter ablation. The organization indices presented in Chapter 9 extend the analysis of intracardiac AFCL by measuring its variability. These indices characterized the mean frequency and variance of the oscillations around the mean AFCL. These measures might be more sensitive in tracking the organization during stepwise catheter ablation "en route" to AF termination and might help to titrate the amount of ablation required to restore SR.

Long-term outcome and termination mode of catheter ablation

In this thesis, the prediction of outcome was investigated on the acute termination of first-time catheter ablation in patients with long-standing persistent AF. A logical continuation of the present work is to study the long-term outcome (3, 6, and 12 months) of stepwise catheter ablation in terms of AF recurrence. Acute termination of AF during catheter ablation does not necessarily ensure a long-term SR maintenance. In fact, patients with long-standing persistent AF may need several attempts of catheter ablation in order to ensure long-term SR maintenance. Hence, this future work should investigate if the organization indices are still discriminative in terms of AF recurrence in the long-term.

Moreover, as presented in Chapter 5, AF can be terminated according to one of these three scenarios: 1) AF directly converts into SR; 2) AF converts to AT and subsequently to SR; and 3) catheter ablation fails to terminate AF and DCC is delivered in order to restore a SR. In patients with long-standing persistent AF, conflicting results were reported regarding the impact of the termination mode during catheter ablation on the long-term SR maintenance [119–124]. On one hand, some groups have shown that the termination mode had no impact on the long-term maintenance of SR [119, 120]. On the other hand, other groups have shown that AF termination into SR had a better long-term clinical outcome [121, 122], whereas other studies have shown that AF termination into AT was associated with a higher likelihood of SR maintenance [123, 124]. Associated with the long-term prediction, the study should also investigate if the organization indices are predictive of the impact of termination mode, and furthermore to establish their association with the long-term SR maintenance.

Multivariate analysis on a larger population

This thesis is mainly limited by the small size of the study population. Future work should compare on a larger population the predictive performance of the new organization indices with the duration of sustained AF (if known) to separate LT and NLT patients at baseline. This limitation also prevented the completion of a multivariate statistical analysis. This kind of statistical analysis would also pave the way for the development of a robust classifier for predicting AF catheter ablation outcome.

Characterization of CFAEs

In human AF, fragmented potentials were first identified in 1997 by Konings et al. who showed that they were largely present in atrial regions displaying either slow conductions or locations of wavelet pivots [125]. Later on, Nademanee et al. proposed the term of CFAE for describing sites with continuous high frequency activities and showed that ablation of CFAEs throughout the atria was associated with the restoration of SR in patients with long-standing persistent AF [53]. During the ablation procedure, CFAEs are visually identified by the operator which is challenging and highly subjective. CFAEs ablation results in extensive atrial lesions that may preclude any recovery of atrial contractile function despite SR restoration. The exact pathological mechanisms of CFAEs are not yet fully understood and are currently an open debate in the medical community, which is reflected by the considerable number of publications on this subject. Nonetheless, it has been shown that catheter ablation at sites displaying a greater percentage of continuous activity or a temporal activation gradient is associated with slowing or termination of chronic AF [7]. However, it is unknown if some proportion of ablated CFAE sites that do not enable AFCL slowing or AF termination play a role in the AF perpetuation process and if their ablation increases or decreases AF organization. Recently, algorithms for time-domain analysis of CFAEs were implemented in the available electroanatomical mapping systems. Despite these recent advances, physicians still do not have a tool to discriminate between culprit and non culprit CFAEs. To the best of our knowledge, to date, no study has been undertaken on CFAE characteristics predictive of an organizational increase during AF. Using the novel organization indices presented in the current thesis, these variations of organization can be assessed globally (from the ECG) as well as within the atria. As such, it would possible to determine whether some CFAE displaying specific characteristics play a hidden role in AF perpetuation and ultimately to define a fully automated fractionation index estimation algorithm, suitable for off-line and on-line electrogram analysis. Such an approach would be of benefit for the physician and for the patients comfort. Indeed, the automated discrimination between culprit and non-culprit CFAEs would greatly reduced the amount of useless ablation, and consequently the procedural time.

From standard 12-lead ECG to body surface potential maps

One of the major drawback of the standard 12-lead ECG is that it was specifically designed to follow the depolarisation and repolarisation of the ventricles, which renders difficult the estimation of the spatial information of the atrial activity. In the present thesis, the precordial lead V_6 was placed in the patients back and this simple replacement has proven to be very useful in assessing non-invasively the LA activity. Moreover, in the present work, the ECG results have shown that lead V_5 was useless in predicting the procedural outcome of catheter ablation. Hence, one might think of using this electrode as an additional dorsal lead in order to improve the spatial resolution of the posterior recording of the atria. However, another device is available for increasing the spatial resolution of surface ECG recordings. This tool, known as *body surface potential maps* (BSPM), is an adjustable vest made of an array of electrodes (between 32 to 300) distributed anteriorly, posteriorly and on the lateral sides of the patients chest.

In the context of AF catheter ablation, recent clinical studies have used BSPM combined with anatomical information of the atria assessed by computed tomography [109, 126, 127]. From the imaging data, the precise position on the patients chest of each BSPM electrode is acquired and a three-dimensional model of the atrial epicardial geometry is reconstructed. The signals recorded from the BSPM are then combined with the geometrical information by the use of specifically designed algorithms in order to estimate a map of atrial epicardial electrical potentials. This process, also known as *ECG imaging*, was originally developed by Rudy's group for ventricular mapping in order to detect local heart rate variability and was later on adapted to atrial mapping [109]. The main goal of these algorithms is to solve what is known as the *inverse problem*. Importantly, solving the inverse problem is a non-trivial task, in particular when studying the atrial epicardial dynamic during AF, and is hindered by three major characteristics. First, the solution of the inverse problem is not unique. Indeed, the same set of surface recordings could result from more than one source configuration. Typically, this difficulty is circumvented by using simplified models of the cardiac current sources [128]. Second, the inverse problem is by its very nature ill-posed, i.e., any small variations on the BSPM can cause an erratic large modification of the equivalent source solution. This important issue mainly results from the smoothing and attenuation of the electrical fields caused by the subject's torso. The desired solution is therefore unstable and highly sensitive to noise, or perturbation in the electrical input data. Actually, this ill-posedness increases with the complexity of the assumed heart (or atrial) model [128]. Bypassing the ill-posed nature of the inverse problem is very arduous and needs the assumption of additional spatial and temporal constraints on the heart/atrial model parameters. These relaxations may alter the estimation of the atrial epicardial electrical activity, providing a possible solution, which can be different from the real electrophysiological dynamic. Lastly, in the particular context of AF, as for the signals recorded on the standard 12-lead ECG, the ventricular activity is predominant in BSPM recordings. The clinical studies using BSPM usually circumvent this issue by acquiring segmented f-waves occurring between several consecutive spontaneous or drug-induced QRS pauses [109, 126, 127]. The resulting sequential recordings are of few seconds duration (typically < 10 seconds). As surface f-waves rapidly vary over time, such approach may not be appropriate for assessing the temporal variations of AF dynamics.

Recently, Haïssaguerre et al. published a very interesting study in which ECG imaging was used to identify atrial regions harboring AF drivers and to characterize them according to the type of AF [127]. Epicardial fibrillatory driver density maps were estimated in order to identify the atrial sites possibly anchoring a source of AF. Then, sequential ablation started from the region with highest density activity to the lowest one until AF termination. If AF was not terminated, linear ablations were performed within the LA. The authors report AF termination in 75% of patients with persistent AF, while for patients with long-standing persistent AF the success rate dropped to 15%. Importantly, the authors noted that in patients with persistent AF, most of the drivers were located in the PV-left atrium regions, while in patients with long-standing persistent AF sources were found beyond the PV region. Although their method clearly suggested time-critical mechanisms for persistent AF, it did not reveal different dynamical behaviors in patients in whom AF was terminated compared to those whose AF was not terminated. The method proposed by Haïssaguerre et al. has raised a call for more understanding within the medical community. First, the process of solving the inverse problem inevitably adds critical assumptions on the atrial model, and cannot take into account the presence of fibrosis for instance. Second, a recent study from Verheule et al. has shown that AF must be considered as a three dimensional arrhythmia characterized by an electrical dissociation between the epicardial layer and the endocardial bundle network [129]. In [127], the drivers are located on an epicardial map, while the ablation is performed within the atria. Hence, the site of ablation does not correspond to the activity estimated on the epicardial density map. Finally, some authors have suggested that a more refined evaluation of AF dynamics is required in order to improve the understanding of AF [130]. Such improvement was achieved by the study of Guillem et al. in which spectral

analysis of body surface recordings during AF helped to characterize the global distribution of the atrial DFs and to identify non-invasively the atria with the highest frequency [86].

As a perspective for the ECG processing schemes presented in the current thesis, a similar approach to that proposed by Guillem et al. of BSPM recordings could be performed. In addition to classical spectral analysis, the computation of the organization indices derived from the adaptive frequency tracking algorithm would enhance the assessment of AF complexity. Indeed, the AOI and aPD have shown to be more robust than time-invariant measures in predicting the procedural outcome of catheter ablation in patients with long-standing persistent AF. Combined with the high spatial resolution provided by BSPM, the amount of organization in different atrial segments could be characterized non-invasively with a better spatial accuracy.

Appendix

A

Definitions

This appendix aims at providing medical and mathematical definitions. First, various medical definitions are presented (Section A.1). Then, the concept of instantaneous frequency and the discrete Hilbert transform are explained (Section A.2). Finally, the binary logistic regression model (Section A.3) as well as the receiver operating characteristic curve analysis are described (Section A.4).

A.1   Medical definitions

– **Thromboembolism**: a thromboembolism is a condition in which a clot (thrombus) in the blood is formed and carried from its site of formation, leading to the obstruction of a blood vessel.

– **Body Mass Index (BMI):** is a measurement of relative weight, based on an individual's mass and height. In other words, it quantifies the relative percentages of fat and muscle mass in the human body. More specifically, it is defined as the individual's body mass in kilogram divided by the square of the height in meters. The unit of the BMI is therefore kg/m^2. By convention a BMI < 18.5 kg/m^2 is categorized as underweight. A BMI in the range $18.5 - 25$ kg/m^2 is considered as normal. Overweight is when the BMI is in the interval $25 - 30$ kg/m^2. Finally, a BMI > 30 kg/m^2 is considered as obese.

– **Hypercholesterolemia:** refers to the presence of high level of cholesterol in the blood.

– **Sleep apnea syndrome:** is a serious type of sleep disorder in which breathing is characterized by pauses (lasting from at least ten seconds up to several minutes), or instances of shallow or irregular episodes. Many studies have established a link between atrial fibrillation and sleep apnea, however the interplay between the two diseases is complex.

– **CHA_2DS_2 VASc score:** is a risk factor for patients with non-valvular AF used as a clinical prediction rule. The meaning of the acronym CHA_2DS_2 VASc is the following: [Congestive heart failure, hypertension, age ≥ 75, diabetes, stroke, vascular disease, age $65 - 74$, and sex category]. The score is computed on a point system in which 2 points are given for a history of stroke, or age ≥ 75; and one point is assigned respectively for age $65 - 74$ years, a history of hypertension, diabetes, recent cardiac failure, vascular disease, and female sex [4]. The maximum CHA_2DS_2 VASc score is therefore 9.

– **Dilated cardiomyopathy:** is a progressive disease of the heart muscle in which the ventricles are importantly enlarged, which consequently alters the efficient pumping of the blood throughout the body.

– **Hypertrophic cardiomyopathy:** is a disease in which the heart muscle (and in particular the ventricular walls) becomes abnormally thick. Despite this thickening, the ventricle size often remains normal. This thickening may, however, block the blood flow out of the ventricles.

– **Congestive heart failure:** occurs when the heart is unable to pump sufficient blood in order to maintain a normal flow to meet the needs of the body. A heart failure happens when the heart muscle cannot pump properly the blood out of the ventricles (in this case it is called a systolic failure), or when the muscles are stiff and do not fill up with blood correctly (in this case it is called a diastolic heart failure).

– **Left ventricular fraction ejection:** measures the percentage of blood being pumped out of the left ventricle each time the heart contracts. A left ventricular fraction ejection of $\geq 55\%$ is considered normal, while $\leq 50\%$ is considered reduced.

– **Beta-blockers:** or β-blockers, are a class of drugs that block the action of the sympathetic nervous system of the heart, thus reducing the stress on the heart. Consequently, these drugs slow down the heart beat and decrease blood vessel contraction in the heart. β-blockers are used to treat certain cardiac arrhythmias as well as hypertension.

– **Calcium channel blockers:** also called calcium channel antagonists, are a group of medication that disturbs the movement of calcium through calcium channels. More specifically, these drugs prevent the calcium from entering the cells of the heart and blood vessel walls. These types of drugs are mainly used against hypertension.

– **Amiodarone:** is an antiarrhythmic medication commonly used for different types of ventricular and atrial cardiac arrhythmias. The amiodarone prolongs phase 3 of the cardiac action potential (i.e. the repolarization phase, see Section 2.1.3 of Chapter 2).

– **Enzyme conversion inhibitors:** is a pharmacological drug primarily used for the treatment of hypertension and congestive heart failure.

– **Angiotensin receptor inhibitors:** are medication commonly used to treat high blood pressure, diabetic nephropathy (kidney damage due to diabetes), and congestive heart failure.

– **Statins:** are a class of drugs used to lower the cholesterol level.

A.2 Instantaneous frequency and the Hilbert transform

This section presents a brief introduction on the concept of instantaneous frequency [1]. Then, the discrete Hilbert transform is briefly explained in A.2.2.

A.2.1 The concept of instantaneous frequency

Frequency is defined as the number of oscillations observed per unit of time. In contrast, the instantaneous frequency is the frequency at a given time. In many applications, the spectral characteristics of a given signal vary over time. Such signals are referred as non-stationary. For these particular signals, the concept of instantaneous frequency reflects a time-varying parameter which defines the location of the signal spectral peaks as they vary over time [131].

The concept of instantaneous frequency was originally introduced by Carson and Fry who defined it as the rate of change of phase angle at a given time [132]. The authors argued that the concept of instantaneous frequency is a generalization of the definition of constant frequency. Later, van der Pol [133] provided an extension of this definition by considering amplitude- and frequency-modulated sinusoids of the following form:

$$x(t) = a(t)\cos(\phi(t)), \qquad (A.1)$$

where $a(t)$ and $\phi(t)$ are the time-varying amplitude and phase respectively. In their work, the authors showed that the instantaneous frequency is defined as the derivative of the phase with respect to time:

$$\omega_i(t) = \frac{d\phi(t)}{dt}. \qquad (A.2)$$

In order to extract the phase from any types of signals, Gabor proposed a method for generating a unique complex signal from a real one, known as the *analytic signal* [60]. His method consisted first in taking the Fourier transform of the real signal. Then, the amplitudes corresponding to negative frequencies were set to zero and the amplitudes corresponding to positive frequencies were multiplied by two. Finally, in order to obtain the analytic signal, the modified spectrum was transformed back to the time domain. Gabor showed that this procedure was equivalent to the following time-domain procedure:

$$x_a(t) = x(t) + j\mathcal{H}\{x(t)\} = x(t) + jx_h(t) = a(t)e^{j\phi(t)}. \qquad (A.3)$$

where $a(t)$ and $\phi(t)$ are the instantaneous amplitude and phase, $x_a(t)$ is the analytic signal, $x(t)$ is the real signal, $\mathcal{H}\{\cdot\}$ denotes the Hilbert transform, and $x_h(t)$ is the Hilbert transformed original signal defined as:

$$x_h(t) = \mathcal{H}\{x(t)\} = \frac{1}{\pi}\,\text{p.v.}\int_{-\infty}^{\infty}\frac{x(\tau)}{t-\tau}\,d\tau, \qquad (A.4)$$

where p.v. denotes the Cauchy principal value of the integral [131]. Moreover, the Hilbert transform can be seen as the convolution of $x(t)$ with the function $\frac{1}{\pi t}$. Indeed, in order to compute the Hilbert transform, due to the integration interval, knowledge of $x(t)$ over the entire time domain is required. However, the main contribution of the integral defined in equation A.4 comes from the region around a particular time t. As such, the Hilbert transform is expressed in the Fourier domain as:

$$X_h(f) = \mathcal{F}\left\{\frac{1}{\pi t}\right\} \cdot X(f). \qquad (A.5)$$

Using the following Fourier transform pair [134],

$$\frac{1}{t} \overset{\mathcal{F}}{\longleftrightarrow} -j\pi\,\text{sgn}(f), \qquad (A.6)$$

---

1. For a more detailed introduction on the concept of instantaneous frequency see [131].

$X_h(f)$ can be expressed as

$$X_h(f) = \begin{cases} jX(f) & \text{for } f < 0, \\ 0 & \text{for } f = 0, \\ -jX(f) & \text{for } f > 0. \end{cases} \tag{A.7}$$

Thus, the Hilbert transform consists in performing a phase shift of $-\frac{\pi}{2}$ (respectively $\frac{\pi}{2}$) for every positive (respectively negative) frequencies. In other words, the imaginary part of the analytic signal corresponds to the original signal delayed by a phase of $\frac{\pi}{2}$. As such, the analytic signal of an harmonic oscillation $x(t) = A_0 \cos(\omega_0 t)$ is $x_a(t) = A_0 \cos(\omega_0 t) + jA_0 \sin(\omega_0 t)$.

Finally, based on the previous works of Carson and Fry [132], van der Pol [133], and Gabor [60], Ville went further in defining the instantaneous frequency as the derivative of the instantaneous phase $\phi(t)$ of the analytic signal $x_a(t)$ with respect to time:

$$\omega_i(t) = \frac{d}{dt} \arg\{x_a(t)\}. \tag{A.8}$$

A.2.2   The discrete Hilbert transform

The concept introduced previously were presented for continuous-time signal. However, the approach is also applicable to discrete-time signals. The most classical method is based on the discrete Hilbert transform which is briefly explained [2].

For a discrete-time signal $x[n]$, the analytic signal $x_a[n]$ is defined as:

$$x_a[n] = x[n] + jx_h[n] = a[n]e^{j\phi[n]}, \tag{A.9}$$

where $x_h[n]$ is the discrete Hilbert transform of $x[n]$. Similarly to the continuous case, the discrete Hilbert transform can be computed by convolving a signal with the discrete-time Hilbert filter: $x_h[h] = h[n] * x[n]$ [81]. This infinite impulse filter is given by:

$$h[n] = \begin{cases} 0 & \text{for } n \text{ even}, \\ \frac{2}{\pi n} & \text{for } n \text{ odd}. \end{cases} \tag{A.10}$$

However, in practical situations, the Hilbert filter A.10 can be approximated with a finite impulse response. In the frequency domain, the discrete Hilbert transform can also be computed as:

$$X_h(e^{j\omega}) = \text{DTFT}\{x_h[n]\} = \text{DTFT}\{h[n] * x[n]\} = H(e^{j\omega}) \cdot X(e^{j\omega}), \tag{A.11}$$

where the discrete-time Fourier transform (DTFT) of the Hilbert filter (A.10) is defined as

$$H(e^{j\omega}) = \begin{cases} j & \text{for } -\pi < \omega < 0, \\ 0 & \text{for } \omega = 0, \\ -j & \text{for } 0 < \omega < \pi. \end{cases} \tag{A.12}$$

Thus, the discrete Hilbert transform is obtained by performing a phase shift for the components of positive (respectively negative) frequencies by $-\frac{\pi}{2}$ (respectively by $\frac{\pi}{2}$).

In practice, the DTFT is not applicable, and consequently the discrete Fourier transform (DFT) is used instead. As such, the frequency response of the Hilbert filter of length N is given by

$$H[k] = \begin{cases} 0 & \text{for } k = 0, \\ -j & \text{for } 1 \leq k \leq \frac{N}{2} - 1, \\ 0 & \text{for } k = \frac{N}{2}, \\ j & \text{for } \frac{N}{2} + 1 \leq k \leq N - 1, \end{cases} \qquad \text{when } N \text{ is even,} \tag{A.13a}$$

---

2. For a more thorough presented on the discrete Hilbert transform see [81]

and

$$H[k] = \begin{cases} 0 & \text{for } k = 0, \\ -j & \text{for } 1 \leq k \leq \frac{N-1}{2}, \\ j & \text{for } \frac{N+1}{2} \leq k \leq N - 1, \end{cases} \qquad \text{when } N \text{ is odd.} \qquad (A.13b)$$

Then, $X_a[k]$ is computed directly from the DFT of a real signal of length N [78]:

$$X_a[k] = \begin{cases} X[0] & \text{for } k = 0, \\ 2X[k] & \text{for } 1 \leq k \leq \frac{N}{2} - 1, \\ X[N/2] & \text{for } k = \frac{N}{2}, \\ 0 & \text{for } \frac{N}{2} + 1 \leq k \leq N - 1, \end{cases} \qquad \text{when } N \text{ is even,} \qquad (A.14a)$$

and

$$X_a[k] = \begin{cases} X[0] & \text{for } k = 0, \\ 2X[k] & \text{for } 1 \leq k \leq \frac{N-1}{2}, \\ 0 & \text{for } \frac{N+1}{2} \leq k \leq N - 1, \end{cases} \qquad \text{when } N \text{ is odd.} \qquad (A.14b)$$

A.3   Binary logistic regression and odds ratio

In medical studies, when a set of variables are to be used for prediction, the most commonly employed technique is the logistic regression. The logistic regression (also called the logit regression) models the relationship between the explanatory variables and the outcome, so that an outcome can be predicted for a new set of explanatory variables. More specifically, the outcome of the explanatory variables is binary (or dichotomous, i.e., only two outcomes are possible, for example "treatment success" or "treatment failure"). The goal of the logistic regression is to find the best fitting model describing the relationship between the outcome variable and a set of independent (explanatory) variables.

Let $X_1, \ldots, X_N$, be a set of N explanatory variables and Y be a dichotomous variable. For example, Y can be defined as:

$$Y = \begin{cases} 1 & \text{for treatment success,} \\ 0 & \text{for treatment failure.} \end{cases}$$

The goal is to model the probability that Y takes the value 1 as a function of the explanatory variables X. In other words, the aim is to derive an equation to predict the probability of the occurrence of the outcome of interest. This conditional probability of Y given X is denoted as $\pi(X)$. The logistic regression fits the probability distribution of the following form:

$$\pi(X) = \frac{\exp(\beta_0 + \beta_1 X)}{1 + \exp(\beta_0 + \beta_1 X)} \tag{A.15}$$

where β_0 and β_1 are the regression coefficients to be estimated. The most commonly used technique to estimate these parameters is maximum likelihood, in which the estimate of a parameter maximizes the probability of the observed data. For more details about the estimation of the regression coefficients, see [135].

The Equation defined in (A.15) describes a family of sigmoid curves. Figure A.1 illustrates several regression curves for different parameter values. As it can be observed, as $x \to -\infty$, $\pi(X) \to 0$, conversely, as $x \to \infty$, $\pi(X) \to 1$. The model given in equation (A.15) satisfies therefore the important requirement that $0 \le \pi(X) \le 1$. The parameter β_1 controls how fast $\pi(X)$ rises from zero to one. The value of X at which $P(Y = 1) = 0.5$ is given by $-\beta_0/\beta_1$ and provides useful information. For example, if the output is either "success" or "failure" of a particular medical treatment, this would reflect the level such that there is a $50 - 50$ chance that, for a certain patient, this specific treatment will be effective.

From Equation (A.15), it follows that $\pi(X)/(1 - \pi(X)) = \exp(\beta_0 + \beta_1 X)$, and thus:

$$\log\left(\frac{\pi(X)}{1 - \pi(X)}\right) = \beta_0 + \beta_1 X \tag{A.16}$$

Since Equation (A.16) results from using a *logistic transform* (also called a logit transform), the model described above is called a binary logistic regression model. The left side of Equation (A.16) is called the *log odds ratio*. Moreover, from Equation (A.16), β_1 represents the amount by which the log odds changes per unit change in X. It is somewhat more meaningful, however, to state that a one-unit increase in X increases the odds by the multiplicative factor $\exp(\beta_1)$ (by exponentiating both sides of Equation (A.16)) [135]. Therefore, the expression $\exp(\beta_1)$ represents the *odd ratio*. A property of logistic regression is that this ratio remains constant for all values of X. Thus, the odds ratio represents the change in the odds of the outcome by increasing X by one unit.

Odds ratio are commonly used to compare the relative odds of the occurrence of the outcome (e.g., "treatment success" or "treatment failure"), given exposure to the variable of interest (e.g., age, health characteristics, organization indices). Moreover, the odds ratio can also be used to
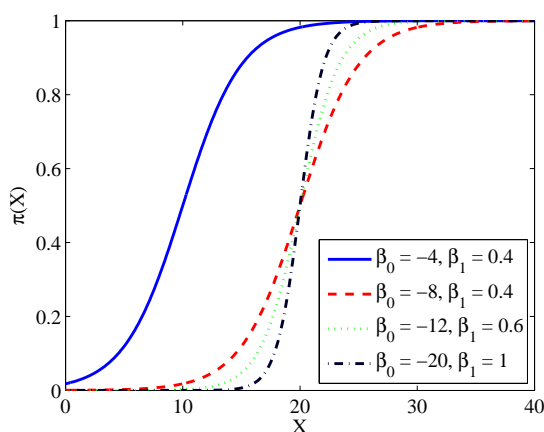
Figure A.1: Examples of different regression curves.

determine whether the value of a particular explanatory variable (e.g., age > 80) , also called exposure, is a risk factor for a particular outcome (e.g., "treatment success). More specifically:

– $\exp(\beta_1) = 1$: the exposure does not affect the odds of outcome. In other words, $\beta_1 = 0$ and therefore the odds and probability are at the same level for all X.

– $\exp(\beta_1) > 1$: the exposure is associated with higher odds of outcome. In other words, $\beta_1 > 0$ and therefore the odds and probability increase as X increases.

– $\exp(\beta_1) < 1$: the exposure is associated with lower odds of outcome. In other words, $\beta_1 < 0$ and therefore the odds and probability decrease as X increases.

In other words, the odds ratio shows the strength of association between a predictor and the response of interest.

Associated with the odds ratio, the 95% confidence interval is used to estimate the precision of the odds ratio. This confidence interval is closely related to the confidence interval for β_1 which is obtained as $[\beta_1 \pm z_{\alpha/2}\sigma_{\beta_1}]$, where $z_{\alpha/2}$ denotes the standard normal deviate with a tail area of $\alpha/2$ and σ_{β_1} is the standard error of the estimation of β_1 [135]. A large confidence interval is indicative of a low precision of the odds ratio and conversely, a small confidence interval is indicative of a high precision of the odds ratio.

A.4   Receiver operating characteristic curve analysis

Training data are used to construct the classification rule. Once the classification rule (or model) has been established, it is of interest to know how effective it will be in assigning future objects to classes. Let us suppose that the studied population is composed of N patients and that a binary classification is performed in which the outcomes are labelled as *positive* (P) or *negative* (N). There are four possible outcomes from a binary classifier:

- True positive (TP): the prediction outcome is positive and the actual outcome is positive.
- True negative (TN): the prediction outcome is negative and the actual outcome is negative.
- False positive (FP): the prediction outcome is positive and the actual outcome is negative.
- False negative (FN): the prediction outcome is negative and the actual outcome if positive.

Classification effectiveness is measured by the number of TP and TN relative to the total number of cases. These two ratios are used to define the two complementary measures of the classification performance and they are known as *sensitivity* and *specificity*. Therefore:

$$\text{Sensitivity} = \frac{\text{TP}}{\text{TP} + \text{FN}} \tag{A.17}$$

$$\text{Specificity} = \frac{\text{TN}}{\text{FP} + \text{TN}} \tag{A.18}$$

The receiver operating characteristic (ROC) curve is defined as a graphical plot of sensitivity vs. $(1 - \text{specificity})$ for a binary classifier model as its discriminant threshold varies. Figure A.2 shows an example of a hypothetical ROC curve. The best prediction method would yield a point in the upper left corner at coordinate $(0, 1)$, representing 100% sensitivity (no FN) and 100% specificity (no FP). A complete random guess would yield a point along the diagonal (also called the *chance diagonal*). Intuitively, it can be observed that points above the diagonal represent good classification results (i.e. better than random), and conversely points below the diagonal represent poor classification results (i.e. worst than random). Following this observation, two indices are commonly used for characterizing the ROC curve, and therefore the classification performance.
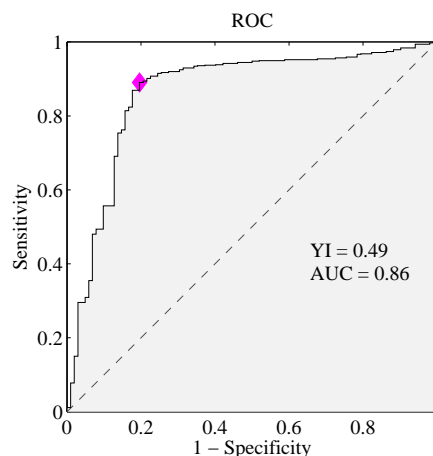

Figure A.2: Examples of a ROC curve. AUC: Area under curve (gray area); YI: Youden Index (pink dash-dotted line). *Data from [136].*

The first measure for characterizing the ROC curve is the area under the curve (AUC). The AUC measures the average true positive rate, taken uniformly over all possible false positive

rates in the range $(0, 1)$. The closer to 1 the AUC is, the more unbalanced the ROC curve is, implying that both sensitivity and specificity of the classification are high. In Figure A.2, the AUC corresponds to the gray area and is equal to 0.89, indicative of a good classification performance.

The second measure is the *Youden* index (YI), which is defined as the maximum difference between the TP and FP rates. In Figure A.2, the YI is illustrated by the pink diamond marker. As illustrated in Figure A.2, the point on the ROC curve corresponding to the YI is therefore the most distant from the diagonal. Thus, the YI is the distance of the farthest point $[(1 -$ specificity), sensitivity] on the ROC curve from the diagonal. Moreover, the threshold at the point on the ROC curve corresponding to the YI is often taken to be the optimal classification threshold.

In summary, the ROC curve provides an assessment of the classifier performance over the whole range of potential threshold values.

Devices

B

In the first part of this appendix, technical details on the catheters are provided (Section B.1). For each ablation procedure four different catheters were used, consisting of one ablation catheter (Section B.1.1) and three mapping catheters (Section B.1.2). Section B.2 presents the system used for the recording and export of the ECG and EGM signals.

B.1 Catheters

B.1.1 Ablation catheter

The ablation was performed with a NaviStar$^{®}$ ThermoCool$^{®}$ catheter from Biosense Wester. The cooling system is of the type open-loop providing therefore a uniform cooling (see Section 4.1.2 in Chapter 4). Figure B.1a illustrates the tip electrode of the ablation catheter. During ablation, a saline solution is passed through the holes as shown Figures B.1a and B.1b. The RF current is delivered to the tip electrode.
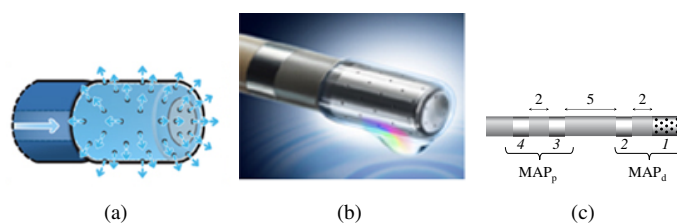

Figure B.1: (a) electrode tip and cooling; (b) NaviStar$^{®}$ ThermoCool$^{®}$ ablation catheter (Biosense Wester$^{®}$); and (c) illustrates the spacing between the electrodes (distances are indicated above the catheter). The numbers in italic below the catheter correspond to the electrode number. *Images from:* `https://www.biosensewebster.com/thermocoolsf.php`.

The tip is deflectable, which facilitates the electrophysiological mapping of the atria and the transmission of the RF current to the tip electrode. The size of the tip electrode is 3.5 *mm* (electrode number 1 in Figure B.1c).

In total the catheter has four electrodes. Typically, for deriving bipolar EGMs, recordings between adjacent electrode pairs are used (e.g. between electrodes $1-2$, $2-3$ and $3-4$), with a dis-

tance of 1 to 5 *mm* between electrodes. The electrode spacing of the NaviStar® ThermoCool®
ablation catheter is $2-5-2$ *mm*, as illustrated in Figure B.1c. Table B.1 summarizes the technical
specificities of the NaviStar® ThermoCool® ablation catheter. The two bipolar signals MAP_d
and MAP_p are derived from the pair of electrodes $1-2$ and $3-4$ respectively and represent the
most distal and proximal pairs of electrodes of the catheter. In this manuscript, this catheter is
denoted as the *MAP* catheter.

Tip electrode	Electrode spacing	Number of electrodes	Bipolar signals labels
3.5 *mm*	$2-5-2$ *mm*	4	MAP_d, MAP_p

Table B.1: Characteristics of the NaviStar® ThermoCool® ablation catheter.

B.1.2   Mapping catheters

Lasso catheter

The Lasso® 2515 variable circular mapping catheter from Biosense Webster (Figure B.2)
was used during the baseline acquisition to map the LA; during the PVI step to localize the
earliest activation at each PV antrum and to monitor the LAA AFCL once each PV was elec-
trically isolated; and finally during post-PVI for a constant monitoring of the LAA AFCL (see
Section 5.2.3 of Chapter 5 for the description of the ablation protocol).

Figure B.2: Lasso® 2515 variable circular mapping catheter (Biosense Wester®). *Picture from*
`http://www.stryker.com`

Table B.2 summarizes the technical specificities of the Lasso® 2515 variable circular map-
ping catheter. The Lasso® 2515 catheter has a variable loop allowing it to adjust and fit any
vein antrum of size between 15 and 25 *mm*. The catheter has 20 electrodes with a spacing of
$2-6-2$ *mm* (Figure B.2 and Table B.2). This catheter is specifically designed to facilitate the
electrophyisological mapping of the atria.

Diameter	Electrode spacing	Number of electrodes	Bipolar signals label
$15-25\ mm$	$2-6-2\ mm$	20	Lasso_{1-2}, Lasso_{3-4}, Lasso_{5-6}, Lasso_{7-8}, Lasso_{9-10}, Lasso_{10-11}, Lasso_{11-12}, Lasso_{13-14}, Lasso_{15-16}, Lasso_{17-18}, Lasso_{19-20}

Table B.2: Characteristics of the Lasso® 2515 variable circular mapping catheter.

Coronary sinus catheter

The Biosense Webster Coronary Sinus with EZ Steer® Bi-directional Technology was placed within the coronary sinus during the entire duration of the ablation procedure. This catheter is specifically designed to map the electrical activity within the coronary sinus. The catheter has a tip electrode of $2\ mm$ and 10 electrodes with a spacing of $2-8-2\ mm$ (Table B.3). The catheter is also bi-directionally deflectable in order to facilitate an accurate positioning of the catheter at the desired location. For each patient, the electrode CS_{9-10} was placed at the CS ostium in order to avoid inter-patient spatial variability. In this manuscript, this catheter is denoted as the *CS-cath* catheter.

Tip electrode	Electrode spacing	Number of electrodes	Bipolar signals labels
$2\ mm$	$2-8-2\ mm$	10	CS_{1-2}, CS_{3-4}, CS_{5-6}, CS_{7-8}, CS_{9-10}

Table B.3: Characteristics of the Coronary Sinus with EZ Steer® Bi-directional Technology catheter.

Quadripolar catheter

The Supreme® Quadripolar Electrophysiology catheter from St. Jude Medical® was placed within the RAA during the entire procedure for a constant monitoring of the RA. As illustrated in Figure B.3, this catheter has four electrodes with a spacing of 5 *mm*. Table B.4 summarizes the technical specificities of the Supreme® Quadripolar Electrophysiology catheter. In this manuscript, this catheter is denoted as the *HRA* catheter.
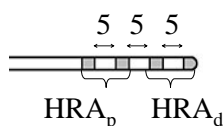
$$5 \quad 5 \quad 5$$

$$\text{HRA}_p \qquad \text{HRA}_d$$

Figure B.3: The Supreme® Quadripolar Electrophysiology catheter (St. Jude Medical®). *Picture from* `http://www.sjm.com`.

Electrode spacing	Number of electrodes	Bipolar signals labels
$5-5-5$ *mm*	4	HRA_d, HRA_p

Table B.4: Characteristics of the Supreme® Quadripolar Electrophysiology catheter.

B.2   Siemens AXIOM Sensis XP

All the ECG and EGMs signals were recorded and exported through the AXIOM Sensis XP® (Siemens®) at a sampling frequency of 2 *kHz*. Because of the electrical interference induced by the common AC current, a notch filter was applied at the frequency of 50 *Hz* reducing therefore all undesired noise at this frequency. Moreover, specific bandpass filters were applied in with respect to the input signal:

– all signals from the ECG were filtered with a passband of $[0.05-200]$ *Hz*.
– all signals from the HRA catheter were filtered with a passband of $[40-400]$ *Hz*.
– all signals from the MAP, CS-cath and HRA catheters were filtered with a passband of $[30-400]$ *Hz*

Ventricular Activity Cancellation

C

The signals recorded from the surface ECG reflect the global activity of the heart, so both ventricular and atrial components are present (Chapter 2, Section 2.2). In studies aiming at characterizing the atrial activity (AA) during AF from the ECG, the major problem is that the ventricular component is of much higher amplitude than the atrial one. Moreover, in the spectral domain, the atrial and ventricular components overlap. Therefore, extracting the atrial signal cannot be achieved using classical linear filters and thus requires nonlinear signal processing techniques. A few approaches have been proposed, among which source separation [137], average beat subtraction (ABS) [57, 138, 139], and single beat subtraction (SB) [56].

Approaches based on source separation schemes exploit the property that the AA and ventricular activity (VA) arise from different biolectrical sources, each of which exhibiting different statistical properties. The main hypothesis is that ECG signals can be considered as a weighted sum of atrial and ventricular sources, noise and artifacts. Source separation algorithms try to find uncorrelated components using principal component analysis, or to find independent components using independent component analysis [137]. In principal component analysis, the VA is characterized in terms of intrabeat correlation. The principal component analysis projects each beat on the "ventricular subspace," and a QRST waveform can be estimated and removed by subtracting a linear combination of the "ventricular" eigenvectors [140]. The performance of this method is critically dependent on the algorithm being employed for subspace identification and in the case of a poor identification, the extracted AA contains undesired components. When algorithms base on independent component analysis are used, it is assumed that the ECG signals are a mixture of various single point sources such as the AA, VA and extracardiac activity. The signals obtained with source separation algorithms cannot therefore represent the complete spatial information contained in a standard 12-lead surface ECG. These schemes may not be the ones with the best performance for extracting the AA from the ECG.

One of the most widely used techniques for the AA extraction from the ECG during AF is the ABS [57, 138, 139]. This approach relies on two main hypotheses; during AF, 1) the AA is uncoupled with the VA and 2) in the same patient, ventricular complexes generally exhibit a limited number of shapes. Typically, an average beat (a template), representative of the ventricular cycle during the period of recording, is subtracted from a single ECG lead in order to remove the VA. Ideally, the resulting signal would be devoid of any VA and would only contain the fibrillatory waveforms. Obviously, when using this approach, a large number of beats is desirable in order to increase the performance of the cancellation. In [139], this technique was refined by adding two major features to the standard ABS approach: reduction of the fibrillatory wave and spatiotem-

poral alignment. One of the major problem of ABS approaches is that the template estimation becomes unreliable when the fibrillatory waves are complex and disorganized, which is often the case in long-standing persistent AF. Also, several beats for each morphology are needed to create the templates. Therefore, the ABS approach is more suitable when the ECG contains a sufficient number of ventricular complexes and when the ventricular complexes are highly regular. In this thesis, patients with long-standing persistent AF were studied. This type of AF is extremely irregular, and therefore an ABS approach was not suitable.

The SB approach also subtracts the QRST complex from the ECG, but unlike the ABS technique, it treats each cardiac cycle in an independent manner [56]. The SB method is more appropriate when the morphology of the ventricular complexes is variable. Most importantly, this approach does not depend on the duration of the ECG recording.

The purpose of this appendix is to briefly present the SB method originally proposed by Lemay et. al [56]. In Section C.1, the pre-processing including the fiducial point detection and baseline correction are presented. In Section C.2, the SB approach is exposed. For more details about cancellation techniques, the reader should refer to [108].

C.1   Pre-processing

C.1.1   Fiducial point detection

Among the six bipolar limb leads of the standard 12-lead ECG, only two of them are linearly independent, i.e. V_{RA} and V_{LA} (see Section 2.2.1). This justifies the expression of the pertinent information contained in the 12-lead ECG by an T-by-8 matrix $\mathbf{X}$ that comprises T samples from eight leads: two limb leads (V_{RA} and V_{LA}) and six precordial leads (V_1 to V_6). The remaining limb leads are recovered by the appropriate linear combination of leads V_{RA} and V_{LA}. A derivative-based method is applied to the root mean square (RMS) signal to detect ventricular complexes [141]. In the ith cardiac cycle, as illustrated in Figure C.1, let:

  – q_i denotes the timing of the onset of the ventricular depolarization,
  – r_i denotes the timing of the R wave (defined as the middle point between the closest samples on either side, below 50% of the maximum value of the RMS curve),
  – k_i denotes the timing of the subsequent T wave,
  – j_i denotes the local minimum of the RMS curve between r_i and k_i.

This RMS signal from which the fiducial points are derived, is defined as:

$$RMS(t) = \sqrt{\frac{1}{8} \sum_{l=1}^{8} x_l(t)^2}, \quad t = 1, \dots, T, \tag{C.1}$$

where $x_l(t)$ denotes the sample t of the lth lead signal.

C.1.2   Baseline correction

On each of the eight lead signals, a baseline correction is applied by means of a cubic spline interpolation anchored on the onset points q_i [142]. The fiducial point detection presented previously and the baseline correction are iteratively applied until no further changes in the various timings were observed. Finally, the eight resulting ECG signals are smoothed by applying a zero-phase fifth-order lowpass Butterworth filter with a cutoff frequency of 50 Hz [108]. Figure C.2 shows an example of a raw excerpt on lead V_2 and its cleaned version after baseline correction.
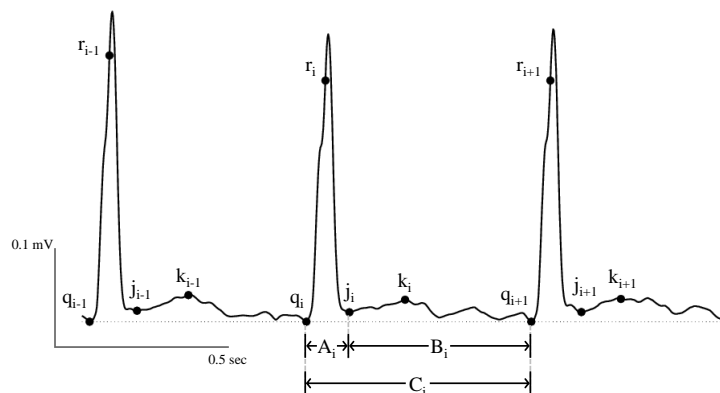
Figure C.1: Fiducial points defined on a RMS signal of duration 2 seconds. The timing of the onset of the ventricular depolarization, the R wave timing, the T wave peak and the J point timings are denoted as q_i, r_i, k_i and j_i respectively. The A_i segment indicates the location of the QRS complex, the B_i segment defines the JQ interval, and the C_i segment corresponds to the cardiac cycle. *Figure adapted from [108].*
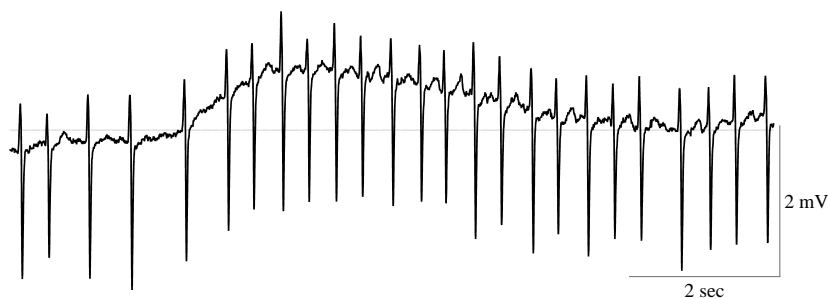
(a) Excerpt on lead V_2 of duration 10 *sec* recorded during AF.
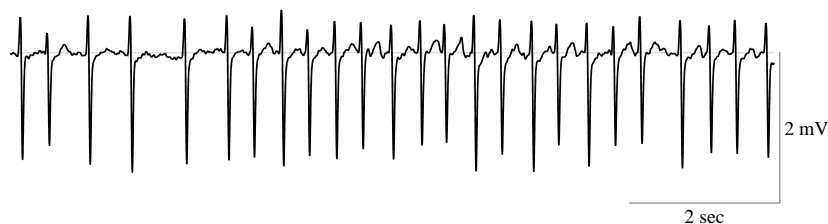
(b) Cleaned up version of (a) after pre-processing.

Figure C.2: Example of a raw excerpt of duration 10 *sec* on lead V_2 (a) and its cleaned version after baseline correction (b). *Figures from [108].*

C.2   Single beat cancellation

The main idea of the SB approach is that each cardiac cycle is treated independently. More-over, the ventricles depolarization (QRS complexes) and repolarization (T and U waves) are treated separately. The two main steps consist in cancelling the repolarization waves using dominant T and U wave, and estimating the AA located in the QRS complexes. A flowchart summarizing the SB scheme is shown in Figure C.3.
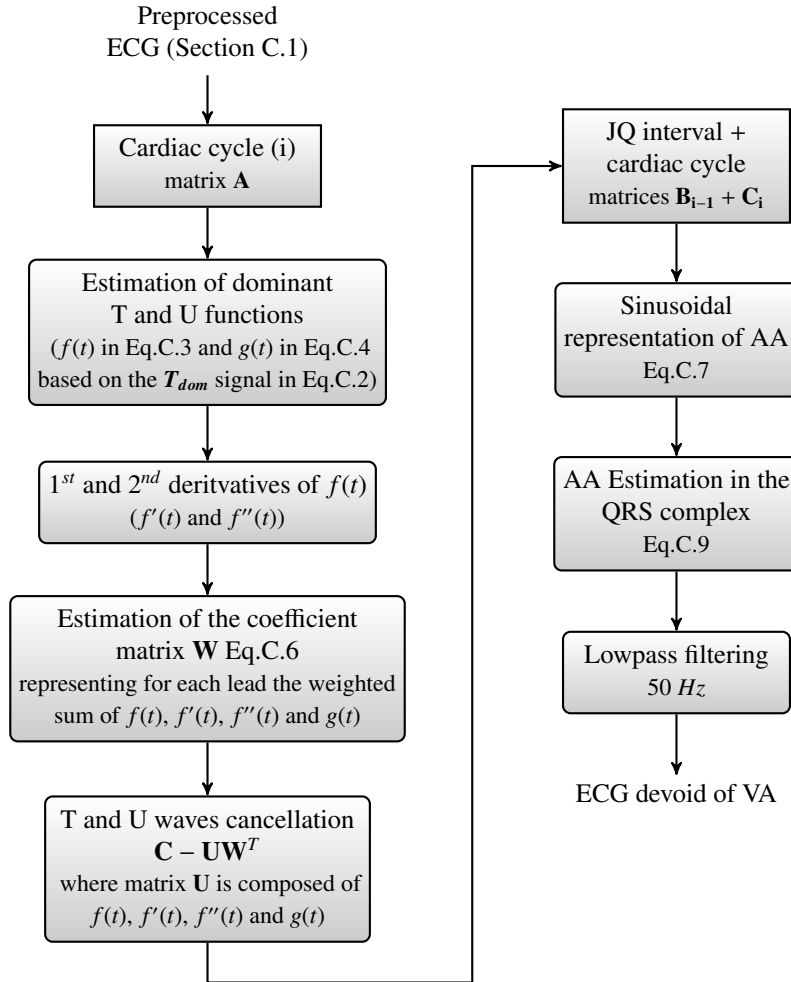

Figure C.3: Flowchart of the single beat cancellation scheme. *Figure adapted from [108].*

T and U waves cancellation

It has been observed that the T wave morphology is quite similar in different leads. This observation has been referred to as the *dominant T wave* and is useful for representing individual T waves [143]. Let the V-by-8 matrix $\mathbf{\Phi}$ contains the V samples of the eight ECG leads during the $ST - T$ interval. The 8-vector $\mathbf{e}$ represents the first eigenvector associated with the largest eigenvalue of the estimated covariance matrix of $\mathbf{\Phi}$. The dominant T wave may be estimated by the first principal component over the $ST - T$ interval as such:

$$\boldsymbol{T_{dom}} = \mathbf{e}^{\mathrm{T}}\boldsymbol{\Phi}^{\mathrm{T}}, \tag{C.2}$$

$\boldsymbol{T_{dom}}$ represents therefore $T_{dom}(t)$ over the $ST - T$ interval.
In order to provide a flexible representation of each individual T wave, the dominant T wave is defined as a linear combination of the function $T_{dom}(t)$ [144]. However, in the context of AF, it was found that taking third-order derivatives generally resulted in components that could hardly be distinguished from noise. Therefore, in the current framework, derivatives up to the second-order only are included [108]. For this purpose, it was necessary to first fit a smooth analytical function to the eigenvector and then to compute the time derivatives from the fitted function. This function is the product of two logistic functions [145]:

$$f(t) = p_1\left(p_2 + \frac{1}{1 + e^{p_3(t-p_5)}} \cdot \frac{1}{1 + e^{p_4(t-p_5)}}\right), \tag{C.3}$$

where p_1 is an overall scaling factor, p_2 defines the initial amplitude, p_3 and p_4 are parameters for the positive and negative slopes respectively, and p_5 sets the timing of the dominant T wave apex [108].
During AF, most ECGs may contain U waves and, thus, due to this occasional presence of U waves, an additional function may be incorporated. It has been observed that the shape of these U waves is similar to that of a Gaussian function. Correspondingly, the general dominant shape of the U wave can be expressed as:

$$g(t) = p_6\, e^{-[(t-p_8)/p_7]^2}, \tag{C.4}$$

where p_6 is an overall scaling factor of the U wave amplitude, p_7 represents its width, and p_8 is the timing of its apex [108].
The VA cancellation in the JQ interval is therefore based on the two dominant functions $f(t)$ and $g(t)$. The eight parameters $p_i, i = 1, \ldots, 8$ are found by fitting the function $f(t) + g(t)$ to the function $\boldsymbol{T_{dom}}$. A nonlinear optimization method (the Levenberg-Marquadt algorithm [146]) is used to estimate these parameters.
Finally, the lth lead is modelled as a linear combination of the function $f(t)$, $f'(t)$, $f''(t)$ and $g(t)$ which was fitted to the observed data matrix $\mathbf{B}$ (for recall, the matrix $\mathbf{B}$ contains the JQ interval, see Figure C.1). The time series $x(t)$ of the lth lead can therefore be expressed as:

$$x_l(t) = w_{0,l}f(t) + w_{1,l}f'(t) + w_{2,l}f''(t) + w_{3,l}g(t) \tag{C.5}$$

where $w_{0,l}, \ldots, w_{3,l}$ denote the weight coefficients for the lth lead. Equation (C.5) constitutes a linear parameter estimation problem for one lead, which can also be expressed in the matrix form as follows:

$$\mathbf{W} = (\mathbf{U}^{\mathrm{T}}\mathbf{U})^{-1}\mathbf{U}^{\mathrm{T}}\mathbf{B}, \tag{C.6}$$

where the matrix $\mathbf{W}$ represents the weight for the individual leads, and the columns of the matrix $\mathbf{U}$ are the functions $f(t)$, $f'(t)$, $f''(t)$ and $g(t)$ over the JQ interval. Within the JQ interval, the AA estimate is thus produced by the difference $\mathbf{B} - \mathbf{UW}$.

Figure C.4 illustrates on a single cardiac cycle recorded on lead V_2 (Figure C.4a) the various steps described previously (Figures C.4b, C.4c, C.4d and C.4e), as well as the final result (Figure C.4f).
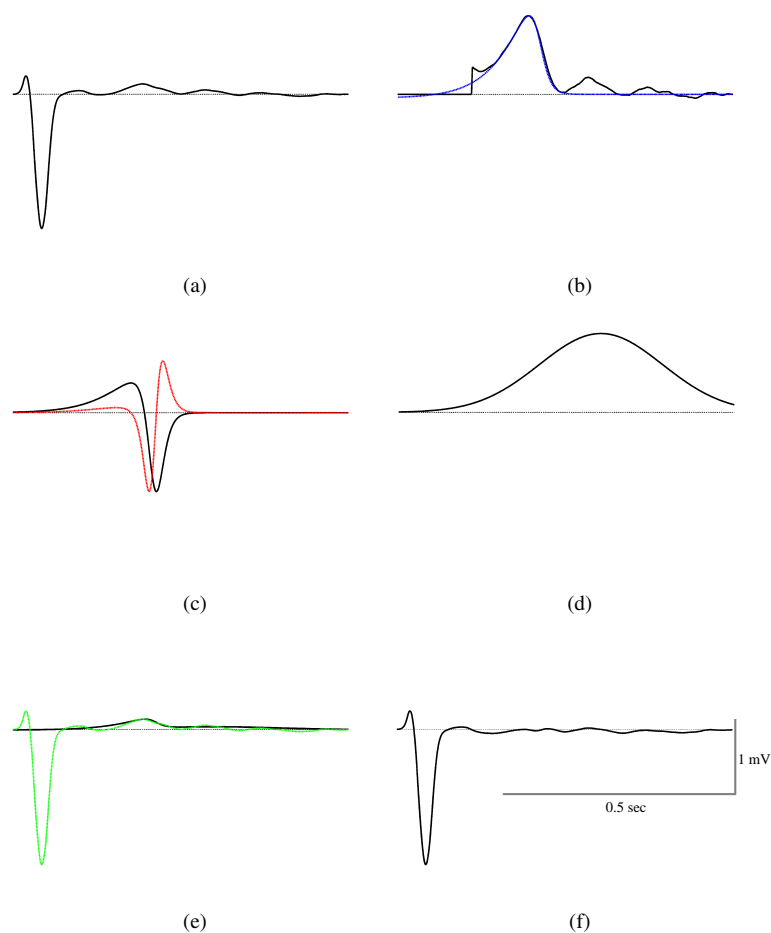
Figure C.4: Illustrative example of the various steps involved in the T and U wave cancellation. Figure (a) shows one cardiac cycle on lead V_2. In Figure (b), the estimated T_{dom} over the JQ interval is represented by a solid line while its dominant function $f(t)$ is represented by a blue line. Figure (c) displays the first $f'(t)$ (solid blue line) and second $f''(t)$ (solid red line) derivatives of $f(t)$. In Figure (d), the dominant function $g(t)$ representing the U wave in T_{dom} is plotted. Figure (e) displays the original signal (solid green line) as well as the final estimate of the ventricular repolarization (solid black line). Finally, Figure (f) shows the signal after the cancellation of the T and U waves. *Figures from [108].*

Atrial activity estimation during the QRS intervals

Within the JQ intervals, the ventricular involvement in the QRS interval A_i remains to be treated. In the scheme of Lemay, et al., rather then using a cancellation method, the AA in segment A_i was estimated from the AA observed in the neighboring cleaned up segments B_{i-1} and B_i [108]. This approach assumes that over one cardiac cycle, the AA signals are stationary. The AA signal over a given QRS interval A_i of a single lead can be expressed as a finite sum of sinusoids:

$$s(t) = \sum_{k=1}^{P} s_k(t) = \sum_{k=1}^{P} \alpha_k \cos(2\pi f_k t) + \beta_k \sin(2\pi f_k t). \tag{C.7}$$

where P defines the number of cosine and sinus functions which fit the AA in the neighboring cleaned up segments B_{i-1} and B_i, the frequencies f_k are uniformly distributed at P values between 0 and 10 Hz, and the P coefficients α_k and β_k define the linear combination of sines and cosines at the frequencies f_k which can be determined using leasts square estimation.
Equation (C.7) can be extented to the complete set of leads as such:

$$\mathbf{A}_i = \mathbf{S}_i \mathbf{E}_i, \tag{C.8}$$

where the matrix $\mathbf{S}_i$ contains the P cosine and P sinus functions during the interval A_i, and the matrix $\mathbf{E}_i$ contains the P parameters α_k and β_k of each lead (and is therefore of size 2P-by-8). The matrix $\mathbf{E}_i$ can be computed as:

$$\mathbf{E}_i = \mathbf{S}_i^{\dagger} \mathbf{B}_i^{C}, \tag{C.9}$$

where $\mathbf{S}_i^{\dagger}$ is the pseudoinverse of $\mathbf{S}_i^{C}$, which contains the P cosine and P sinus functions during the neighboring segments B_{i-1} and B_i, and the matrix $\mathbf{B}_i^{C}$ is the concatenation of the JQ matrices $\mathbf{B}_{i-1}$ and $\mathbf{B}_i$.

Finally, the atrial signal is obtained by concatenating the neighboring JQ intervals with the sinusoidal signal perviously obtained. Because the concatenated signal may contain void segments at the interval boundaries, a low-pass Butterworth filter with a cutoff frequency of 50 Hz was applied.

Figure C.5 illustrates an example of the AA estimation during the QRS interval.
As an illustrative example of the performance of the SB scheme, an excerpt of 10 seconds on lead V_2 is shown in Figure C.6a, the resulting signal after baseline correction is shown in Figure C.6b, while Figures C.6c and C.6d show the results obtained by the ABS and the SB methods respectively. In this example, the SB technique produces considerably smaller QRS residues than ABS does. A theoretical analysis on simulated and clinical ECGs of the performance of the ABS and SB methods is detailed in [108]. Moreover, clinical results have demonstrated that the SB approach produced significantly smaller QRS residues than the ABS method.
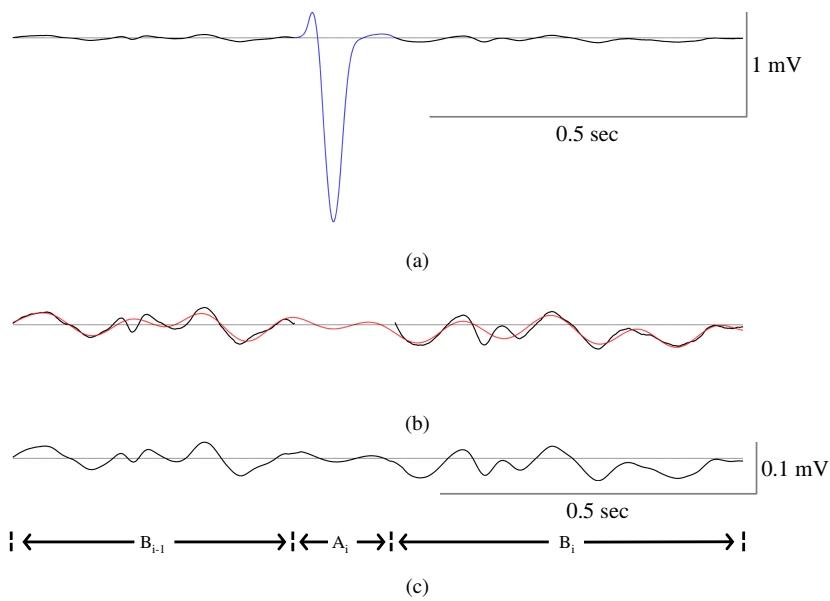
1 mV

0.5 sec

(a)

(b)

0.1 mV

0.5 sec

$\vdots \longleftarrow\!\!\!\!-\!\!\!\!- B_{i-1} \longrightarrow\!\!\vdots\!\!\longleftarrow A_i \longrightarrow\!\!\vdots\!\!\longleftarrow\!\!\!\!- B_i \longrightarrow\!\!\vdots$

(c)

Figure C.5: Estimation of the atrial activity located within the QRS intervals. Figure (a) displays an excerpt of a ith QRS complex from lead V_2 from the timing of the J point j_{i-1} to the timing of the following onset of the Q wave (q_{i+1}). The solid lines constitute the estimated AA located in the $i-1^{th}$ and the ith JQ intervals after cancellation of the T and U waves. The $A_{i^{th}}$ QRS complex is plotted in a blue line. In Figure (b), the solid lines are the magnified AA estimated segments after cancellation of the T and U waves located in the $i-1^{th}$ and the ith JQ intervals, while the red line represents the AA estimated segments by the sum of sinusoids ($P = 50$). Finally, Figure (c) shows the magnified AA estimates of the entire signal after filtering at 50 *Hz*. *Figures from [108].*
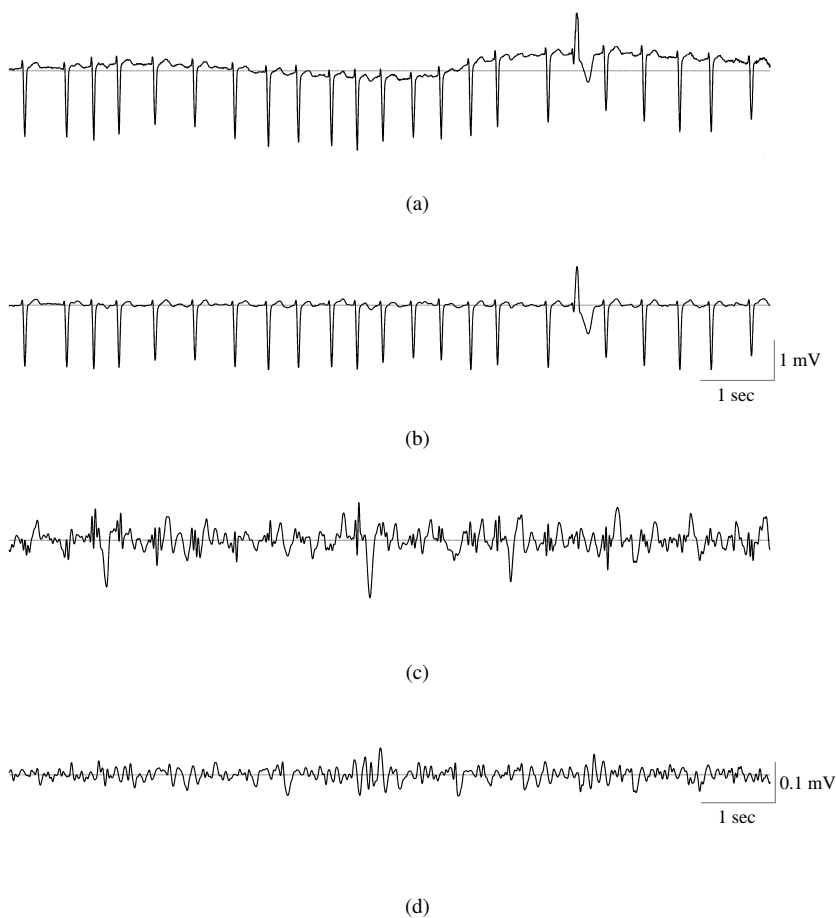
(a)

(b)

(c)

(d)

Figure C.6: Example of the ventricular activity cancellation. Figure (a) displays an excerpt of 10 seconds acquired on lead V_2 while Figure (b) shows the resulting signal after baseline correction. Figure (c) shows the estimated AA with an ABS approach where the 3rd and 11th QRS residues were considered significant. Figure (d) displays the estimated AA obtained with the SB scheme where no QRS complex residue was considered significant. *Figures from [108].*

Bibliography

[1] S. S. Chugh, R. Havmoeller, K. Narayanan, D. Singh, M. Rienstra, E. J. Benjamin, R. F. Gillum, Y.-H. Kim, J. H. McAnulty, Jr, Z.-J. Zheng, M. H. Forouzanfar, M. Naghavi, G. A. Mensah, M. Ezzati, and C. J. L. Murray, "Worldwide epidemiology of atrial fibrillation: A global burden of disease 2010 study." *Circulation*, Dec 2013.

[2] D. M. Lloyd-Jones, T. J. Wang, E. P. Leip, M. G. Larson, D. Levy, R. S. Vasan, R. B. D'Agostino, J. M. Massaro, A. Beiser, P. A. Wolf, and E. J. Benjamin, "Lifetime risk for development of atrial fibrillation: the Framingham Heart Study." *Circulation*, vol. 110, no. 9, pp. 1042–1046, Aug 2004.

[3] A. Alonso and L. G. S. Bengtson, "A rising tide: The global epidemic of atrial fibrillation." *Circulation*, pp. 829–830, Dec 2013.

[4] E. H. R. Association, E. A. for Cardio-Thoracic Surgery, A. J. Camm, P. Kirchhof, G. Y. H. Lip, U. Schotten, I. Savelieva, S. Ernst, I. C. V. Gelder, N. Al-Attar, G. Hindricks, B. Prendergast, H. Heidbuchel, O. Alfieri, A. Angelini, D. Atar, P. Colonna, R. D. Caterina, J. D. Sutter, A. Goette, B. Gorenek, M. Heldal, S. H. Hohloser, P. Kolh, J.-Y. L. Heuzey, P. Ponikowski, F. H. Rutten, E. S. C. C. for Practice Guidelines, A. Vahanian, A. Auricchio, J. Bax, C. Ceconi, V. Dean, G. Filippatos, C. Funck-Brentano, R. Hobbs, P. Kearney, T. McDonagh, B. A. Popescu, Z. Reiner, U. Sechtem, P. A. Sirnes, M. Tendera, P. E. Vardas, P. Widimsky, D. Reviewers, P. E. Vardas, V. Agladze, E. Aliot, T. Balabanski, C. Blomstrom-Lundqvist, A. Capucci, H. Crijns, B. Dahlöf, T. Folliguet, M. Glikson, M. Goethals, D. C. Gulba, S. Y. Ho, R. J. M. Klautz, S. Kose, J. McMurray, P. P. Filardi, P. Raatikainen, M. J. Salvador, M. J. Schalij, A. Shpektor, J. Sousa, J. Stepinska, H. Uuetoa, J. L. Zamorano, and I. Zupan, "Guidelines for the management of atrial fibrillation: the Task Force for the Management of Atrial Fibrillation of the European Society of Cardiology (ESC)." *Europace*, vol. 12, no. 10, pp. 1360–1420, Oct 2010.

[5] Z. Issa, J. Miller, and D. Zipes, *Clinical Arrhythmology and Electrophysiology: A Companion to Braunwald's Heart Disease*, ser. Saunders W.B. Elsevier - Health Sciences Division, 2012.

[6] M. Haïssaguerre, P. Sanders, M. Hocini, Y. Takahashi, M. Rotter, F. Sacher, T. Rostock, L.-F. Hsu, P. Bordachar, S. Reuter, R. Roudaut, J. Clémenty, and P. Jaïs, "Catheter ablation of long-lasting persistent atrial fibrillation: critical structures for termination." *J. Cardiovasc. Electrophysiol.*, vol. 16, no. 11, pp. 1125–1137, Nov 2005.

[7] Y. Takahashi, M. D. O'Neill, M. Hocini, R. Dubois, S. Matsuo, S. Knecht, S. Mahapatra, K.-T. Lim, P. Jaïs, A. Jonsson, F. Sacher, P. Sanders, T. Rostock, P. Bordachar, J. Clémenty, G. J. Klein, and M. Haïssaguerre, "Characterization of electrograms associated with termination of chronic atrial fibrillation by catheter ablation." *J. Am. Coll. Cardiol.*, vol. 51, no. 10, pp. 1003–1010, Mar 2008.

[8] T. Rostock, T. V. Salukhe, D. Steven, I. Drewitz, B. A. Hoffmann, K. Bock, H. Servatius, K. Müllerleile, A. Sultan, N. Gosau, T. Meinertz, K. Wegscheider, and S. Willems, "Long-term single and multiple procedure outcome and predictors of success after catheter ablation for persistent atrial fibrillation." *Heart Rhythm*, vol. 8, no. 9, pp. 1391–1397, Apr 2011.

[9] J. L. Wells, R. B. Karp, N. T. Kouchoukos, W. A. MacLean, T. N. James, and A. L. Waldo, "Characterization of atrial fibrillation in man: studies following open heart surgery." *Pacing Clin Electrophysiol*, vol. 1, no. 4, pp. 426–438, Oct 1978.

[10] K. B. Kim, M. D. Rodefeld, R. B. Schuessler, J. L. Cox, and J. P. Boineau, "Relationship between local atrial fibrillation interval and refractory period in the isolated canine atrium." *Circulation*, vol. 94, no. 11, pp. 2961–2967, Dec 1996.

[11] A. R. Misier, T. Opthof, N. M. van Hemel, J. J. Defauw, J. M. de Bakker, M. J. Janse, and F. J. van Capelle, "Increased dispersion of "refractoriness" in patients with idiopathic paroxysmal atrial fibrillation." *J. Am. Coll. Cardiol.*, vol. 19, no. 7, pp. 1531–1535, Jun 1992.

[12] M. C. Wijffels, C. J. Kirchhof, R. Dorland, and M. A. Allessie, "Atrial fibrillation begets atrial fibrillation. A study in awake chronically instrumented goats." *Circulation*, vol. 92, no. 7, pp. 1954–1968, Oct 1995.

[13] M. Allessie, J. Ausma, and U. Schotten, "Electrical, contractile and structural remodeling during atrial fibrillation." *Cardiovasc. Res.*, vol. 54, no. 2, pp. 230–246, May 2002.

[14] T. E. Walters, A. W. Teh, S. Spence Grad, P. M. Kistler, J. B. Morton, and J. M. Kalman, "The relationship between the electrocardiographic atrial fibrillation cycle length and left atrial remodelling: A detailed electroanatomic mapping study." *Heart Rhythm*, vol. 11, no. 4, pp. 670–676, Dec 2013.

[15] T. Sasaki, S. Niwano, S. Sasaki, R. Imaki, M. Yuge, S. Hirasawa, D. Satoh, M. Moriguchi, A. Fujiki, and T. Izumi, "Long-term follow-up of changes in fibrillation waves in patients with persistent atrial fibrillation: spectral analysis of surface ECG." *Circ. J.*, vol. 70, no. 2, pp. 169–173, Feb 2006.

[16] A. Bollmann, N. K. Kanuru, K. K. McTeague, P. F. Walter, D. B. DeLurgio, and J. J. Langberg, "Frequency analysis of human atrial fibrillation using the surface electrocardiogram and its response to ibutilide." *Am. J. Cardiol.*, vol. 81, no. 12, pp. 1439–1445, Jun 1998.

[17] A. Bollmann, D. Husser, L. Mainardi, F. Lombardi, P. Langley, A. Murray, J. J. Rieta, J. Millet, S. B. Olsson, M. Stridh, and L. Sörnmo, "Analysis of surface electrocardiograms in atrial fibrillation: techniques, research, and clinical applications." *Europace*, vol. 8, no. 11, pp. 911–926, Nov 2006.

[18] A. Bollmann, M. Mende, A. Neugebauer, and D. Pfeiffer, "Atrial fibrillatory frequency predicts atrial defibrillation threshold and early arrhythmia recurrence in patients undergoing internal cardioversion of persistent atrial fibrillation." *Pacing Clin. Electrophysiol.*, vol. 25, no. 8, pp. 1179–1184, Aug 2002.

[19] K. Yoshida, A. B. Rabbani, H. Oral, D. Bach, F. Morady, and A. Chugh, "Left atrial volume and dominant frequency of atrial fibrillation in patients undergoing catheter ablation of persistent atrial fibrillation." *J. Interv. Card. Electrophysiol.*, vol. 32, no. 2, pp. 155–161, Jun 2011.

[20] S. Matsuo, N. Lellouche, M. Wright, M. Bevilacqua, S. Knecht, I. Nault, K.-T. Lim, L. Arantes, M. D. O'Neill, P. G. Platonov, J. Carlson, F. Sacher, M. Hocini, P. Jaïs, and M. Haïssaguerre, "Clinical predictors of termination and clinical outcome of catheter ablation for persistent atrial fibrillation." *J. Am. Coll. Cardiol.*, vol. 54, no. 9, pp. 788–795, Aug 2009.

[21] T. H. Everett, J. R. Moorman, L.-C. Kok, J. G. Akar, and D. E. Haines, "Assessment of global atrial fibrillation organization to optimize timing of atrial defibrillation," *Circulation*, vol. 103, no. 23, pp. 2857–2861, Jun 2001.

[22] R. Klabunde, *Cardiovascular Physiology Concepts*.   Lippincott Williams & Wilkins, 2005.

[23] B. Alberts, D. Bray, J. Lewis, M. Raff, K. Roberts, and J. Watson, *Molecular Biology of the Cell*, 4th ed.   Garland, 2002.

[24] Y. Kubo, J. P. Adelman, D. E. Clapham, L. Y. Jan, A. Karschin, Y. Kurachi, M. Lazdunski, C. G. Nichols, S. Seino, and C. A. Vandenberg, "International Union of Pharmacology. LIV. Nomenclature and molecular relationships of inwardly rectifying potassium channels." *Pharmacological reviews*, 2005.

[25] N. Sperelakis, Y. Kurachi, A. Terzic, and M. Cohen, *Heart Physiology and Pathophysiology*, 4th ed.   Academic Press, 2000.

[26] F. Wilson, F. Johnston, A. Macleod, and P. Barker, "Electrocardiograms that represent the potential variations of a single electrode." *Am. Heart J.*, vol. 9, pp. 447–71, 1934.

[27] J. Malmivuo and R. Plonsey, *Bioelectromagnetism-Principles and Applications of Bioelectric and Biomagnetic Fields*.   Oxford University Press, 1995.

[28] J. Goldberger and J. Ng, *Practical Signal and Image Processing in Clinical Cardiology*.   Springer, 2010.

[29] W. G. Stevenson and K. Soejima, "Recording techniques for clinical electrophysiology." *J. Cardiovasc. Electrophysiol.*, vol. 16, no. 9, pp. 1017–1022, Sep 2005.

[30] S. Stewart, C. L. Hart, D. J. Hole, and J. J. V. McMurray, "A population-based study of the long-term risks associated with atrial fibrillation: 20-year follow-up of the Renfrew/Paisley study." *Am. J. Med.*, vol. 113, no. 5, pp. 359–364, Oct 2002.

[31] V. Fuster, L. E. Rydén, D. S. Cannom, H. J. Crijns, A. B. Curtis, K. A. Ellenbogen, J. L. Halperin, G. N. Kay, J.-Y. Le Huezey, J. E. Lowe, S. B. Olsson, E. N. Prystowsky, J. L. Tamargo, and L. S. Wann, "2011 ACCF/AHA/HRS focused updates incorporated into the ACC/AHA/ESC 2006 Guidelines for the management of patients with atrial fibrillation: a report of the American College of Cardiology Foundation/American Heart Association Task Force on Practice Guidelines developed in partnership with the European Society of Cardiology and in collaboration with the European Heart Rhythm Association and the Heart Rhythm Society." *J. Am. Coll. Cardiol.*, vol. 57, no. 11, pp. e101–e198, Mar 2011.

[32] G. Y. Lip, D. J. Golding, M. Nazir, D. G. Beevers, D. L. Child, and R. I. Fletcher, "A survey of atrial fibrillation in general practice: the West Birmingham Atrial Fibrillation Project." *Br. J. Gen. Pract.*, vol. 47, no. 418, pp. 285–289, May 1997.

[33] M. Haïssaguerre, P. Jaïs, D. C. Shah, A. Takahashi, M. Hocini, G. Quiniou, S. Garrigue, A. L. Mouroux, P. L. Métayer, and J. Clémenty, "Spontaneous initiation of atrial fibrillation by ectopic beats originating in the pulmonary veins." *N. Engl. J. Med.*, vol. 339, no. 10, pp. 659–666, Sep 1998.

[34] H. Calkins, K. H. Kuck, R. Cappato, J. Brugada, A. J. Camm, S.-A. Chen, H. J. G. Cri-
     jns, R. J. Damiano, Jr, D. W. Davies, J. DiMarco, J. Edgerton, K. Ellenbogen, M. D.
     Ezekowitz, D. E. Haines, M. Haïssaguerre, G. Hindricks, Y. Iesaka, W. Jackman, J. Jalife,
     P. Jaïs, J. Kalman, D. Keane, Y.-H. Kim, P. Kirchhof, G. Klein, H. Kottkamp, K. Kumagai,
     B. D. Lindsay, M. Mansour, F. E. Marchlinski, P. M. McCarthy, J. L. Mont, F. Morady,
     K. Nademanee, H. Nakagawa, A. Natale, S. Nattel, D. L. Packer, C. Pappone, E. Prys-
     towsky, A. Raviele, V. Reddy, J. N. Ruskin, R. J. Shemin, H.-M. Tsao, and D. Wilber,
     "2012 HRS/EHRA/ECAS Expert Consensus Statement on Catheter and Surgical Abla-
     tion of Atrial Fibrillation: recommendations for patient selection, procedural techniques,
     patient management and follow-up, definitions, endpoints, and research trial design." *Eu-
     ropace*, vol. 14, no. 4, pp. 528–606, Apr 2012.

[35] G. K. Moe and J. A. Abildskov, "Atrial fibrillation as a self-sustaining arrhythmia inde-
     pendent of focal discharge." *Am. Heart. J.*, vol. 58, no. 1, pp. 59–70, Jul 1959.

[36] M. Allessie, W. Lammers, F. Bonke, and J. Holen, *Cardiac Electrophysiology and Ar-
     rhythmias*.   New York: Grune & Stratton, 1985, ch. Experimental evaluation of Moe's
     multiple wavelet hypothesis of atrial fibrillation, pp. 265—-276.

[37] J. L. Cox, T. E. Canavan, R. B. Schuessler, M. E. Cain, B. D. Lindsay, C. Stone, P. K.
     Smith, P. B. Corr, and J. P. Boineau, "The surgical treatment of atrial fibrillation. Intraop-
     erative electrophysiologic mapping and description of the electrophysiologic basis of atrial
     flutter and atrial fibrillation." *J. Thorac. Cardiovasc. Surg.*, vol. 101, no. 3, pp. 406–426,
     Mar 1991.

[38] J. Jalife, O. Berenfeld, and M. Mansour, "Mother rotors and fibrillatory conduction: a
     mechanism of atrial fibrillation." *Cardiovasc. Res.*, vol. 54, no. 2, pp. 204–216, May 2002.

[39] O. Berenfeld, R. Mandapati, S. Dixit, A. C. Skanes, J. Chen, M. Mansour, and J. Jal-
     ife, "Spatially distributed dominant excitation frequencies reveal hidden organization in
     atrial fibrillation in the Langendorff-perfused sheep heart." *J. Cardiovasc. Electrophysiol.*,
     vol. 11, no. 8, pp. 869–879, Aug 2000.

[40] D. Wyse, A. Waldo, J. DiMarco, M. J. Domanski, Y. Rosenberg, E. Schron, J. Kellen,
     H. Greene, M. Mickel, J. Dalquist, S. Corley, and Atrial Fibrillation Follow-up Investiga-
     tion of Rhythm Management (A.F.F.I.R.M.) Investigators, "A comparison of rate control
     and rhythm control in patients with atrial fibrillation." *N. Engl. J. Med.*, vol. 347, no. 23,
     pp. 1825–1833, Dec 2002.

[41] I. C. Van Gelder, V. E. Hagens, H. A. Bosker, J. H. Kingma, O. Kamp, T. Kingma, S. A.
     Said, J. I. Darmanata, A. J. M. Timmermans, J. G. P. Tijssen, H. J. G. M. Crijns, and Rate
     Control versus Electrical Cardioversion for Persistent Atrial Fibrillation Study Group, "A
     comparison of rate control and rhythm control in patients with recurrent persistent atrial
     fibrillation." *N. Engl. J. Med.*, vol. 347, no. 23, pp. 1834–1840, Dec 2002.

[42] B. Lown, R. Amarasingham, and J. Neuman, "New method for terminating cardiac ar-
     rhythmias. Use of synchronized capacitor discharge." *J.A.M.A.*, vol. 182, pp. 548–555,
     Nov 1962.

[43] J. L. Cox, R. B. Schuessler, D. G. Lappas, and J. P. Boineau, "An 8 1/2-year clinical
     experience with surgery for atrial fibrillation." *Ann. Surg.*, vol. 224, no. 3, pp. 267–73;
     discussion 273–5, Sep 1996.

[44] J. L. Cox, "Cardiac surgery for arrhythmias." *J. Cardiovasc. Electrophysiol.*, vol. 15, no. 2,
     pp. 250–262, Feb 2004.

[45] D. L. Packer, S. Asirvatham, and T. M. Munger, "Progress in nonpharmacologic therapy of atrial fibrillation." *J. Cardiovasc. Electrophysiol.*, vol. 14, no. 12 Suppl, pp. S296–S309, Dec 2003.

[46] A. Natale, "Advances in catheter-ablation treatment of atrial fibrillation." *Nat. Rev. Cardiol.*, vol. 10, no. 2, pp. 63–64, Feb 2013.

[47] C. Pappone, G. Oreto, F. Lamberti, G. Vicedomini, M. L. Loricchio, S. Shpun, M. Rillo, M. P. Calabrò, A. Conversano, S. A. Ben-Haim, R. Cappato, and S. Chierchia, "Catheter ablation of paroxysmal atrial fibrillation using a 3D mapping system." *Circulation*, vol. 100, no. 11, pp. 1203–1208, Sep 1999.

[48] C. Pappone, S. Rosanio, G. Oreto, M. Tocchi, F. Gugliotta, G. Vicedomini, A. Salvati, C. Dicandia, P. Mazzone, V. Santinelli, S. Gulletta, and S. Chierchia, "Circumferential radiofrequency ablation of pulmonary vein ostia: A new anatomic approach for curing atrial fibrillation." *Circulation*, vol. 102, no. 21, pp. 2619–2628, Nov 2000.

[49] M. Hocini, I. Nault, M. Wright, G. Veenhuyzen, S. M. Narayan, P. Jaïs, K.-T. Lim, S. Knecht, S. Matsuo, A. Forclaz, S. Miyazaki, A. Jadidi, M. D. O'Neill, F. Sacher, J. Clémenty, and M. Haïssaguerre, "Disparate evolution of right and left atrial rate during ablation of long-lasting persistent atrial fibrillation." *J. Am. Coll. Cardiol.*, vol. 55, no. 10, pp. 1007–1016, Mar 2010.

[50] M. Haïssaguerre, P. Sanders, M. Hocini, L.-F. Hsu, D. C. Shah, C. Scavée, Y. Takahashi, M. Rotter, J.-L. Pasquié, S. Garrigue, J. Clémenty, and P. Jaïs, "Changes in atrial fibrillation cycle length and inducibility during catheter ablation and their relation to outcome." *Circulation*, vol. 109, no. 24, pp. 3007–3013, Jun 2004.

[51] S. Ernst, F. Ouyang, F. Löber, M. Antz, and K.-H. Kuck, "Catheter-induced linear lesions in the left atrium in patients with atrial fibrillation: an electroanatomic study." *J. Am. Coll. Cardiol.*, vol. 42, no. 7, pp. 1271–1282, Oct 2003.

[52] S. Matsuo, M. Wright, S. Knecht, I. Nault, N. Lellouche, K.-T. Lim, L. Arantes, M. D. O'Neill, M. Hocini, P. Jaïs, and M. Haïssaguerre, "Peri-mitral atrial flutter in patients with atrial fibrillation ablation." *Heart Rhythm*, vol. 7, no. 1, pp. 2–8, Jan 2010.

[53] K. Nademanee, J. McKenzie, E. Kosar, M. Schwab, B. Sunsaneewitayakul, T. Vasavakul, C. Khunnawat, and T. Ngarmukos, "A new approach for catheter ablation of atrial fibrillation: mapping of the electrophysiologic substrate." *J. Am. Coll. Cardiol.*, vol. 43, no. 11, pp. 2044–2053, Jun 2004.

[54] R. J. Hunter, I. Diab, M. Tayebjee, L. Richmond, S. Sporton, M. J. Earley, and R. J. Schilling, "Characterization of fractionated atrial electrograms critical for maintenance of AF: a randomized controlled trial of ablation strategies (the CFAE AF trial)," *Circ. Arrhythm. Electrophysiol.*, vol. 4, no. 5, pp. 622–629, Oct 2011.

[55] S. Petrutiu, A. V. Sahakian, W. Fisher, and S. Swiryn, "Manifestation of left atrial events and interatrial frequency gradients in the surface electrocardiogram during atrial fibrillation: contributions from posterior leads." *J. Cardiovasc. Electrophysiol.*, vol. 20, no. 11, pp. 1231–1236, Nov 2009.

[56] M. Lemay, J.-M. Vesin, A. van Oosterom, V. Jacquemet, and L. Kappenberger, "Cancellation of ventricular activity in the ECG: evaluation of novel and existing nethods," *IEEE Trans. Biomed. Eng*, vol. 54, no. 3, pp. 542–546, Mar 2007.

[57] M. Holm, S. Pehrson, M. Ingemansson, L. Sörnmo, R. Johansson, L. Sandhall, M. Sune-mark, B. Smideberg, C. Olsson, and S. B. Olsson, "Non-invasive assessment of the atrial cycle length during atrial fibrillation in man: introducing, validating and illustrating a new ECG method." *Cardiovasc. Res.*, vol. 38, no. 1, pp. 69–81, Apr 1998.

[58] M. H. Raitt and W. Kusumoto, "Correlations among the frequencies of atrial activity on the surface electrocardiogram, intracardiac atrial electrograms, and the atrial effective re-fractory period in patients with atrial fibrillation." *J. Electrocardiol.*, vol. 45, no. 3, pp. 296–303, Jan 2012.

[59] M. Stridh, D. Husser, A. Bollmann, and L. Sörnmo, "Waveform characterization of atrial fibrillation using phase information." *IEEE Trans. Biomed. Eng.*, vol. 56, no. 4, pp. 1081–1089, Apr 2009.

[60] D. Gabor, "Theory of communication," *J. IEE.*, vol. 93, no. 26, pp. 429–457, Nov 1946.

[61] W. Nho and P. J. Loughlin, "When is instantaneous frequency the average frequency at each time?" *IEEE Signal Proc. Let.*, vol. 6, no. 4, pp. 78–80, Apr 1999.

[62] M. Chavez, M. Besserve, C. Adam, and J. Martinerie, "Towards a proper estimation of phase synchronization from time series." *J. Neurosci. Methods.*, vol. 154, no. 1-2, pp. 149–160, Jun 2006.

[63] A. Bollmann, D. Husser, M. Stridh, L. Sörnmo, M. Majic, H. U. Klein, and S. B. Olsson, "Frequency measures obtained from the surface electrocardiogram in atrial fibrillation research and clinical decision-making." *J. Cardiovasc. Electrophysiol.*, vol. 14, no. 10 Suppl, pp. S154–S161, Oct 2003.

[64] K. T. Konings, C. J. Kirchhof, J. R. Smeets, H. J. Wellens, O. C. Penn, and M. A. Allessie, "High-density mapping of electrically induced atrial fibrillation in humans." *Circulation*, vol. 89, no. 4, pp. 1665–1680, Apr 1994.

[65] S. R. Dibs, J. Ng, R. Arora, R. S. Passman, A. H. Kadish, and J. J. Goldberger, "Spatiotem-poral characterization of atrial activation in persistent human atrial fibrillation: multisite electrogram analysis and surface electrocardiographic correlations–a pilot study." *Heart Rhythm*, vol. 5, no. 5, pp. 686–693, May 2008.

[66] J. Tuan, F. Osman, M. Jeilan, S. Kundu, R. Mantravadi, P. J. Stafford, and G. A. Ng, "Increase in organization index predicts atrial fibrillation termination with flecainide post-ablation: spectral analysis of intracardiac electrograms." *Europace*, vol. 12, no. 4, pp. 488–493, Apr 2010.

[67] K. Yoshida, A. Chugh, E. Good, T. Crawford, J. Myles, S. Veerareddy, S. Billakanty, W. S. Wong, M. Ebinger, F. Pelosi, K. Jongnarangsin, F. Bogun, F. Morady, and H. Oral, "A critical decrease in dominant frequency and clinical outcome after catheter ablation of persistent atrial fibrillation." *Heart Rhythm*, vol. 7, no. 3, pp. 295–302, Mar 2010.

[68] Y. Takahashi, P. Sanders, P. Jaïs, M. Hocini, R. Dubois, M. Rotter, T. Rostock, C. J. Nal-liah, F. Sacher, J. Clémenty, and M. Haïssaguerre, "Organization of frequency spectra of atrial fibrillation: relevance to radiofrequency catheter ablation." *J. Cardiovasc. Electro-physiol.*, vol. 17, no. 4, pp. 382–388, Apr 2006.

[69] J. Tuan, M. Jeilan, S. Kundu, W. Nicolson, I. Chung, P. J. Stafford, and G. A. Ng, "Re-gional fractionation and dominant frequency in persistent atrial fibrillation: effects of left atrial ablation and evidence of spatial relationship." *Europace*, vol. 13, no. 11, pp. 1550–1556, Jun 2011.

[70] J. W. E. Jarman, T. Wong, P. Kojodjojo, H. Spohr, J. E. R. Davies, M. Roughton, D. P. Francis, P. Kanagaratnam, M. D. O'Neill, V. Markides, D. W. Davies, and N. S. Peters, "Organizational index mapping to identify focal sources during persistent atrial fibrillation." *J. Cardiovasc. Electrophysiol.*, vol. 25, no. 4, pp. 355–363, Jan 2014.

[71] A. R. Jones, D. E. Krummen, and S. M. Narayan, "Non-invasive identification of stable rotors and focal sources for human atrial fibrillation: mechanistic classification of atrial fibrillation from the electrocardiogram." *Europace*, vol. 15, no. 9, pp. 1249–1258, Feb 2013.

[72] S. Lee, K. Ryu, A. L. Waldo, C. M. Khrestian, D. M. Durand, and J. Sahadevan, "An algorithm to measure beat-to-beat cycle lengths for assessment of atrial electrogram rate and regularity during atrial fibrillation." *J. Cardiovasc. Electrophysiol.*, vol. 24, no. 2, pp. 199–206, Nov 2012.

[73] Q. Xi, A. V. Sahakian, J. Ng, and S. Swiryn, "Atrial fibrillatory wave characteristics on surface electrogram: ECG to ECG repeatability over twenty-four hours in clinically stable patients." *J. Cardiovasc. Electrophysiol.*, vol. 15, no. 8, pp. 911–917, Aug 2004.

[74] M. Stridh, L. Sörnmo, C. J. Meurling, and S. B. Olsson, "Characterization of atrial fibrillation using the surface ECG: time-dependent spectral properties." *IEEE Trans. Biomed. Eng.*, vol. 48, no. 1, pp. 19–27, Jan 2001.

[75] L. Uldry, C. Duchêne, Y. Prudat, M. M. Murray, and J.-M. Vesin, "Adaptive tracking of EEG frequency components," in *Advanced Biosignal Processing*. Springer, 2009, pp. 123–144.

[76] J. Van Zaen, L. Uldry, C. Duchêne, Y. Prudat, R. A. Meuli, M. M. Murray, and J.-M. Vesin, "Adaptive tracking of EEG oscillations," *J. Neurosci. Meth.*, vol. 186, no. 1, pp. 97–106, Jan 2010.

[77] J. Van Zaen, "Efficient schemes for adaptive frequency tracking and their relevance for EEG and ECG," Ph.D. dissertation, Ecole Polytechnique Fédérale de Lausanne, 2012.

[78] S. L. Marple, "Computing the discrete-time analytic signal from the FFT," *IEEE T. Signal Proces.*, vol. 47, no. 9, pp. 2600–2603, Sep 1999.

[79] S. Haykin, *Adaptive filter theory*, 4th ed. Prentice Hall, 2001.

[80] Y. Prudat and J.-M. Vesin, "Multi-signal extension of adaptive frequency tracking algorithms," *Signal Process.*, vol. 89, no. 6, pp. 963–973, Jun. 2009.

[81] A. V. Oppenheim and R. W. Schafer, *Discrete-time signal processing*, 3rd ed. Pearson, 2010.

[82] I. Nault, N. Lellouche, S. Matsuo, S. Knecht, M. Wright, K.-T. Lim, F. Sacher, P. Platonov, A. Deplagne, P. Bordachar, N. Derval, M. D. O'Neill, G. J. Klein, M. Hocini, P. Jaïs, J. Clémenty, and M. Haïssaguerre, "Clinical value of fibrillatory wave amplitude on surface ECG in patients with persistent atrial fibrillation." *J. Interv. Card. Electrophysiol.*, vol. 26, no. 1, pp. 11–19, Oct 2009.

[83] M. Meo, V. Zarzoso, O. Meste, D. G. Latcu, and N. Saoudi, "Non-invasive prediction of catheter ablation outcome in persistent atrial fibrillation by exploiting the spatial diversity of surface ECG." *Conf. Proc. IEEE. Eng. Med. Biol. Soc.*, vol. 2011, pp. 5531–5534, Aug 2011.

[84] N.-W. Hsu, Y.-J. Lin, C.-T. Tai, T. Kao, S.-L. Chang, W. Wongcharoen, L.-W. Lo, A. R. Udyavar, Y.-F. Hu, H.-W. Tso, Y.-J. Chen, S. Higa, and S.-A. Chen, "Frequency analysis of the fibrillatory activity from surface ECG lead V1 and intracardiac recordings: implications for mapping of AF." *Europace*, vol. 10, no. 4, pp. 438–443, Apr 2008.

[85] P. G. Platonov, I. Cygankiewicz, M. Stridh, F. Holmqvist, R. Vazquez, A. Bayes-Genis, S. McNitt, W. Zareba, and A. B. de Luna, "Low atrial fibrillatory rate is associated with poor outcome in patients with mild to moderate heart failure." *Circ. Arrhythm. Electrophysiol.*, vol. 5, no. 1, pp. 77–83, Jan 2012.

[86] M. S. Guillem, A. M. Climent, J. Millet, A. Arenal, F. Fernández-Avilés, J. Jalife, F. Atienza, and O. Berenfeld, "Non-invasive localization of maximal frequency sites of atrial fibrillation by body surface potential mapping." *Circ. Arrhythm. Electrophysiol.*, vol. 6, no. 2, pp. 294–301, Feb 2013.

[87] J. Sahadevan, K. Ryu, L. Peltz, C. M. Khrestian, R. W. Stewart, A. H. Markowitz, and A. L. Waldo, "Epicardial mapping of chronic atrial fibrillation in patients: preliminary observations." *Circulation*, vol. 110, no. 21, pp. 3293–3299, Nov 2004.

[88] F. Sarmast, A. Kolli, A. Zaitsev, K. Parisian, A. S. Dhamoon, P. K. Guha, M. Warren, J. M. B. Anumonwo, S. M. Taffet, O. Berenfeld, and J. Jalife, "Cholinergic atrial fibrillation: I(K,ACh) gradients determine unequal left/right atrial frequencies and rotor dynamics." *Cardiovasc. Res.*, vol. 59, no. 4, pp. 863–873, Oct 2003.

[89] K. Lemola, M. Ting, P. Gupta, J. N. Anker, A. Chugh, E. Good, S. Reich, D. Tschopp, P. Igic, D. Elmouchi, K. Jongnarangsin, F. Bogun, F. Pelosi, F. Morady, and H. Oral, "Effects of two different catheter ablation techniques on spectral characteristics of atrial fibrillation." *J. Am. Coll. Cardiol.*, vol. 48, no. 2, pp. 340–348, Jul 2006.

[90] K. Yoshida, M. Ulfarsson, H. Tada, A. Chugh, E. Good, M. Kuhne, T. Crawford, J. F. Sarrazin, N. Chalfoun, D. Wells, K. Jongnarangsin, F. Pelosi, F. Bogun, F. Morady, and H. Oral, "Complex electrograms within the coronary sinus: time- and frequency-domain characteristics, effects of antral pulmonary vein isolation, and relationship to clinical outcome in patients with paroxysmal and persistent atrial fibrillation." *J. Cardiovasc. Electrophysiol.*, vol. 19, no. 10, pp. 1017–1023, Oct 2008.

[91] S. Lazar, S. Dixit, F. E. Marchlinski, D. J. Callans, and E. P. Gerstenfeld, "Presence of left-to-right atrial frequency gradient in paroxysmal but not persistent atrial fibrillation in humans." *Circulation*, vol. 110, no. 20, pp. 3181–3186, Nov 2004.

[92] L.-W. Lo, C.-T. Tai, Y.-J. Lin, S.-L. Chang, A. R. Udyavar, Y.-F. Hu, K.-C. Ueng, W.-C. Tsai, T.-C. Tuan, C.-J. Chang, T. Kao, H.-M. Tsao, W. Wongcharoen, S. Higa, and S.-A. Chen, "Predicting factors for atrial fibrillation acute termination during catheter ablation procedures: implications for catheter ablation strategy and long-term outcome." *Heart Rhythm*, vol. 6, no. 3, pp. 311–318, Mar 2009.

[93] M. K. Stiles, A. G. Brooks, B. John, Shashidhar, L. Wilson, P. Kuklik, H. Dimitri, D. H. Lau, R. L. Roberts-Thomson, L. Mackenzie, S. Willoughby, G. D. Young, and P. Sanders, "The effect of electrogram duration on quantification of complex fractionated atrial electrograms and dominant frequency." *J. Cardiovasc. Electrophysiol.*, vol. 19, no. 3, pp. 252–258, Mar 2008.

[94] J. Ng and J. J. Goldberger, "Understanding and interpreting dominant frequency analysis of AF electrograms." *J. Cardiovasc. Electrophysiol.*, vol. 18, no. 6, pp. 680–685, Jun 2007.

[95] D. Husser, M. Stridh, D. S. Cannom, A. K. Bhandari, M. J. Girsky, S. Kang, L. Sörnmo, S. B. Olsson, and A. Bollmann, "Validation and clinical application of time-frequency analysis of atrial fibrillation electrocardiograms." *J. Cardiovasc. Electrophysiol.*, vol. 18, no. 1, pp. 41–46, Jan 2007.

[96] P. Sanders, O. Berenfeld, M. Hocini, P. Jaïs, R. Vaidyanathan, L.-F. Hsu, S. Garrigue, Y. Takahashi, M. Rotter, F. Sacher, C. Scavée, R. Ploutz-Snyder, J. Jalife, and M. Haïssaguerre, "Spectral analysis identifies sites of high-frequency activity maintaining atrial fibrillation in humans." *Circulation*, vol. 112, no. 6, pp. 789–797, Aug 2005.

[97] M. Hocini, P. Jaïs, P. Sanders, Y. Takahashi, M. Rotter, T. Rostock, L.-F. Hsu, F. Sacher, S. Reuter, J. Clémenty, and M. Haïssaguerre, "Techniques, evaluation, and consequences of linear block at the left atrial roof in paroxysmal atrial fibrillation: a prospective randomized study." *Circulation*, vol. 112, no. 24, pp. 3688–3696, Dec 2005.

[98] M. D. O'Neill, P. Jaïs, Y. Takahashi, A. Jönsson, F. Sacher, M. Hocini, P. Sanders, T. Rostock, M. Rotter, A. Pernat, J. Clémenty, and M. Haïssaguerre, "The stepwise ablation approach for chronic atrial fibrillation–evidence for a cumulative effect." *J. Interv. Card. Electrophysiol.*, vol. 16, no. 3, pp. 153–167, Sep 2006.

[99] M. Haïssaguerre, M. Hocini, Y. Takahashi, M. D. O'Neill, A. Pernat, P. Sanders, A. Jonsson, M. Rotter, F. Sacher, T. Rostock, S. Matsuo, L. Arantés, K. Teng Lim, S. Knecht, P. Bordachar, J. Laborderie, P. Jaïs, G. Klein, and J. Clémenty, "Impact of catheter ablation of the coronary sinus on paroxysmal or persistent atrial fibrillation." *J. Cardiovasc. Electrophysiol.*, vol. 18, no. 4, pp. 378–386, Apr 2007.

[100] A. Forclaz, S. M. Narayan, D. Scherr, N. Linton, A. S. Jadidi, I. Nault, L. Rivard, S. Miyazaki, N. Linton, L. Uldry, M. Wright, A. J. Shah, X. Liu, O. Xhaet, N. Derval, S. Knecht, F. Sacher, P. Jaïs, M. Hocini, and M. Haïssaguerre, "Early Temporal and Spatial Regularization of Persistent Atrial Fibrillation Predicts Termination and Arrhythmia-Free Outcome Short title: Regularization Index for Persistent AF Ablation." *Heart Rhythm*, vol. 8, pp. 1374–1382, May 2011.

[101] M. D. O'Neill, M. Wright, S. Knecht, P. Jaïs, M. Hocini, Y. Takahashi, A. Jönsson, F. Sacher, S. Matsuo, K. T. Lim, L. Arantes, N. Derval, N. Lellouche, I. Nault, P. Bordachar, J. Clémenty, and M. Haïssaguerre, "Long-term follow-up of persistent atrial fibrillation ablation using termination as a procedural endpoint." *Eur. Heart. J.*, vol. 30, no. 9, pp. 1105–1112, May 2009.

[102] Y. Takahashi, A. Takahashi, T. Kuwahara, T. Fujino, K. Okubo, S. Kusa, A. Fujii, A. Yagishita, S. Miyazaki, T. Nozato, H. Hikita, K. Hirao, and M. Isobe, "Clinical characteristics of patients with persistent atrial fibrillation successfully treated by left atrial ablation." *Circ. Arrhythm. Electrophysiol.*, vol. 3, no. 5, pp. 465–471, Aug 2010.

[103] E. K. Heist, F. Chalhoub, C. Barrett, S. Danik, J. N. Ruskin, and M. Mansour, "Predictors of atrial fibrillation termination and clinical success of catheter ablation of persistent atrial fibrillation." *Am. J. Cardiol.*, vol. 110, no. 4, pp. 545–551, May 2012.

[104] Task Force of The European Society of Cardiology and The North American Society of Pacing and Electrophysiology, "Heart rate variability. Standards of measurement, physiological interpretation, and clinical use. Task Force of the European Society of Cardiology and the North American Society of Pacing and Electrophysiology." *Eur. Heart. J.*, vol. 17, no. 3, pp. 354–381, Mar 1996.

[105] C. Julien, "The enigma of Mayer waves: facts and models." *Cardiovasc. Res.*, vol. 70, no. 1, pp. 12–21, Apr 2006.

[106] P. Pascale, A. J. Shah, L. Roten, D. Scherr, Y. Komatsu, A. S. Jadidi, K. Ramoul, M. Daly, A. Denis, S. B. Wilton, N. Derval, F. Sacher, M. Hocini, M. Haïssaguerre, and P. Jaïs, "Pattern and timing of the coronary sinus activation to guide rapid diagnosis of atrial tachycardia after atrial fibrillation ablation." *Circ. Arrhythm. Electrophysiol.*, vol. 6, no. 3, pp. 481–490, Apr 2013.

[107] L. Y. Di Marco, D. Raine, J. P. Bourke, and P. Langley, "Characteristics of atrial fibrillation cycle length predict restoration of sinus rhythm by catheter ablation." *Heart Rhythm*, vol. 10, no. 9, pp. 1303–1310, Jun 2013.

[108] M. Lemay, "Data processing techniques for the characterization of atrial fibrillation," Ph.D. dissertation, Ecole Polytechnique Fédérale de Lausanne, 2008.

[109] P. S. Cuculich, Y. Wang, B. D. Lindsay, M. N. Faddis, R. B. Schuessler, R. J. Damiano, L. Li, and Y. Rudy, "Noninvasive characterization of epicardial activation in humans with diverse atrial fibrillation patterns." *Circulation*, vol. 122, no. 14, pp. 1364–1372, Oct 2010.

[110] L. Mirmohamadsadeghi, S. Fallet, A. Buttu, J. Saugy, T. Rupp, R. Heinzer, J.-M. Vesin, and G. P. Millet, "Sleep Apnea Detection Using Features from the Respiration and the ECG Recorded with Smart-Shirts," *IEEE Biomedical Circuits and Systems Conference (BIOCAS 2014)*, 2014.

[111] American Academy of Sleep Medicine Task Force, "Sleep-related breathing disorders in adults: recommendations for syndrome definition and measurement techniques in clinical research. the report of an american academy of sleep medicine task force." *Sleep*, vol. 22, no. 5, pp. 667–689, Aug 1999.

[112] O. Schleusing, P. Renevey, M. Bertschi, S. Dasen, and R. Paradiso, "Detection of mood changes in bipolar patients though monitoring of physiological and behavioral signals," in *5th European Conference of the International Federation for Medical and Biological Engineering*, ser. IFMBE Proceedings, k. Jobbágy, Ed. Springer Berlin Heidelberg, 2012, vol. 37, pp. 1106–1109.

[113] O. Gilad, C. A. Swenne, L. R. Davrath, and S. Akselrod, "Phase-averaged characterization of respiratory sinus arrhythmia pattern." *Am J Physiol Heart Circ Physiol*, vol. 288, no. 2, pp. H504–H510, Feb 2005.

[114] A. Buttu, A. Forclaz, P. Pascale, S. Narayan, E. Pruvot, and J.-M. Vesin, "Morphological study of intracardiac signals as a new tool to track the efficiency of stepwise ablation of persistent atrial fibrillation," in *Computing in Cardiology, 2011*, Sept 2011, pp. 169–172.

[115] A. Buttu, S. Volorio, A. Forclaz, P. Pascale, S. Narayan, E. Pruvot, and J.-M. Vesin, "Tracking of stepwise ablation of persistent atrial fibrillation using synchronization of nearby electrograms," in *Computing in Cardiology, 2011*, Sept 2011, pp. 505–508.

[116] L. Faes, G. Nollo, M. Kirchner, E. Olivetti, F. Gaita, R. Riccardi, and R. Antolini, "Principal component analysis and cluster analysis for measuring the local organisation of human atrial fibrillation." *Med Biol Eng Comput*, vol. 39, no. 6, pp. 656–663, Nov 2001.

[117] L. Faes, G. Nollo, R. Antolini, F. Gaita, and F. Ravelli, "A method for quantifying atrial fibrillation organization based on wave-morphology similarity." *IEEE Trans Biomed Eng*, vol. 49, no. 12 Pt 2, pp. 1504–1513, Dec 2002.

[118] V. Jacquemet, N. Virag, and L. Kappenberger, "Wavelength and vulnerability to atrial fibrillation: Insights from a computer model of human atria." *Europace*, vol. 7 Suppl 2, pp. 83–92, Sep 2005.

[119] M. D. O'Neill, M. Wright, S. Knecht, P. Jaïs, M. Hocini, Y. Takahashi, A. Jönsson, F. Sacher, S. Matsuo, K. T. Lim, L. Arantes, N. Derval, N. Lellouche, I. Nault, P. Bordachar, J. Clémenty, and M. Haïssaguerre, "Long-term follow-up of persistent atrial fibrillation ablation using termination as a procedural endpoint." *Eur Heart J*, vol. 30, no. 9, pp. 1105–1112, May 2009.

[120] C. S. Elayi, L. D. Biase, C. Barrett, C. K. Ching, M. al Aly, M. Lucciola, R. Bai, R. Horton, T. S. Fahmy, A. Verma, Y. Khaykin, J. Shah, G. Morales, R. Hongo, S. Hao, S. Beheiry, M. Arruda, R. A. Schweikert, J. Cummings, J. D. Burkhardt, P. Wang, A. Al-Ahmad, B. Cauchemez, F. Gaita, and A. Natale, "Atrial fibrillation termination as a procedural endpoint during ablation in long-standing persistent atrial fibrillation." *Heart Rhythm*, vol. 7, no. 9, pp. 1216–1223, Sep 2010.

[121] Y. M. Park, J.-I. Choi, H. E. Lim, S. W. Park, and Y.-H. Kim, "Is pursuit of termination of atrial fibrillation during catheter ablation of great value in patients with longstanding persistent atrial fibrillation?" *J Cardiovasc Electrophysiol*, May 2012.

[122] S. Ammar, G. Hessling, T. Reents, M. Paulik, S. Fichtner, P. Schön, R. Dillier, S. Kathan, C. Jilek, C. Kolb, B. Haller, and I. Deisenhofer, "Importance of sinus rhythm as endpoint of persistent atrial fibrillation ablation." *J Cardiovasc Electrophysiol*, vol. 24, no. 4, pp. 388–395, Apr 2013.

[123] T. Rostock, T. V. Salukhe, B. A. Hoffmann, D. Steven, I. Berner, K. Müllerleile, C. Theis, K. Bock, H. Servatius, A. Sultan, and S. Willems, "The prognostic role of subsequent atrial tachycardias occurring during ablation of persistent atrial fibrillation: A prospective randomized trial." *Circ Arrhythm Electrophysiol*, vol. 6, no. 6, pp. 1059–1065, Oct 2013.

[124] M. Faustino, C. Pizzi, D. Capuzzi, T. Agricola, G. M. Costa, M. E. Flacco, C. Marzuillo, M. Nocciolini, L. Capasso, and L. Manzoli, "The impact of atrial fibrillation termination mode during catheter ablation procedure on maintenance of sinus rhythm." *Heart Rhythm*, May 2014.

[125] K. T. Konings, J. L. Smeets, O. C. Penn, H. J. Wellens, and M. A. Allessie, "Configuration of unipolar atrial electrograms during electrically induced atrial fibrillation in humans." *Circulation*, vol. 95, no. 5, pp. 1231–1241, Mar 1997.

[126] H. Cochet, R. Dubois, F. Sacher, N. Derval, M. Sermesant, M. Hocini, M. Montaudon, M. Haïssaguerre, F. Laurent, and P. Jaïs, "Cardiac Arrythmias: Multimodal Assessment Integrating Body Surface ECG Mapping into Cardiac Imaging." *Radiology*, p. 131331, Dec 2013.

[127] M. Haissaguerre, M. Hocini, A. Denis, A. J. Shah, Y. Komatsu, S. Yamashita, M. Daly, S. Amraoui, S. Zellerhoff, M.-Q. Picat, A. Quotb, L. Jesel, H. Lim, S. Ploux, P. Bordachar, G. Attuel, V. Meillet, P. Ritter, N. Derval, F. Sacher, O. Bernus, H. Cochet, P. Jais, and R. Dubois, "Driver domains in persistent atrial fibrillation." *Circulation*, vol. 130, no. 7, pp. 530–538, Aug 2014.

[128] R. M. Gulrajani, "The forward and inverse problems of electrocardiography." *IEEE Eng Med Biol Mag*, vol. 17, no. 5, pp. 84–101, 122, 1998.

[129] S. Verheule, J. Eckstein, D. Linz, B. Maesen, E. Bidar, A. Gharaviri, and U. Schotten, "Role of endo-epicardial dissociation of electrical activity and transmural conduction in the development of persistent atrial fibrillation." *Prog Biophys Mol Biol*, Jul 2014.

[130] J. Kalifa and U. M. R. Avula, "Ablation of driver domains during persistent atrial fibrillation: A call for more understanding." *Circulation*, Jul 2014.

[131] B. Boashash, "Estimating and interpreting the instantaneous frequency of a signal — Part 2: algorithms and applications," *P IEEE*, vol. 80, no. 4, pp. 540–568, April 1992.

[132] J. R. Carson and T. C. Fry, "Variable frequency electric circuit theory with application to the theory of frequency-modulation," *Bell Syst Tech J*, vol. 16, no. 4, pp. 513–540, October 1937.

[133] B. van der Pol, "The fundamental principles of frequency modulation," *J IEE*, vol. 93, no. 23, pp. 153–158, May 1946.

[134] D. W. Kammler, *A first course in Fourier analysis*. Prentice Hall, 2000.

[135] T. Ryan, *Modern Regression Methods*, ser. Wiley Series in Probability and Statistics. John Wiley & Sons, 2008.

[136] B. Vidakovic, *Statistics for Bioengineering Sciences: With MATLAB and WinBUGS Support*, ser. Springer Texts in Statistics. Springer, 2011.

[137] J. J. Rieta, F. Castells, C. Sánchez, V. Zarzoso, and J. Millet, "Atrial activity extraction for atrial fibrillation analysis using blind source separation." *IEEE Trans. Biomed. Eng.*, vol. 51, no. 7, pp. 1176–1186, Jul 2004.

[138] A. Bollmann, K. Sonne, H. D. Esperer, I. Toepffer, J. J. Langberg, and H. U. Klein, "Noninvasive assessment of fibrillatory activity in patients with paroxysmal and persistent atrial fibrillation using the Holter ECG." *Cardiovasc. Res.*, vol. 44, no. 1, pp. 60–66, Oct 1999.

[139] M. Stridh and L. Sörnmo, "Spatiotemporal QRST cancellation techniques for analysis of atrial fibrillation." *IEEE Trans. Biomed. Eng.*, vol. 48, no. 1, pp. 105–111, Jan 2001.

[140] L. T. Mainardi, L. Sörnmo, and S. Cerutti, *Understanding Atrial Fibrillation: The Signal Processing Contribution, Part II*, ser. Synthesis Lectures on Biomedical Engineering. Morgan & Claypool Publishers, 2008.

[141] Z. Ihara, A. van Oosterom, and R. Hoekema, "Atrial repolarization as observable during the PQ interval." *J. Electrocardiol.*, vol. 39, no. 3, pp. 290–297, Jul 2006.

[142] L. Sörnmo and P. Laguna, *Bioelectrical signal processing in cardiac and neurological applications*. Academic Press, 2005.

[143] A. van Oosterom, "The dominant T wave and its significance." *J. Cardiovasc. Electrophysiol.*, vol. 14, no. 10 Suppl, pp. S180–S187, Oct 2003.

[144] A. van Oosterom, "Singular value decomposition of the T wave: Its link with a biophysical model of repolarization," *Int. J. Bioelectromagnetism*, vol. 4, p. 59, Jul 2003.

[145] A. van Oosterom and V. Jacquemet, "A parametrized description of transmembrane potential used in forward and inverse procedures," in *Folia Cardiologica*, vol. 12 (suppl. D), 2005, p. 111.

[146] D. W. Marquardt, "An algorithm for least-squares estimation of nonlinear parameters," *J. Soc. Ind. Appl. Math.*, vol. 2, pp. 431–441, 1963.

Index

Andrea Buttu

133 route de Lully
CH-1233 Bernex
Phone: +41 79 448 97 50
Email: andrea.buttu@gmail.com

Date of birth: May 2nd, 1982
Nationality: Swiss
Marital status: Single

Education

2010 – 2014	ÉCOLE POLYTECHNIQUE FÉDÉRALE DE LAUSANNE, Switzerland. Ph.D. in Biomedical Signal Processing under the direction of Dr. J.-M. Vesin. Thesis entitled : *Novel ECG and Intracardiac Electrograms Signal Processing Schemes for Predicting the Outcome of Atrial Fibrillation Catheter Ablation.*
2007 – 2008	OXFORD SCIENCE ENTERPRISE CENTRE SAÏD BUSINESS SCHOOL, UNIVERSITY OF OXFORD, United Kingdom. "Building a Business" program.
2002 – 2008	ÉCOLE POLYTECHNIQUE FÉDÉRALE DE LAUSANNE, Switzerland. Bachelor and M.Sc. in Communication Systems. Specialization : Wireless Communications.

Academic Experience

2007 – 2008	ÉCOLE POLYTECHNIQUE FÉDÉRALE DE LAUSANNE, Switzerland. Teaching assistant for lab sessions and exercises in the course *Digital photography* given by Prof. S. Süsstrunk..

Professional Experience

2008 – 2009	IMAGE AND VISUAL REPRESENTATION GROUP, ÉCOLE POLYTECHNIQUE FÉDÉRALE DE LAUSANNE, Switzerland. Research assistant.
2007 – 2008	YOTTA DCL - OXFORD METRICS GROUP, Oxford, United Kingdom. Master thesis entitled : *Road surface reconstruction using structured light and stereo vision.*
Apr. – Sept. 2006	SIEMENS, Munich, Germany. Internship in the field of wireless networks. Patent : *Method for Establishing Bidirectional Data Transmission Paths in a Wireless Meshed Communication Network.*

Language

French, Romanian :	native languages.
English :	advanced.
German, Spanish :	basic.

Computer Skills

Environment :	Windows (good working knowledge) and Linux (basic).
Programming :	Matlab, wide experience. Java and C/C++, good experience. UML, basic knowledge.
Tools :	Network Simulator ns-2, Microsoft Office, and LaTeX.

Interests and Activities

· Sailing, Tennis, Badminton, Mountain, Wakeboard.
· Music, Travelling, Reading.

References

Available upon request.

Publications

Journal Papers

A. Buttu, J. Van Zaen, A. Viso, A. Forclaz, P. Pascale, P. Maury, A. Rollin, E. Pruvot, and J.-M. Vesin, "Long-standing persistent atrial fibrillation terminating within the left atrium displays high organization from the ECG," *Circulation: Arrhythmia and Electrophysiology*, 2014, in preparation.

A. Buttu, J. Van Zaen, A. Viso, A. Forclaz, P. Pascale, S. M. Narayan, E. Pruvot, and J.-M. Vesin, "Adaptive frequency tracking of the baseline ECG identifies the site of atrial fibrillation termination by catheter ablation," *Biomedical Signal Processing and Control*, vol. 8 no 6, pp. 969–980, November 2013

Conference Papers

L. Mirmohamadsadeghi, S. Fallet, A. Buttu, J. Saugy, T. Rupp, R. Heinzer, J.-M. Vesin, and G.P. Millet, "Sleep apnea detection using features from the respiration and the ECG recorded with smart-shirts," *The 2014 IEEE Biomedical Circuits & Systems Conference Proceedings*, Lausanne, Switzerland, October 2014.

A. Buttu, A. Forclaz, P. Pascale, P. Maury, A. Rollin, J.-M. Vesin, and E. Pruvot, "Measures of right atrial organization as a mean to select candidates for sinus rhythm restoration by catheter ablation," *Computing in Cardiology*, Zaragoza, Spain, September 2013.

A. Buttu, J. Van Zaen, A. Viso, A. Forclaz, P. Pascale, S. M. Narayan, J.-M. Vesin, and E. Pruvot, "Termination of atrial fibrillation by catheter ablation can be successfully predicted from baseline ECG," *Computing in Cardiology*, Kraków, Poland, September 2012.

A. Buttu, J. Van Zaen, A. Viso, A. Forclaz, P. Pascale, S. M. Narayan, J.-M. Vesin, and E. Pruvot, "A new method for ECG tracking of persistent atrial fibrillation termination during stepwise ablation," *Computing in Cardiology*, Hangzhou, China, September 2011.

A. Buttu, A. Forclaz, P. Pascale, S. M. Narayan, E. Pruvot, and J.-M. Vesin, "Morphological study of intracardiac signals as a new tool to track the efficiency of stepwise ablation of persistent atrial fibrillation," *Computing in Cardiology*, Hangzhou, China, September 2011.

A. Buttu, S. Volorio, A. Forclaz, P. Pascale, S. M. Narayan, J.-M. Vesin, and E. Pruvot, "Tracking of stepwise ablation of persistent atrial fibrillation using synchronization of nearby electrograms," *Computing in Cardiology*, Hangzhou, China, September 2011.

A. Cabasson, L. Dang, J.-M. Vesin, A. Buttu, R. Abächerli, R. Leber, and L. Kappenberger, "P-wave indices to detect susceptibility to atrial fibrillation," *Computing in Cardiology*, Hangzhou, China, September 2011.

Abstracts

A. Buttu, J.-M. Vesin, A. Forclaz, P. Pascale, P. Maury, A. Rollin, L. Roten, and E. Pruvot, "Long-standing persistent atrial fibrillation terminating within the left atrium displays high temporal bi-atrial stability of activation wavefront," *Cardiostim*, Nice, France, June 2014.

A. Buttu, E. Pruvot, A. Forclaz, P. Pascale, S. M. Narayan, P. Maury, A. Rollin, and J.-M. Vesin, "High bi-atrial organization in patients with long-standing persistent atrial fibrillation terminated within the left atrium," *EHRA Europace*, Athens, Greece, June 2013.

A. Buttu, J. Van Zaen, A. Viso, A. Forclaz, P. Pascale, P. Maury, A. Rollin, S. M. Narayan, J.-M. Vesin, and E. Pruvot, "High pre-ablation ECG organization in long-standing persistent atrial fibrillation terminated within the left atriaum," *EHRA Europace*, Athens, Greece, June 2013.

A. Buttu, A. Forclaz, P. Pascale, S. M. Narayan, E. Pruvot, and J.-M. Vesin, "Contribution of left and right atrial appendage activities to ECG fibrillation waves," *Heart Rhythm Society (HRS) 33rd Annual Scientific Sessions*, Boston, USA, May 2012.

A. Buttu, J. Van Zaen, A. Viso, A. Forclaz, P. Pascale, S. M. Narayan, J.-M. Vesin, and E. Pruvot, "Termination of atrial fibrillation by catheter ablation can be successfully predicted from baseline ECG," *Cardiostim*, Nice, France, June 2012.

A. Buttu, J. Van Zaen, A. Viso, A. Forclaz, P. Pascale, S. M. Narayan, J.-M. Vesin, and E. Pruvot, "Termination of atrial fibrillation by catheter ablation can be successfully predicted from baseline ECG," *Swiss Society of Cardiology Annual Meeting*, Lausanne, Switzerland, June 2012.

J. Van Zaen, L. Uldry, A. Buttu, L. Kappenberger, and J.-M. Vesin, "Harmonic frequency tracking algorithm for predicting the success of pharmacological cardioversion of atrial fibrillation," *EHRA Europace*, Madrid, Spain, June 2011.

A. Buttu, A. Viso, J. Van Zaen, J.-M. Vesin, A. Forclaz, P. Pascale, S. M. Narayan, and E. Pruvot, "ECG periodic components as a promising tool for complexity assessment during stepwise ablation of atrial fibrillation," *Swiss Society of Cardiology Annual Meeting*, Basel, Switzerland, June 2011.

A. Buttu, S. Volorio, J.-M. Vesin, A. Forclaz, P. Pascale, S. M. Narayan, and E. Pruvot, "Mechano-electrical contribution of ventricular contractions to the complexity of atrial fibrillation electrograms," *Swiss Society of Cardiology Annual Meeting*, Basel, Switzerland, June 2011.

Invited Talks

A. Buttu, "Adaptive organization analyses of the surface ECG to predict left atrial sites of termination of long-standing persistent AF during ablation," *Cardiostim*, Nice, France, June 2014.

A. Buttu, and J.-M. Vesin, "Adaptive tracking of atrial fibrillation ECG oscillations," *7th TRM Forum on Computer Simulation and Experimental Assessment of Cardiac Function*, Lugano, Switzerland, December 2013.